UNIVERSITY OF BIRMINGHAM

Studies on the Chemical Recycling of Poly(lactic acid) *via* Alcoholysis

By

Fabio Michele Lamberti

A thesis submitted to
The University of Birmingham
For the degree of
DOCTOR OF PHILOSOPHY

School of Chemical Engineering
College of Engineering and Physical Sciences
The University of Birmingham
December 2022

Abstract

Continual reduction of landfill space, rising CO_2 levels, and plastic pollution are global issues that will only grow in time if not correctly addressed. The opportunity exists to replace petroleum-derived plastics with bioplastics. This, in conjunction with mechanical and chemical recycling, is a potential remedy that enables a circular economy. PLA is a leading bioplastic; its growing production capacity means its end-of-life treatment is becoming increasingly important. One beneficial disposal route for PLA is its chemical recycling *via* alcoholysis. The alcoholysis of PLA leads to the generation of value-added products alkyl lactates; this route also has potential for a circular economy. In this work, the alcoholysis of PLA was studied in a autoclave reactor. A range of alcohols were used as reactants to generate various alkyl lactates. Discrete synthesised catalysts and commercially available catalysts were investigated, as well as dual catalysis systems. Three kinetic models were applied to the experimental data: a simple first order model that only considers the initial degradation of PLA, a two-step consecutive model with irreversible second step, and a two-step consecutive model with the second step in equilibrium.

This work concluded that increasing the nucleophilic alcohol chain length decreases alcoholysis reaction rate; the increased steric hinderance of a larger alcohol inhibits coordination to the catalyst and PLA ester groups. This work also concluded that dual catalyst synergy is only present if there is a great enough difference in pK_a for each catalyst in addition to having both acid and base character. Further research is needed to fully explore synergistic Lewis acids-base pairs; an understanding of their coordination and mechanism is required in order to fully exploit dual-catalysts systems for enhanced chemical recycling. The chemical recycling of PLA *via* alcoholysis is a promising end-of-life solution, adding value to the PLA supply chain through the generation of value-added ALs.

This thesis is dedicated to the loving memory of Michelangelo and Maria Taverna.

Acknowledgments

My deepest thanks and gratitude to Prof Joe Wood for his leadership and supervision, and for providing the opportunity for my PhD research. Thanks goes to Prof Andrew Ingram for his co-supervision. I want to thank them both for the enthusiasm and guidance throughout this project.

I am greatly indebted to Dr Román-Ramírez for his help with MATLAB modelling, and greatly appreciate the help of Dr Paul Mckeown and Prof. Matthew D. Jones during our collaboration. I would also like to thank Prof Andrew Dove for his help and contribution towards dual catalysis. My gratitude goes to Zoe Simon for her help with GC maintenance. The Chemical Engineering Workshop team is also thanked for their contribution in the reactor maintenance. Special thanks to Cécile Le Duff for her guidance and help with ^{1}H NMR. Thanks to the school of School of Chemical Engineering University of Birmingham for the scholarship as part of my financial support. Thanks also goes to ESPRC for their funding which allowed for the equipment used in this project. I would like to thank the past and current students that also undertook PhDs in this research group, the conversations and discussions had during lab time made the whole experience more enjoyment. Special thanks goes to Pushpa and Abu for cultivating a welcoming office environment, your support during rough times was greatly appreciated.

My heartfelt thanks goes to my father and mother for the motivation and financial support throughout this study. Special thanks to my brother and sister for their moral support and encouragement. I also want express thanks to my nonna, nonno, aunties, uncles, and my cousins, for their support. Big shout out to my boys Carmz and Peppus for the continual banter and good times. Last but not least, my deepest thanks and gratitude to my beautiful wife Megan for her unconditional love and support. Without her this journey would have been significantly harder.

CONTENTS

List of Figures

List of Tables

Nomenclature

B_0	Applied magnetic field
E_a	Activation energy of reaction kJ·mol^{-1}
ee	Enantiomeric excess
I	angular momentum quantum number
M_n	Number average molecular weight
M_r	Relative molecular mass
M_w	Mass average molecular weight
pK_a	The negative base 10 logarithm of the acid dissociation constant
T_1	Longitudinal relaxation
T_2	Spin – spin transverse relaxation
T_g	Glass transition temperature
T_m	Melting temperature
$\nu°$	Resonance frequency
ω_0	Larmor frequency
γ	gyromagnetic ratio
δ	Chemical shift ppm

Acronyms

AD	Azeotropic distillation
AL	Alkyl lactates / alkyl lactate methine group
ATR	Attenuated total reflectance
Backbiting	Intramolecular transesterification

Bakelite	Phenol-formaldehyde resin
BuLa	Butyl lactate
BuOH	Butan-1-ol
CE	Chain end oligomer methine
CMR	A catalytic membrane reactor
CO_2	Carbon dioxide
CSTR	Continuous stirred-tank reactors
DMAP	4-(dimethylamino)pyridine
DP	Degree of polymerisation
ED	Electrodialysis
EG	Ethylene glycol
EoL	End-of-Life
EPLA	Expanded poly(lactic acid)
EPS	Expanded PS
EtLa	Ethyl lactate
EtOH	Ethanol
ExD	Extractive distillation
FBR	Fixed bed reactor
FTIR	Fourier transform infrared spectroscopy
GC	Gas chromatography
GHG	Green house gas
GWP	Global warming potential
HDPE	High density poly(ethylene)
HOMO	Highest occupied molecular orbital

^{1}H NMR	Proton nuclear magnetic resonance
IL	Ionic liquids
Int	Internal methine groups of a PLA chain
LCA	Life cycle assessment
LDPE	Low density poly(ethylene)
LUMO	Lowest unoccupied molecular orbital
MeLa	Methyl lactate
MeOH	Methanol
$Mg(OAc)_2$	Magnesium acetate tetrahydrate
MSA	Methanesulfonic acid
PET	Poly(ethylene terephthalate)
PHB	Poly(3-hydroxybutyrate)
PHBV	Poly(3-hydroxybutyrate-co-3 hydroxyvalerate)
PLA	Poly(lactic acid)
PFR	Plug flow reactor
PP	Poly(propylene)
PrLa	Propyl lactate
PrOH	Propan-1-ol
PS	Poly(styrene)
PUR	Poly(urethane)
PVC	Poly(vinylchloride)
RF	Radio frequency
TA	terephthalic acid
TBD	triazabicyclodecene

TGA	Thermogravimetric analysis
TMS	Tetramethylsilane
$Zn(OAc)_2$	Zinc acetate dihydrate

Chapter 1 – Introduction

1.1 Background and Motivation

Plastics (man-made polymers) are a group of relatively modern materials that have become ubiquitous in everyday life. They are utilized globally in a diverse range of applications: textile fibres, medical sutures, cosmetic enhancers, packaging materials and in the construction sector. Since their industrialisation in the 1950's plastic production has grown at an extraordinary rate. By 2050 it is estimated that annual plastic production will reach 1.1 Gt, consuming 20% of global oil production [1,2]. Plastic's astonishing growth has surpassed most other man-made materials with notable exceptions such as steel and cement [1].

The excellent mechanical and barrier properties of plastics, coupled with a low bulk density, often make them the superior choice of material for an application. Further in their favour is the fact that traditional plastics have relatively cheap production costs when synthesised from petroleum, even when accounting for rising crude oil prices. The issues surrounding plastics arise at end-of-life, their robust mechanical properties lead to extremely long biodegradation times in the natural environment. The majority of postconsumer plastic is disposed of in landfill or the ocean, causing environmental damage as well as an economic loss [1–3]. Plastics are now so ubiquitous in the environment they can be found in every location on earth and have been suggested as a geological indicator of the proposed Anthropocene era [1,4]. Plastic pollution is an alarming issue, considering its production growth this problem is only set to increase in the future.

The problems associated with plastic pollution could be mitigated by implementing a circular economy. In theory all thermoplastics can be collected and recycled at end-of-life. A circular plastic economy would reuse and mechanically recycle waste plastics when possible. Reuse and mechanical recycling have the lowest environmental impacts in comparison to other

disposal routes. The downside to mechanical recycling is that the recycled plastic will have diminished mechanical properties, furthermore the material will be of a lower quality in comparison to virgin polymer. During mechanical recycling polymer chains are exposed to thermo-mechanical degradation, the combination of mechanical stresses and high temperatures causes chain scissions reactions that shorten the polymer chains [5]. Each mechanical cycle will degrade the polymer chains further and diminish the final material properties, the mechanical recycling of PLA is discussed further in section § 2.5.4. To combat this plastics are often mechanically recycled alongside virgin polymer. Once recyclate polymer material becomes low-grade, mechanical recycling is no longer possible. While disposal routes such as landfill or incineration are still possible, chemical recycling exists as a third option that offers many advantages [3,6]. Chemical recycling routes are numerous, with many different strategies that generate either a value-added product or monomeric units of the recycled plastic. Recovered monomer could be used as a feedstock for new polymer synthesis, thus lowering the requirement for fossil fuels [7]. Chemical recycling offers the potential to reduce global warming impacts and fossil resource depletion [8].

A leading bioplastic is poly(lactic acid) (PLA), which makes up a growing 13.9% of the bioplastic market; it is considered a bioplastic as it is both bio-based and biodegradable [9]. PLA is limited by its more expensive cost and brittleness in comparison to fossil-based plastics. Despite this, its main potential could be to replace poly(styrene) (PS) (6% of the total plastic production) as a more environmentally friendly polymer [1]. At end-of-life PLA should be chemically recycled instead of composted to recover the embedded energy of its molecular chains. Although it is possible to chemically recycle PLA *via* hydrolysis to generate its monomer lactic acid (LA), a more desirable recycling route from an environmental perspective is alcoholysis. LCAs have reported alcoholysis of PLA to have the most environment benefits

across impact categories, such as global warming, acidification, eutrophication, resource use, and photochemical ozone formation [10]. Alcoholysis provides the opportunity to generate value-added products alkyl lactates (AL) in addition to having a smaller activation energy (E_a) than hydrolysis. In comparison to end-of-life (EoL) treatments of other polyesters such as PET (Poly(ethylene terephthalate)), EoL of PLA is relatively under researched. A simple search of the terms 'PET chemical recycling', and 'PLA chemical recycling', on the web of science generated 1054 and 188 results respectively. Likewise, a search for these terms on google scholar generated 160000 and 47500 results respectively. PLA's production capacity is expected to significantly increase in the future making its lack of literature around EoL treatment critical. Thus, PLA and specifically its chemical recycling *via* alcoholysis was investigated for this thesis.

The work presented in this thesis focuses on the chemical recycling of PLA, specifically recycling is achieved *via* alcoholysis to generate AL. This depolymerisation process is considered a transesterification reaction; where an alcoholic nucleophile selectively cleaves PLA's ester linkages, where the R group of the alcohol nucleophile swaps with the R group of the ester. The specific AL produced depends on the alcohol used: methanol (MeOH) will result in methyl lactate (MeLa), ethanol (EtOH) will result in ethyl lactate (EtLa), etc. These different alcoholysis reactions were optimised in terms of reactor parameters; additionally different catalysts were explored as well as the synergistic utilization of dual-catalyst systems. The specific details are addressed in the objectives below.

1.2 Objectives of the Present Study

After surveying the range of information about plastic pollution and the literature reported for PLA alcoholysis, the following objectives were set for the present study to address prior knowledge gaps:

i) To evaluate PLA alcoholysis and the kinetics of AL formation, using collaboration Zn (II) complexes, synthesised by the University of Bath

a) To investigate different alcohol chain lengths and their effects on AL formation, to interpret reaction results and establish a kinetic model for the experimental data.

b) To compare the catalytic performance of the two synthesised Zn (II) complexes and optimise their reactivity towards PLA transesterification.

Work carried out in Objective (i) was part of an EPSRC project (EP/P016405/1) and collaboration with University of Bath. The discrete Zn complexes were developed and prepared by the research group of Prof. Matthew Jones in the School of Chemistry at the University of Bath. The synthesis of these discrete Zn complexes is detailed in section §3.3. The experimental data were fitted to kinetic model in MATLAB, the MATLAB script was provided by Dr. Luis A. Román-Ramírez from the School of Chemical Engineering University of Birmingham and is detailed in section §3.6.

ii) To compare the catalytic performance of commercially available catalysts: zinc acetate dihydrate ($Zn(OAc)_2$), and 4-(dimethylamino)pyridine (DMAP), on the rate of PLA alcoholysis.

a) To explore catalyst mixtures and Lewis acid-base synergy and investigate the enhanced reactivity towards PLA depolymerisation.

b) To investigate and compare the effect of MeOH and EtOH towards PLA depolymerisation.

c) To establish a simplified kinetic model and fit the experimental data.

iii) To evaluate and optimise PLA methanolysis and MeLa formation, using a range of commercially available catalysts: $Zn(OAc)_2$, magnesium acetate tetrahydrate ($Mg(OAc)_2$), DMAP and triazabicyclodecene (TBD).

a) To explore catalyst mixtures and acid-base synergies further exploiting enhanced reactivity for PLA depolymerisation.

b) To investigate the molar equivalent of MeOH on the production rate of MeLa.

c) To investigate the kinetics of catalyst mixtures using three kinetic models: a first order model that only considers the initial degradation of PLA, a two-step consecutive model with the second step being irreversible, a two-step consecutive model with the second step being in equilibrium. To compare resulting activation energies from these different kinetic models.

1.3 Thesis Layout

Given the range of objectives stated above the structure of this thesis is set as the following 8 chapters.

Chapter 1 provides a brief introduction and background information about current work as well as providing the objectives of this project.

Chapter 2 presents an in-depth literature review discussing the background of plastics as well as its market share, pollution, motivation for recycling, and different recycling routes. Bioplastics are then introduced along with biodegradation. PLA is then discussed, covering its synthesis, mechanical properties, and its potential to mitigate climate change. PLA recycling routes are discussed, including mechanical recycling and various chemical recycling routes. One route alcoholysis is discussed in depth as this is the focus of the thesis; different catalysts are presented as well as the exploration of synergistic catalyst pairs. Issues associated with PLA on the already well-established mechanical recycling of PET are discussed, as well as a brief discussion of reactor types and plastic separation. This chapter includes parts from the publication, Recycling of Bioplastics: Routes and Benefits [11]. This paper comprises of work entirely from the thesis author.

Chapter 3 is a compilation of the list of materials and instruments used in this project, descriptions of the collaboration catalyst synthesis, the experimental set up, operating procedures, and analytical methods are described. Detailed information regarding the reactor and characterisation techniques are provided.

Chapter 4 presents the investigation of alcohol chain length and its effect on the alcoholysis of PLA, collaboration synthesised catalysts were utilized here. This chapter is based on the publication, Kinetics of Alkyl Lactate Formation from the Alcoholysis of Poly(lactic Acid) [12]. While the catalyst synthesis and model were provided by colleagues on this collaboration, this paper comprises of work entirely from the thesis author.

Chapter 5 reports the investigation of two commercially available catalysts $Zn(OAc)_2$ and DMAP on the alcoholysis of PLA using both MeOH and EtOH. This chapter is based on the publication, Synergistic Dual Catalytic System and Kinetics for the Alcoholysis of Poly(Lactic Acid) [13]. Prof. Andrew Dove provided help in the original discussion of dual catalysis. This paper comprises of work entirely from the thesis author.

Chapter 6 presents the study of four commercially available catalysts $Zn(OAc)_2$, $Mg(OAc)_2$, DMAP and TBD, comparing their catalytic reactivity towards alcoholysis of PLA. This chapter is based on the publication, Methanolysis of Polylactic acid Using Catalyst Mixtures and the Kinetics of Methyl Lactate Production [14]. While this paper utilized the model provided by Dr. Luis A. Román-Ramírez, the work comprises entirely from the thesis author.

Chapter 7 brings the results of the previous 3 chapters together into final conclusions. Important questions that should be addressed in future work are identified.

Chapter 8 appendices such as experimental data, instrument calibrations, material characterisations, example calculations and MATLAB kinetic modelling scripts.

Chapter 2 – Literature Review

2.1 Plastic Background

Polymers have existed in nature long before the formation of the first cellular structures. A living cell is comprised of multiple organic polymer structures, such as cells walls, proteins, enzymes, and DNA, to name a few [15,16]. While the term 'polymer' was originally coined in 1827 by Berzelius its modern definition differs significantly from its inception [17,18]. We now think of polymers as substances that are comprised of macromolecular chains, a macromolecule being defined as a structure comprised of multiple repeating units of low relative molecular mass (M_r) [16]. The macromolecular structure of polymers was not recognised until the landmark paper published by Staudinger in 1920, who was eventually awarded a Nobel Prize in 1953 [16,18,19].

One of the earliest accounts of natural polymer usage was by the Ancient Mesoamericans. By 1600 B.C they were producing rubber by mixing latex from *Castilla elastica* trees with juice from *Ipomoea alba* vines [20,21]. Similar to material chemists today, Mesoamericans could tailor the final properties of the polymer by changing initial reaction conditions [20,21]. By using different ratios of latex and *I.alba* juice they were able to make rubber balls with high elasticity that bounce, high wear resistance rubber sandal soles, and rubber bands used in tool making [21]. Over two millennia later in 1839 Goodyear discovered natural rubber (polyisoprene) can be vulcanized with sulphur. This process crosslinks the polymer chains and hardens the final rubber material [16,20]. Many developments relating to natural rubber and cellulose were made during the 19th at the start of the 20th century.

The next major development was carried out by Baekeland in the years 1905 to 1909, where he discovered a phenol-formaldehyde resin (Bakelite) [16]. The commercialisation of Bakelite is significant as it is considered to be the first completely synthetic thermosetting plastic [17,18].

The success of Bakelite led to the rapid development of many other types of polymers, notably PET was developed by ICI in 1943 [18]. The true commercialisation of plastics began in the 1950's with the discoveries of Ziegler's organometallic catalyst systems and Natta's stereoselective olefin polymerisation [22]. Their combined efforts won them the 1963 Nobel prize in chemistry, and their discoveries led to the application of Ziegler-Natta catalysts for olefin polymerisation ushering in the "age of plastics" [23]. The ensuing rapid growth in plastic production is extraordinary surpassing most other man-made materials [1].

2.2 Plastic Definition

Plastics can be made with a near limitless variety of structures and can be tailored in terms of both their repeating monomer units and the way their polymer chains are linked together. Based solely on chain linkage, polymers can be separated into four distinct groups: thermoset, thermoplastic, elastomer, and thermoplastic elastomer [3]. A thermoset polymer undergoes irreversible polymerisation from a liquid to solid state when heated, forming a highly cross-linked molecular structure that cannot easily be melted and therefore is difficult to recycle [24,25]. (A special class of thermosets known as vitrimers have dynamic covalent bonds so can easily be recycled [26]). Elastomers, like thermosets, also consist of cross-linked polymer chains but can undergo elastic deformation when exposed to a load, and will return to their original shape once the load is removed [27]. Unlike thermosets, a thermoplastic can be repeatedly softened upon heating and will harden when cooled, opening up the potential to be recycled. A thermoplastic has an internal structure consisting of linear macromolecular chains held together by relatively weak intermolecular forces, such as Van der Waals forces, dipole-dipole interactions, and hydrogen bonding, to name just a few [25,27]. Thermoplastic elastomers are polymers that exhibit both thermoplastic and elastomeric properties [28].

Tacticity is the relative stereochemistry of adjacent chiral centres within a macromolecule. The tacticity of a thermoplastic is significant as it determines the physical properties of the material. The regularity of polymer chains in addition to substituent steric effects, determines the degree of crystalline long-range order and amorphous long-range disorder. The tacticity of a thermoplastic determines its crystallinity, typical range of crystallinity can be defined as completely amorphous (0%) to highly crystalline (>90%). An amorphous thermoplastic, such as poly(vinylchloride) (PVC), and polystyrene (PS), has random arrangements of molecular chains [29–31]. Due to long-range disorder amorphous thermoplastics lack a sharp melting point and will soften gradually as temperature increases. Semi-crystalline thermoplastics, such as polypropylene (PP), and high-density polyethylene (HDPE), have both crystalline regions of molecular chains in addition to amorphous regions [29–31]. Semi-crystalline thermoplastics have a sharp melting point and will quickly change state into a low viscosity liquid above its melting temperature (T_m).

2.3 Plastic Market Share and Application

The global plastic market size was valued at £432 billion in 2020 [32]. The proportion (by mass) of different polymer types that make up the plastic production year 2017 was as follows: PP 17%, LDPE 16%, HDPE 13%, PVC 9%, PET 8%, poly(urethane) (PUR) 7%, PS 6%, other 4%, additives 6% and PP&A 14%. PP&A is fibre production which consists primary of poly(ester), poly(amide) and poly(acrylic) fibre with PET accounting for 70%. These eight polymer groups and their additives made up 96% of plastic production that year [1,33]. Packaging applications used 42% of all nonfibre plastics (mostly PP, LDPE, HDPE, and PET); the next largest consuming sector is building and construction which used 69% of all PVC and 19% of the total nonfibre plastics [1].

In general plastics have excellent mechanical and barrier properties as well as relatively cheap production costs; this has allowed them to replace classic materials (metal, paper, glass) in many applications as the superior choice. Using plastic components in vehicles results in a lower environmental impact, HDPE fuel tanks have a smaller life cycle energy consumption of 3.6 GJ per tank in comparison to steel at 4.9 GJ per tank [34]. Comparing the life cycle assessment (LCA) for beverage-packaging materials made out of glass, aluminium cans, PET, and PLA, PLA followed by PET displayed the smallest greenhouse gas (GHG) emissions [35]. Another LCA study reported recycled PET bottles has the smallest Global Warming Potential (GWP) followed by virgin PET, then glass [36]. HDPE bags have been reported to have a 2.5× smaller environmental impact than paper bags [37]. Another study compared the LCA for single use bags and reusable bags. The study concluded after 50 instances of reuse PP non-woven bags have the smallest GWP, followed by HDPE, biodegradable plastic, cotton woven, and kraft paper bags at 14, 16, 17 and 81 times higher GWP impacts respectively [38]. Despite public perception, plastics are often the more environmentally friendly material in comparison to classic materials.

2.3.1 Recycling Motivation

Plastics have revolutionised global sectors such as transportation, healthcare and communications, greatly improving the quality of human life [39]. Despite the advantages of plastic materials their production from fossil-fuels and lack of EoL treatment is unsustainable. In 2014 plastic production reached 311 Mt, 26% by volume (approximately 81 Mt) was used in packaging applications [2]. Only 5% of the 81 Mt of plastic packaging was collected and recycled for subsequent use. This means a staggering 95% of packaging material was lost after short/single use which had an estimated value of £59 – 90 billion [2]. The unsustainability is attributed to the lack of a circular economy; as of 2015 it was estimated that only 9% of all

plastic ever produced was recycled; 12% was incinerated, and alarmingly 79% has accumulated in landfills or the natural environment [1].

In the year 2010 an estimated 5-13 Mt of plastic waste entered the ocean [40]. An estimated 100 Mt of plastic waste will end up disposed of in the oceans in just a 15 year period after 2010 [41]. Approximately 30% of this is HDPE and PP; these polyolefins have been reported to have a maximum weight loss of only 0.8% and 0.6% respectively after six months in the ocean [1,42]. Once plastic enters the ocean it will slowly degrade and fragment into increasingly smaller sizes ranging from: macro >5 mm, micro <5 mm, and nano <100 nm. At all sizes plastics have been reported to negatively impact marine organisms causing widespread contamination of ocean ecosystems [43,44]. It is well reported that microplastics ingested by zooplankton and phytoplankton/algae inhibit growth and cause other negative impacts on their health and function [43–46]. Considering that approximately 70% of the world's oxygen is produced from photosynthesizing marine plants, microplastic pollution could have serious consequences for climate change and global warming [43,47]. Ultimately microplastics bioaccumulate up the food chain and enter the human body, annual microplastic consumption in humans ranges from 74,000 – 121,000 particles [48]. Once inside the body, constituent monomers, additives, and toxins are released, causing physiological harm ranging from oxidative stress to carcinogenic behaviour [49]. Ingestion of microplastics have also been reported to act as endocrine disrupters, causing disruption of spermatogenesis and sperm maturation which could lead to male infertility [50,51].

2.3.2 Recycling Methods

Before plastic waste can be recycled several key steps are required: collection, sorting, cleaning, size reduction, and separation by polymer types [52]. Collection of postconsumer plastic largely depends on governmental legislation and regional collection schemes [53]. After size reduction

a range of separation techniques can be applied to separate plastic flakes into polymer type. One commonly used technique is sink/float separation which separates polymers based on their density. Using water allows for the easy separation of the polyolefins (PP, HDPE, and LDPE) from the other commodity plastics (PVC, PET and PS) [52]. Using different solvents can allow for the separation of PS from PET; however, this technique is limited and cannot separate PLA or PVC from PET as they have too similar densities [52]. Other techniques such as X-ray detection or Fourier-transform near-infrared, are capable of characterising similar density polymers allowing for separation [52]. One practical (low cost and simple to use) separation technique is froth flotation which is able to separate PVC and PLA from PET [54,55]. Another promising characterisation technique is triboelectric separation. This technique works by applying electrostatic charge to mixed plastics, by measuring the rate of charge relaxation it is possible to separate into polymer groups such as PP, PET/ PS, PVC, and HDPE [56,57].

Once separated into polymer type there are four possible recycling routes as shown in Figure 2.1. Reuse and primary recycling (closed-loop mechanical), secondary recycling (open-loop mechanical), tertiary recycling (chemical), and quaternary recycling (energy recovery). Primary and secondary recycling are both mechanical recycling techniques. These methods reprocess plastic waste material into new plastic products e.g the manufacturing of plastic bottles from used plastic bottles. Tertiary recycling is the reprocessing of waste plastic by chemical means into basic chemicals and monomers. Quaternary recycling are methods that recover energy through combustion of plastic turning the waste into energy for power and heating [58].

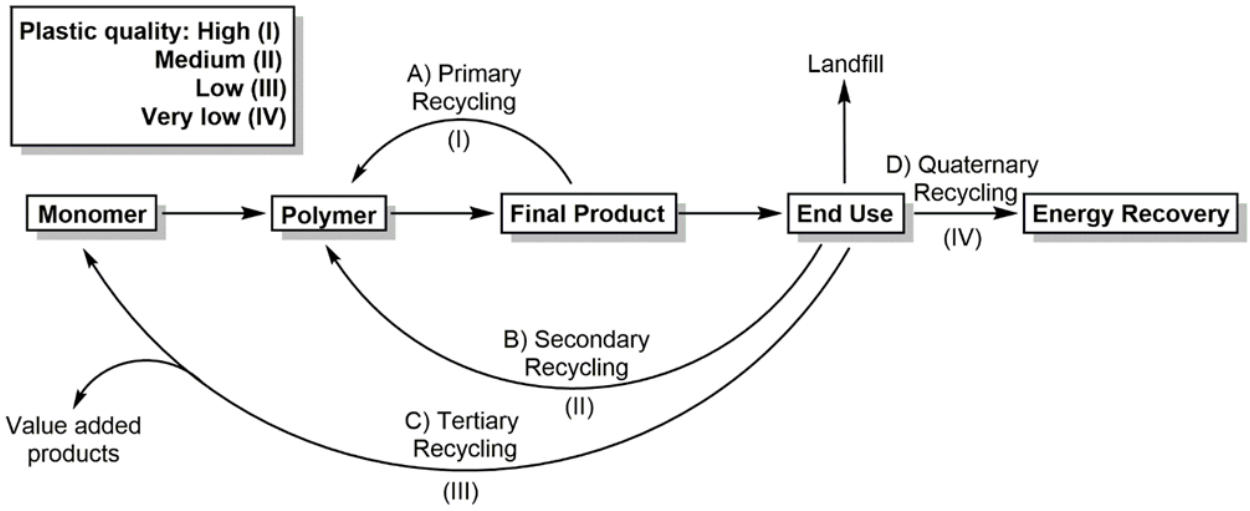

Figure 2.1 Different plastic waste treatment options and associated plastic quality.

A) Primary recycling is a closed loop recycling method that can only be carried out on high quality plastic scrap of known history. It refers to either the reuse of the material or the closed loop mechanical recycling of scrap plastic to produce products with the original structure [59,60]. An example of this is the recycling of scrap PET that arises during PET bottle production; the scrap PET is remelted with virgin PET to generate new bottles. This is the most efficient and cost-effective type of recycling, a market for the recycled material is certain and it reduces the need for virgin material. However, only a clean uncontaminated single type of plastic can be recycled and there is still a limit on the number of cycles of the material.

B) Secondary recycling refers to the transformation/downgrading of waste plastic into a less demanding product *via* mechanical means (screw extrusion, injection moulding, blow moulding, etc.) [25,58–60]. Mechanical recycling offers the following advantages over chemical recycling: a lower processing cost, lower global warming potential, less non-renewable energy use, and less acidification and eutrophication [61]. Secondary recycling is considered downgrading because the final product will have diminished properties that deteriorate with each cycle. Deterioration is due to a build-up of contaminates, water, and impurities, that cause chain-scission reactions along the polymer chains. These scission

reactions lower the mass average molecular weight (M_w) of the polymer and decrease its mechanical properties [25,62]. To combat this, plastics are often mechanically recycled alongside their virgin polymer. For example, the mechanical recycling of poly(ethylene terephthalate) (PET) bottles often has a virgin to recyclate ratio of 7 : 3 [6]. While this partially improves some mechanical properties, overall downgrading still occurs, meaning mechanical recycling alone it is not a long-term solution to the global plastic waste problem [63].

C) Tertiary recycling (chemical recycling) is used to describe chemical processes which depolymerise and degrade plastic waste into monomeric units or directly into other useful materials. Chemical recycling methods are diverse and numerous, and depending on the polymer type each technique will have its advantages and disadvantages. Some of the more common methods are: pyrolysis, alcoholysis, glycolysis, hydrogenation, gasification, and hydrolysis [60,64]. Once the monomer has been obtained it can be used as a feedstock for the production of virgin plastic resulting in a closed loop circular economy [58,63,64]. Chemical recycling has the following advantages over mechanical recycling: the opportunity to produce value-added material, and a truly circular economy as polymers can be chemically recycled for an indefinite amount of cycles [52,63]. Even though chemical recycling techniques have been long established and offer clear advantages over mechanical recycling, widespread utilization has been limited. This is mainly due to high start-up and processing costs relative to cheap petrochemical feedstocks.

D) Quaternary recycling Quaternary recycling refers to the process of energy recovery from the incineration of plastic waste. Plastics are high-yielding energy sources; when they are burned the resulting heat energy is used to generate steam, turn a turbine and generate electricity [59,60,65]. As plastic waste is mechanically recycled *via* primary and secondary techniques its material properties are downgraded with each cycle [62]. Low-grade plastic material is not

suitable for mechanical recycling so the majority of low-grade plastic is discarded in landfills; this is tremendously unstainable and leads to the contamination of ecosystems [58]. Quaternary recycling is beneficial since it helps to reduce the plastic volume in landfills and is obtaining value from waste material. However, during combustion, hazardous substances such as halogenated additives and dioxins can be released into the atmosphere [65,66]. Usage of quaternary recycling has increased because of higher levels of efficiency of new incinerators [65]. Although the incineration of low-grade plastic is better than landfilling it should only be undertaken when other methods of recycling are no longer possible. This type of recycling should only be carried out as a last resort as it completely destroys the polymer, meaning any intrinsic valve imbedded in the polymers' molecular structure is lost. Other recycling methods such as chemical recycling retain the molecular structure, thus making better use of the embedded energy [59,66].

2.4 Bioplastics

A bioplastic is defined as either bio-based, biodegradable, or a combination of both [9,67,68]. A polymer is considered bio-based if its feedstock is a renewable biomass source such as vegetable fats, cellulose, and corn starch. A polymer can be either fully or partially bio-based [69]. Bio-based plastics are more sustainable materials than fossil-based plastics. The plants which provide the biomass feedstocks for biopolymers absorbed CO_2 as they grew, and in this way the net carbon footprint of bioplastic production is reduced [70]. There is an important distinction between first- and second-generation biomass; the first refers to food biomass (e.g. sugar cane) whereas the latter refers to inedible biomass (lignocellulosic material) [71]. Using a second-generation biomass such as forest residues to synthesize bioplastics, would mitigate climate change effects due to smaller carbon footprints than first generation [72,73]. For bioplastics to replace conventional fossil-based plastics several issues need to be addressed.

There needs to be a cost reduction in their production, a need to improve their thermomechanical and barrier properties, improved speed of biodegradability, and a wider availability [67]. As the bioplastic market continues its rapid growth, its total production capacity increases and so its production prices will fall [74]. The key issue then is if the properties of bioplastics can be improved to become competitive with fossil-based plastics. While bioplastics are a solution to fossil-based commodity plastic it is entirely possible to synthesise fossil-based plastics such as PE, PET, and PP, from 100% biomass sources and thus make bioplastics.

To limit the scope of this discussion only bio-PET is discussed. The majority of bio-based PET currently in circulation is only 30% partially bio-based where only one of its monomers, ethylene glycol (EG), is produced from biomass [75]. Technical constraints have limited terephthalic acid (TA) production from fossil fuels [76]. A possible solution is to use abundant lignocellulosic biomass from forest residues to generate bio-based TA [72,77]. Yeast microorganisms can be used to convert lignocellulosic biomass into isobutanol, isobutanol can be further processed into paraxylene a precursor to TA [78,79]. While a variety of biomass sources can be used to generate bio-versions of TA and EG, different sources will have different environmental impacts. Bio-PET bottles with precursor TA obtained from forest residues have a CO_2 emission of 4.14 – 4.92 kg CO_2 equivalent per kg PET bottle. This is 27% lower than bio-PET with precursor TA derived from corn stover, and 21% lower than bio-PET with fossil derived TA [77]. This highlights that synthesis from a renewable resource does not necessarily mean a lower environmental impact than synthesis from fossil fuels [77,80,81].

Bio-PET, bio-PE, and bio-PP, have identical properties to their fossil-based versions but have significantly lower carbon footprints (when the biomass source is second generation). However, sourcing monomers from biomass is typically more expensive than obtaining monomers from

fossil fuels; thus, production of these bioplastics has been limited. If the majority of PET, PE, and PP in circulation was sourced from biomass it would make PLA less attractive as a bioplastic. However, PLA's biggest potential is to replace PS in its applications as a lower carbon footprint material. While bio-based functional styrene monomers and copolymers have been produced, 100% Bio-PS has not yet been synthesised [82,83].

2.4.1 Biodegradation

When a polymer biodegrades it is a combination of abiotic reactions (photodegradation, oxidation, hydrolysis) and enzymatic cleavage of polymer chains into metabolic products (H_2O, CO_2, biomass, etc.) [84,85]. Microbial characteristics affecting the biodegradation rate include: the type of microorganism present, the microorganisms distribution, the growth conditions of the microbes (pH, temperature, moisture content, oxygen, nutrients), and the types of enzymes used by the microbes (intracellular, extracellular) [84,86–88]. Plastic characteristics that affect the biodegradation rate include the surface conditions (hydrophilic, hydrophobic), the first order structure (chemical structure, molecular weight) and the high order structure (Glass transition temperature (T_g), T_m, crystallinity) [87,88].

Biodegradation occurs in two discrete stages. In the first stage polymer chains are degraded and shortened by both abiotic reactions and extracellular enzymatic attack. Enzymes preferentially degrade the less-ordered amorphous regions of a plastic. During biodegradation amorphous regions rapidly decrease, while the proportion of crystalline regions increases and level off near 100% [88]. The second stage occurs when the polymer chains have reached a sufficiently small size, allowing for transportation into the cells of the microorganisms where they can bioassimilate and mineralize [85]. There are several international standards which define the biodegradability of bioplastics, each under specific conditions. The standard EN 13432:2000, for instance, states that for bioplastics to be compostable they must decompose by 90% and

mineralize within 3 months in an industrial composter between 50 – 60 °C [89]. In principle, it is not necessary to collect biodegradable plastics since they can be left to biodegrade in the environment which offers several advantages: increased soil fertility, lower accumulation of plastic in landfills, and a reduction in the cost of waste management [67,86,90]. Depending on the type of bioplastic and the conditions of the compost its rate of degradation may be significantly less than desired. Another disadvantage of biodegradation is that any value imbedded in the polymer's molecular structure is lost.

It should be noted that composting in oxygen is considered aerobic digestion, while anaerobic digestion involves composting in the absence of oxygen and produces biogas. While anaerobic digestion is slower is it considered better for the environment. One study found that anaerobic digestion of PLA cups performs better in the majority of impact categories in comparison to aerobic composting and incineration [91]. While anaerobic digestion has potential for energy recovery it is still more beneficial to recycle postconsumer PLA mechanically, and once low-grade recycle chemically to recapture more material value [63,92,93].

2.5 Poly(lactic acid)

PLA is a polyester thermoplastic that makes up a growing 13.9% of the bioplastic market [9]. It is considered a bioplastic as it is biodegradable and its feedstock is a renewable biomass resource. Depending on its tacticity it can have semi-crystalline or even completely amorphous characteristics. Traditionally PLA has been manufactured through the inexpensive polycondensation of its monomer lactic acid (LA). This condensation reaction only yields low molecular weight (M_w) PLA due to: a viscous polymer melt, the liberation of water, and intramolecular transesterification (*"*backbiting") reactions that form lactide [63,94–97]. The industrially preferred method of synthesis is the catalytic ring-opening polymerisation (ROP) of lactide (cyclic dimer of LA), *via* the coordination-insertion of tin(II) octoate, Figure 2.2

[23,63,94,98]. Other ROP pathways are possible such as anionic, cationic and organocatalytic; however, coordination-insertion has been accepted as the most effective method in terms of high M_w (M_w >100,000 g/mol) and microstructure of PLA [99]. Although the ROP of lactide is unfavourable entropically, the relief of its ring strain acts as the thermodynamic driving force for the reaction [99].

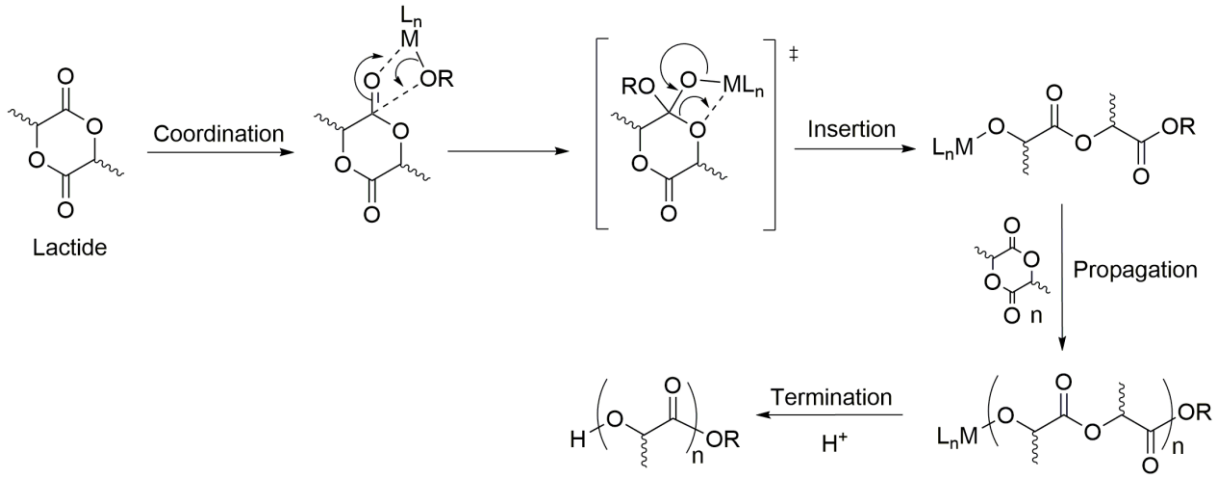

Figure 2.2. Coordination insertion ring opening polymerisation. H^+ represents a proton source.

The mechanical properties of PLA depend on both the M_w and the degree of crystallinity (dictated by its tacticity), Table 2.1 [29,100,101]. A higher M_w will increase the glass transition temperature (T_g) and the melting temperature (T_m) as well as the tensile strength and the elastic modulus. PLA is limited by its inferior barrier properties and its relative brittleness compared to existing fossil-based plastics, Table 2.2 [102]. PLA's brittleness can be improved by blending with tough polymers or *via* plasticization block copolymerisation, which has been shown to increase the strain at break but reduces the material's tensile strength [103].

Table 2.1. Thermomechanical properties of different PLA tacticities vs other and fossil-based plastics.

Properties	**PLA**	**P*L*LA**	**P*DL*LA**	**PET**	**LDPE**	**HDPE**	**PP**
Tensile strength (MPa)	21 - 60	15.5 - 150	27.6 - 50	31.9	10	155	38
Tensile modulus (GPa)	0.35 - 3.5	2.7 - 4.14	1 - 3.45	1.98	0.2	7.5	1.7
Ultimate strain %	2.5 - 6	3 - 10	2 - 10	1.7	620	65	400
T_g (°C)	45 - 60	55 - 65	50 - 60	67 - 80	-30	-	-10
T_m (°C)	150 - 162	170 - 200	*Am*	168 - 182	130	130	176

Am = amorphous thus no melting point.

Table 2.2. Barrier properties of PLA in comparison to other fossil-based plastics at 30°C.

Permeation gas [x10^{-10} cm^3 (STP)· cm cm^{-2} s^{-1} $cmHg^{-1}$]	**PLA**	**LDPE**	**PS**	**PET**
N_2	1.3	1.9	2.2	0.008
CO_2	10.2	28	10.5	0.2
O_2	3.3	6.9	2.6	0.04
CH_4	1	4	2.3	0.004

Despite these limitations PLA is still a promising bioplastic; its main potential could be to replace PS in its applications (6% of the total plastic production) as a more environmentally friendly polymer [1]. Using blowing agents such as CO_2 it is possible to manufacture low-density expanded PLA (EPLA); this material is a sustainable alternative to expanded PS (EPS) [104]. Despite having similar mechanical properties, EPLA has some drawbacks in comparison to EPS. EPLA is limited by its relatively low T_g (50 – 60 °C) in comparison to EPS which has a higher T_g (100 °C). The low T_g results in poor heat resistance so EPLA may deform when used at temperatures in the vicinity of its T_g. This is particularly problematic during storage or transportation where EPLA could be exposed to relatively high temperatures [105]. EPLA's poor heat resistance is improved by increasing the degree of crystallinity; however, EPLA suffers from very slow crystallization kinetics [106]. Finally EPLA is also limited by its low melt strength which causes a smaller expansion ratio; this results in a foam that is less light weight, has a lower cushioning and heat insulating ability [105,106].

2.5.1 Production of Lactic Acid

While it is possible to produce LA directly from chemical synthesise the majority in circulation has been produced *via* microbial fermentation of carbohydrates [95,107,108]. A fermentation broth contains a complex mixture of impurities (nutrients and cell debris) which makes the purification of LA a costly and crucial step [109]. In fact, the complexities associated with fermentation and separating LA from mixtures accounts for 50% of the overall costs for PLA

synthesis [23,109,110]. A further 30% of the overall cost is attributed to lactide synthesis. Typically, industry synthesises lactide *via* a two-step process: first polymerisation of LA to low M_w PLA, followed by thermal degradation and backbiting reactions of low M_w PLA to generate lactide. Depending on the optical properties of the low M_w PLA will determine the yields of *L*-lactide, *D*-lactide and *meso*-lactide [95,110]. Only 20% of the overall cost of PLA synthesis is due to the ROP step; these additional costs make PLA less competitive with fossil-based plastics [23,111]. Instead, these extra costs could be avoided by recovering LA or lactide directly from the chemical recycling of postconsumer PLA. LA has been identified as one of the top 30 building blocks to access a large variety of commodity chemicals shown in Figure 2.3. LA production is projected to increase annually by 5 – 8% [112,113]. The versatility of LA along with growing climate change pressures has caused a significant increase in PLA and PLA depolymerisation research.

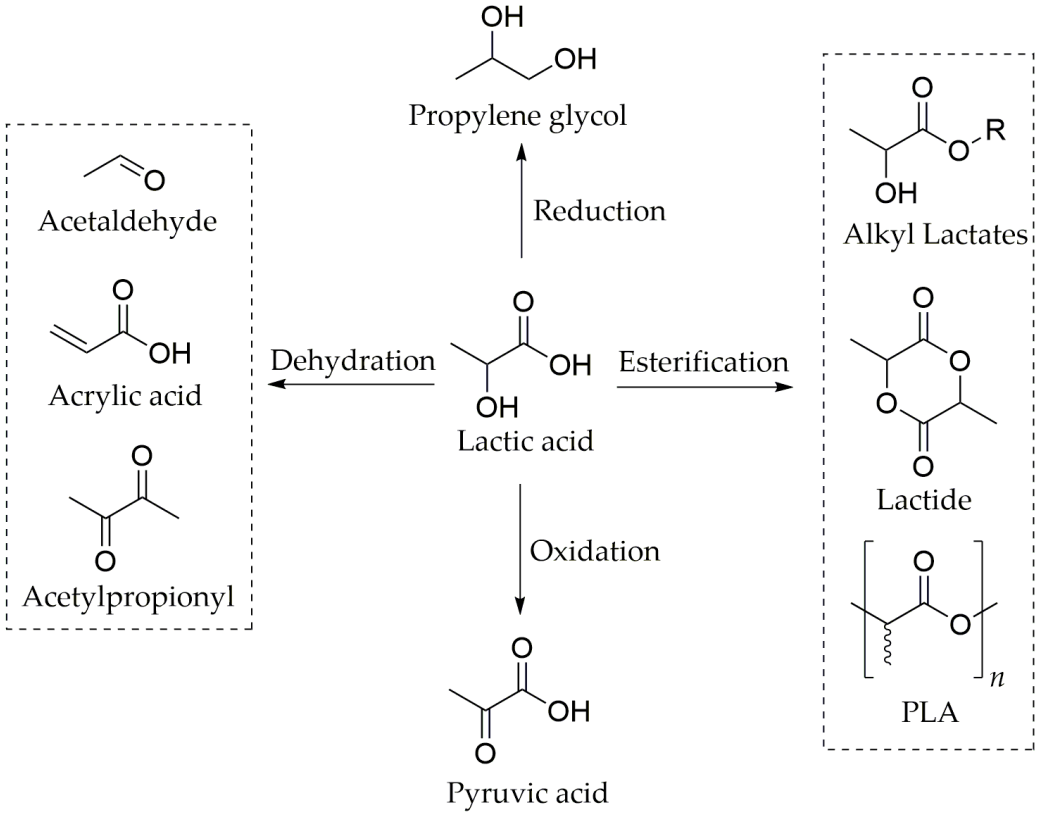

Figure 2.3. The versatility of LA as a platform chemical.

Depending on the bacteria used, fermentation processes are classified as either *homofermentative or heterofermentative*. *Homofermentative* bacteria generate two molecules of LA per molecule of glucose, whereas *heterofermentative* bacteria generate only one molecule of LA per molecule of glucose, as well as EtOH and CO_2. Industrial fermentation typically utilise *homofermentative* bacteria; most often a genus of *Lactobacilli* is used which produces a high yield/rate of lactic acid [95]. Industrial fermentation is carried out in large-scale batch reactors with conditions: pH (5.4 – 6.4), temperature (38 – 42 °C), low oxygen concentration, and a simple carbohydrate such as glucose [108]. Fermentation offers numerous advantages such as: utilisation of second generation biomass, low energy consumption, and the generation of optically pure *D*-lactic acid (*D*-LA), or *L*-lactic acid (*L*-LA) [107,114]. Since a LA molecule has only one chiral carbon there are two optically active forms *D*-LA and *L*-LA, shown in Figure 2.4 [69]. Lactide is the cyclic dimer of LA so contains two stereocenters, it exists in three possible stereoisomeric forms: a pair of enantiomers *L*-LA (*S*,*S*), and *D*-LA (*R*,*R*), or as *meso*-lactide. *Meso*-lactide refers to a lactide molecule with both (*S*) and (*R*) chiral carbons, whereas *rac*-lactide refers to a racemic mixture of the enantiomers *L*-LA and *D*-LA [69,96,108].

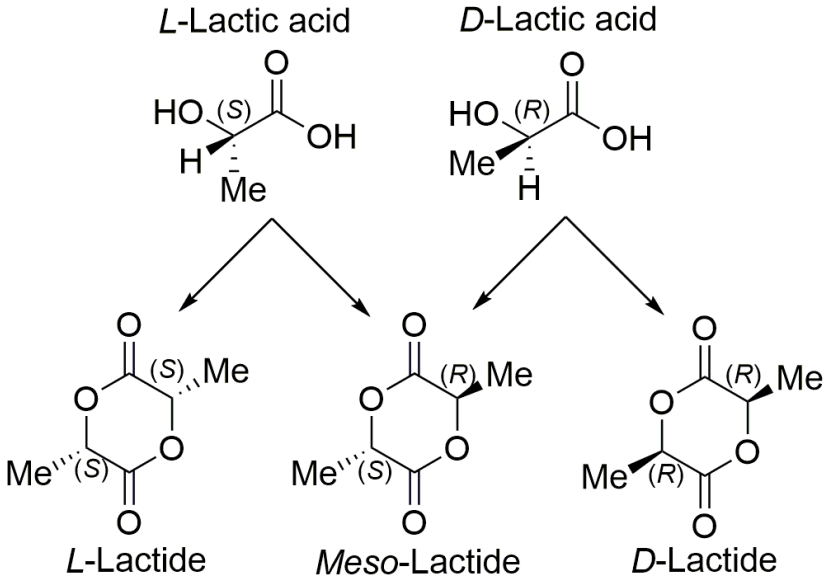

Figure 2.4. Stereoisomeric forms of lactic acid and lactide.

2.5.2 Stereoisomerism

The polymerisation of three lactide stereoisomers and *rac*-lactide leads to 5 possible tacticities for PLA: isotactic, isotactic stereoblock, syndiotactic, heterotactic, and atactic, Figure 2.5 [63,69,96,115,116]. **Isotactic** PLA is semi-crystalline and is synthesized *via* ROP of either enantiopure monomer *L*-lactide or *D*-lactide, to produce P*L*LA and P*D*LA respectively. The stereocenters of the repeat unit either (*S*) or (*R*) are maintained along the whole PLA chain [117].

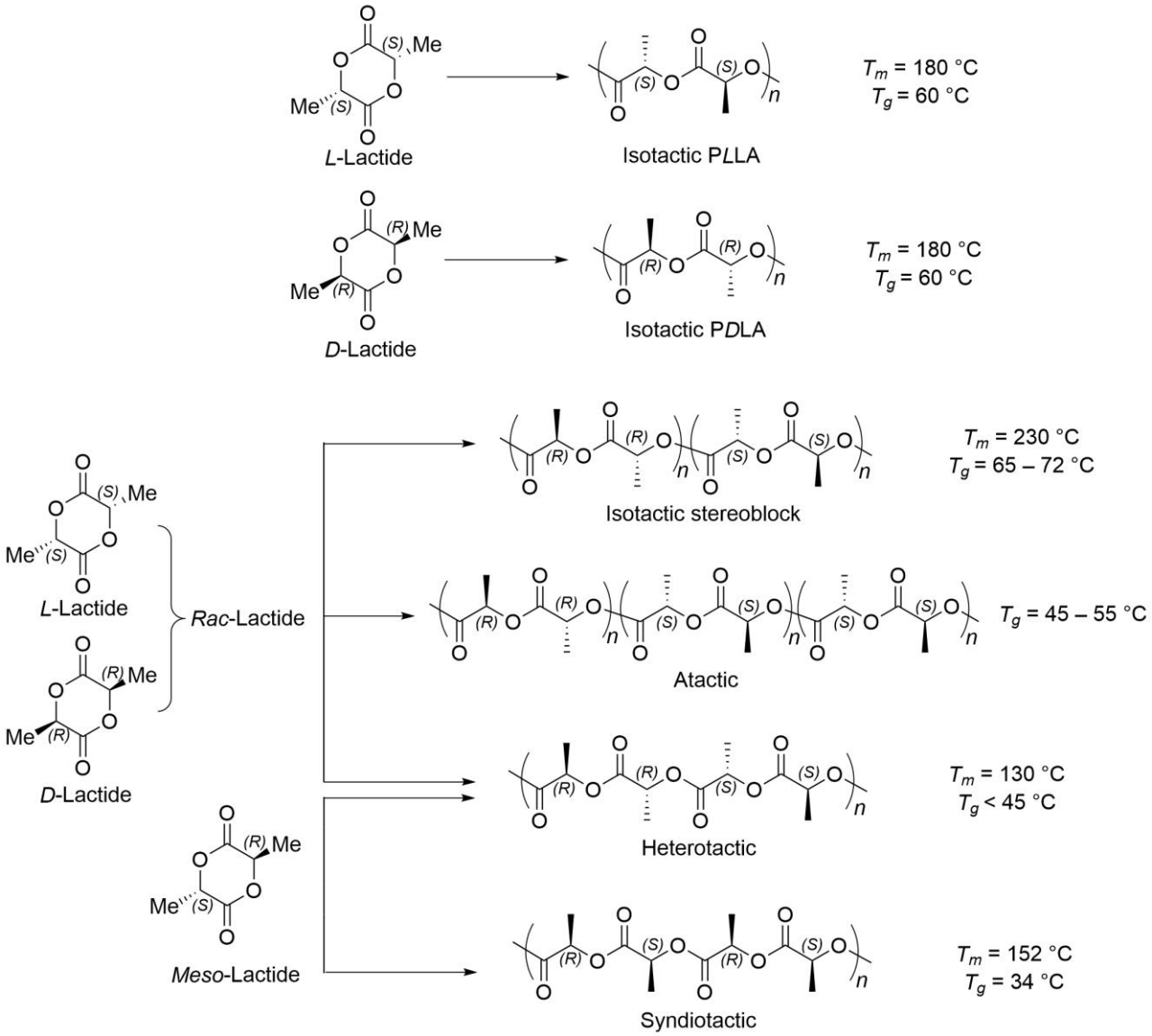

Figure 2.5. Stereochemical configurations of PLA.

This regularity means isotactic PLA chains pack well so exhibit higher crystallinity and have stronger intermolecular forces compared other tacticities. This is reflected in its well defined high melting point (T_m =180 °C) [69,96]. **Isotactic stereoblock** is also semi-crystalline but is synthesized *via* ROP of *rac*-lactide utilizing a racemic catalyst [69,96,118]. **Syndiotactic** PLA is also semi-crystalline and is produced *via* ROP of *meso*-lactide to produce P*DL*LA; the stereocenter of the repeat unit will alternate along the polymer backbone. **Heterotactic** PLA is amorphous and is produced *via* ROP of *meso*-lactide using a racemic catalyst. This tacticity can also be produced *via* ROP of *rac*-lactate where the insertion of *D*- and *L*-lactide alternates, producing linkages of –(*R*)(*R*)(*S*)(*S*)– along the polymer backbone. **Atactic** PLA is also amorphous and its polymer backbone consists of a random arrangement of stereocenters (*S*)/(*R*), impairing any long range order, which explains its undefined melting point and a low glass transition temperature (T_g) [27,63,69,96,117].

2.5.3 Biodegradation

It is important to define the environmental conditions needed to decompose a biodegradable polymer. PLA biodegradation only occurs in a favourable environment of high temperature and humidity when appropriate microbes are present [119,120]. While PLA fully decomposes into CO_2 and H_2O in a large scale composter at 50 – 60 °C in 90 days, its biodegradation in land littering or seawater is less than desired [87,94]. PLA degrading microorganisms occur significantly less in the environment compared to other polyester degraders. The percentage of PLA degrading microbes in soil is only 0 – 0.04%, whereas degrading microbes for another biopolymer poly(3-hydroxybutyrate) (PHB) is between 0.2 – 11.4% [121]. After one year in a marine environment at 30 °C PLA only biodegrades by about 8%, whereas biopolymer poly(3-hydroxybutyrate-co-3-hydroxyvalerate) (PHBV) biodegrades by about 80%, Table 2.3 [122]. PLA composites have been reported to increases PLA biodegradability. In soil, the rate of

weight loss of pure PLA is ≈ 0% annually, whereas starch/PLA composites have a weight loss of 0 – 15% annually, and a starch/poly(hydroxyester-ether)/PLA composites have a weight loss of 4 – 50% /year [123]. The anaerobic biodegradability of PCL, PHB, and PLA was studied in soil at an average temperature of 10 °C , the biodegradability was 90% in 9 days, 29 – 49% in 277 days, and 3 – 22% in 277 days respectively [124].

Table 2.3. Marine biodegradation for PLA, LDPE and PHA after 1 year.

Polymer	**% Biodegradation after 1 year**
PLA	8.41
LDPE	5.63
PHBV	81.81

2.5.4 Mechanical Recycling

Comparing the LCA of different disposal routes, mechanical recycling shows the lowest environment impact, followed by chemical recycling, and composting [125]. Mechanical recycling offers several advantages such as relative simplicity, a low investment, and controlled technological parameters [59,126]. On the other hand, mechanical recycling causes unavoidable downgrading of the polymer material, limiting the number of cycles possible [125]. During the mechanical recycling of a PLA its polymer chains are exposed to thermo-mechanical degradation. The combination of mechanical stresses and high temperatures causes chain scissions reactions that shorten the polymer chains [5]. The service life of the plastic also exposes it to degrading sources such as: oxygen, light, and water. Degradation causes physical and chemical changes to the polymer's molecular structure, increasing structural heterogeneity and changing the thermal, viscoelastic, and mechanical properties of the polymer [5,126,127]. The following mechanistic routes occur during the thermal degradation of PLA: (i) hydrolysis, which forms hydroxyl and carboxyl linear oligomers with a shorter chain length; (ii) esterification; (iii) intramolecular transesterification, 'backbiting' reactions occurring both from

the chain ends and the middle of the chain, forming cyclic oligomers and linear species with shorter lengths; (iv) intermolecular transesterification, where ester units of different polymer chains interchange; (v) chain scission reactions, consisting of acyl-oxygen, alkyl-oxygen, and β-scission homolysis at temperature above melting; (vi) other radical reactions, which produce random chain cleavage forming linear hydroxyl and carboxyl terminated species [126,127]. *Beltrán et al.* simulated the effects of mechanical recycling processes on the structure and properties of PLA [128]. Attenuated total reflectance infrared (FTIR-ATR) spectroscopy and differential scanning calorimetry (DSC) revealed that after one melt reprocess recycled PLA displayed insignificant change in optical, mechanical, and gas barrier properties compared to with virgin PLA [128].

Karasiewicz *et al.* studied the effect of multiple (10 times) extrusion cycles on PLA and its effect on its mechanical properties [129]. After 10 extrusion cycles there was no significant effect on the T_g, the crystallisation temperature decreased with each extrusion cycle, and the T_m only slightly decreased after 10 cycles [129]. The mechanical properties of PLA decreased with each extrusion cycle: after 10 cycles the tensile strength displayed a 5.2% reduction, the ultimate strain at break had a 8.3% reduction, the impact strength had a 20.2% reduction, the permeability of water vapour and oxygen had increased in transmission rate by 39% and 18% respectively [129]. These results highlight the mechanical recycling of PLA up to 10 times causes only a small reduction in mechanical and gas barrier properties. However, the reduction in properties is enough to prevent the utilization of the recycled material from the same application as its virgin counterpart.

One way to counteract the material downgrading that comes with mechanical recycling PLA is to add a chain extender during the extrusion cycle. This helps partially recover the diminished M_n and other mechanical properties, making the recycled PLA more comparable with virgin

PLA [130]. Another way to combat downgrading is to mechanically recycle postconsumer PLA alongside virgin PLA, similarly to PET mechanical recycling that uses a recyclate to virgin ratio of 3:7 [6]. This is useful as it generates a 'recycled' PLA material that still has sufficient mechanical properties to meet the same application as the virgin PLA. A downside to mechanically recycling with virgin polymer is production is still somewhat linear; a truly circular economy is only possible using chemical recycling routes. Taking this all into account the mechanical recycling of postconsumer PLA is a promising recycling route. It has been estimated that in order for postconsumer PLA mechanical recycling to be profitable, there needs to be a global production of at least 200 kt and the recycling facility should be able to process at least 5 – 18 kt annually [131,132]. PLA makes up 13.9% (293 kt) of the bioplastic market (2.11 Mt), so there is enough PLA in global circulation to make its mechanical recycling profitable [9]. Since PLA production is predicted to increase in the future its mechanical recycling becomes even more feasible.

2.5.5 Chemical Recycling Routes

Chemical recycling offers up a unique opportunity for a circular plastic economy, gaining value from waste plastics generating either monomeric units or value-added products. Depending on the polymer type being recycled, each chemical recycling route will have its advantages and disadvantages. Chemical recycling is an excellent option when dealing with the disposal of low-grade plastics that can no longer be mechanically recycled. LCAs have shown the chemical recycling of PLA to have clear environmental benefits when compared to composting or incineration [10,125]. The most common chemical recycling routes for PLA include hydrolysis, pyrolysis, and alcoholysis. A simple search of the terms 'PLA hydrolysis', 'PLA pyrolysis', and 'PLA alcoholysis' on the web of science generated 1866, 218, and 32 results respectively. Likewise, a search for these terms on google scholar generated 127000, 19400, and 1830 results

respectively. As alcoholysis is relatively under researched it is important to cover both hydrolysis and pyrolysis as catalysts and catalytic mechanisms for these two routes could have overlap with alcoholysis. Despite having the least amount of research alcoholysis is a promising depolymerisation route and allows for the generation of value-added product ALs.

2.5.5.1 Hydrolysis

The hydrolysis of PLA is its most researched chemical recycling route. The rate of hydrolytic degradation of PLA depends on several factors such as temperature, pH, molecular weight, and the degree of crystallinity [133,134]. Hydrolysis of PLA arises when water diffuses into the material and cleaves its polymer chains. Ester bonds are cleaved to yield carboxyl and hydroxyl end groups. The carboxyl end groups are capable of catalysing the reaction causing additional cleavage of ester bonds; this effect is called *autocatalysis* [135]. Hydrolysis should be thought of as two components occurring simultaneously: the rate of water diffusion into polymer mass and the rate of hydrolysis. Depending on the rate of diffusion and rate of hydrolysis three different erosion mechanisms are possible: surface erosion (heterogeneous erosion), bulk erosion (homogeneous erosion), and autocatalytic bulk erosion [136]. If water diffusion is slower compared to rate of hydrolysis, degradation and mass loss of the polymer occurs primarily on the surface, which is known as surface erosion. If water diffusion is faster compared to the rate of hydrolysis, degradation and uniform mass loss of the polymer occurs through the bulk, which is known as bulk erosion [137]. However, if the hydrolysis products LA and LA oligomers cannot diffuse out of the polymer mass quickly enough, their carboxyl end groups catalyst the reaction, known as autocatalytic bulk erosion [135,136].

Hydrolysis of PLA occurs preferentially in amorphous regions due to lower resistance, crystalline rises to 99% before hydrolysis ensues in crystalline regions [133]. The hydrolysis mechanism is determined by the acidity of the solution. The use of acids and bases provide

different catalysed mechanisms for the reaction, shown in Figure 2.6. **Acid-catalysed** hydrolysis primarily occurs through chain-end scissions where terminal hydroxyl groups are protonated and then hydrolysed directly to LA; the rate of degradation is independent of chain length [134,138]. **Base-catalysed** and neutral hydrolysis occurs through random chain scissions *via* backbiting reactions that generate lactide; the lactide is subsequently hydrolysed to LA [134,138]. Basic conditions greatly enhance the hydrolysis rate so that degradation occurs *via* surface erosion, while bulk erosion is observed for acidic and neutral conditions [139].

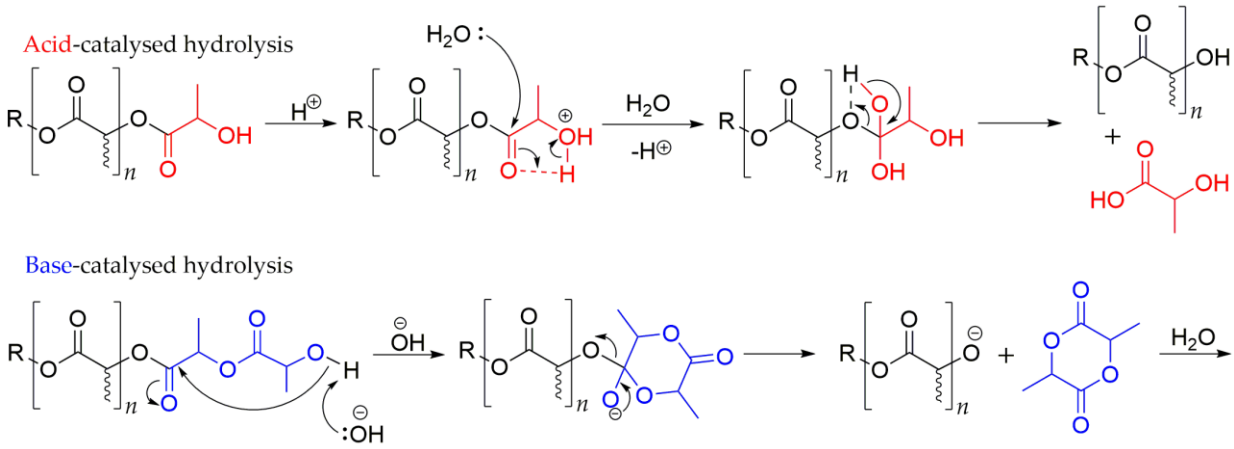

Figure 2.6. Acidic and basic mechanisms for PLA hydrolysis.

One clear example of the potential of chemical recycling is in the recovery of LA through the hydrolysis of PLA. This route of LA production avoids the costs associated with LA purification after glucose fermentation. Furthermore, LA production from the hydrolysis of PLA has a lower carbon footprint. The energy required to generate LA from the fermentation of corn glucose has been estimated as 55 MJ·kg^{-1} of LA produced, versus only 14 MJ·kg^{-1} of LA produced *via* hydrolysis [137]. Tsuji *et al.* studied the hydrolysis of PLLA (M_n 170,000 g·mol^{-1}) in the melt at high temperature and pressure [140]. Hydrolysis at 250 °C produced the best results, achieving a LA yield of 90% in 20 min [140]. Significant racemization of LA occurs at temperatures ≥ 240 °C, while hydrolysis at 350 °C caused decomposition of LA and reduced the maximum LA yield to 30%. In the temperature range 180 – 250 °C the activation

energy (E_a) for P*L*LA in the melt was calculated to be E_a = 51.04 kJ·mol^{-1}. In the temperature range 21 – 45 °C for solid P*L*LA the E_a = 83.68 kJ·mol^{-1}, whereas for P*DL*LA the E_a = 83.26 kJ·mol^{-1} [140]. Tsuji *et al.* again studied the hydrolysis of P*L*LA in solid state vs melt but at a different temperature range. At the temperature range 170 – 250 °C the E_a was evaluated to be 49.6 kJ·mol^{-1} for P*L*LA in the melt, the E_a for the solid phase temperature range 120 – 160 °C was evaluated to be 69.6 kJ·mol^{-1} [141].

Another group studied the kinetics for the PLA hydrolysis using high pressure steam in the temperature range 100 – 130 °C [142]. Degradation proceeded through the auto-catalytic mechanism with the E_a estimated to be 87.2 kJ·mol^{-1} [142]. Piemonte and Gironi studied the kinetics of PLA hydrolysis and proposed a model that accounts for both the autocatalytic mechanism and a two-reaction phase theory [143]. Two activation energies were estimated: the first 53.23 kJ·mol^{-1} is assigned to the two-phase theory and the second 36.85 kJ·mol^{-1} is assigned to the autocatalytic mechanism. A range of PLA concentrations 5 – 50 wt% were hydrolysed. 95% conversion of PLA to MeLa was achieved in 120 min at the temperature range 160 – 180 °C; the reaction rate was not dependent on PLA concentration [143]. Hirao *et al.* carried out the hydrolysis of P*L*LA using conventional heating and microwave irradiation [144]. In both cases the reaction temperature was 170 °C and weight ratio of P*L*LA:H_2O was 3:1 [144]. Using conventional heating, a maximum LA yield of 45% was attained in 800 min, whereas the same yield of LA was reached in only 120 min using microwave irradiation. When the maximum LA yield was reached using conventional heating, the optical purity had decreased to 94% enantiomeric excess (ee), whereas microwave irradiation attained the same yield while maintaining a higher optical purity of 98% ee [144].

Soto-Valdez *et al.* studied H_2O / EtOH mixtures for PLA hydrolysis [145,146]. PLA films were immersed in either pure H_2O, 50% EtOH, or a 95% EtOH solution for 180 days at 40 °C;

changes in molecular weight, LA release, and the sorption of water and EtOH were monitored. Hydrolysis of PLA film and LA production was most accelerated by immersion in 50% EtOH, in comparison to both 95% EtOH and pure H_2O [145]. EtOH acts to swell the polymer which helps facilitate the sorption of water, allowing for hydrolytic degradation. The kinetics were then investigated for a 50% EtOH solution in comparison to pure H_2O. Hydrolysis was carried out in 50% EtOH in the temperature range 40 – 80 °C and the E_a was estimated to be 93.41 kJ·mol^{-1} [146]. in pure H_2O in the temperature range 60 – 90 °C the E_a was estimated to be 101.43 kJ·mol^{-1} [146]. Song *et al.* employed a range of ionic liquids (IL) for the hydrolysis of PLA. After hydrolysis, calcium carbonate was added to precipitate the product [147]. Out of the tested ILs, 1-butyl- 3-methylimidazolium acetate ([Bmim][OAc]) displayed the best results, achieving a PLA conversion of 93.93% and calcium lactate yield of 76.08% in 2 h at 130 °C. Other notable ILs are [HSO_3-pmim][HSO_4], and [Emim][OAc], which achieved PLA conversions of 85.21% and 90.86%, respectively under the same reaction conditions [147]. Hydrolysis using [Bmim][OAc] in the temperature range 120 – 135 °C proceeded *via* first-order kinetics with an estimated E_a of 133.9 kJ·mol^{-1}. The IL was reused 7 times and showed no significant reduction in PLA conversion or yield of calcium lactate.

2.5.5.2 Pyrolysis

The chemical recycling of PLA *via* pyrolysis is less researched than hydrolysis but there is still substantial literature. Pyrolysis is the thermal degradation of a polymer by heating in an inert environment with or without catalysts [60]. The thermal degradation of PLA is a complex process that produces a range of products. Additionally, the E_a for PLA pyrolysis has been reported to vary irregularly as the reaction progresses. Early work on catalyst-free pyrolysis of PLA was carried out by McNeil *et al.* [148]. They reported that PLA broke down in a single stage between 250 – 450 °C, and more than 50% (by weight) of the degradation products were

cyclic oligomers [148]. *L*-lactide was also produced, along with *meso*-lactide and *D*-lactide due to racemization at high temperatures. In another paper they demonstrated that temperature had a significant effect on the product composition [149]. Ethylene and propylene were only observed at high temperatures ≥ 362 °C, while the proportion of acetaldehyde was greatest at 230 °C. From pyrolysis experiments at 240 – 270 °C the E_a was estimated to be 119 kJ·mol^{-1} [149]. Various pyrolysis degradation mechanisms for PLA have been proposed, consisting of: random homolytic chain scissions, unzipping depolymerisation, hydrolysis, oxidative degradation, *cis*-elimination, backbiting, and intermolecular transesterification, as shown in Figure 2.7 [134,149–153].

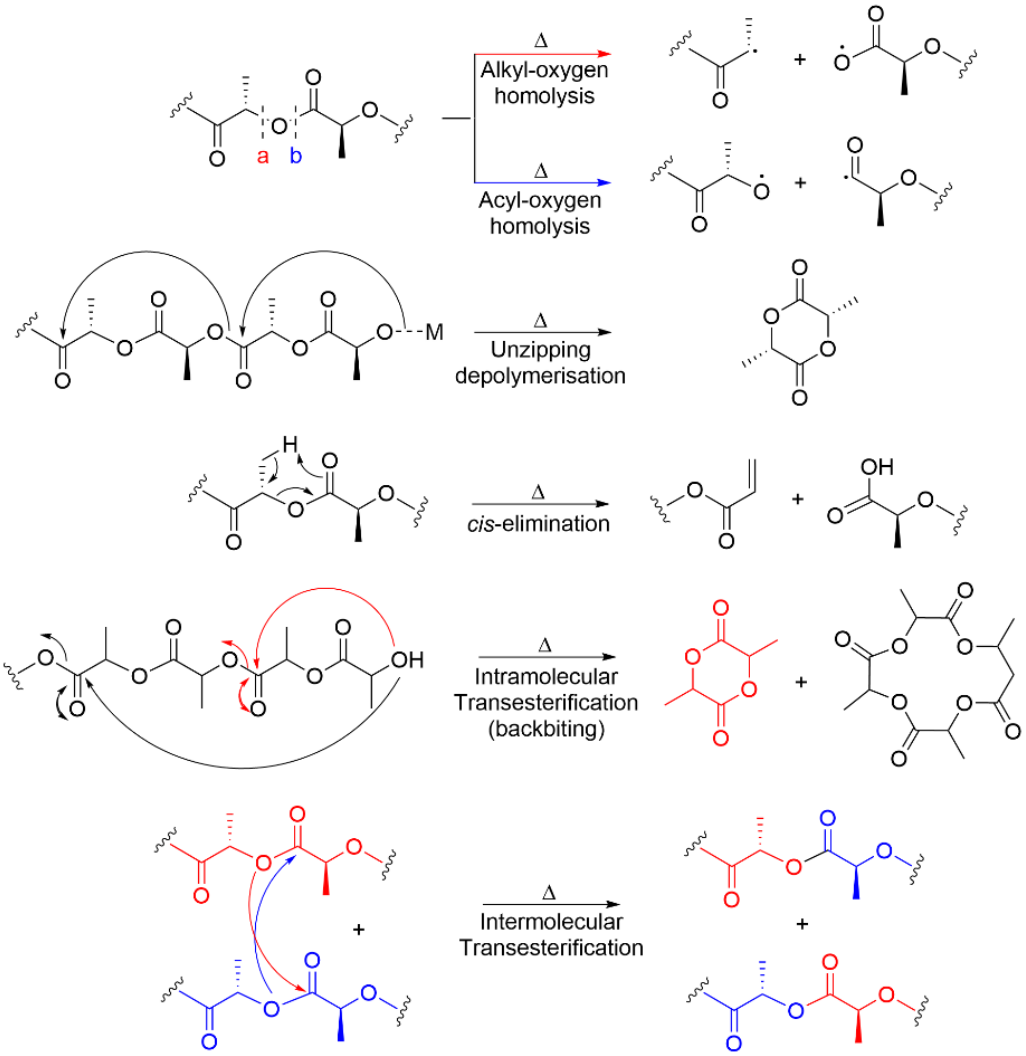

Figure 2.7. Thermal degradation mechanisms. M = metal salt = Sn(II), Mg(II), Zn(II), Fe(III), Al(III).

Backbiting reactions occur at both chain ends forming a range of cyclic oligomers, linear species with shorter lengths, acetaldehyde, and CO [149]. At higher temperatures (≥ 270 °C), radical reactions consisting of alkyl-oxygen homolysis or acyl-oxygen homolysis dominate, generating carbon dioxide and methylketene respectively [149]. The thermal degradation mechanisms for PLA pyrolysis can be controlled to selectively produce *L*-lactide, this is extremely useful as enantiopure *L*-lactide is the precursor for industrial ROP to commercial grade P*L*LA. The factors that influence the thermal degradation mechanism are: molecular weight, moisture, residual monomer, oligomer, and most importantly residual metals [151]. In fact residual metals or the addition of metal salts during pyrolysis can help control product selectivity, as well as decreasing a polymer's thermal stability. Noda *et al.* studied the activity of a series of metals as intramolecular transesterification catalysts for the pyrolysis of P*L*LA oligomer [154]. They reported the activity of each metal was in the following order Sn > Zn > Zr > Ti > Al [154]. Sn complexes are typically utilized as catalysts for commercial ROP of lactide to P*L*LA, so residual Sn content can often be found in the material.

Nishida *et al.* carried out the pyrolysis of P*L*LA in the temperature range 40 – 400 °C, using PLA samples ranging in Sn content from 20 to 607 ppm [155]. The pyrolysis of P*L*LA with Sn content 607 ppm selectively produced *L*-lactide as the degradation product, whereas pyrolysis with Sn content 20 ppm produced cyclic oligomers as the main product. Moreover, the higher Sn content decreased the E_a, from 185 kJ·mol^{-1} to 119 kJ·mol^{-1} [155]. To clarify the pyrolysis mechanism, three P*L*LA samples with different chain end structures and Sn amount were thermally degraded. Pyrolysis was carried out on two P*L*LA samples with Sn content 1006 ppm and 689 ppm; they exhibited a zero-order weight loss with an estimated E_a of 80 – 90 kJ·mol^{-1} and 120 – 130 kJ·mol^{-1} respectively [156]. Both P*L*LA samples selectively produced *L*-lactide, implying repeated backbiting reactions and an unzipping depolymerisation that selectively

produces lactide. Pyrolysis was also carried out on P*L*LA samples with Sn content 23 ppm; these samples exhibited a random weight degradation with an estimated E_a of 176 kJ·mol^{-1}, forming a large amount of diastereoisomers and cyclic oligomers [156]. A further study was carried out using calcium end capped P*L*LA in the temperature range 280 – 370 °C [157]. These samples displayed first order weight loss with an estimated E_a of 98 kJ·mol^{-1}, the dominating reaction mechanism proceeding by unzipping transesterification generating mostly lactides [157]. The effect of calcium oxide (CaO) and magnesium oxide (MgO) on the pyrolysis of PLA was also explored; both metal oxides caused the pyrolysis mechanism to proceed *via* unzipping transesterification and lowered the E_a [158].

2.5.5.3 Alcoholysis

In general, alcoholysis requires milder operating conditions and a thus lower E_a than pyrolysis and hydrolysis. Alcoholysis leads to the formation of value-added ALs. A circular economy can be achieved by first converting AL to lactide, which can then be converted into PLA *via* ROP, shown in Figure 2.8 [159–162].

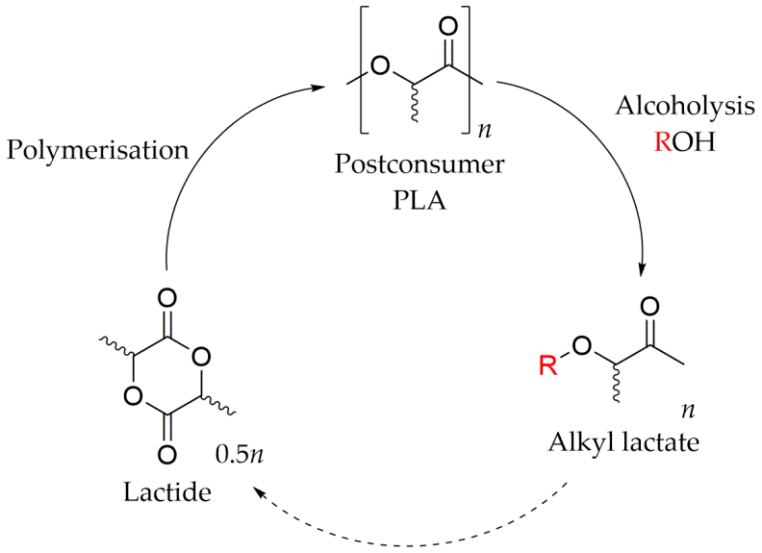

Figure 2.8. General scheme for the circular economy of PLA via alcoholysis of postconsumer PLA.

Arguably alcoholysis is the most beneficial recycling route as it offers several advantages, such as a high yield of industrially valuable AL from waste, simple product purification, and lower environment impacts [10,163]. ALs are versatile green solvents that are biodegradable and have a low toxicity. They have the potential to replace many fossil-based chemicals in applications, such as pharmaceuticals, agriculture, food, coating, cosmetic industries, plasticizers, and solvents [23,164,165]. The specific AL produced depends on the alcohol used: MeOH results in MeLa, EtOH results in EtLa, etc. A transesterification catalyst is also required for sufficient depolymerisation with relatively mild reaction conditions. Alcoholysis adds value to the PLA supply chain; the market price for EtLa is almost double that of PLA [166,167].

One of the earliest reports of PLA alcoholysis was in 1945, in which methanolysis was carried out using H_2SO_4 as the catalyst; high conversions of MeLa were achieved (75 – 80%) at 150 °C within 4 h [168]. The same study also carried out ethanolysis achieving an conversion to EtLa of 57% at 100°C within 4h. A patented process by DuPont in 1993 depolymerised PLA *via* alcoholysis to various ALs (MeLa, EtLa and butyl lactate (BuLa)) using H_2SO_4 as the catalyst; high conversions of ALs were attained (69 - 87%) at 150 – 190 °C within 2 h [169]. Despite both these studies achieving high conversions of AL at a moderate temperature and time, both processes are limited by using H_2SO_4 due to its high corrosivity and toxicity. Literature has since explored many other catalysts for the alcoholysis of PLA: commercial metal salts, ionic liquids, organocatalysts, and discrete metal complexes.

2.5.5.3.1 Catalyst-Free

Catalytic alcoholysis offers advantages such as faster reaction rates and greater product selectivity. However, possible downsides include increased cost, increased toxicity, and more complicated downstream separation. Catalyst-free alcoholysis is a simple alternative that avoids these problems. One study carried out the catalyst-free alcoholysis of PLA using EtOH at 140

– 190 °C, BuOH at 130 – 190 °C, and BuOH at 170 – 210 °C, both with and without microwave assistance [170]. The E_a values for each were estimated to be 112.97, 58.88, and 108.78 kJ·mol^{-1} respectively. The E_a was unchanged if microwave or conventional heating was used. Surprisingly alcoholysis using BuOH at the lower temperature range had the smallest E_a. The paper inferred that around 170 °C the mechanism for BuOH alcoholysis changes. Microwave irradiation was found to increase the reaction rate by increasing the reaction frequency factor, but had no effect on the E_a or racemization of AL [170].

Petrus *et al.* also carried out catalyst-free PLA ethanolysis [171]. The standard procedure involved heating PLA and EtOH in a reactor to 180 – 260 °C for 1 h using EtOH / PLA (per ester unit) ratios ranging from 1 to 10 [171]. In all the experiments conversion of PLA to EtLa increased with increasing temperature. The amount of alcohol was found to significantly influence the reaction kinetics. When the EtOH / PLA ratio was 1:1 after 1 h at 260 °C EtLa conversion reached 50%. At the same conditions but changing the ratio to 2:1, 4:1, and 10:1, the conversions increased to 77%, 96%, and 99% respectively. The paper recommends using an EtOH / PLA ratio of 4:1 at 220 – 260 °C; this way a smaller excess of alcohol must be removed while still gaining the increased reactivity from a higher EtOH / PLA ratio [171].

2.5.5.3.2 Commercial Metal Salts

Metal salts that are active towards transesterification can be used as catalysts for PLA alcoholysis. Their main advantages as catalysts are they are relatively cheap, simple to use, and have a large variety available. A range of studies has been performed using commercially available metal salts for PLA alcoholysis. One study reported $Zn(OAc)_2$ as an effective catalyst for PLA alcoholysis using either MeOH or EtOH at their respective boiling points [172]. Using MeOH attained a MeLa yield of 70% in 15 h at 65 °C, while EtOH attained a EtLa yield of only 21% in 15 h at 78 °C [172]. The authors noted a IR spectroscopy peak at 1600 cm^{-1} which was

identified as a chelate complex of $Zn(lactate)_2$ resulting from $Zn(OAc)_2$ and MeLa. The methanolysis of mixed waste PLA / PET was also carried out; a MeLa yield of 65% was attained in 15 h at 65 °C while the PET remained unreacted and was recovered by filtration [172]. The pre-treatment of PLA / PET waste with a mild alcoholysis method is uniquely useful and is discussed further in section § 2.5.6.

A series of commercially available metal salts ($ZnCl_2$, $AlCl_3$, $FeCl_3$, $Zn(OAc)_2$, $Na(OAc)_2$, NaOH and zinc octoate) was investigated for the methanolysis of PLA [173]. All these catalysts achieved a high PLA conversion and AL yield, but $FeCl_3$ produced the best results. Using $FeCl_3$, solventless methanolysis was carried out at 130 °C and achieved a PLA conversion of 96% and MeLa yield of 87.2% within 4 h [173]. $FeCl_3$ was reused directly as a catalyst without any treatment; PLA conversion and MeLa yield was maintained up to six instances of reuse. The reaction was determined to proceed by a first-order kinetics with an E_a of 32.41 $kJ \cdot mol^{-1}$ [173]. Petrus *et al.* used metal alkoxides synthesized *in situ* for the alcoholysis of P*L*LA [171]. $Mg(OEt)_2$ was prepared *in situ* from $MgBu_2$ and EtOH, using an EtOH / Mg / PLA (per ester unit) ratio of 4 : 0.01 : 1, an EtLa conversion of 95% was achieved at 140 °C in 1 h. Following this procedure a wide range of ALs were generated using a range of alcohols (MeOH, PrOH, BuOH, *sec*-butyl alcohol, isobutyl alcohol, pentanol, isopentyl alcohol and hexanol) and $Mg(Bu)_2$ as a precatalyst. Despite all the alcohols displaying effective PLA alcoholysis; it was concluded that the alcohol reactivity decreases with an increasing number of carbon atoms in the main chain [171]. The activities of a range of catalysts (metal halides, hydroxides, carboxylates, alkoxides, metallic chips and organometallic compounds) for the ethanolysis of P*L*LA at 200°C was also examined. Mg and Ca alkoxides generated *in situ* had the highest catalytic activities attaining a EtLa conversion of 89% and 91% in 1 h respectively. Good

catalytic activates were also observed for $SnCl_2$, $ZnCl_2$, and TBD, reaching EtLa conversions of 86%, 85%, and 81% in 1 h respectively [171].

2.5.5.3.3 Ionic Liquids

Song *et al.* reported the methanolysis of PLA using a range of ILs as catalysts [174]. Out of the investigated ILs only 1-butyl-3-methylimidazolium acetate ([Bmim][OAc]), and [Bmim][HSO_4] exhibited catalytic activity. Using these ILs produced a PLA conversion of 97.2% and 90.2%, and a MeLa yield of 92.5% and 87.9% respectively, at 115 °C using 6 molar equivalents of MeOH in 3h. [Bmim][OAc] was explored further for PLA methanolysis at 90 – 115 °C; the reaction was considered to proceed by first-order kinetics with an E_a of 38.29 $kJ \cdot mol^{-1}$ [174]. Additionally [Bmim][OAc] was recycled 6 times without a reduction in catalytic activity.

More recently Song *et al.* reported methanolysis of PLA using IL [Bmim][OAc] coupled with metal salts $Zn(OAc)_2$, $Cu(OAc)_2$, and $FeCl_3$, at 110 °C using 5 molar equivalents of MeOH [175,176]. Using either 1 mol% 2[Bmim][OAc]-$Zn(OAc)_2$ or 1 mol% 2[Bmim][OAc]-$Cu(OAc)_2$ resulted in PLA conversions of 79.20% and 48.32%, and MeLa yields of 73.35% and 44.22% respectively after 1 h [175]. Using 2 mol% [Bmim][Ac]-$FeCl_3$ resulted in the greatest catalytic activity, reaching a PLA conversion of 92.83% and a MeLa yield of 87.50% within 3 h [176]. Although [Bmim][OAc]-$FeCl_3$ had the greatest conversion and yield it should be noted that it was at a higher catalyst loading and the reaction ran for longer. In all the studied experiments the combination of an IL with a metal salt resulted in an enhanced reactivity when compared to the IL or metal salt alone. The synergistic effect can be explained by the IL solubilising PLA, allowing for easier access to its carbonyls. The Lewis acid metal then coordinates to the carbonyl, increasing its electrophilicity and susceptibility to nucleophilic attack by the alcohol [23,134,175]. 2[Bmim][OAc]-$Zn(OAc)_2$ was explored further for PLA

methanolysis at 90 – 110 °C. The reactions were considered to proceed by pseudo-first order kinetics with a small E_a of 20.96 kJ·mol^{-1} [175]. Likewise [Bmim][OAc]-$FeCl_3$ was tested for PLA methanolysis at 100 – 125 °C; the reactions were determined to proceed by first order kinetics with an E_a of 21.28 kJ·mol^{-1} [176]. Both IL were reused up to 5 times without a significant decrease in catalyst performance. Despite excellent activity and recyclability their industrial use is limited by their high costs and intrinsic viscosity [23,175,176].

DBU-based protic ILs consisting of protonated DBU cations and anions such as acetate, lactate, and propionate, have been studied for the methanolysis of PLA [177]. The best performance was seen with 5 mol% [HDBU][OAc] achieving a PLA conversion of 100% and MeLa yield of 91%, at 100 °C and 5 molar equivalents of MeOH in 5 h [177]. In all the studied experiments the combination [HDBU] with an anion resulted in increased reactivity compared to DBU alone. A range of alcohols were investigated (MeOH, EtOH, PrOH, BuOH, isopropyl alcohol and isobutyl alcohol) the 1-alkanols displayed a better reactivity than iso-alcohols as the increased steric hindrance obstructs nucleophilic attack [177]. The proposed mechanism involves [HDBU] cation coordinating to the PLA carbonyl through hydrogen bonding increasing its electrophilicity making it more susceptible to attack. The [OAc] anion coordinates to the alcohol through hydrogen bonding making the oxygen atom more nucleophilic; the alcohol then attacks the PLA carbonyl through a transesterification reaction [177]. The use of [HDBU] coupled with an imidazole anion for PLA methanolysis showed excellent catalytic activity, achieving 100% PLA conversion and a MeLa yield of 87% at only 70 °C using 5 molar equivalents of MeOH in 1 h [178].

2.5.5.3.4 Organocatalysts

Organocatalysts (DMAP, DBN, DBU and TBD) have successfully been applied to the alcoholysis of PET, as this is another polyester these catalysts could also be applied to PLA

alcoholysis [179]. Both organocatalysts DMAP and TBD can be considered bifunctional hydrogen bonding catalysts; both have previously shown to be effective catalysts for transesterification reactions [179–182]. TBD is an effective catalyst as its bifunctional acid/base character simultaneously coordinates to the nucleophilic alcohol, while also activating the ester carbonyl *via* hydrogen bonding [179]. In a similar way DMAP acts as a bifunctional catalyst. Its base character coordinates to the nucleophilic alcohol bringing it closer for attack, while its proton in the *ortho*-position activates the ester carbonyl making it more prone to nucleophilic attack [182]. Figure 2.9 shows the proposed TBD and DMAP transition states during PLA methanolysis.

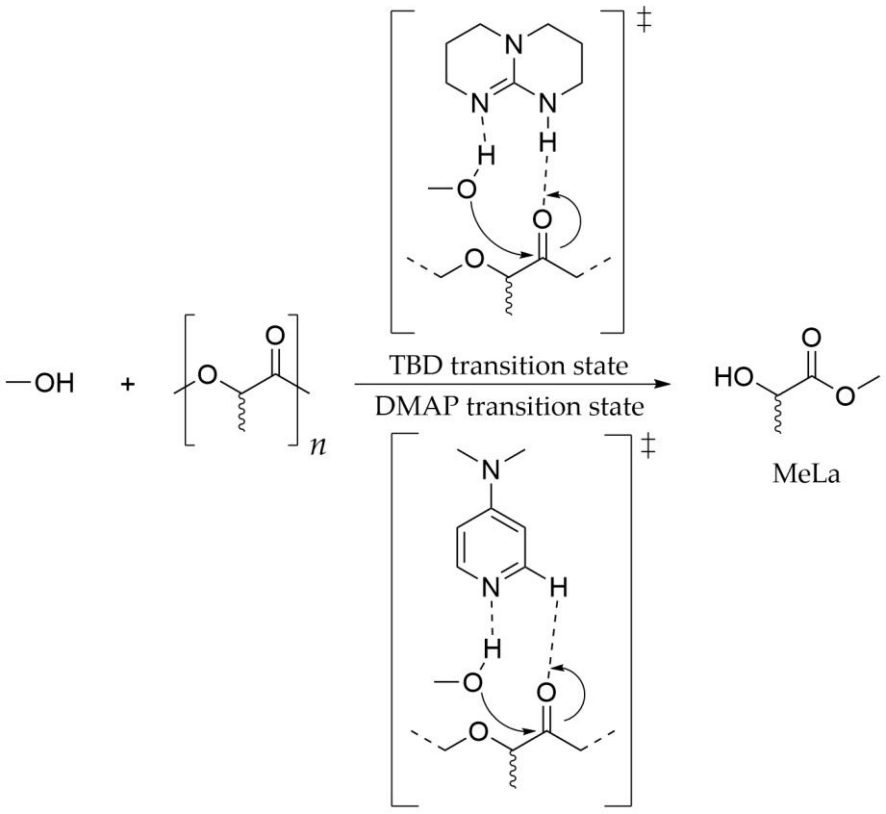

Figure 2.9. Proposed transition state for TBD and DMAP catalysed PLA methanolysis.

Leibfarth *et al.* explored using organocatalyst TBD for alcoholysis of PLA, various alcohols ranging in length from MeOH to BuOH as well as allylic alcohols and branching alcohols were tested [163]. 1 mol% of TBD and 3 equivalents of alcohol provided fast and efficient

depolymerisation at room temperature. The allylic and branching alcohols required longer reaction times to achieve complete depolymerisation. Additionally, the amount of TBD was found to significantly affect alcoholysis rate. Using 1 mol% of TBD and 3 equivalents of EtOH resulted in 100% conversion of PLA in 2 min producing a mixture of EtLa to dimer 1:5 (After 10 min a 90% yield of EtLa was observed). Increasing the TBD amount to 2.5 mol% resulted in 100% conversion of PLA and a 95% yield of EtLa in only 2 min [163]. The transesterification of the EtLa dimer was slower than expected, the authors postulated that the dimer's intramolecular alcohol outcompetes intermolecular alcohols in hydrogen bonding to TBD [163]. Although these are outstanding results at room temperature and resulted in retention of stereochemistry, the amount of PLA in each experiment was only 0.3 g so these results might not reflect larger scale experiments.

Organocatalysts 4-pyrrolidinopyridine (PPY) and DMAP have been used as effective transesterification catalysts for the controlled alcoholysis of PLA [183]. PLA molecular weight (M_n 100,000) and degree of polymerisation (DP) (approximately 1388) was reduced to an average DP of 53, 23, and 55, through alcoholysis using benzyl alcohol, pentaerythritol, and poly(ethylene glycol) respectively at 185 °C in only 30 min [183]. Alberti *et al.* also studied a range of organocatalysts for PLA methanolysis using microwave heating at 180 °C [184]. DMAP, DBU, DABCO, and TBD showed effective transesterification, resulting in MeLa yields of 97%, 99%, 61%, and 99% respectively, at 5 mol% loading using 23 equivalents of MeOH in only 10 min [184]. Decreasing catalyst loading resulted in decreased activity, 2.5 mol% DMAP attained a MeLa yield of 74%, whereas 1 mol% DMAP attained a MeLa yield of only 4% under the same conditions. Increasing the MeOH equivalents to 46 and decreasing the MeOH equivalents to 3 both resulted in reduced activities and reduced MeLa yields of 68% and

11% respectively [184]. Although these are excellent results the amount of PLA in each experiment was only 0.1 g.

2.5.5.3.5 Discrete Metal Complexes

Discrete metal complexes are not commercially available and must be synthesised before they can be utilized for PLA alcoholysis. While this is considered a disadvantage, discrete metal complexes have the potential to be tailored and modified. There is a huge variety of metals and ligands that are active towards transesterification. The ligands themselves can be tailored by adding or removing functional groups. The way the ligands and metals coordinate together can also be tailored to attain complexes with different coordination number and structure (e.g. tetrahedral, octahedral, etc). Whitelaw *et al.* reported the use of group 4 salalen complexes for both the production of PLA and its degradation by methanolysis [185]. Hafnium (IV) salalen complexes were able to depolymerise PLA samples to MeLa with a moderate conversion of 75% after 24 h at room temperature [185]. Little difference was observed between the degradation of either atactic or isotactic PLA. Payne *et al.* reported the use of mono and dimeric Zn(II) complexes for both the production of PLA and its degradation by methanolysis [186]. All the Zn(II)-complexes were able to facilitate PLA methanolysis, however, the mono Zn(2-3)$_2$ complexes outperformed the rest reaching 100% conversion of PLA to MeLa within 8 h at 80 °C [186].

Román-Ramírez *et al.* reported the use of Zn (II) ethylenediamine Schiff-based complexes (Zn(**1**^{Et})$_2$) as effective catalysts for the methanolysis of PLA, Figure 2.10a [187]. Results revealed that the main parameters affecting methanolysis are temperature and catalyst concentration; there was no dependence on the PLA type/molecular weight. Different solvents (THF, 2-MeTHF, acetone) were investigated for methanolysis at 40 °C; THF generated the best results in terms of PLA conversion and MeLa yield [187]. The kinetic model was proposed as

two consecutive first-order reactions; the experimental data was fitted to this model in MATLAB. The first step consists of a PLA ester group undergoing transesterification forming two chain end oligomers, the second step consists of a chain end oligomer being converted to MeLa through a reversible reaction. The activation energies for the first step were determined at different catalyst concentrations, the E_a values were estimated to be 65 , 44, and 39 kJ·mol^{-1} at catalyst concentrations 4, 8, and 16 wt% respectively [187]. The MATLAB script provided by Román-Ramírez was used in Chapter 4 and 6, the script is detailed in appendix §8.1.3 [12,14].

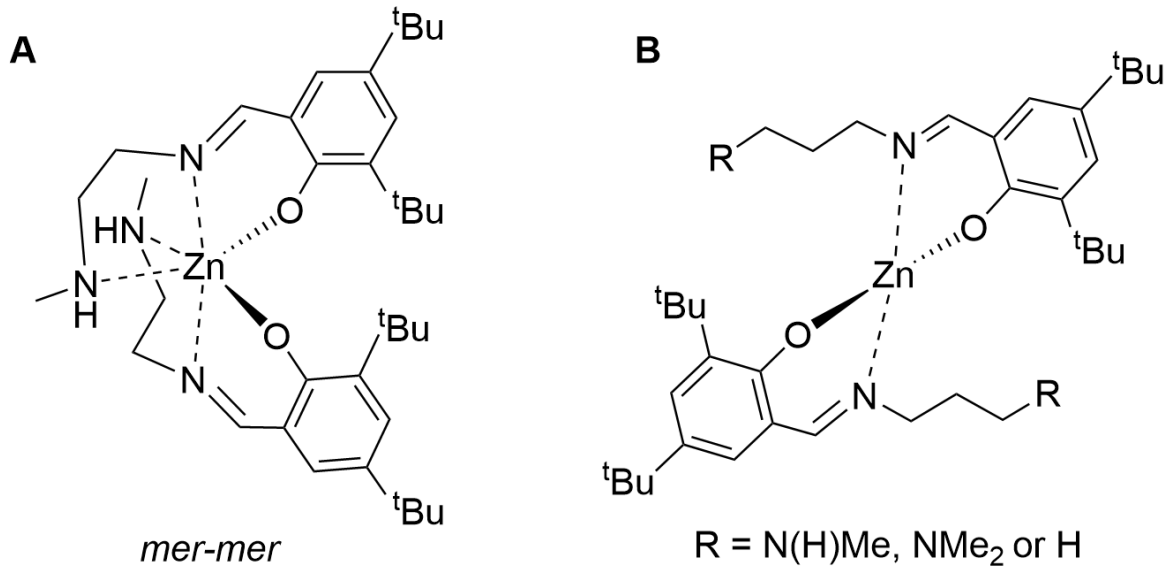

Figure 2.10. Zn(II) complexes for PLA alcoholysis: **A**) Ethylenediamine Zn(II) complex (Zn(**1**^{Et})$_2$, **B**) Propylamine Zn(II) complex (Zn(**2**^{Pr})$_2$).

McKeown *et al.* made a minor variation to the ligand backbone of the octahedral Zn(**1**^{Et})$_2$ complex, increasing the chain length by one carbon and changing the anime R group [188]. This led to the generation of Zn(**2**^{Pr})$_2$ complexes that demonstrated high activity, shown in Figure 2.10b. Using Zn(**2**^{Pr})$_2$ (R = NMe$_2$) a scaled up (12.5 g) PLA methanolysis reaction was carried out achieving a PLA conversion of 97% and a MeLa yield of 77% within 1 h at only 50 °C. The same catalyst was used for ethanolysis and took a longer reaction time to reach similar

PLA conversion and MeLa yield. Zn($\mathbf{2}^{Pr}$)$_2$ (R = NMe_2) was also used for mixed PLA / PET waste methanolysis and found the rate of degradation of PLA was not impaired by the addition of PET [188]. Comparing the different Zn($\mathbf{2}^{Pr}$)$_2$ complexes for methanolysis at 50 °C, R = N(H)Me took 30 min for a PLA conversion of 100% and MeLa yield of 81%, and R = NMe_2 took 1 h for a PLA conversion of 100% and MeLa yield of 84% [188]. While using R = H took 3 h to reach a PLA conversion of 29% and a MeLa yield of only 5%, the reduced activity implies the additional amine group has a significant role in the reaction mechanism. Similar to the bifunctional organcatalysts previously mentioned, the additional nitrogen uses its lone pair to form hydrogen bonds with the nucleophilic alcohol, while the Zn(II) centre simultaneously activates the PLA carbonyl group [188]. As to why R=N(H)Me produces better results than R=NMe_2, NMe_2 has more electron density to form hydrogen bonds but the additional Me group sterically impedes coordination to the alcohol. Both Zn($\mathbf{1}^{Et}$)$_2$ and Zn($\mathbf{2}^{Pr}$)$_2$ R=NMe_2 provided by McKeown *et al.*, were used in Chapter 4; their synthesis is detailed in section §3.3 [12].

Román-Ramírez *et al.* investigated the kinetics of PLA methanolysis using these complexes, Zn($\mathbf{1}^{Et}$)$_2$, Zn($\mathbf{2}^{Pr}$)$_2$ R=NMe_2, and Zn($\mathbf{2}^{Pr}$)$_2$ R = N(H)Me [189]. The experimental data were modelled to a two-step constitutive reaction with a second step in equilibrium. The activation energies for Zn($\mathbf{1}^{Et}$)$_2$ and Zn($\mathbf{2}^{Pr}$)$_2$ R = NMe_2 were calculated to be E_{a1} = 37.89 and −5.7 kJ mol^{-1}, E_{a2} = 39.6 and 10.5 kJ mol^{-1}, E_{a-2} = 37.2 and -17.1 kJ mol^{-1}, respectively [189]. Unlike previous literature the complex Zn($\mathbf{2}^{Pr}$)$_2$ R=NMe_2 was more active towards methanolysis than Zn($\mathbf{2}^{Pr}$)$_2$ R=N(H)Me. At 90 °C after 1 h using R=NMe_2 attained a PLA conversion of 72% and MeLa yield of 21%, whereas under the same conditions R=N(H)Me attained a PLA conversion of 63% and MeLa yield of 16% [188,189]. Interestingly Zn($\mathbf{2}^{Pr}$)$_2$ exhibited unusual behaviour depolymerising PLA at -20 °C producing a curved Arrhenius plot and barrierless E_{a1}.

Despite the achievement of a barrierless E_{a1}, Zn(**2**^{Pr})$_2$ is limited by its susceptibility to oxygen and moisture when in solution.

2.5.6 Issues with PLA Contamination during PET Recycling

Arguably, PET has the most established infrastructure for mechanical recycling; in particular PET bottles are often mechanically recycled for subsequent use. One report estimated that 500 kt of plastics was collected at the kerbside in the UK in 2016, 202 kt of which was PET, 57.9% was bottles (148 kt) and 40.1% (54 kt) was rigid packaging [190]. The mechanical recycling of PET bottles is so well established in part due to: a large enough and constant supply of material, reprocessing techniques such as solid-state post-condensation and the addition of chain extenders to counter the reduction in M_w, and the reprocessing of postconsumer PET to virgin PET ratio of 3:7 [6,132]. The growing production and application of PLA is a controversial issue; specifically, PLA causes major issues if it is present during PET mechanical recycling [131]. PLA content as low as 1000 ppm causes significant hazing and degradation of the recycled PET during melt reprocessing, the yield of recycled PET is greatly diminished and the quality is impaired [131,132]. As PLA and PET are both polyesters with similar densities, they are not separated using conventional sorting techniques such as density floating. Furthermore, the production capacity of PLA is predicted to increase which will result in a larger proportion of PLA in waste circulation, which could have large consequence for PET mechanical recycling.

PLA as a contaminant can easily be addressed using chemical recycling as the solution, shown in Figure 2.11. It is possible to pretreat PET waste with a mild chemical recycling method such as alcoholysis; no PET will be depolymerised, but any PLA will depolymerise to generate AL. Two literature examples show the methanolysis of mixed PLA / PET results in the depolymerisation of PLA while leaving PET unreacted [172,188]. These routes provide a

strategy to selectively recycle PLA from mixed PET waste by converting PLA to a AL and recovering the unreacted PET by filtration [172,188]. Chemical recycling of PLA first not only ensures a purer PET stream for its mechanically recycling, but also makes the whole process more feasible due to the generation of valuable AL which can be sold for an additional profit [191]. It is thus suggested that the methods reported here for PLA alcoholysis could be extended to PLA / PET mixtures in future research.

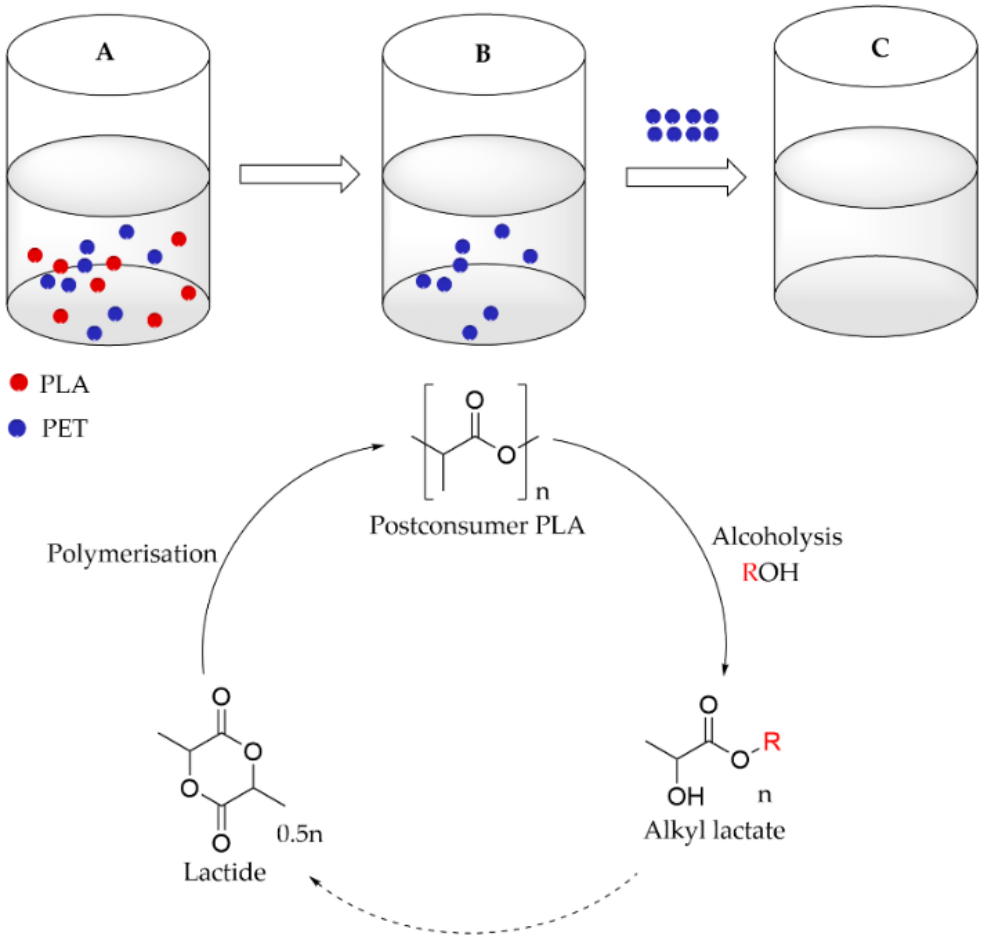

Figure 2.11. Chemical recycling of PLA / PET mixed waste. **A**) Mixed PLA / PET waste placed in a solvent. **B**) Mild alcoholysis conditions depolymerise PLA and leave PET unreacted. **C**) Unreacted PET is then removed for mechanical recycling.

2.5.7 Incineration

Incineration and heat energy recovery is defined as a quaternary recycling method. Since plastics are high-yield energy sources when they are incinerated the resulting heat energy can

be used to generate electricity. Based on current European infrastructure municipal solid waste (MSW) incineration has an assumed average heat efficiency of 22%. Furthermore, only 60% of European incineration plants are equipped with energy recovery units recovering 15% electricity for every GJ of waste incinerated [192]. If the electric production efficiency of a waste incineration plant is assumed to be about 30% then 20 kWh of electric energy will be generated from the incineration of 1000 PLA bottles [193]. From an energy recovery perspective it is more beneficial to incinerate low-grade PLA over composting, generating electricity from waste materials [91,192,193]. However, if the incineration plant is not equipped with an energy recovery unit, then composting waste PLA becomes the better disposal option as it still offers some benefits such as: increased soil fertility, and a reduction in the cost of waste management [67,86,90].

LCAs have shown that other recycling routes for PLA, such as mechanical and chemical recycling perform much better from an environmental perspective compared to incineration [10,194]. While benefits of incineration include a reduction of plastic volume in landfill and easy application to a mixed waste stream, incineration should only be carried out as a last resort when chemical recycling is not possible. This is because the embedded energy of the polymer's molecular structure is lost and harmful chemicals are released into the atmosphere [65,66]. For each tonne of MSW that is incinerated 15 – 40 kg of hazardous waste is produced which requires further treatment [195].

2.5.8 Chemical Recycling Scale up

The majority of the literature for PLA chemical recycling discussed in § 2.5.5 was carried out on a small laboratory scale. In order for these results to be applicable to industry, reaction scale up should be considered. When scaling up a reaction, heat and mass transfer become increasingly important [196]. Large vessels may contain variations in both temperature and

reactant composition; understanding this is critical for reactor design. Moreover, many industrial reactions will contain complex mixtures of products, reactants, intermediates, and side products. This makes downstream processing and product separation equally important when considering a scaled-up reaction. The scope for reactor type and separation is extremely varied so only a few of the more common techniques are discussed here. Additional, only a small amount of literature exists that explores rector and separation design for PLA chemical recycling, so the following discussion is generic.

2.5.8.1 Reactor types

The three classic ideal chemical reactors are batch reactors, plug flow reactors (PFR), and continuous stirred-tank reactors (CSTR). However, there are many other reactor types; each type has unique characteristics, advantages, and disadvantages [197–199]. A reactor type should be carefully selected for each specific application. On a smaller scale, most reactors can be assumed to behave isothermally. It can also be assumed that the system is homogeneous and fluid properties such as density are constant throughout the reaction. While these assumptions will hold true for some industrial reactions, for others it is completely unrealistic [197–199].

The batch reactor – is an unsteady-state system where reactants are charged in the vessel and sealed before initiating the reaction [197,199]. Batch reactors are operated discontinuously, with periods for charging, reaction, and discharging/cleaning. Mixing is typically carried out using a mechanical agitator, while temperature is regulated using external coils or a vessel jacket for heating and using a condenser and refrigerated circulator for cooling. Batch reactors are the most common type of industrial rector and can have volumes exceeding 10000 L. The larger the reactor volume the more likely heat and mass transfer limitations will emerge, resulting in internal variations in temperature and composition [196,198]. Batch reactors are typically utilized for small-volume speciality chemicals, e.g. most pharmaceutical products are

produced in batch processes. While batch systems can match the volume productivity of flow reactors this is only achieved while the reactor is in operation; the cyclical nature of charging and discharging means flow reactors have the greater overall productivity [196–198]. Other disadvantages include: more difficult product separation, greater labour costs, and greater mass transfer limitations [200].

Continuous flow reactors – are usually preferred for long production runs of high-volume chemicals. These reactors are typically utilized in the petrochemical industry; their continuous nature leads to greater productivities and greater economies of scale in comparison to batch reactors. Continuous reactors offer several advantages; improved heat and mass transfer, production cost for the same annual capacity is lower, a uniform quality of product, and easier scale up and control for industrial-scale production [197,200]. Continuous flow reactors come in two types, PFR and CSTR. These reactors different significantly with respect to conversion and selectivity. The reaction rate throughout the CSTR is lower than in a PFR at any point at the same reaction conditions. PFR is substantially better than the CSTR for obtaining higher conversions and product selectivity [197]. Both PFR and CSTR are designed to operate at a steady state while reactants are continuously charged and products removed. Both PFR and CSTR have good potential to be utilized for PLA chemical recycling; their continuous nature leads to better economics [199]. Especially when considered the plastic pollution problem as a whole, the large volumes are such that batch operation is much less feasible than continuous operation. When comparing these two types of reactors, reactions that have low conversion are better performed in a CSTR while high conversion reactions get better results in a PFR [199]. The results later in this chapter show all the alcoholysis reactions to have relatively high conversions, particularly at higher temperatures; it would then be recommend to use a PFR for the scaled up alcoholysis of PLA.

A fixed bed reactor – (FBR) is a vessel filled with catalyst pellets packed in a static bed. Typically these reactors are used with gas-phase reactions but FBR can also be used with liquid phase reactants [201]. The main advantage of a FBR is that the catalyst is heterogeneous, meaning no separation process is required and product purification is simplified [200,201]. By having the catalyst modules immobilized on pellets decreases catalyst deactivation. This in turn reduces production costs and is useful when the catalyst is expensive to manufacture [200–202].

A catalytic membrane reactor – (CMR) incorporates catalysts onto membranes to produce a unit that simultaneously acts as a separator and a reactor. Combining the reaction and separation into a single step can improve yield, reaction selectivity and also decrease downstream separation costs [203]. For equilibrium limited reactions, the membrane selectively removes a reaction product from equilibrium in order to increase the yield compared to conventional membranes [204]. The continuous extraction of products enhances yield by shifting the equilibrium; these reactions include dehydrogenation and esterification [205]. A key area of research for this field is the uniform distribution of nanosized clusters throughout a polymeric matrix. Precise preparation and distribution of the catalytic clusters is crucial for high performance of the membrane in terms of turn over and permselectivity. When used for liquid phase reactions, the catalyst can either be inorganic (metal, zeolites) or metalorganic complexes. The membranes are usually made from polydimethylsiloxane (PDMS) since the polymer offers mechanical, chemical and thermal stability with a high permeability [206].

2.5.8.2 Separation

As previously mentioned, the majority of LA in circulation is generated from fermentation mixtures, and downstream processing and purification of LA accounts for 50% of the overall cost of PLA synthesis [109,110]. Product separation remains a significant challenge in biorefinery reactors, and the growth of the bioplastic industry has led to an increased demand

for separation processes. These separation technologies are already utilized in the biorefinery and petrochemical industrials, and their utilization will be critical for the developing chemical recycling industries. There are several membrane separation processes, which can be defined as concentration driven membrane separation, pressure driven membrane separation, and electrically driven membrane separation.

Concentration driven membrane separation – this form of separation functions on the difference in concentration between the feed and permeate, causing mass transport across the membrane. Two types of concentration driven separation include membrane extraction and pervaporation. Both of these techniques are well established as industrial processes and are used for both the recovery of alcohols from fermentation broths and for alcohol dehydration [207]. Membrane extraction functions on the transfer of low concentrated solutes across a membrane when two immiscible liquids are in contact. Either a flat sheet membrane or a hollow fibre membrane is used. Typically hollow fibre membranes are chosen as they offer advantages such as high membrane area and self-supporting structure [208,209]. Pervaporation functions in the same way as membrane extraction but it has an additional phase change where the feed fluid is partially vaporized at the permeate side of the membrane [210]. Pervaporation systems are typically used for the recovery of liquid alcohols from diluted fermentation broths; these systems have been used as early as 1986 where polymeric silicone rubber membranes were used to recover ethanol, i-propanol, and n-propanol from solutions with alcohol mass fractions of 5 wt% [211].

Pressure driven membrane separation – is used in fermentation processes to recover the product and simultaneously reject microorganisms, recovering valuable side products from spent fermentation broth [207]. Colón *et al.* reported the removal of volatile fatty acids from an anaerobic bioreactor using a 10 kDa tubular ceramic membrane; it was found that permeate flux

linearly increased with increasing pressure [212]. Timmer *et al.* tested several reverse osmosis and nanofiltration membranes for the separation of lactic acid from a fermentation broth [213,214]. A broth containing 4 wt% of lactic acid was fed through the membranes at pressures of 10-40 bar; all the membranes partially rejected lactic acid. NF membranes fared better that RO membranes in terms of lactic acid rejection of about 50% while RO membranes had much higher rejection of about 80%. The permeability of the membranes rapidly dropped within a few hours of operation due to fouling affecting the membrane [213].

Electrically driven membrane separation – or electrodialysis (ED) has applications in multiple processes for biomass conversion and can use a variety of membrane configurations [207]. A large focus of research is for the recovery of valuable organic acids from fermentation broths; one of the most investigated recoveries is for lactic acid since it is already industrially produced on a large scale. By 1986 an electrically driven membrane separation process had already been used to recover lactic acid from a fermentation broth [215]. Wang *et al.* used conventional ED processes to recover lactic acid from a fermentation broth [216]. Interestingly the feed for the broth was not glucose but kitchen garbage, the garbage containing 95% organic components consisting of bread, vegetables and fruits; once fermentation finished ammonia lactate was recovered as lactic acid with a yield of 90% [216].

Distillation separation –is a simpler method than the use of membranes and has been utilized in industry for decades. Distillation is simple and cost effective but can only be used to separate products from systems that have different and clearly defined boiling points [217,218]. A superior distillation method is reactive distillation which shares similarities with the catalytic membrane reactor; a reactive distillation combines product separation with the reaction itself [217,219,220]. There are two further distillation methods: azeotropic distillation (AD) and extractive distillation (ExD) [221]. AD involves adding a third volatile component called an

entrainer, which forms an azeotrope with the two components, changing their relative volatilities and altering their separation factor. Cyclohexane is commonly used as an entrainer for separation of ethanol from an azeotropic mixture with water [221,222]. ExD also involves the addition of a third component, typically a high boiling solvent, which alters the activity coefficients of the distillation mixture, increasing the separation factor [221]. Out of these separation techniques, reactive distillation is best suited for scaled up alcoholysis of PLA; combining the reaction and separation into a single step can improve yield, and reaction selectivity. Moreover the product of alcoholysis AL has a much higher boiling point than the alcohols used for alcoholysis, making distillation possible.

2.5.9 Dual Catalyst Systems

Chemical recycling offers beneficial disposal routes for postconsumer plastic waste, and a wide variety of catalysts can be used for each of these methods. Over the past two decades, the use of dual catalyst systems, consisting of transition metal complexes coupled with organocatalysts or simple acid-base mixtures, has received increasing attention [223–225]. Careful selection of synergistic catalysts can cause unprecedented reactivities, which would not be accessible using either catalyst alone. While this is a relatively new field, synergistic catalysis has always existed in nature as many enzymes function through cooperative mechanisms with two or more catalysts to afford a specific transformation [226]. The enhanced reactivity of synergistic catalysts could be utilized in industrial chemical recycling making the process more economically viable. The concept of dual catalysis generally falls into the categories of cooperative synergistic catalysis or cascade catalysis, and is related to the chemistry of frustrated Lewis pairs [226–229]. Synergistic dual catalysis is defined as both the activation of the nucleophile and the electrophile using two distinct catalysts. The activated species have a higher HOMO (highest occupied molecular orbital) and lower LUMO (lowest unoccupied

molecular orbital) in comparison to the respective ground state starting materials, Figure 2.12 [226]. When considering the reaction between the two activated species the HOMO-LUMO gap is smaller in comparison to only one activated species; a smaller HOMO-LUMO gap means a smaller E_a and thus greater rate constant at the same temperature [226].

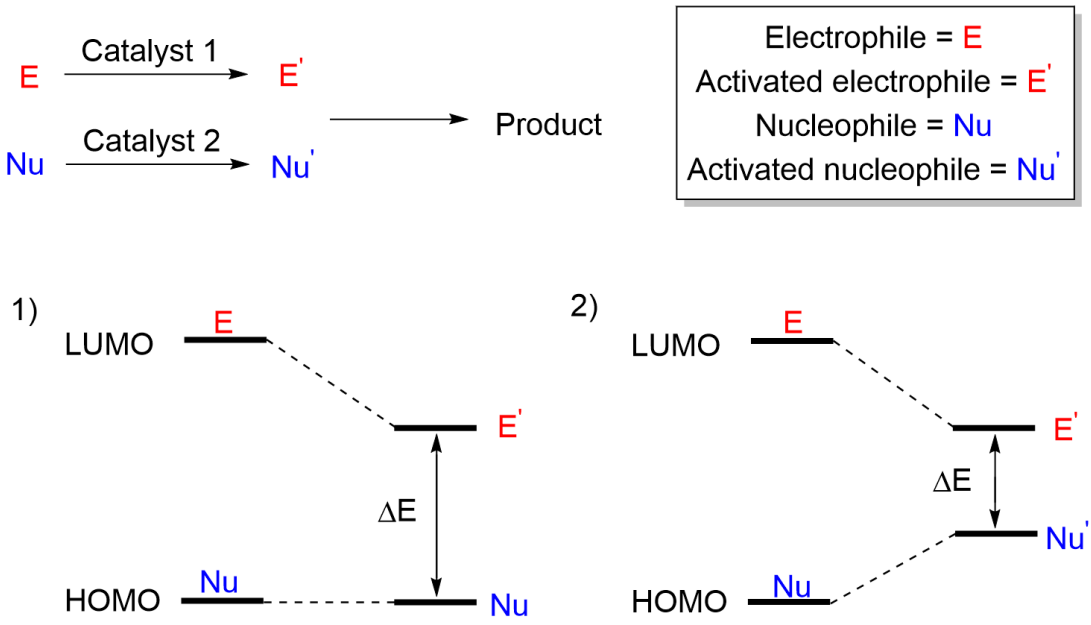

Figure 2.12. The concept of synergistic catalysis. 1) Shows the HOMO/LUMO for traditional catalysis. 2) Shows the HOMO/LUMO for synergistic catalysis.

Romiti *et al.* discussed the four types of synergistic dual catalytic reactions [225]. Type I is for fully cooperative catalysts where each catalyst reacts exclusively with only one substrate. Type II is for partially cooperative catalysts where using either of the catalysts alone would result in the formation of the desired product, but at a significantly slower rate and/or with lower stereoselectivity compared to using both catalysts. Type III is for partially cooperative catalysts but in this case one of the catalysts used alone would result in slow and/or minimally enantioselective reaction, while the other catalyst alone would cause substrate decomposition

and formation of undesirable side products. Type IV is for non-cooperative catalysts that require correct synchronization in order to be useful [225].

One of the earliest dual catalyst systems for polyesters was reported by Del Monte *et al.*, they used acid-base organocatalysts methanesulfonic acid (MSA) and TBD for the enhanced ROP of of ε-caprolactone [230]. In order for an enhancing dual catalyst complex to form there needs to be a great enough difference in pK_a between the two catalysts; a sufficient difference leads to proton transfer and the formation of a stable acid-base complex [231]. One potential problem with synergistic dual catalysis is self-quenching. Careful selection of the two catalysts is necessary to prevent self-quenching; appropriate catalysts will form labile bonds with reversible binding [226]. The strength of the acid-base interaction has a significant effect on the activity and stability of the catalyst complex. If the coordination between the Lewis acid and base is too strong, both catalysts can become inactive. Additionally, redox events could occur which render the catalyst inactive. If the catalysts bind too weakly then the catalyst complex will be too unstable so no activity enhancement is observed [226,232]. Recent literature has reported the use of synergistic dual catalysis for polyester recycling and found it outperformed single catalysis [231–234]. These Lewis acid-base pairs were prepared by simple physical interactions, allowing for dual catalyst systems to be a scalable process relevant for industry [231]. Dove *et al.* reported a synergistic effect for $Zn(OAc)_2$ coupled with DMAP resulting in an increased PET depolymerisation rate [232]. These catalysts were provided by Dove and used in the work reported in Chapter 5 and 6 [13,14].

2.5.10 Market Size of PLA, AL, LA, and *L*-lactide

The three most common chemical recycling methods for PLA are pyrolysis, hydrolysis, and alcoholysis, which produce lactide, LA, and AL respectively. It is important to know the market size for each of these products and of PLA. Data for market sizes is provided from market

research groups instead of traditional literature. Even so, there are gaps in the data and conflicting estimates of different market values. One group reported the global market values of PLA and LA will reach $2.31 billion and $2.43 billion by 2028, with compound growth rates (CAGR) of 16.3% and 9.6% [235,236]. Another group predicted market values for PLA an LA to reach $1.98 billion and $2.7 billion by 2028, with CAGR of 18.1% and 8% [237,238]. Another group predicted the market size for PLA, LA, and *L*-lactide to reach $1.7 billion, $4 .9 billion, and $2.4 billion respectively by 2027 [239–241]. Representing CAGR of 13.86%, 8.92%, and 12.6%. This group also predicted the global market for AL to reach $109 million by 2028 with a CAGR of 2.3% [242]. With EtLa making up the largest proportion of the AL market estimated at $92 million by 2024 [243]. Summarising the data, LA has the greatest market value followed by PLA, *L*-lactide, and AL; PLA has the greatest market growth, followed by, *L*-lactide, LA, and LA.

2.5.11 Optimal Chemical Recycling Route

Determining which chemical recycling route is optimal on an industrial scale depends on many factors. Some of the key factors that should be considered are: the LCA for each route, the reaction rate, the reagents and catalysts, the product yield and selectivity, the E_a of reaction, the operating conditions (heat, pressure, and stirring), as well as the reactor type/size. The level of research of each method should also be considered when deciding which chemical recycling route to utilize in industry. Alcoholysis being the least researched depolymerisation route means there is a large potential for investigation. Three chemical recycling routes are compared in Table 2.4. Hydrolysis has clear advantages: its product LA has a significantly greater market size than lactide or AL, its reaction has a relatively low E_a 49.6 kJ·mol^{-1} at moderate temperatures 170 – 250 °C, and high conversions of PLA can be achieved without catalysts. Pyrolysis could be considered the best route for a direct circular economy. Its product, lactide,

is the precursor for ROP to generate virgin PLA. Pyrolysis avoids the environmental and economic costs of first having to convert AL or LA to lactide. Although high conversions of PLA can also be achieved without catalysts this reaction requires high temperatures ≥ 270 °C and has the greatest E_a 119 kJ·mol^{-1}. The presence of Sn (1006 ppm) or calcium (121 ppm) lowers the E_a to 80 – 90 kJ·mol^{-1} and 98 kJ·mol^{-1} respectively. However, it is still greater than the E_a for hydrolysis or alcoholysis routes. Alcoholysis is favoured by having the smallest E_a 39 kJ·mol^{-1} at mild reaction temperatures 40 – 130 °C while attaining high conversions of PLA. Arguably this makes alcoholysis the best disposal route for the postconsumer PLA from an environmental perspective. LCAs have reported alcoholysis of PLA to have the most environment benefits across impact categories such as global warming, acidification, eutrophication, resource use, and photochemical ozone formation [10]. Hydrolysis of PLA shows the highest benefit concerning land use and water scarcity [10]. The lowest PLA depolymerisation E_a values are all alcoholysis routes; the lowest E_a being -5.7 kJ·mol^{-1} was accomplished *via* methanolysis using Zn(**2**^{Pr})$_2$ [189]. Like other discrete metal complexes, a downside is this catalyst must first be synthesised and is not commercially available. Additionally Zn(**2**^{Pr})$_2$ is also limited by its sensitivity as it easily becomes deactivated. The next lowest E_a (20.96 kJ·mol^{-1}) belongs to the ionic liquid 2[Bmim][OAc]:Zn(OAc)$_2$ [175]. The synergistic effect of the IL combined with the Zn(OAc)$_2$ salt explains why [Bmim][OAc] alone has a greater E_a (38.29 kJ·mol^{-1}) [174]. Despite IL exhibiting superior activity its scalability remains limited by their high cost and intrinsic viscosity [23]. Interestingly, when [Bmim][OAc] was used for methanolysis at only 2 wt% and 90 – 115 °C the E_a (38.29 kJ·mol^{-1}) was significantly lower than the E_a for hydrolysis (133.9 kJ·mol^{-1}); despite the hydrolysis reaction using 50 wt% of [Bmim][OAc] and a higher temperature of 120 – 135 °C

[147,175]. This result implied that catalysts that are effective for PLA hydrolysis might be even more active towards PLA alcoholysis.

Table 2.4. The activation energies (E_a) of different chemical recycling routes for PLA.

Degradation route	Catalyst	E_a (kJ·mol^{-1})	Temperature (°C)	Ref.
Hydrolysis	-	83.68	21 – 45	[140]
Hydrolysis (P*L*LA in melt)	-	49.6	170 – 250	[141]
Hydrolysis (P*L*LA in solid)	-	69.6	120 – 160	[141]
Hydrolysis	-	53.23 ± 6.81	140 – 180	[143]
Hydrolysis	-	51.04	180 – 250	[140]
Hydrolysis	-	101.4	40 – 80	[146]
Hydrolysis	EtOH, 50% by volume	93.41	60 – 90	[146]
Hydrolysis	[Bmim][OAc], 50 wt%	133.9	120 – 135	[147]
Pyrolysis	-	119	240 – 270	[149]
Pyrolysis	Sn 1006 ppm	80 – 90	40 – 400	[156]
Pyrolysis	Sn 689 ppm	120 – 130	40 – 400	[156]
Pyrolysis	Sn 23 ppm	176	40 – 400	[156]
Pyrolysis	Ca 121 ppm	98	280 – 370	[157]
Methanolysis	$FeCl_3$, 1 wt%	32.41	110 – 135	[173]
Methanolysis	[Bmim][OAc], 2 wt%	38.29	90 – 115	[174]
Methanolysis	2[Bmim][OAc]-$Zn(OAc)_2$, 1 wt%	20.96	90 – 110	[175]
Methanolysis	2[Bmim][OAc]-$FeCl_2$, 0.25 wt%	21.28	100 – 125	[176]
Methanolysis	$Zn(\mathbf{1}^{Et})_2$, 4 – 16 wt%	39 – 65	40 – 130	[187]
Methanolysis	$Zn(\mathbf{2}^{Pr})_2$, 4 wt%	−5.7	50 – 70	[189]
Ethanolysis	-	112.97	140 – 190	[170]
Butanolysis	-	58.88	130 – 190	[170]
Butanolysis	-	108.78	170 – 210	[170]

Bmim = 1-butyl-3-methylimidazolium, Et = Ethylenediamine, Pr = Propylamine

Considering that alcoholysis routes are the least researched but already have the lowest E_a means there is enormous potential for their development. Discovery of different catalytic mechanisms could lead to an even smaller E_a for PLA alcoholysis. As E_a decreases further the overall process of alcoholysis recycling becomes more economically feasible and environmentally friendly, meaning that less energy is required to generate products from waste material.

2.6 Conclusions and Rationale for Current Studies

Some of the following conclusions can be made from the above discussion:

- Current levels of plastic pollution are unsustainable, so that the transition from a linear single use plastic economy to a circular economy is critical. A circular approach offers both a financial incentive and climate change mitigation.
- Bioplastics and in particular bio-based plastics, represent an emerging market of polymers capable of replacing fossil-based plastics as more environmentally friendly materials.
- PLA is a leading bioplastic with mechanical and barrier properties competitive with PS, and its market size (13.9% of the bioplastic market) is projected to increase in the future. The limitations of PLA in comparison to fossil-based plastics are: its inferior barrier properties, its relative brittleness, and its relatively expensive synthesis. In addition, PLA causes a large disruption during the mechanical recycling of PET.
- Chemical recycling routes such as pyrolysis, hydrolysis, and alcoholysis, serve as ideal recycling routes for low-grade postconsumer PLA that can no longer be mechanically recycled. Each of these routes offers pros and cons: pyrolysis allows for the most direct circular economy but requires the greatest E_a, hydrolysis generates LA which has the largest market size but requires a moderate E_a, alcoholysis has the lowest impact LCA and requires the smallest E_a but its product AL has the smallest market value.

- Both hydrolysis and alcoholysis directly make PLA a more competitive material. Hydrolysis avoids the expensive costs associated with LA generation from fermentation, making the overall cost of PLA much cheaper. Alcoholysis can easily be applied to mixed PLA / PET waste to selectively depolymerise PLA to AL; unreacted PET is then suitable for mechanical recycling.
- A large variety of catalysts and alcohols can be applied to PLA alcoholysis to generate a range of ALs. The use of synergistic dual catalysts is a developing field; early literature shows promising results applying synergistic catalysts to the alcoholysis of polyesters.

Based on the literature review provided, the transition from a linear plastic economy to a circular economy is paramount to combat plastic pollution and climate change. The bioplastics market is emerging as a replacement to fossil-based plastics to decrease usage of fossil fuels. PLA is a crucial biopolymer with an EOL that is particularly important because of the issues related to PET mechanical recycling. The work in this thesis deals with the alcoholysis of PLA using a semi batch reactor. The first part of this work examines the use of discrete metal complexes Zn(**1**^{Et})$_2$ and Zn(**2**^{Pr})$_2$ (R = NMe_2), testing the effect of increasing alcohol chain length. The second part of this work focuses on the synergistic interaction of $Zn(OAc)_2$ and DMAP investigating the effect of different ratios of the two catalysts. This is expanded in the third part of this work; where mixtures of four catalysts $Zn(OAc)_2$, $Mg(OAc)_2$, DMAP, and TBD, are explored to find any synergetic relationships, in addition to testing the effect of MeOH equivalents on the methanolysis rate. Detailed kinetics were estimated for each experimental section of this thesis. The reaction kinetics aid in understanding the depolymerisation mechanism for PLA alcoholysis.

Chapter 3 – Experimental Setup and Analytical Methods

3.1 Chapter Overview

This chapter describes the experimental procedures and methods that were used in this thesis, broken down into the following sections: i) materials and equipment, ii) zinc complex synthesis and characterisation, iii) the apparatus and procedures used in each publication, and iv) the methodologies and techniques for sample analysis. Section §3.2 provides a full list of the commercial materials and a brief specification of the instruments used in this project. This is followed by Section §3.3 which details the synthesis of Zn(**1**^{Et})$_2$ and Zn(**2**^{Pr})$_2$ complexes. This was part of an ESPRC project collaboration with the University of Bath. McKeown *et al.* synthesised the Zn(**1**^{Et})$_2$ and Zn(**2**^{Pr})$_2$ complexes and they were tested for PLA alcoholysis at the University of Birmingham. The setup of a Parr batch autoclave is then described in detail in Section §3.4, also specifying the operating procedure, reagent charging and sampling method. The analytical methods used during this study include gas chromatography (GC) and proton nuclear magnetic resonance (^{1}H NMR) spectroscopy, described in Section §3.5.1 and §3.5.2 respectively. Both techniques were used to identify and quantify the reaction products from PLA alcoholysis. GC was primarily used as quick and convenient screening to monitor reaction progress, whereas ^{1}H NMR provided more detail regarding the relative concentrations of PLA, oligomers, and AL. These data were used to carry out a model fitting procedure in MATLAB to calculate the reaction kinetics. The MATLAB script used during this project was provided by Román-Ramírez from the School of Chemical Engineering University of Birmingham and is detailed in detailed in Appendix §8.1.3.

3.2 Materials and Equipment

A full list of commercial chemicals and materials used in this study is provided in Table 3.1. A full list of the instruments used during the project for is provided in Table 3.2.

Table 3.1. Commercial chemicals and materials used in this study.

Material	Supplier	Specification
For Alcoholysis Reactions		
Methanol	Fisher Scientific, Loughborough UK	99.8% (Methanolysis reactant)
Methyl (*S*)-lactate	Fisher Scientific, Loughborough UK	97% (GC analytical standard)
Ethanol	Fisher Scientific, Loughborough UK	99.8% (Ethanolysis reactant)
Ethyl (*S*)-lactate	Fisher Scientific, Loughborough UK	97% (GC analytical standard)
Propan-1-ol	Fisher Scientific, Loughborough UK	99% (Propanolysis reactant)
Butan-1-ol	Fisher Scientific, Loughborough UK	99% (Butanolysis reactant)
Butyl (*S*)-lactate	Sigma-Aldrich, Gillingham UK	97% (GC analytical standard)
Tetrahydrofuran	Fisher Scientific, Loughborough UK	99.8% (Alcoholysis solvent)
Zinc acetate dihydrate	Sigma-Aldrich, Gillingham UK	99.9% (Alcoholysis catalyst)
Magnesium acetate tetrahydrate	Sigma-Aldrich, Gillingham UK	99.9% (Alcoholysis catalyst)
Triazabicyclodecene	Sigma-Aldrich, Gillingham UK	98% (Alcoholysis catalyst)
4-(dimethylamino)pyridine	Sigma-Aldrich, Gillingham UK	99.9% (Alcoholysis catalyst)
Gas		
Compressed air zero grade	BOC, UK	99.9%
Hydrogen	BOC, UK	99.9%
Nitrogen	BOC, UK	99.9%
Helium	BOC, UK	99.9%)
*For Zn(**1**^{Et})$_2$ and Zn(**2**^{Pr})$_2$ Synthesis*		
3,5-Di-*tert*-butyl-2-hydroxybenzaldehyde	Sigma-Aldrich, Gillingham UK	99% (Zn (II) complex synthesis)
N-Methylethylenediamine	Sigma-Aldrich, Gillingham UK	95% (Zn (II) complex synthesis)
3-(Dimethylamino)-1-propylamine	Sigma-Aldrich, Gillingham UK	99% (Zn (II) complex synthesis)
Hexane	Sigma-Aldrich, Gillingham UK	95% (Zn (II) complex synthesis)
Diethylzinc	Sigma-Aldrich, Gillingham UK	≥52 wt% Zn basis (Zn (II) complex synthesis)

Table 3.2. Instruments involved in this study

Instrument	Manufacturer	Note
A&D analytical balance	A&D Instruments Ltd.	Series: HR-200
Agilent 6890N Network Gas Chromatography	Agilent Technologies Inc	Flame Ionisation Detector (FID), column: Agilent HP-5
Oil Bath heating circulator IKA CBC 5 Control	IKA England Ltd.	-
CORIO CP-600F refrigerated / heating circulator	Julabo UK Ltd.	-
400 MHz Bruker Avance II spectrometer	Bruker Inc	-
HPLC PUMP	-	-

3.3 Discrete Zn(**1**^{Et})$_2$ and Zn(**2**^{Pr})$_2$ synthesis

Synthesis of these complexes was carried out and provided by Prof. Matthew Jones and Dr. Paul Mckeown from the School of Chemistry, University of Bath. For Zn(**1**^{Et})$_2$ **synthesis**, the required ligand was made directly prior to complexation with Zn(II). The ligand was first prepared in a Schlenk tube *via* a simple condensation reaction. 3,5-Di-*tert*-butyl-2-hydroxybenzaldehyde (2 mmol) dissolved in methanol (3 mL) and *N*-Methylethylenediamine (2mmol) was added dropwise. After complete addition the solution was left at 25 °C for 16 h, after which the solvent was removed *in vacuo*. The solid ligand was added to toluene (10 mL) along with diethylzinc (1 mmol) and stirred for an hour before solvent removal. The desired complex was purified by *via* washing or recrystallisation from hexane. For Zn(**2**^{Pr})$_2$ **synthesis**, the required ligand was made directly prior to complexation with Zn(II). The ligand was first prepared in a Schlenk flask *via* a simple condensation reaction. 3,5-di-*tert*-butyl-2-hydroxybenzaldehyde (2 mmol) was dissolved in methanol (5 mL), and 3-(dimethylamino)-1-propylamine (2 mmol) was added dropwise. After complete addition the solution was stirred for 3 h, after which the solvent was removed *in vacuo* and the product dried at 40 °C under a dynamic vacuum. The solid ligand was added to hexane (10 mL) along with diethylzinc (1

mmol) added dropwise and stirred for 3 hour before the complex was purified and isolated. Both Zn($\mathbf{1}^{Et}$)$_2$ and Zn($\mathbf{2}^{Pr}$)$_2$ complexes were stable in ambient conditions.

3.4 Parr Reactor for Alcoholysis Reactions

Figure 3.1 shows a schematic diagram of the Parr reactor used in this study.

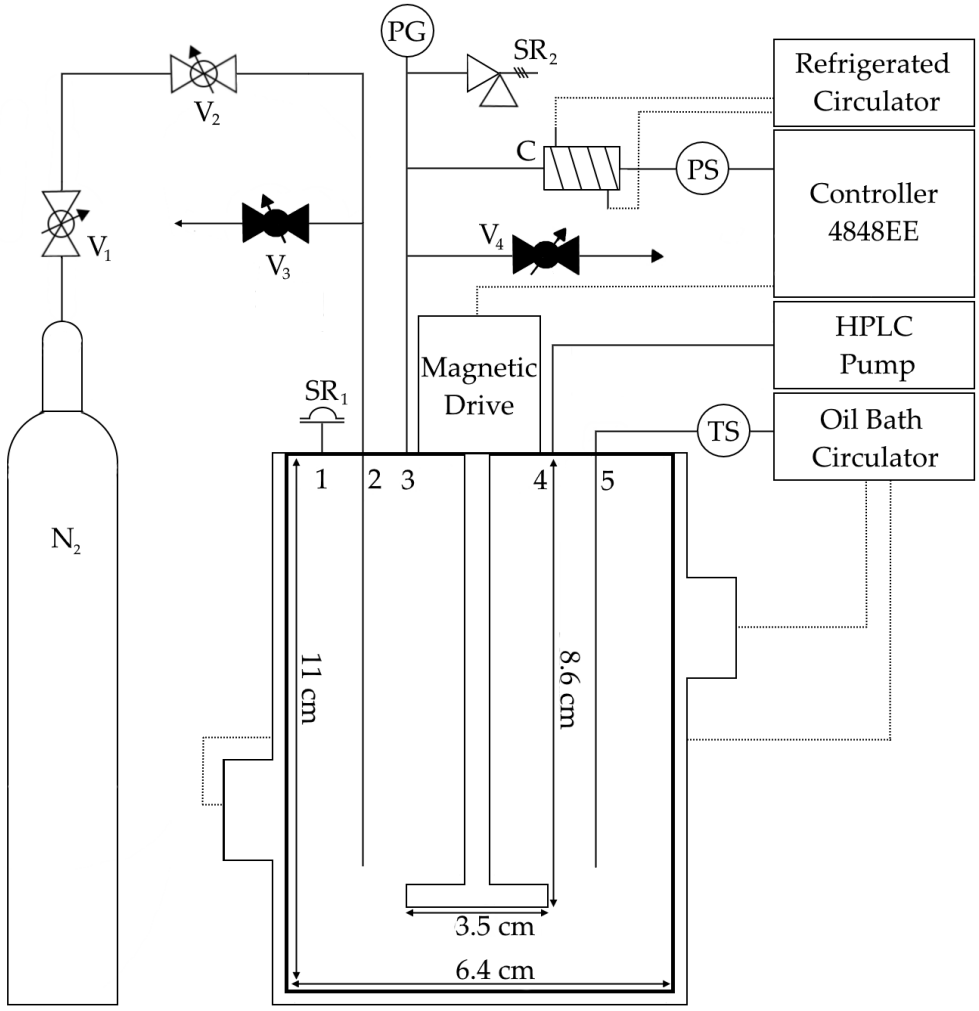

Valves:		Indicators	
V_1	Gas cylinder regulator	TS	Temperature sensor
V_2	Gas inlet control valve	PS	Pressure Sensor
V_3	Sampling valve	PG	Mechanical pressure gauge
V_4	Gas release valve		
Others:			
SR_1		Relief valve (set at 40 bar)	
SR_2		Safety rupture disc (set at 20 bar)	
C		Condenser	

Figure 3.1 Schematic of the Parr autoclave reactor used for alcoholysis experiments.

Alcoholysis reactions were conducted in a stainless-steel semi-batch autoclave reactor (max pressure 200 bar, temperature range from -10 to 350 °C) manufactured by Parr Instrument Company, Illinois, US. This 300 mL autoclave is a cylindrical and flat-bottomed vessel with the inside dimensions of 6.4 cm (diameter) × 11 cm (height). The liquid sampling valve (V_4) is attached to the same fitting as the gas inlet valve (V_3) connected to the same line (2). Incoming gas is always introduced below the surface of the liquid and the operator is provided with a means for clearing the line to be sure that any sample taken during a run will be representative.

3.4.1 Procedure used in Chapter 4

For each experiment, 12.5 g of PLA, 250 mL of THF and 1 g of Zn(**1**^{Et})$_2$ (8 wt% ≈ 9 mol%) were charged to the reactor. The autoclave was then sealed and degassed with N_2 for 20 min before bringing the reactor to the desired working temperature (50 – 130 °C) at a stirring speed of 300 rpm. The reactor was left at the desired temperature for a further 20 min to ensure all the PLA pellets were dissolved. The reactions were initiated in a semi-batch manner with the addition of 50 mL of alcohol (either EtOH ≈ 5 molar equivalents relative to ester groups, PrOH ≈ 4 equivalents, or BuOH ≈ 3 equivalents) fed into the reactor *via* an HPLC pump at a rate of 10 mL·min^{-1}. The calculation of molar equivalent is detailed in appendix §8.3.1. Reaction samples were taken periodically throughout each experiment and analysed by GC and ^{1}H NMR analysis. Multiple reactions were carried out at each temperature and results were averaged. The protocol was identical for Zn(**2**^{Pr})$_2$ experiments except the stirring speed was 800 rpm since Zn(**2**^{Pr})$_2$ displayed mass transport limitations at 300 rpm. A range of concentrations of EtLa and BuLa were injected into the GC to determine a calibration plot, detailed in appendix §8.2.1. The gradient of these plots allowed for the quantitative analysis and calculation of EtLa and BuLa concentration during the reactions. At the time of experiments, propyl lactate (PrLa) was

not available to be purchased. Therefore, it was not possible to determine a calibration plot for this component, so GC analysis for propanolysis was only qualitative.

More specifically the **ethanolysis** Zn(**1**^{Et})$_2$ and Zn(**2**^{Pr})$_2$ experiments in Section §4.2, were carried out at in temperatures 50 – 110 °C. The **propanolysis** Zn(**1**^{Et})$_2$ experiments in Section §4.3, were carried out at in temperatures in the range 90 – 130 °C. The Zn(**2**^{Pr})$_2$ experiments were carried out at in temperatures in the range 50 – 110 °C. The **butanolysis** Zn(**1**^{Et})$_2$ experiments in Section §4.4, were carried out at in temperatures in the range 50 – 130 °C. The Zn(**2**^{Pr})$_2$ experiments were carried out at temperatures in the range 50 – 110 °C.

3.4.2 Procedure used in Chapter 5

For the **preliminary mixed catalyst methanolysis** experiments in Section §5.2, 2 g of PLA, 10 mL of MeOH (≈ 9 molar equivalents relative to ester groups), 40 mL of THF, and a various amounts of $Zn(OAc)_2$ and DMAP (total = 0.1 g, 5 wt%) were charged in the reactor. Various stirring speeds ranging from 0 to 700 rpm were also investigated. Once the reactor was charged, the autoclave was sealed and degassed with N_2 for at least 10 min before bringing the reactor to the desired working temperature (130 °C) at stirring speed ranging from 0 to 700 rpm. The reactor was left at 130 °C for a further 10 min to ensure all the PLA pellets were dissolved before 10 mL of MeOH was fed into the reactor *via* an HPLC pump at a rate of 10 mL·min^{-1}. Samples were taken periodically and tested by gas chromatograph (GC).

For the **dual catalyst alcoholysis** experiments in Section §5.3, in each of the methanolysis experiments, 2 g of PLA, 40 mL of THF, and 0.05 g $Zn(OAc)_2$ + 0.05 g DMAP (0.8 mol% / 1.5 mol%) were charged in the reactor. In each ethanolysis experiment, 2 g of PLA, 35.5 mL THF, and 0.05 g $Zn(OAc)_2$ + 0.05 g DMAP were charged in the reactor. Once the reactor was charged, the autoclave was sealed and degassed with N_2 for at least 10 min before bringing the reactor to the desired working temperature (100 – 130 °C) at a stirring speed of 300 rpm. The

reactor was left at the desired temperature for a further 10 min to ensure that all the PLA pellets were dissolved. Then, either 10 mL of MeOH or 14.5 mL EtOH was fed into the reactor *via* an HPLC pump at a rate of 10 mL·min^{-1}. The volumes of the two alcohols were varied to ensure both MeOH and EtOH experiments had approximately 9 equivalents of alcohol per ester bond of PLA. Then, the volume of THF was adjusted to ensure the same concentration of PLA in both MeOH and EtOH experiments. Samples were taken periodically and tested by GC. For the **dual methanolysis** reactions in Section §5.3.2 the same protocol was followed but samples were also analysed by ^{1}H NMR.

3.4.3 Procedure used in Chapter 6

For the **preliminary methanolysis Zn(OAc)$_2$ experiments** in Section §6.2, the procedure was as follows: 2 g of PLA, 2 mol% of Zn(OAc)$_2$ (relative to mol of PLA), and THF were added to the autoclave, which was then sealed and degassed with N_2 for 5 min. The amount of THF depended on the amount of MeOH; enough THF was added so that each reaction volume was 50 mL total. Afterward, the temperature was brought to 130 °C for a further 10 min to ensure that all the PLA pellets had dissolved. Several stirring speeds were tested (0 rpm, 300 rpm, 600 rpm). Various amounts of MeOH (5.6 mL ≈ 5 equivalents, 10 mL ≈ 9 equivalents, 15 mL ≈ 13 equivalents or 19 mL ≈ 17 equivalents) in different runs were then fed into the reactor *via* an HPLC pump at a rate of 10 mL·min^{-1}. Reaction samples were taken periodically and tested *via* Agilent 6890N gas chromatograph.

For the **single and mixed catalyst methanolysis experiments** in Section §6.3 and §6.4, the procedure was as follows: 2 g PLA, various ratios of catalysts (Zn(OAc)$_2$, Mg(OAc)$_2$, TBD, and DMAP) always totalling 2 mol%, and either 40 mL or 31 mL of THF (depending on MeOH amount, total volume = 50 mL), was added to the autoclave, which was then sealed and degassed with N_2 for 5 min. Afterwards, the temperature was brought to 130 °C for a further

10 min to ensure that all the PLA pellets had dissolved. Two stirring speeds were tested: 300 rpm or 600 rpm. Two MeOH amounts were tested: 10 mL ≈ 9 equivalents and 19 mL ≈ 17 equivalents, which were fed into the reactor *via* an HPLC pump at a rate of 10 mL·min^{-1}. Reaction samples were taken periodically and tested *via* gas chromatograph (GC).

For the **final methanolysis $Zn(OAc)_2$ and dual $Zn(OAc)_2$ / TBD experiments** in section §6.4.2, the procedure was as follows: 2 g of PLA, 2 mol% of $Zn(OAc)_2$, and 31 mL of THF were added to the autoclave, which was then sealed and degassed with N_2 for 5 min. A stirring speed of 600 rpm was used. A range of temperatures were investigated 100 – 130 °C. Once the reactor had reached the desired temperature, 19 mL ≈ 17 equivalents of MeOH were fed into the reactor *via* an HPLC pump at a rate of 10 mL·min^{-1}. Reaction samples were taken periodically and tested by ^{1}H NMR spectroscopy.

3.5 Analytical methods

3.5.1 Gas chromatography (GC)

The reaction mixtures used throughout this project were analysed using an Agilent 6890N Network Gas Chromatography equipped with an Flame Ionisation Detector (FID), a simplified schematic shown in Figure 3.2. An FID uses flame fuelled by hydrogen and zero air to ionize organic compounds that are carried by an inert gas through a retention column. Liquid sample is injected into the GC and vaporized; its components are then separated in the retention column, and each analyte then passes through the flame becoming ionized. These ions are detected by FID and their current is converted to an electrical signal. Signals appear at different retention times corresponding to each analyte. Signal intensity is proportional to the quantity of each analyte injected into the GC. An inert make-up gas is required to ensure that sufficient gas flow is provided throughout the column and FID, typically helium or nitrogen are used. It is important that the gas contains minimal impurities as they could interfere with the analysis.

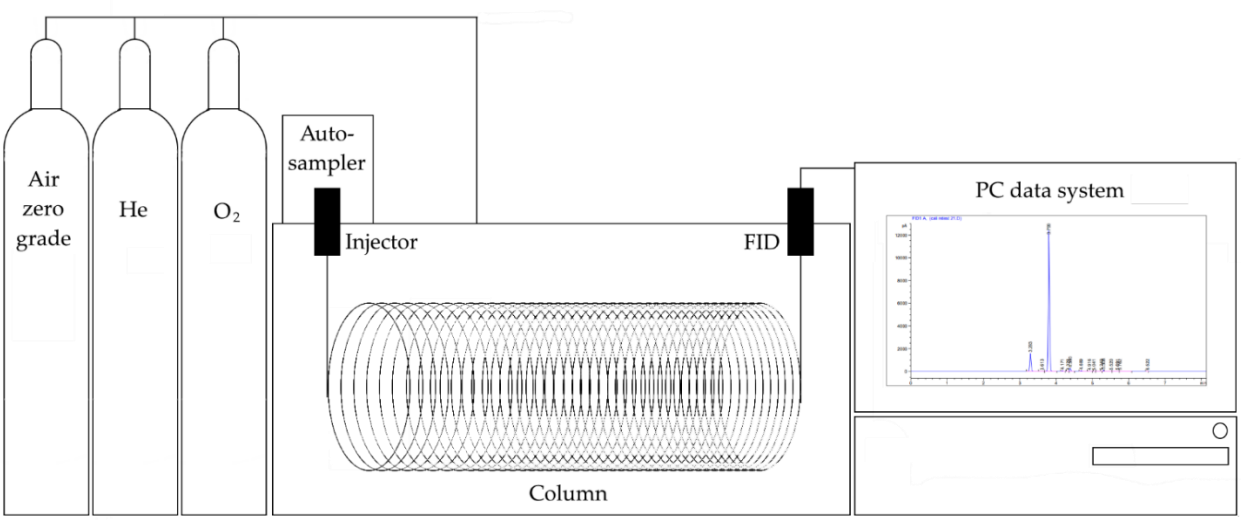

Figure 3.2 Simplified schematic of the Agilent 6890N Network Gas Chromatography system.

Optimised separation of reaction mixture analytes depends largely on the correct selection of a capillary column – the stationary phase (match polarity of sample), the column I.D. (dependent on the size of the sample), the film thickness (dependent on the volatility of the sample), and the column length (to increase the resolution when needed). An appropriate oven method is also critical and needs to be developed. A good method holds the column at a certain temperature with or without a temperature ramp that allows for each analyte to sufficiently separate. A good method will result in distinct signal peaks but still within a reasonable time frame. Once a proper method has been developed, chemical standards at a series of known concentrations are injected, and the corresponding retention time is used to identify similar compounds in reaction mixtures. As the intensity of a GC signal is related to the amount of analyte injected, a calibration plot can be generated from the known concentrations. This allows for the quantitative analysis of similar chemicals in a reaction mixture.

The specific column and oven method used during this study is summarised: the GC was coupled with a Flame-Ionization Detector (FID) (Agilent Technologies, 6890N, Cheadle, UK), samples were injected by an autosampler (Agilent Technologies, 7683B. Cheadle, UK), to a 30 m × 0.32 mm ID, 0.25 µm film thickness HP-5 Agilent capillary column. Helium was used as

a carrier and make-up gas with the following conditions: inlet temperature of 150 ◦C, 1 μL injection volume, 1:400 split ratio, 250 °C detector temperature, with an initial oven temperature of 65 °C (held for 4 min), then 100 °C·min^{-1} ramp to 195 °C (held for 1 min), followed by 100 °C·min^{-1} ramp to 230 °C (held for 5 min). The initial flow rate was 0.8 mL·min^{-1} (held for 5 min), then 100 mL·min^{-1} ramp to 3 mL·min^{-1} (held for 5 min). A multiple point external standard calibration curve was prepared using standard solutions covering the range of AL concentrations, detailed in Appendix §8.2.1. A linear response of the detector was determined for MeLa, EtLa, and BuLa (R^2 = 0.9998, 0.9998, and 0.9969 respectively). For PrLa the GC analysis was only qualitative.

3.5.2 Proton nuclear magnetic resonance (^{1}H NMR) spectroscopy

The Stern – Gerlach experiment in 1921 shot a beam of Ag atoms through an inhomogeneous magnetic field; the result was discrete bands of silver atoms. This result was significant as it implied the silver atoms behaved like tiny magnets interacting with the external field [244,245]. NMR was co-discovered in 1946, nuclei such as ^{1}H, and ^{31}P were able to absorb radio frequency (RF) energy when place in an external magnetic field at specific strength [245]. Different nuclei within a molecule resonated at different frequencies which allows for the detailed analysis of the molecule structure. Nuclei that have an even number of protons and neutrons have zero spin. All other nuclei have either half integer or integer spin and can be imaged as spinning on their axes. Quantum mechanics tells us that the orientation of angular momentum is quantized; thus the subsequent magnetic moment has discrete orientations. Nuclei with spin can be described by an angular momentum quantum number (I), and the magnetic moment may lie in $2I$ +1 different orientations relative to an axis [244]. A hydrogen proton has I = ½ so its spin adopts either of two orientations; in the absence of an external magnetic field both these orientations are of equal energy. When a magnetic field is applied the spin states align with

(lower energy – α spin state) or against (higher energy – β spin state) the external field. The initial populations of spin energy levels are determined by thermodynamics and the Boltzmann distribution. Lower energy levels contain slightly more nuclei than the higher levels. In an applied magnetic field (B_0) the protons undergo a motion called precession as they twist round the direction of the field. The rate of precession termed the *Larmor frequency* (ω_0) is proportional to the field strength of B_0, described by the Larmor equation (3.1),

$$\omega_0 = \gamma B_0 \tag{3.1}$$

where the gyromagnetic ratio (γ) is a proportionality constant related to the internal structure of a nucleus. Resonance absorption of spin ½ nuclei occurs when the ω_0 is the same as the applied electromagnetic field. If an applied RF signal matches ω_0, then a proton in the lower energy absorbs energy so its angle of precession 'flips' to the higher energy level. It is possible to excite all the lower energy nuclei so no further RF can be absorbed; the spin system is then saturated. As the proton realigns with the applied field it emits energy at the Larmor frequency. Relaxation processes take place as nuclei return to a lower energy state. There are two major relaxation processes: spin – lattice longitudinal relaxation (T_1), and spin – spin transverse relaxation (T_2). T_1 describes the return to equilibrium in the direction of the magnetic field. T_2 describes the decay of excited magnetization perpendicular to the applied magnetic field.

The precise resonant frequency of the energy transition is dependent on the effective magnetic field of the nuclei. This is affected by electron shielding which depends on the chemical environment. In general, increasing electronegativity deshields a proton so that they experience a greater effective magnetic field. This means a greater energy gap between α and β spin states, thus a higher frequency of radiation absorbed and higher chemical shift for the proton. The difference between the resonance frequency and that of a reference standard is known as the chemical shift. Typically for ^{1}H NMR, tetramethylsilane (TMS) is used as the reference

standard as all its hydrogens share identical environments. Chemical shifts are reported on the δ scale which is defined by the equation (3.2),

$$\delta = \left(\frac{\nu - \nu^{\circ}}{\nu^{\circ}}\right) \times 10^{6} \quad (3.2)$$

where ν° is the resonance frequency of the standard (TMS chemical shift of zero). The advantage of δ scale is that shifts reported are independent of the applied field and is convenient to express in ppm. It is also important to consider spin-spin coupling which causes signals to split depending on neighbouring protons. The number of splitting indicates the number of chemically bonded nuclei in the vicinity of the observed nucleus.

Throughout this project ^{1}H NMR analysis using a 400 MHz Bruker Avance II spectrometer (Bruker Coventry UK) was utilized to determine the alcoholysis reaction mixtures. The NMR was equipped with a Bruker 9.39 T Ultrashield magnet, a Bruker Avance NEO console (2018), and 5 mm BBFO "smart" probe. Reaction samples were withdrawn and analysed at various intervals and ^{1}H NMR analysis used to determine the relative concentrations of PLA, oligomers, and the AL product. Each of these had specific proton resonances. According to equation (3) there are three possible environments for methine functional groups: internal methine protons along the PLA chains (Int) (δ = 5.09 – 5.21 ppm), two types of chain end methine protons belonging to oligomer fragments (CE) (δ = 4.30 – 4.39 ppm / 5.09 – 5.21 ppm), or methine protons belonging to an alkyl lactate molecule (AL) (δ = 4.23 – 4.29 ppm), detailed in Appendix §8.2.2. This enables the determination of the reaction progress, by monitoring the relative concentration of each methine environment *via* ^{1}H NMR spectroscopy. Reaction samples were dissolved in $CDCl_3$ and chemical shifts were referenced against TMS.

3.6 Alcoholysis Rate Equations

The experimental data for Chapters 4 and 6 were modelled using the reaction mechanism shown in Equations (3.3 – 3.6), proposed by Román-Ramírez, et al [187]. The alcohol nucleophile was in excess so was not included in the model.

$$Int \overset{k_1}{\rightarrow} CE \underset{k_{-2}}{\overset{k_2}{\rightleftarrows}} AL \tag{3.3}$$

$$\frac{d[Int]}{dt} = -k_1[Int] \tag{3.4}$$

$$\frac{d[CE]}{dt} = k_1[Int] - k_2[CE] + k_{-2}[AL] \tag{3.5}$$

$$\frac{d[AL]}{dt} = k_2[CE] - k_{-2}[AL] \tag{3.6}$$

In the overall rate equation (3.3), the internal methine protons along the PLA chains are represented by (Int), the chain-end methine protons of the oligomer fragments are represented by (CE), and the alkyl lactate methine protons of the product are represented by (AL). PLA was depolymerized through a two-step reaction, with the second step being reversible. The coefficient k_1 represents the random attack of an ester linkage by a MeOH nucleophile; each cleavage results in the generation of two CE oligomers. The coefficient k_2 represents the forward equilibrium step, which is the formation of the product AL from CE oligomers; this step occurs when MeOH attacks an ester linkage of an oligomer adjacent to its CE. The reverse equilibrium step represented by coefficient k_{-2}, occurs when the alcohol group of AL attacks an ester linkage of the CE oligomer, and itself becomes a larger oligomer. The differential Equations (3.3 – 3.6) were solved in MATLAB according to the script detailed in Appendix §8.1.3. Using a minimisation of least squares fitting procedure in MATLAB, the rate constants were estimated from the experimental ^{1}H NMR data. The rate constants were estimated for the same reaction over a range of temperatures and used to generate Arrhenius plots to obtain E_a

for the reaction. The experimental data for Chapter 5 were modelled using the simplified two step reaction mechanism shown below in equation (3.7).

$$Int \overset{k_1}{\rightarrow} CE \overset{k_2}{\rightarrow} AL \tag{3.7}$$

$$\frac{d[Int]}{dt} = -k_1[Int] \tag{3.8}$$

$$\frac{d[CE]}{dt} = k_1[Int] - k_2[CE] \tag{3.9}$$

$$\frac{d[AL]}{dt} = k_2[CE] \tag{3.10}$$

$$[CE] = \frac{k_1}{k_2 - k_1}[\exp(-k_1 t) - \exp(-k_2 t)][Int]_0 \tag{3.11}$$

The model is simplified from the previous model by not assuming an equilibrium for the second step. This was carried out to investigate if there was a significant difference in estimated E_a for each mechanism. The alcohol in excess was not included in the model. Int represents the internal methines along the PLA chains, CE represents the chain end methines of the oligomer fragments from cleaved PLA chains and, AL represents the alkyl lactate methines of the product. Equations (8 – 10) were solved by sequential integration and substitution (work shown in appendix §8.2.2) to produce equation (11). The ^{1}H NMR data were then fitted to equation (11) using SigmaPlot which enabled for the determination of k_1 and k_2.

Chapter 4 – Kinetics of Alkyl Lactate Formation from the Alcoholysis of Poly(lactic Acid)

4.1 Chapter Overview

This Chapter describes the investigation of two discrete Zn complexes and their effect on the alcoholysis of PLA. A range of alcohols were also explored to see the effect of alcohol chain length on the rate of PLA alcoholysis. All the experiments were carried out in the 300 ml Parr autoclave reactor in a semi-batch manner through the addition of alcohol, as described in Section §3.4.1. The catalysts (Zn($\mathbf{1}^{Et}$)$_2$ and Zn($\mathbf{2}^{Pr}$)$_2$) were synthesised by McKeown *et al.* (the School of Chemistry at the University of Bath), using the synthesis detailed in Section §3.3. The experimental data were fitted to a kinetic model in MATLAB proposed by Román-Ramírez, detailed in Section §3.6. This chapter is based on the publication, Kinetics of Alkyl Lactate Formation from the Alcoholysis of Poly(lactic Acid) [12].

There are several studies that have investigated the methanolysis of PLA using a range of catalysts such as metal salts and ILs [173–176]. Only one previous study was found that investigated the kinetics of PLA alcoholysis using other alcohols such as EtOH and BuOH [170]. Several studies on PLA alcoholysis have been published by collaboration group members. The MATLAB script and kinetic model were originally proposed for PLA methanolysis [187]. McKeown *et al.* developed a range of Zn complexes that were applied to the ROP of *L*-lactide to PLA, and the subsequent alcoholysis of PLA using MeOH or EtOH [188]. The work reported here extends these studies by using Zn($\mathbf{1}^{Et}$)$_2$ and Zn($\mathbf{2}^{Pr}$)$_2$ for PLA alcoholysis, investigating a greater range of alcohols while also studying the reaction kinetics. Different alcohols were used at a fixed volume; in each case the alcohol is in excess relative to the PLA ester groups. For the depolymerisation reaction to occur, the catalyst must coordinate to both PLA and the nucleophilic alcohol. The working hypothesis is that longer chain alcohols

will sterically hinder this coordination, resulting in slower reaction rates. The results for PLA alcoholysis using EtOH, PrOH, and BuOH, are divided into Sections §4.2, §4.3, and §4.4. Each section is subdivided into the reporting of GC results, ^{1}H NMR results, and activation energies (E_a). A comparison and discussion of the data are then presented in Section §4.5. Finally, Section §4.6 summaries this investigation and establishes a conclusion.

4.2 Ethanolysis and Kinetics of Ethyl Lactate Formation

The ethanolysis of PLA is a particularly useful recycling method as its product EtLa has the largest market share and demand out of all the ALs [243]. The protocol for these experiments is detailed in Section §3.4.1. PLA ethanolysis was modelled as a two-step reversible reaction detailed in Section §3.6.

4.2.1 GC Results

Samples were taken throughout each experiment and analysed by GC to determine the concentration of EtLa. Figure 4.1 shows the EtLa concentration ($g \cdot mL^{-1}$) vs time (min) for the ethanolysis of PLA using Zn($\mathbf{1}^{Et}$)$_2$ in the temperature range 50 – 110 °C. Experiments were repeated (2 – 3 times) at each temperature and results averaged. A higher temperature resulted in greater concentrations of EtLa in shorter times. The times taken to reach an EtLa concentration of 0.06 $g \cdot mL^{-1}$ are: 174 min (110 °C), 313 min (90 °C), 1160 min (70 °C), and 4097 min (50 °C). This trend is expected as the average kinetic energy is increased at the higher temperatures, so a larger proportion of molecules overcome the activation energy. There is only a small reduction in the EtLa production rate between 110 °C to 90 °C, with a greater reduction from 90 °C to 70 °C, and the greatest reduction from 70 °C to 50 °C. When considering the ethanolysis of PLA on an industrial scale, a compromise should be made, using higher temperatures generates faster production rates while using lower temperatures leads to lower operating costs. The lower operating temperature of 90 °C still has a relatively high EtLa

production rate while also benefiting from a lower operating cost and smaller GWP. Despite ethanolysis at 70 °C and 50 °C having lower operating costs they may not be viable for industrial production as the EtLa production rate is too slow.

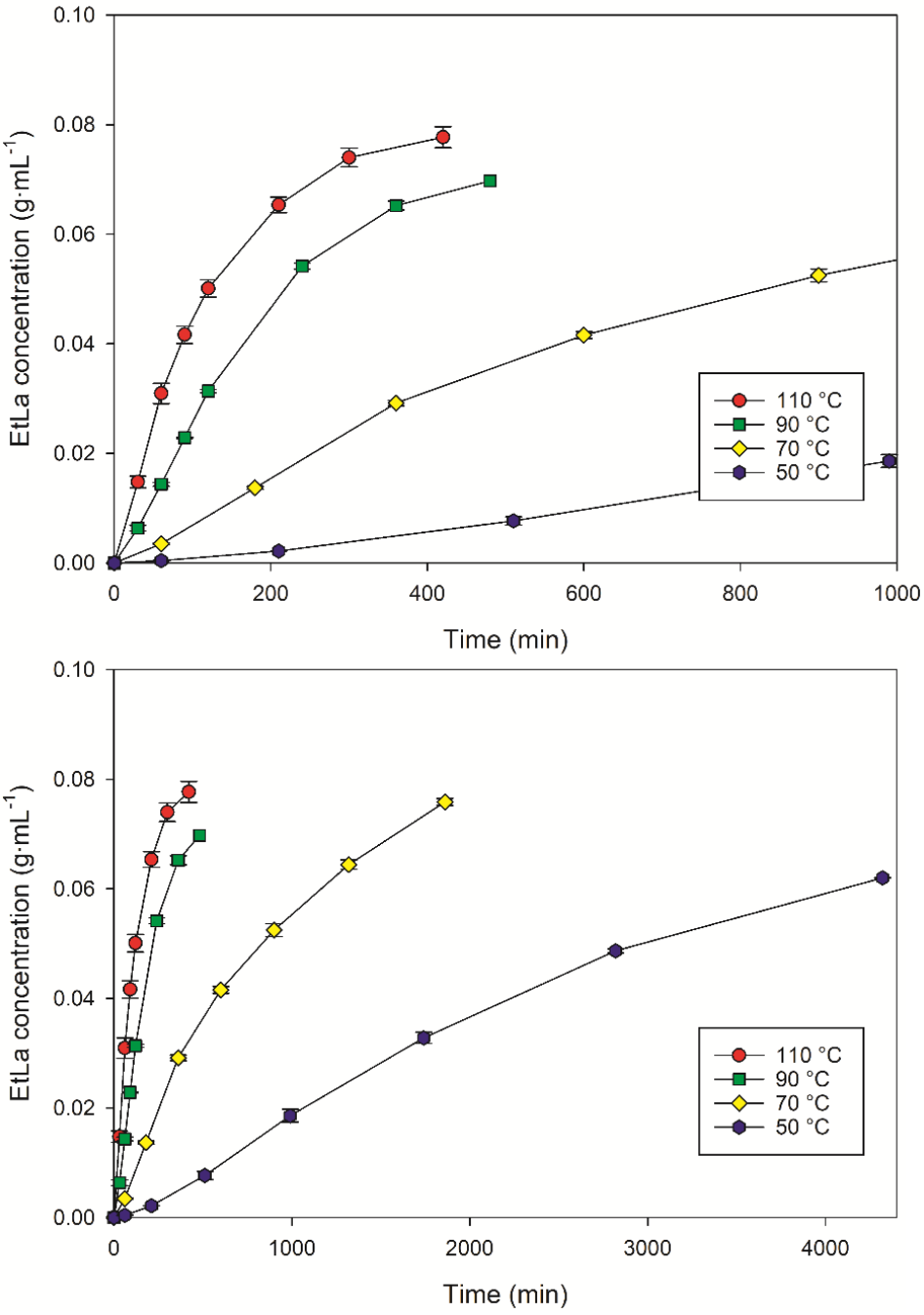

Figure 4.1. Ethanolysis of 12.5 g of PLA at 50 – 130 °C, 300 rpm and 1 g Zn($\mathbf{1}^{Et}$)$_2$.

Figure 4.2 shows the EtLa concentration ($g \cdot mL^{-1}$) vs time (min) for the ethanolysis of PLA using Zn($\mathbf{2}^{Pr}$)$_2$ across the temperature range 50 – 110 °C. Experiments were repeated (2 – 4 times) at each temperature and results were averaged (excluding **7**0 °C and 90 °C). For the most part a higher temperature resulted in a greater EtLa production rate. However, Zn($\mathbf{2}^{Pr}$)$_2$ exhibited non-Arrhenius behaviour at temperatures ≤ 70 °C resulting in enhanced initial reaction rates as temperature decreases. The phenomenon of non-Arrhenius behaviour and variable activation energies has received considerable attention in the literature. A myriad of factors can be considered such as: quantum-mechanical tunnelling effects, the dielectric properties and viscosity of the solvent, quasi-thermodynamic effects, and multi-step mechanisms such as reversible and consecutive reactions which have differing activation energies [246,247]. According to Carvalho-Silva *et al.* non-Arrhenius behaviour can be divided into super-Arrhenius kinetics (convex Arrhenius plot) or sub-Arrhenius kinetics (concave Arrhenius plot) [248,249]. Super-Arrhenius kinetics refer to transport phenomena that increase reactivity as the temperature increases, whereas sub-Arrhenius refers to quantum tunnelling effects that increase reactivity as temperature decreases [248,249]. McKeown *et al*. showed evidence that at 50 °C Zn($\mathbf{2}^{Pr}$)$_2$ undergoes ligand dissociation in addition to the formation of a new species [188]. Román-Ramírez *et al.* used Zn($\mathbf{2}^{Pr}$)$_2$ for the methanolysis of PLA and observed non-Arrhenius behaviour only at low temperatures; a concave Arrhenius plot was obtained [189]. A concave Arrhenius plot (sub-Arrhenius kinetics) implies that quantum tunnelling effects are responsible for the increase in reactivity as temperature decreases [189,248,249]. This phenomenon was observed for Zn($\mathbf{2}^{Pr}$)$_2$ reactions but not Zn($\mathbf{1}^{Et}$)$_2$ reactions. One explanation is that Zn($\mathbf{2}^{Pr}$)$_2$ ligand dissociation and formation of a new species facilitates quantum tunnelling effects, resulting in sub-Arrhenius kinetics that accelerate the reaction as temperature decreases.

Remarkably, ethanolysis at 50 °C had the greatest initial EtLa production rate. The times taken to reach an EtLa concentration of 0.06 $g \cdot mL^{-1}$ at each temperature are: 664 min (50 °C), 762 min (110 °C), 2020 min (90 °C), and 5384 min (70 °C). A small reduction in the EtLa production rate was observed between 110 °C and 90 °C, with a greater reduction between 90 °C and 70 °C. Despite 50 °C exhibiting the greatest initial production rate it also plateaued at a lower EtLa concentration in comparison to 110 °C. This implies the equilibrium in equation (3.3) lies more to the left at 50 °C in comparison to 110 °C, favouring the formation of CE and resulting in a lower concentration of EtLa. Ethanolysis of PLA utilizing $Zn(\mathbf{2}^{Pr})_2$ appears promising for industrial scale-up. This is because a relatively high EtLa production can be achieved at the low temperature 50 °C. Lowering operating temperatures makes the chemical recycling of PLA more economically feasible, in addition to having a smaller environmental impact, for example through lower energy use.

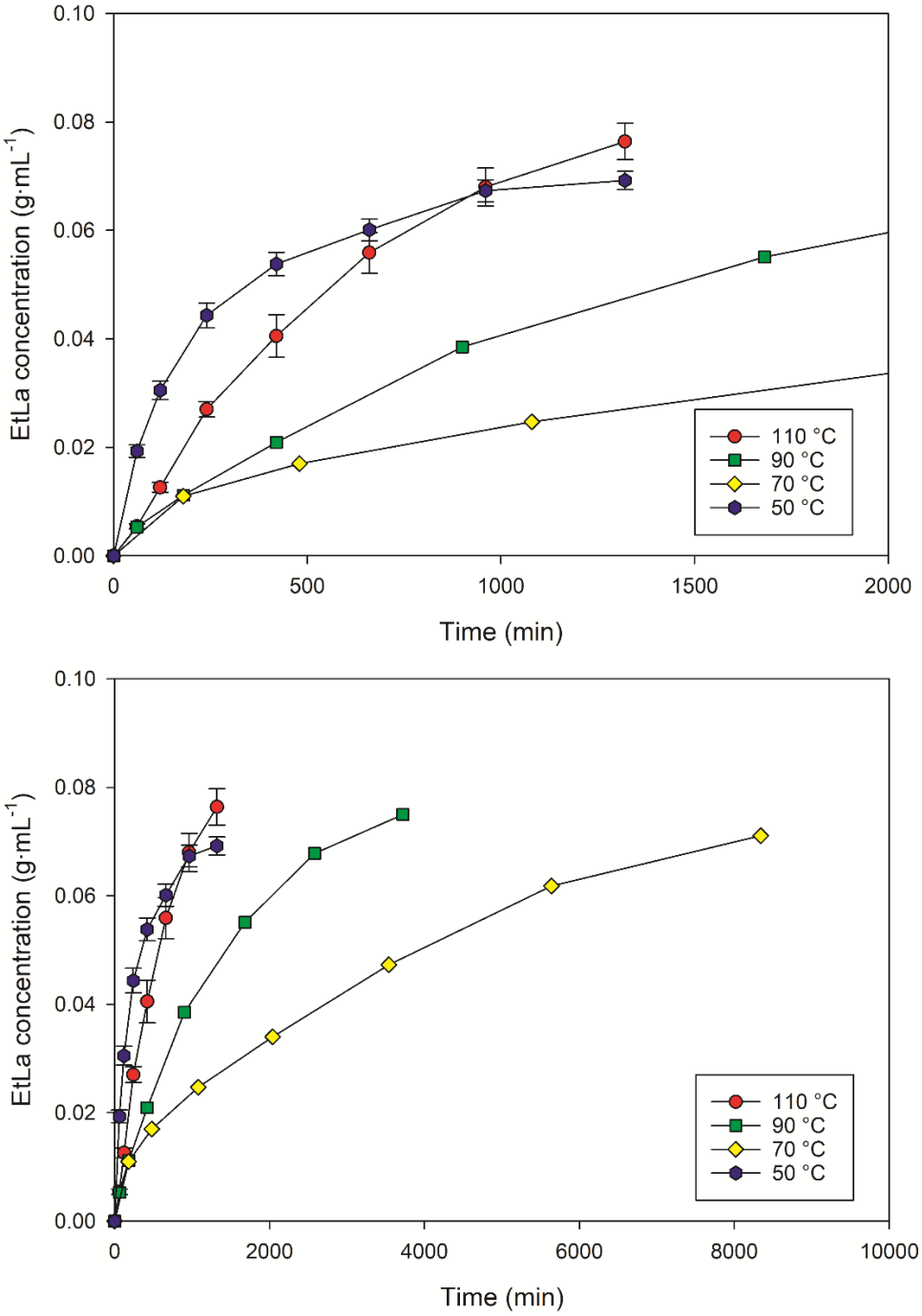

Figure 4.2 Ethanolysis of 12.5 g of PLA at 110 – 50 °C, 800 rpm and 1 g Zn(**2**^{Pr})$_2$.

Table 4.1 presents the EtLa concentrations and rates determined by GC for both catalysts Zn(**1**^{Et})$_2$ and Zn(**2**^{Pr})$_2$ to allow for comparison. Initial rate of EtLa production was determined at 60 min, since at this time the concentration vs time graph is relatively linear. Zn(**1**^{Et})$_2$ follows a clear trend that a higher temperature results in a greater initial rate of EtLa production. Zn(**2**^{Pr})$_2$

follows the opposite trend, its non-Arrhenius behaviour resulting in higher rates of EtLa production at lower temperatures. The greatest initial rate of EtLa production 5.18 x 10^{-4} ($g \cdot mL^{-1} \cdot min^{-1}$) was achieved by Zn(**1**^{Et})$_2$ at 110 °C, just over double what the catalyst could achieve at 90 °C. Surprisingly Zn(**2**^{Pr})$_2$ at 50 °C exhibited a maximum rate of 2.51 x 10^{-4} ($g \cdot mL^{-1} \cdot min^{-1}$), while this is half the rate of Zn(**1**^{Et})$_2$ at 110 °C it was achieved at a significantly lower temperature.

Table 4.1. Ethanolysis of 12.5 g PLA at 50 – 110 °C, using 9 mol% of either Zn(**1**^{Et})$_2$ (300 rpm) or Zn(**2**^{Pr})$_2$ (800 rpm), using 5 equivalents of EtOH. The data representative averages of repeat experiments (2-4 repeats, excluding Zn(**2**^{Pr})$_2$ 70 °C and 90 °C).

Catalyst (1 g, 8 wt%)	**Temperature (°C)**	**Final time (min)**	**Final EtLa concentration ($g \cdot mL^{-1}$)**	**Initial rate of EtLa production ($g \cdot mL^{-1} \cdot min^{-1}$)**
Zn(**1**^{Et})$_2$	110	317	0.0727	5.18 x 10^{-4}
	90	450	0.0689	2.39 x 10^{-4}
	70	1740	0.0745	5.83 x 10^{-5}
	50	4485	0.0616	6.73 x 10^{-6}
Zn(**2**^{Pr})$_2$	110	834	0.0533	7.46 x 10^{-5}
	90	3090	0.0718	8.83 x 10^{-5}
	70	8700	0.0694	9.50 x 10^{-5}
	50	1031	0.0719	2.51 x 10^{-4}

4.2.2 ^{1}H NMR Results

Reaction samples were taken periodically throughout each experiment and analysed by ^{1}H NMR, detailed in section §3.5.2. The relative concentrations of Int, CE, and AL were fitted to the kinetic model described in equation (3.3) and the resulting rate equations were solved in MATLAB. By comparing integrals of interest ^{1}H NMR can be used to determine the ratios of compounds in a reaction mixture; this allows for a relative concentration of each compound to be determined. Since the theoretical maximum concentration of the product is known, the relative concentration can be used to determine its exact concentration (e.g. an 86% relative concentration of AL would be 86% of the theoretical maximum concentration). Relative concentration *versus* time profiles using Zn(**1**^{Et})$_2$ at each temperature are shown in Figure 4.3.

At 110 °C, a maximum concentration of 50% for CE intermediates was reached at 35 min, while 100% conversion of Int groups was reached at 160 min. At 90 °C a maximum concentration of 46% for CE intermediates was reached at 90 min, while 100% conversion of Int groups was reached at 300 min. At 70 °C, a maximum concentration of 49% for CE intermediates occurred at 300 min, while 100% conversion of Int groups was reached at 1500 min. At 50 °C, a maximum concentration of 44% for CE intermediates was reached at 810 min, 100% conversion of Int groups was only reached at 4320 min. The reaction profiles show good fits for the experimental data to the kinetic model. As Zn(**2**^{Pr})$_2$ exhibited non-Arrhenius behaviour at the tested temperature range it was not possible to obtain reliable fits.

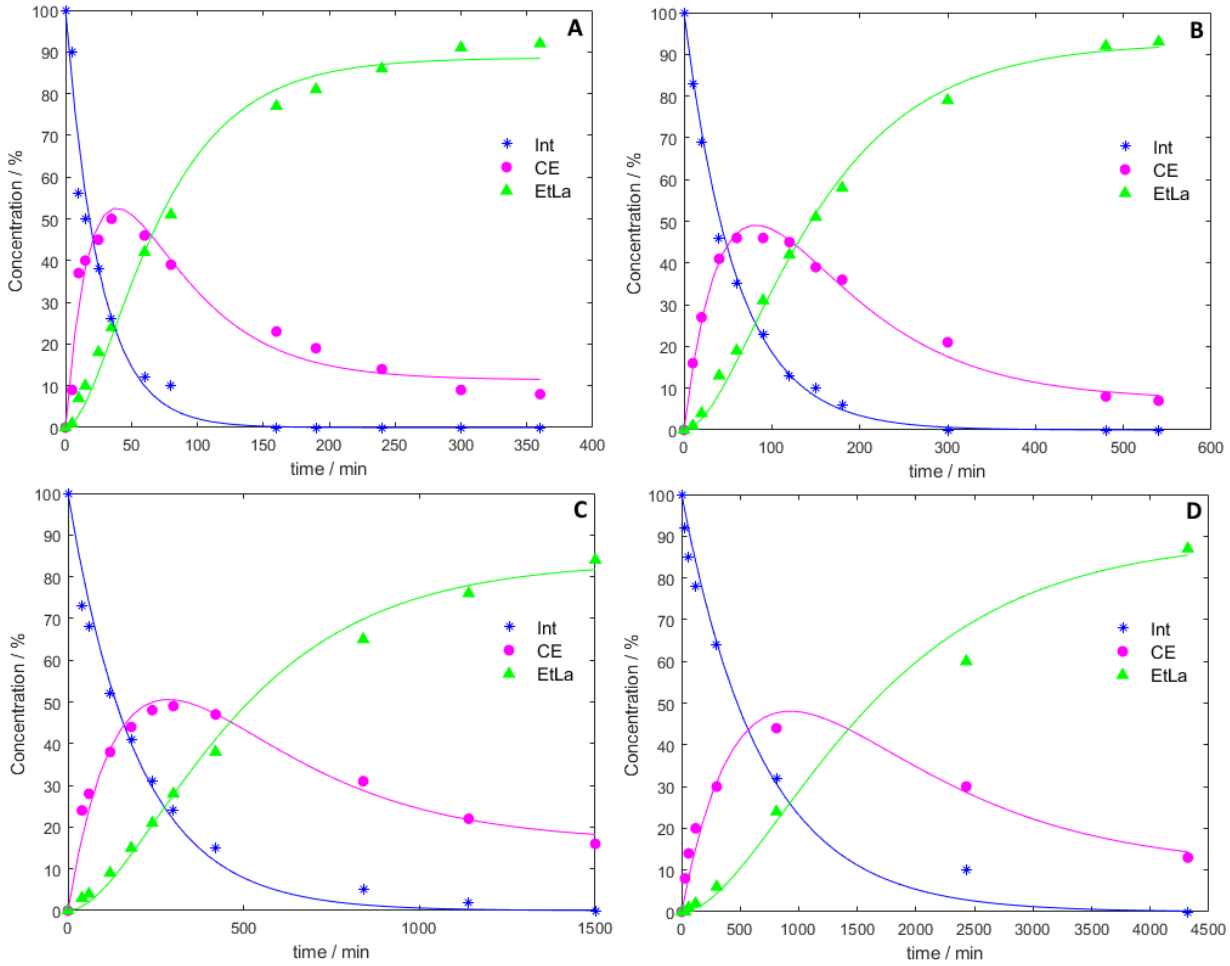

Figure 4.3. Zn(**1**^{Et})$_2$ ethanolysis reaction profiles obtained from ^{1}H NMR data fitted in MATLAB. (**A**) = 110 °C, (**B**) = 90 °C, (**C**) = 70 °C, (**D**) = 50 °C.

Conversion of Int groups (X_{Int}), AL selectivity (S_{AL}), and AL yield (Y_{AL}) were calculated according to equations 4.1 – 4.3,

$$X_{Int} = \frac{Int_0 - Int}{Int_0} \quad (4.1)$$

$$S_{AL} = \frac{AL}{Int_0 - Int} \quad (4.2)$$

$$Y_{AL} = S_{AL} X_{Int} \quad (4.3)$$

Int_0 is the initial concentration of the PLA Int groups (100%). Conversion selectivity and yield of AL were calculated at 60 min for both sets of experiments using Zn(**1**^{Et})$_2$ or Zn(**2**^{Pr})$_2$ catalysts. Averages for X_{Int}, S_{AL}, and Y_{AL}, at each temperature were determined to allow for easier comparison, shown in Table 4.2. Zn(**1**^{Et})$_2$ exhibited a clear trend that a higher temperature resulted in a higher, X_{Int}, S_{AL}, and Y_{AL}. For Zn(**1**^{Et})$_2$ at 110 °C the average values of X_{Int}, S_{AL}, and Y_{AL}, were 85%, 43%, and 37%, whereas for Zn(**2**^{Pr})$_2$ the values were only 47%, 15%, and 7% respectively. At high temperatures Zn(**2**^{Pr})$_2$ exhibits a lower rate of AL production than Zn(**1**^{Et})$_2$, resulting in a smaller yield of AL in a given time. However, at lower temperature the non-Arrhenius behaviour of Zn(**2**^{Pr})$_2$ leads to an increase of activity. At both 70 °C and 50 °C, Zn(**2**^{Pr})$_2$ displayed a significantly higher activity than Zn(**1**^{Et})$_2$, producing a greater conversion of Int and greater yield of AL. Remarkably, Zn(**2**^{Pr})$_2$ at 50 °C outperformed Zn(**1**^{Et})$_2$ at 110 °C, achieving average X_{Int}, S_{AL}, and Y_{AL} values, of 86%, 68%, and 85%, respectively.

Table 4.2. PLA ethanolysis using Zn(**1**^{Et})$_2$ (300 rpm) or Zn(**2**^{Pr})$_2$ (800 rpm) at 50 – 110°C. Conversion of Int groups, AL selectivity, and AL yield, calculated at 60 min. The data represent averaged repeat experiments (2-4 repeats, excluding Zn(**2**^{Pr})$_2$ 70 °C, 90 °C, and 110 °C).

Catalyst (1 g, 8 wt%)	Temperature (°C)	Average X_{Int} (%)	Average S_{AL} (%)	Average Y_{AL} (%)
Zn(**1**^{Et})$_2$	110	85	43	37
	90	61	27	17
	70	33	13	4
	50	12	3	1
Zn(**2**^{Pr})$_2$	110	47	15	7
	90	42	12	5
	70	51	18	9
	50	86	68	58

X_{Int}, S_{AL}, Y_{AL}, are determined at 60 min of reaction.

4.2.3 Activation Energy

The relative concentrations determined in Section §4.2.2 were fitted to the experimental model, equation (3.3) described in Section §3.6. The rate equations (3.4 – 3.6) were solved in MATLAB, generating estimates of rate coefficients for the fitted experimental data at different temperatures, shown in Table 4.3. The greatest difference between values for k between two repeats was k_{-2} at 90 °C. Over the temperature range 50 – 110 °C there was a greater range in values for k_2 and k_{-2} in comparison to k_1. This implies the equilibrium step in equation (3.3) is more sensitive to the specific reaction conditions than the first step.

Table 4.3. Estimated rate coefficients for each ethanolysis experiment.

Catalyst (1 g, 8 wt%)	Temperature (°C)	k_1 (min^{-1})	k_2 (min^{-1})	k_{-2} (min^{-1})
Zn(**1**^{Et})$_2$	110	3.85 x 10^{-2}	1.74 x 10^{-2}	2.25 x 10^{-3}
	110	2.74 x 10^{-2}	1.46 x 10^{-2}	2.42 x 10^{-3}
	90	1.48 x 10^{-2}	8.86 x 10^{-3}	2.07 x 10^{-3}
	90	1.68 x 10^{-2}	9.05 x 10^{-3}	7.01 x 10^{-4}
	70	5.59 x 10^{-3}	2.71 x 10^{-3}	1.68 x 10^{-4}
	70	5.09 x 10^{-3}	2.62 x 10^{-3}	5.14 x 10^{-4}
	50	1.05 x 10^{-3}	7.21 x 10^{-4}	9.87 x 10^{-5}
	50	1.46 x 10^{-3}	8.39 x 10^{-4}	9.82 x 10^{-5}

The estimated rate coefficients were used to generate Arrhenius plots for PLA ethanolysis using Zn($\mathbf{1}^{Et}$)$_2$. According to equation (3.3), alcoholysis of PLA occurs in three steps. Therefore, there are three sets of rate coefficients (k_1, k_2, and k_{-2}) which correspond to three different activation energies (E_{a1}, E_{a2}, and E_{a-2}). The Arrhenius plot for Zn($\mathbf{1}^{Et}$)$_2$ is shown in Figure 4.4. The resulting activation energies are: E_{a1} = 56.3 ± 8.0 kJ·mol^{-1}, E_{a2} = 53.1 ± 6.4 kJ·mol^{-1}, and E_{a-2} = 56.2 ± 18.9 kJ·mol^{-1}. One study estimated the E_a for catalyst free PLA ethanolysis in the temperature range 140 – 190 °C to be 112.97 kJ·mol^{-1} [170]. The value for E_{a1} found in this thesis is significantly lower in addition to being determined at a lower temperature range of 50 – 110 °C. The experimental data show a good fit; each Arrhenius plot has $R^2 \geq 0.098$. The estimated activation energies highlight that E_{a-2} has the greatest range in upper and lower bound values ± 18.9 kJ·mol^{-1}. The activation energy for ethanolysis was also determined according to first order kinetics. First order kinetics only considers the initial cleavage of PLA Int groups. The integrated rate equation was plotted, resulting in a linear graph with a negative gradient, detailed in Appendix §8.1.1. The first order E_a was calculated to be 55.1 ± 10.0 kJ·mol^{-1}, which is similar to the value for E_{a1} (56.3 ± 8.0 kJ·mol^{-1}). The E_a value for first order ethanolysis in literature was reported as 112.97 kJ·mol^{-1}, which significantly greater than E_{a1} and the first order E_a determined in this project [170]. As Zn($\mathbf{2}^{Pr}$)$_2$ exhibited non-Arrhenius behaviour at the tested temperature range it was not possible to obtain reliable fits.

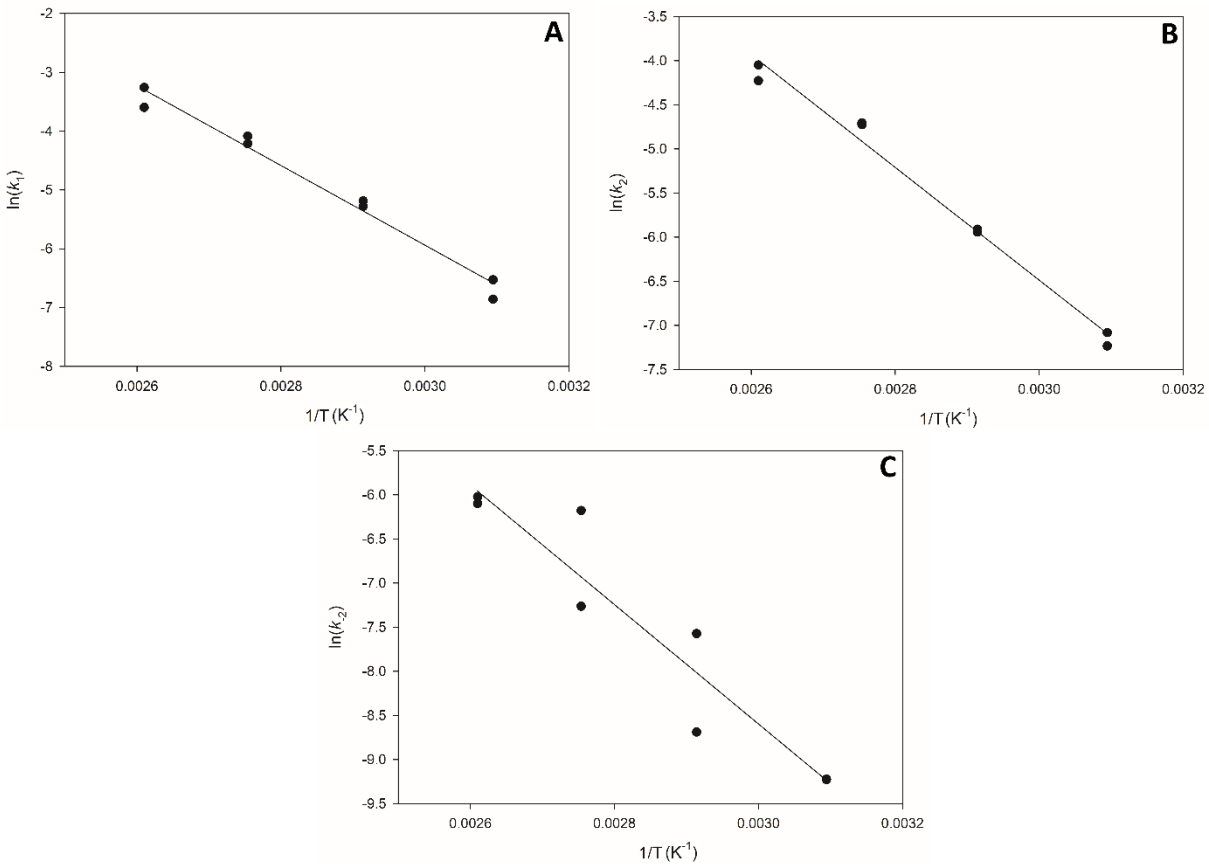

Figure 4.4. Arrhenius plots for ethanolysis of 12.5 g PLA, at 300 rpm, 5 equivalents of EtOH, 9 mol% of Zn(**1**^{Et})$_2$. (**A**) k_1 y = -6778.39x + 14.40 R^2 = 0.980, (**B**) k_2 y = -6393.33x + 12.69 R^2 = 0.986, (**C**) k_{-2} y = -6767.64x + 11.71 R^2 = 0.8986.

4.3 Propanolysis and Kinetics of Propyl Lactate Formation

The propanolysis of PLA is less useful then ethanolysis as its product PrLa has a smaller market share and demand [242]. Nevertheless, PrLa has some uses such as fragrance enhancement in alcoholic beverages [250,251]. PrLa production from the chemical recycling of PLA has environmental benefits in comparison to synthesis from fossil-based sources. The protocol for these experiments is detailed in Section §3.4.1. PLA propanolysis was modelled as a two-step reversible reaction, detailed in Section §3.6. k^{-1}

4.3.1 GC Results

Samples were taken throughout each experiment and analysed by GC. Despite this analysis being only qualitative, a higher GC peak area in a shorter time can be extrapolated to mean a

greater production rate of PrLa. Figure 4.5 shows the GC peak area vs time (min) for the propanolysis of PLA using Zn(**1**^{Et})$_2$ at the temperature range 90 – 130 °C. A clear trend shows a higher temperature resulting in a faster production of PrLa. The times taken to reach a PrLa peak area of 2000 are: 260 min (130 °C), 412 min (110 °C), and 1950 min (90 °C). There is only a small reduction in the rate of PrLa production going from 130 °C to 110 °C, with a significant reduction between 110 °C and 90 °C. The lower operating temperature of 110 °C results in a relatively high PrLa production rate, while also benefiting from lower operating costs and carbon footprint. Despite operation at 90 °C benefiting from lower operating costs the PrLa production rate is likely to be too slow to be viable for industry.

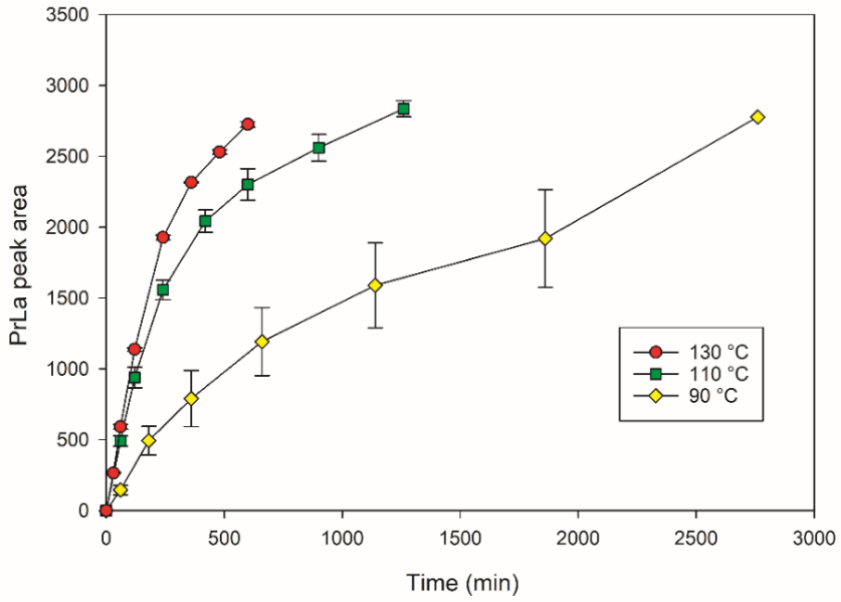

Figure 4.5. Propanolysis of 12.5 g of PLA at 90 – 130 °C, 300 rpm and 1 g Zn(**1**^{Et})$_2$.

Figure 4.6 shows the GC peak area vs time (min) for the propanolysis of PLA using Zn(**2**^{Pr})$_2$ at temperature range 50 – 110 °C. For the most part a higher temperature results in a greater production of PrLa. However, the catalyst Zn(**2**^{Pr})$_2$ displays non-Arrhenius behaviour at temperatures ≤ 70 °C resulting in enhanced initial reaction rates as temperature decreases. Remarkably propanolysis at 50 °C had the greatest PrLa production rate. The reaction times taken to reach a GC peak area of 1000 at each reactor operating temperature are: 194 min (50

°C), 861 min (110 °C), 4250 min (90 °C), and 7999 min (70 °C). There is a significant reduction in the rate of PrLa production between 110 °C to 90 °C, with a smaller reduction between 90 °C to 70 °C. The reduction in rate between 90 °C to 70 °C is smaller than expected. This can be attributed to the non-Arrhenius behaviour exhibited around and below 70 °C. Similarly to Zn(**2**^{Pr})$_2$ ethanolysis, an operating temperature of 50 °C produced the greatest amount of AL in the shortest time. As previously mentioned, quantum tunnelling effects result in sub-Arrhenius kinetics that accelerate the reaction as temperature decreases [189,248,249].

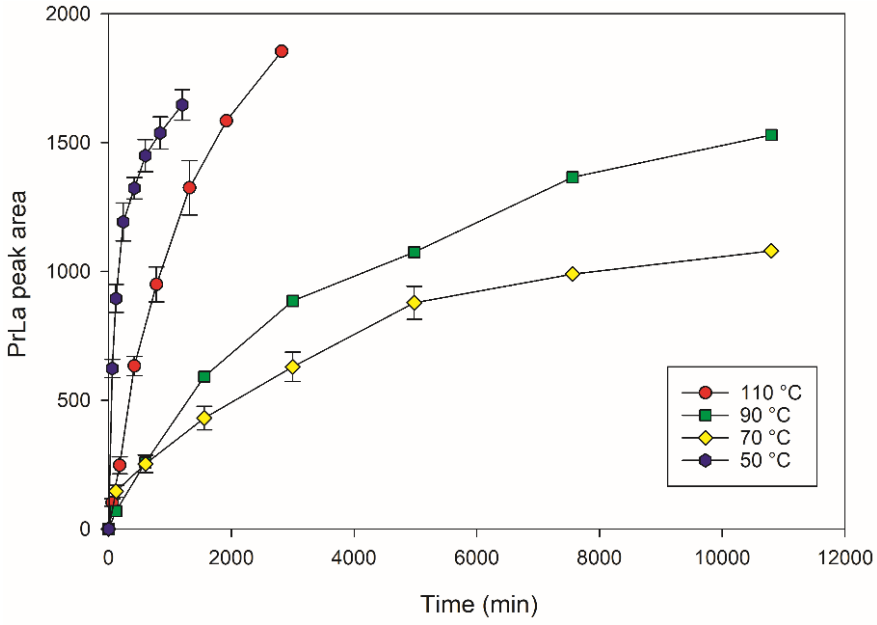

Figure 4.6. Propanolysis of 12.5 g of PLA at 130 – 90 °C, 800 rpm and 1 g Zn(**2**^{Pr})$_2$.

4.3.2 ^{1}H NMR Results

Reaction samples were taken periodically throughout each experiment and analysed by ^{1}H NMR, detailed in Section §3.5.2. The relative concentrations of Int, CE, and AL were fitted to the kinetic model described in equation (3.3) and the resulting rate equations were solved in MATLAB. Reaction profiles using Zn(**1**^{Et})$_2$ at each temperature are shown below in Figure 4.7. At 130 °C a maximum concentration of 51% for CE intermediates was reached at 145 min, and 100% conversion of Int groups was reached at 360 min. At 110 °C a maximum CE

concentration of 50% occurred at 90 min, while 100% conversion of Int groups was reached at 1320 min. At 90 °C a maximum CE concentration of 43% occurred at 120 min, and 100% conversion of Int groups was reached at 2058 min. The reaction profiles show good fits for the experimental data to the kinetic model.

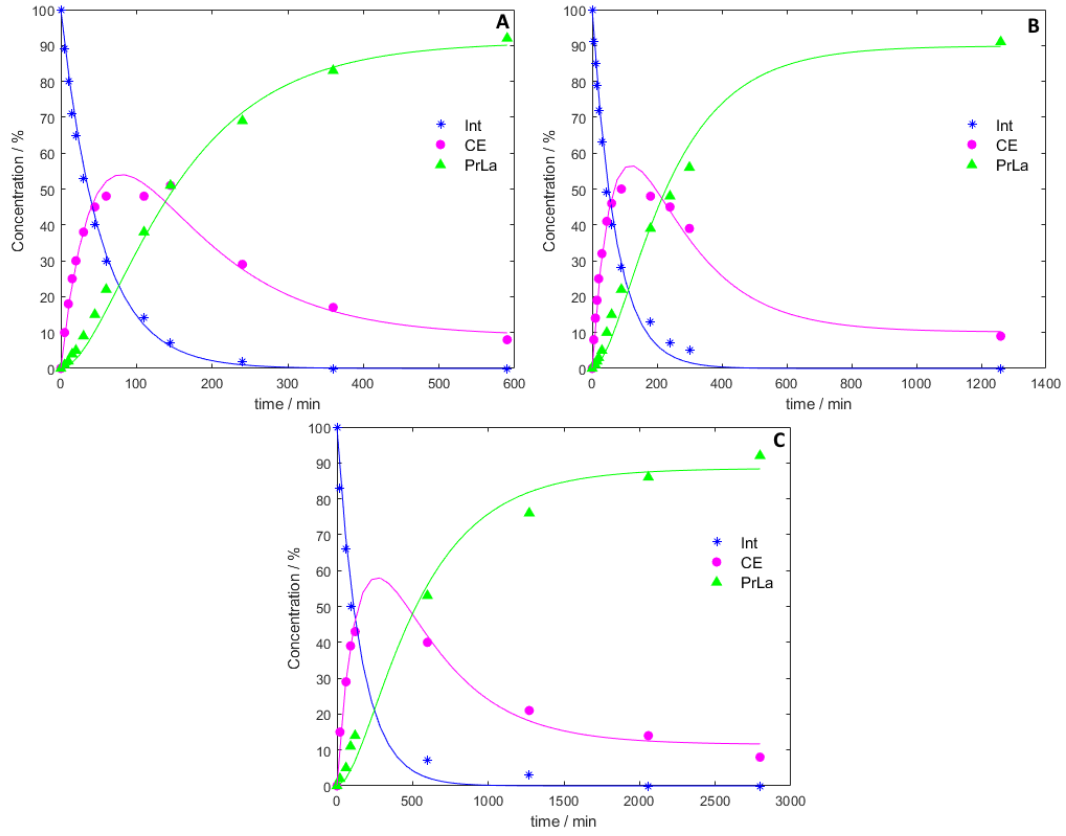

Figure 4.7. Zn(**1**^{Et})$_2$ propanolysis reaction profiles obtained from ^{1}H NMR data fitted in MATLAB. (**A**) = 130 °C, (**B**) = 110 °C, (**C**) = 90 °C.

Conversion selectivity and yield of AL were calculated at 60 min for both sets of experiments using Zn(**1**^{Et})$_2$ or Zn(**2**^{Pr})$_2$. Averages for X_{Int}, S_{AL} and Y_{AL}, at each temperature were determined to allow for easier comparison, as shown in Table 4.4. Comparing the averages for Zn(**1**^{Et})$_2$ there is a clear trend that a higher temperature resulted in higher values of X_{Int}, S_{AL}, and Y_{AL}. For Zn(**1**^{Et})$_2$ at 130 °C the average X_{Int}, S_{AL}, and Y_{AL} values were 66%, 70%, and 46% respectively. In comparison, for Zn(**2**^{Pr})$_2$ at 130 °C the average X_{Int}, S_{AL}, and Y_{AL}, were only 24%, 7%, and 2% respectively. Zn(**2**^{Pr})$_2$ exhibits a lower rate of AL production than Zn(**1**^{Et})$_2$ at high

temperatures, generating smaller yields of AL at 110 °C and 90 °C. At 50 °C Zn($\mathbf{2}^{Pr}$)$_2$ outperformed Zn($\mathbf{1}^{Et}$)$_2$ at 110 °C, achieving average X_{Int}, S_{AL}, and Y_{AL} values of 78%, 56%, and 44% respectively. In comparison to Zn($\mathbf{1}^{Et}$)$_2$ at 130 °C, Zn($\mathbf{2}^{Pr}$)$_2$ at 50 °C generated a greater X_{Int} but smaller S_{AL} and Y_{AL}. As previously stated, the equilibrium from Zn($\mathbf{2}^{Pr}$)$_2$ at 50 °C appears to lie more to the left, favouring the formation of CE over the formation of AL.

Table 4.4. PLA propanolysis using Zn($\mathbf{1}^{Et}$)$_2$ (300 rpm 90 – 130 °C) or Zn($\mathbf{2}^{Pr}$)$_2$ (800 rpm 50 – 110 °C). Conversion of PLA Int groups, AL selectivity, and AL yield, calculated at 60 min. The data represents averaged repeat experiments (2-3 repeats, excluding Zn($\mathbf{1}^{Et}$)$_2$ 90 °C, and Zn($\mathbf{2}^{Pr}$)$_2$ 90 °C).

Catalyst (1 g, 8 wt%)	**Temperature (°C)**	**Average X_{Int} (%)**	**Average S_{AL} (%)**	**Average Y_{AL} (%)**
Zn($\mathbf{1}^{Et}$)$_2$	130	66	70	46
	110	62	28	18
	90	34	15	5
Zn($\mathbf{2}^{Pr}$)$_2$	110	24	7	2
	90	17	6	1
	70	42	13	6
	50	78	56	44

X_{Int}, S_{AL}, Y_{AL}, are determined at 60 min of reaction.

4.3.3 Activation Energy

The relative concentrations determined in Section §4.3.2 were fitted to the experimental model, equation (3.3) described in Section §3.6. The rate equations (3.4 – 3.6) were solved in MATLAB generating estimates of rate coefficients for the fitted experimental data at different temperatures, shown in Table 4.5.

Table 4.5. Estimated rate coefficients for each propanolysis experiment.

Catalyst (1 g, 8 wt%)	**Temperature (°C)**	**k_1 (min^{-1})**	**k_2 (min^{-1})**	**k_{-2} (min^{-1})**
Zn($\mathbf{1}^{Et}$)$_2$	130	1.91×10^{-2}	7.98×10^{-3}	7.86×10^{-4}
	130	1.50×10^{-2}	7.60×10^{-3}	7.64×10^{-4}
	110	1.37×10^{-2}	5.01×10^{-3}	5.64×10^{-4}
	110	1.50×10^{-2}	6.83×10^{-3}	5.17×10^{-4}
	90	6.38×10^{-3}	2.32×10^{-3}	4.14×10^{-4}

The estimated rate coefficients were used to generate Arrhenius plots for PLA propanolysis using Zn(**1**^{Et})$_2$, shown in Figure 4.8. These reactions were carried out in the temperature range 90 – 130 °C. The resulting activation energies are: E_{a1} = 27.5 ± 24.7 kJ·mol^{-1}, E_{a2} = 34.7 ± 25.6 kJ·mol^{-1}, and $E_{a\text{-}2}$ = 19.5 ± 6.4 kJ·mol^{-1}. The experimental data shows a reasonable fit, with each Arrhenius plot having $R^2 \geq 0.807$. The estimated activation energies highlight that E_{a2} has the greatest range, with upper and lower bound values ± 25.6 kJ·mol^{-1}. The activation energy for propanolysis was also determined according to first order kinetics, where only the initial cleave of Int groups was considered. The integrated rate equation was plotted resulting in a linear graph with a negative gradient, detailed in Appendix §8.2.1. The first order E_a was calculated to be 37.3 ± 23.6 kJ·mol^{-1}. While this value is slightly greater than the value for E_{a1} (27.5 ± 24.7 kJ·mol^{-1}) they overlap within their confidence intervals. The first order kinetics was calculated to allow for comparison with reported literature activation energies for PLA alcoholysis which all assumed first order kinetics.

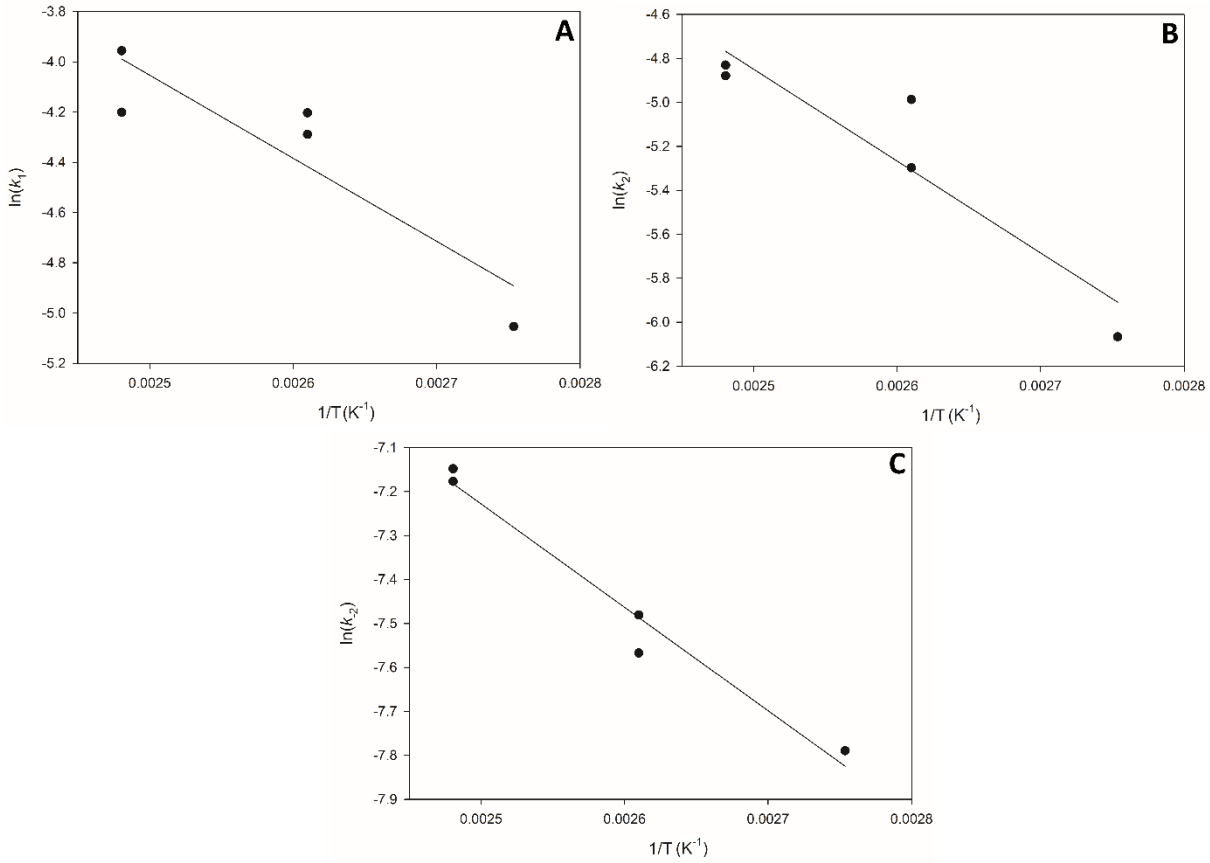

Figure 4.8. Arrhenius plots for propanolysis of 12.5 g PLA, at 300 rpm, 4 equivalents of PrOH, 9 mol% of Zn(**1**^{Et})$_2$. (**A**) k_1 y = -3307.33x + 4.22 R^2 = 0.8075, (**B**) k_2 y = -4177.86x + 5.60 R^2 = 0.8614, (**C**) k_{-2} y = -2351.96x - 1.35 R^2 = 0.9696.

4.4 Butanolysis and Kinetics of Butyl Lactate Formation

The butanolysis of PLA is a less useful than ethanolysis as its product BuLa has a smaller market share and demand [242]. Nevertheless, BuLa has some uses such as solvent for ethyl cellulose, gums, oils, dyes, and paints [252]. Producing BuLa from the chemical recycling of PLA has a lower global warming potential (GWP), in comparison to the synthesis of BuLa from fossil-based sources. The protocol for these experiments is detailed in Section §3.4.1. PLA butanolysis was modelled as a two-step reversible reaction detailed in Section §3.6.

4.4.1 GC Results

Samples were taken throughout each experiment and analysed by GC to determine the concentration of BuLa. Figure 4.9 shows the BuLa concentration (g·mL^{-1}) vs time (min) for the

butanolysis of PLA using Zn($\mathbf{1}^{Et}$)$_2$ at 50 – 130 °C. Experiments were repeated (2 – 4 times) at each temperature and results averaged. A higher temperature resulted in a faster production of BuLa. The times taken to reach an BuLa concentration of 0.04 g·mL^{-1} are: 144 min (130 °C), 301 min (110 °C), 500 min (90 °C), 1519 min (70 °C), and 10096 (50 °C). Initially, there is only a minor reduction in rate of BuLa production decreasing the temperature from 130 °C to 110 °C. However, as the temperature continues to decrease the reduction in production rate increases significantly. The greatest reduction in the rate of BuLa production occurs from 70 °C to 50 °C.

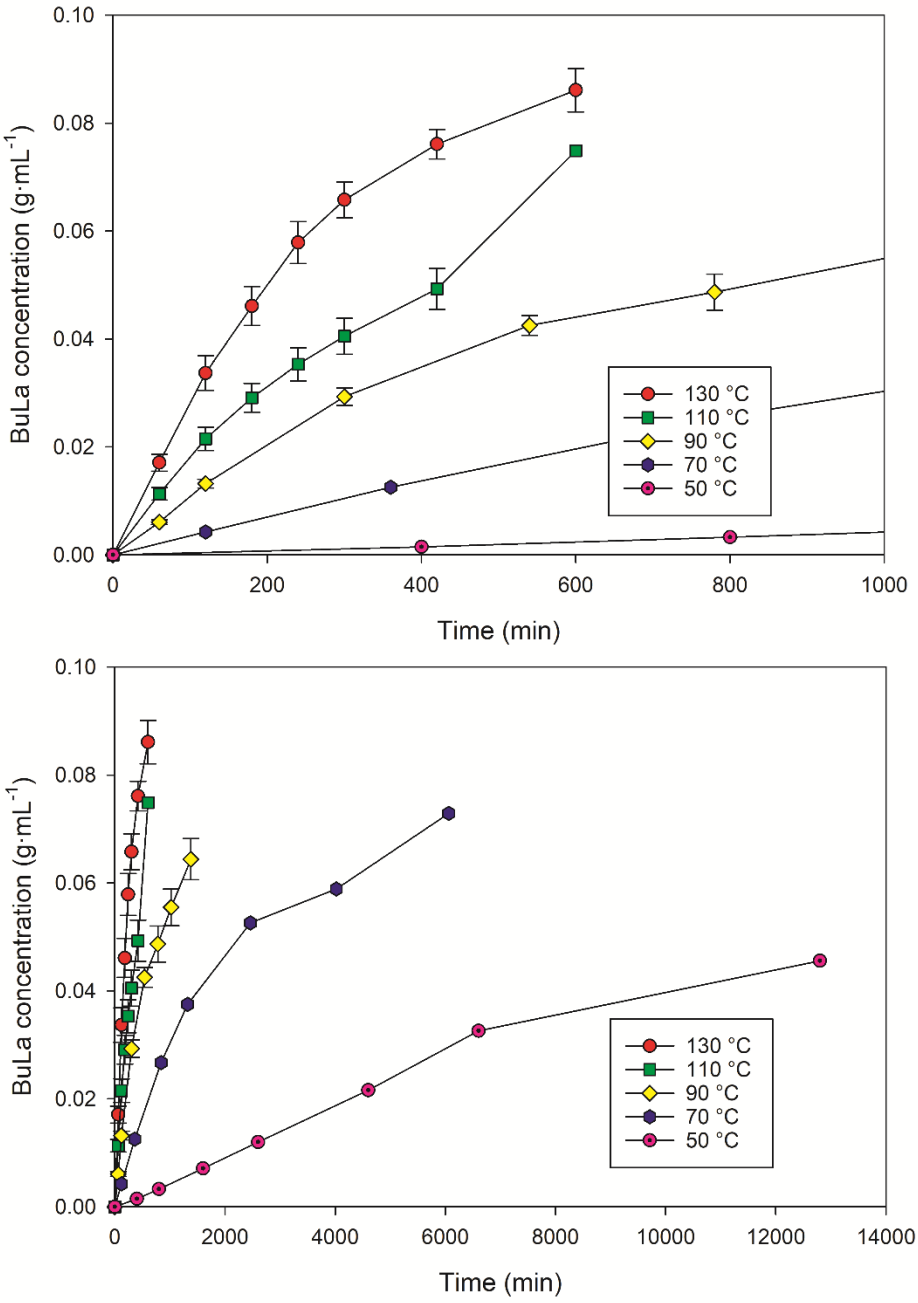

Figure 4.9. Butanolysis of 12.5 g of PLA at 50 – 130 °C, 300 rpm and 1 g Zn(**1**^{Et})$_2$.

Figure 4.10 shows the EtLa concentration (g·mL^{-1}) vs time (min) for the butanolysis of PLA using Zn(**2**^{Pr})$_2$ at 50 – 110 °C. A higher temperature resulted in a greater production rate of BuLa. The times taken to reach an BuLa concentration of 0.04 g·mL^{-1} are: 632 min (110 °C), 1459 min (90 °C), 3045 min (50 °C), and 3337 min (70 °C). There is only a small reduction in the BuLa production rate between 110 °C to 90 °C, with a similar reduction from 90 °C to 70

°C. While reaction at 50 °C displayed an initial production rate greater than at 70 °C its final BuLa concentration plateaued at a lower value. The initial production of BuLa at 70 °C and 50 °C is competitive with 110 °C but quickly falls off past 200 min. While it is evident non-Arrhenius behaviour is taking place at 50 °C, the increase in reaction rate is minor. This is a different result in comparison to ethanolysis and propanolysis at 50 °C. This difference implies that the non-Arrhenius behaviour of the catalyst is affected by its coordination to the alcohol nucleophile. A larger alcohol limits the catalyst's coordination and thus limits its non-Arrhenius effect and increase in activity.

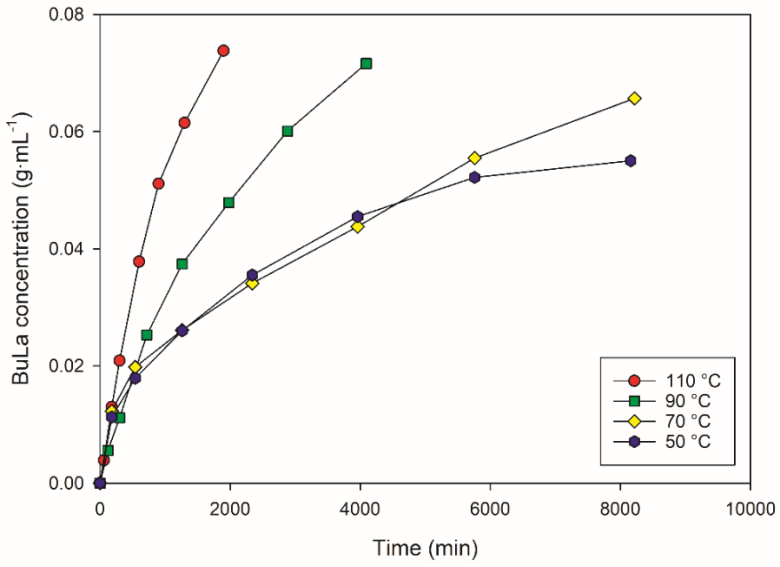

Figure 4.10. Butanolysis of 12.5 g of PLA at 50 – 110 °C, 800 rpm and 1 g Zn(**2**^{Pr})$_2$.

Table 4.6 presents GC data for both catalysts Zn(**1**^{Et})$_2$ and Zn(**2**^{Pr})$_2$ to allow for comparison. Initial rate of BuLa production was determined at 60 min. Zn(**1**^{Et})$_2$ follows a clear trend that a higher temperature results in a higher initial rate of BuLa production. The greatest initial rate of BuLa production 2.85 x 10^{-4} (g·mL^{-1}·min^{-1}) was achieved by Zn(**1**^{Et})$_2$ at 130 °C. The rate of BuLa production approximately doubles with every 20 °C increase in temperature. Zn(**2**^{Pr})$_2$ follows an opposite trend, lower temperatures result in higher rates of BuLa production.

Table 4.6. Butanolysis of 12.5 g PLA, using 9 mol% of either Zn($\mathbf{1}^{Et}$)$_2$ (300 rpm 50 – 130 °C) or Zn($\mathbf{2}^{Pr}$)$_2$ (800 rpm 50 – 110 °C), using 3 equivalents of BuOH. The data representative averages of repeat experiments (2-4 repeats, excluding Zn($\mathbf{1}^{Et}$)$_2$ 70 °C and Zn($\mathbf{2}^{Pr}$)$_2$).

Catalyst (1 g, 8 wt%)	**Temperature (°C)**	**Final time (min)**	**Final EtLa concentration (g·mL^{-1})**	**Initial rate of BuLa production (g·mL^{-1}·min^{-1})**
Zn($\mathbf{1}^{Et}$)$_2$	130	1062	0.0943	2.85 x 10^{-4}
	110	2312	0.0685	1.40 x 10^{-4}
	90	2978	0.0793	9.24 x 10^{-5}
	70	6066	0.0731	4.24 x 10^{-5}
	50	4590	0.0173	8.30 x 10^{-6}
Zn($\mathbf{2}^{Pr}$)$_2$	110	2898	0.0754	4.42 x 10^{-5}
	90	3306	0.0645	5.78 x 10^{-5}
	70	8670	0.0674	1.56 x 10^{-4}
	50	8160	0..0550	1.26 x 10^{-4}

4.4.2 ^{1}H NMR Results

Reaction samples were taken periodically throughout each experiment and analysed by ^{1}H NMR, detailed in Section §3.5.2. The relative concentrations of Int, CE, and AL were fitted to the kinetic model described in equation (3.3) and the resulting rate equations were solved in MATLAB. Reaction concentration *versus* time profiles using Zn($\mathbf{1}^{Et}$)$_2$ at each temperature are shown in Figure 4.11. At 130 °C a maximum CE concentration of 47% occurred at 120 min; 100% conversion of Int groups was reached at 240 min. A maximum CE concentration of 48% occurred at 120 min for 110 °C; 100% conversion of Int groups was reached at 1143 min. A maximum CE concentration of 44% was reached at 582 min for 90 °C; 100% conversion of Int groups was reached at 2862 min. At 70 °C a maximum CE concentration of 48% occurred at 2760 min; 87% conversion of Int groups was reached at 6066 min. At 50 °C a maximum CE concentration of 41% was reached at 5730 min, while 70% conversion of Int groups was reached at 5730 min (not shown in figure). The reaction profiles at 130 °C, 110 °C, and 90 °C, show good fits for the experimental data to the kinetic model. While 70 °C shows a poor fits,

this is likely due to the time scale of the reaction. At 70 °C the reactions are extremely slow, necessitating long reaction times of many hours. These reactions should have been run for longer to capture the reaction completion. Running the reaction to completion and taking fewer samples at the start would allow for better spacing of the sample intervals which should produce better fitting graphs.

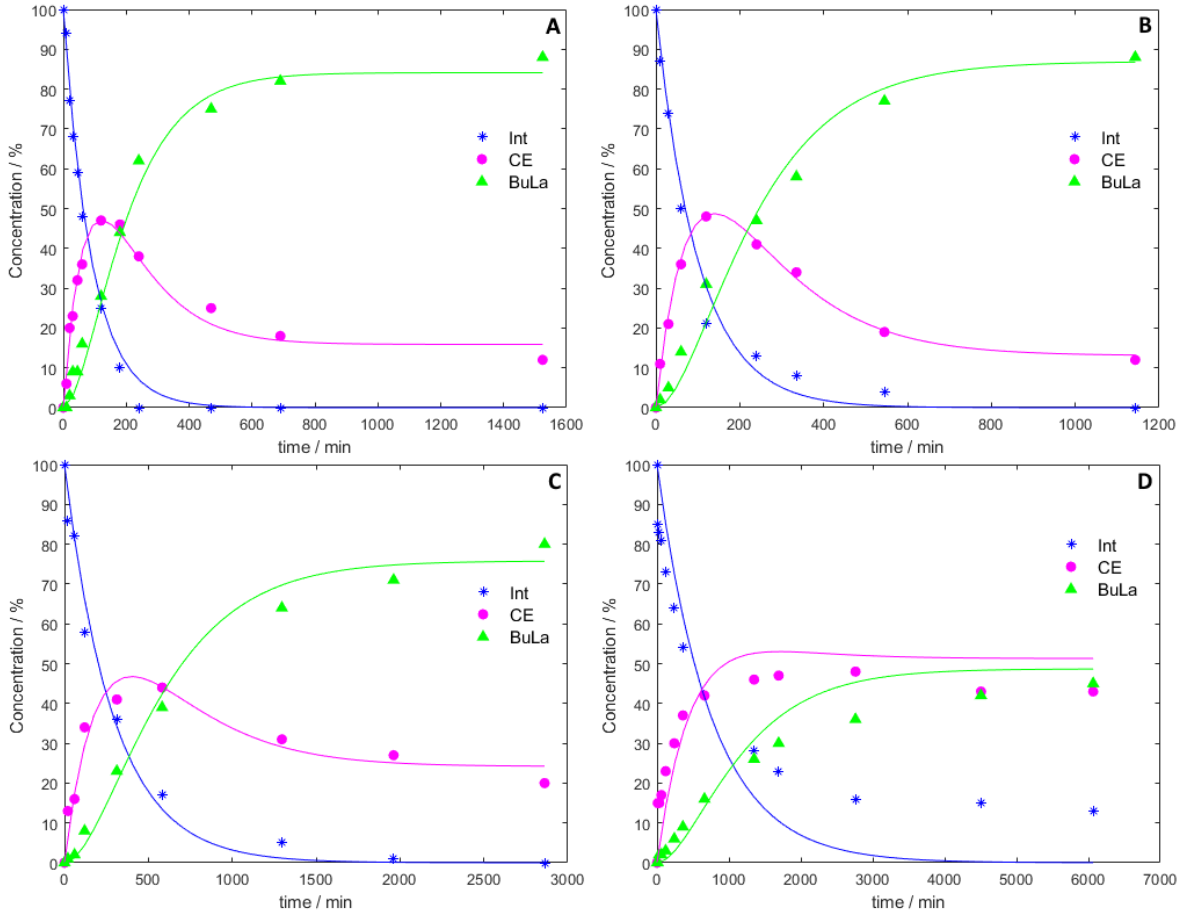

Figure 4.11. Zn(**1**^{Et})$_2$ butanolysis reaction profiles obtained from ^{1}H NMR data fitted in MATLAB. (**A**) = 130 °C, (**B**) = 110 °C, (**C**) = 90 °C, (**D**) = 70 °C.

Conversion selectivity and yield of AL were calculated at 60 min for both sets of experiments using Zn(**1**^{Et})$_2$ or Zn(**2**^{Pr})$_2$. Averages for X_{Int}, S_{AL}, and Y_{AL}, at each temperature were determined to allow for easier comparison, as shown in Table 4.7. Comparing the averages for Zn(**1**^{Et})$_2$ there is a clear trend that a higher temperature results in higher values of X_{Int}, S_{AL}, and Y_{AL}. At 110 °C the average values of X_{Int}, S_{AL}, and Y_{AL}, were 34%, 19%, and 7% respectively. In

comparison for Zn(**2**^{Pr})$_2$ at 110 °C the average X_{Int}, S_{AL}, and Y_{AL}, were only 25%, 4%, and 1% respectively. While Zn(**2**^{Pr})$_2$ exhibits a lower rate of AL production than Zn(**1**^{Et})$_2$ at high temperatures, its non-Arrhenius behaviour produces higher reaction rates at lower temperatures. Zn(**2**^{Pr})$_2$ at 50 °C outperformed Zn(**2**^{Pr})$_2$ at 110 °C, achieving average values of X_{Int}, S_{AL}, and Y_{AL}, of 54%, 17%, and 9%, respectively.

Table 4.7. PLA butanolysis using Zn(**1**^{Et})$_2$ (300 rpm 50 – 130 °C) or Zn(**2**^{Pr})$_2$ (800 rpm 50 – 110 °C). Conversion of PLA Int groups, AL selectivity, and AL yield, calculated at 60 min. The data represents averaged repeat experiments (2-4 times, excluding Zn(**1**^{Et})$_2$ 70 °C, and Zn(**2**^{Pr})$_2$).

Catalyst (1 g, 8 wt%)	**Temperature (°C)**	**Average X_{Int} (%)**	**Average S_{AL} (%)**	**Average Y_{AL} (%)**
Zn(**1**^{Et})$_2$	130	59	29	17
	110	34	19	7
	90	29	15	5
	70	19	11	2
	50	2	0	0
Zn(**2**^{Pr})$_2$	110	25	4	1
	90	27	7	2
	70	53	19	10
	50	54	17	9

X_{Int}, S_{AL}, Y_{AL}, are determined at 60 min of reaction.

4.4.3 Activation Energy

The relative concentrations determined in Section §4.4.2 were fitted to the experimental model equation (3.3) described in Section §3.6. The rate equations (3.4 – 3.6) were solved in MATLAB, generating estimates of rate coefficients for the fitted experimental data at different temperatures, shown in Table 4.8.

Table 4.8. Estimated rate coefficients for each butanolysis experiment.

Catalyst (1 g, 8 wt%)	Temperature (°C)	k_1 (min^{-1})	k_2 (min^{-1})	k_{-2} (min^{-1})
	130	1.11×10^{-2}	6.85×10^{-3}	1.29×10^{-3}
	130	1.65×10^{-2}	7.17×10^{-3}	9.26×10^{-4}
	110	7.39×10^{-3}	3.50×10^{-3}	1.50×10^{-3}
	110	2.92×10^{-3}	1.79×10^{-3}	9.79×10^{-4}
	110	3.05×10^{-3}	1.94×10^{-3}	1.12×10^{-3}
	110	9.93×10^{-3}	5.57×10^{-3}	8.36×10^{-4}
$Zn(\mathbf{1}^{Et})_2$	90	3.44×10^{-3}	2.29×10^{-3}	7.32×10^{-4}
	90	3.49×10^{-3}	1.83×10^{-3}	8.23×10^{-4}
	90	7.96×10^{-3}	4.34×10^{-3}	1.15×10^{-3}
	70	1.33×10^{-3}	9.55×10^{-4}	1.01×10^{-3}
	50	2.20×10^{-4}	2.74×10^{-4}	2.24×10^{-4}
	50	2.19×10^{-4}	2.64×10^{-4}	2.35×10^{-4}

The estimated rate coefficients were used to generate Arrhenius plots for PLA butanolysis using $Zn(\mathbf{1}^{Et})_2$, shown in Figure 4.12.

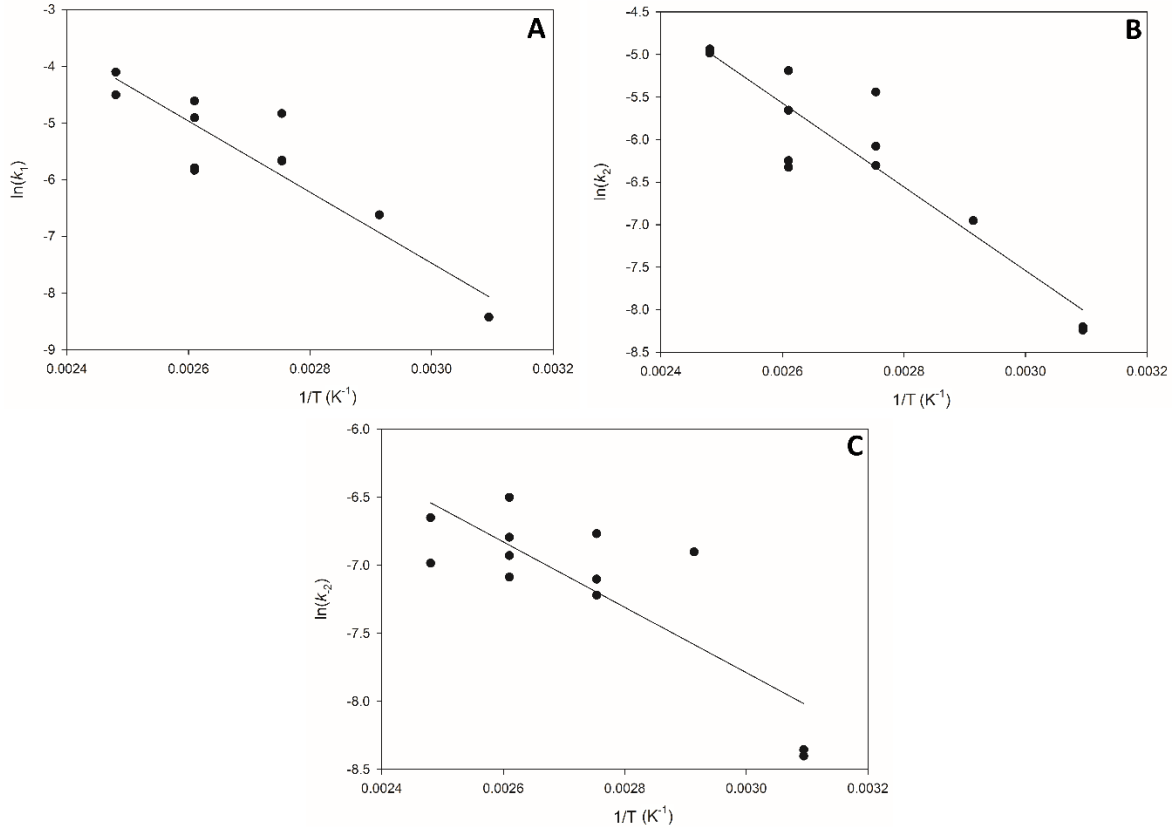

Figure 4.12. Arrhenius plots for butanolysis of 12.5 g PLA, at 300 rpm, 3 equivalents of BuOH, 9 mol% of $Zn(\mathbf{1}^{Et})_2$. (**A**) k_1 y = -6264.44x + 11.32 R^2 = 0.8550, (**B**) k_2 y = -4918.42x + 7.22 R^2 = 0.8508, (**C**) k_{-2} y = -2403.92x – 0.5779 R^2 = 0.6793.

These reactions were carried out in the temperature range 50 – 130 °C. The resulting E_a are: E_{a1} = 52.0 ± 15.1 kJ·mol^{-1}, E_{a2} = 40.9 ± 12.1 kJ·mol^{-1}, and $E_{a\text{-}2}$ = 20.0 ± 9.7 kJ·mol^{-1}. The experimental data for k_1 and k_2 show a reasonable fit; each Arrhenius plot has $R^2 \geq 0.8508$. k_{-2} has only a moderate fit with its coefficient of regression, $R^2 = 0.6793$. E_{a1} has the greatest range, with upper and lower bound values ± 15.104 kJ·mol^{-1}. The lower R^2 values in comparison to ethanolysis and propanolysis are likely due to the incomplete conversion in the low temperature butanolysis experiments, leading to a less comprehensive dataset than the faster reactions with shorter chain alcohols. Similarly to the previous sections, first order kinetics were also calculated for butanolysis where only the initial cleavage of Int groups is considered. The first order E_a was calculated to be 52.7 ± 17.7 kJ·mol^{-1}, which is similar to the value determined for E_{a1} (52.0 ± 15.1 kJ·mol^{-1}). The E_a value for first order butanolysis in literature was reported to be 58.88 kJ·mol^{-1}, which is in line with both E_{a1} and the first order E_a determined in this project [170].

4.5 Comparison of Alcoholysis using EtOH, PrOH, and BuOH

Reaction samples were analysed by ^{1}H NMR allowing for the calculation of relative concentrations of Int, CE, and AL groups during each reaction. The relative concentration of AL formed during Zn(**1**^{Et})$_2$ catalysed alcoholysis of PLA is shown in Figure 4.13. The figure shows the comparison of using either EtOH, PrOH, or BuOH, at 110 °C. Regardless of the alcohol used, each reaction reaches a final relative concentration of around 90%. At this concentration the reaction has reached equilibrium. EtOH displayed the fastest reaction, generating AL concentration of 90% in the shortest time. The next fastest was PrOH, followed by BuOH. These data support the working hypothesis that longer chain alcohols sterically hinder alcoholysis reactions.

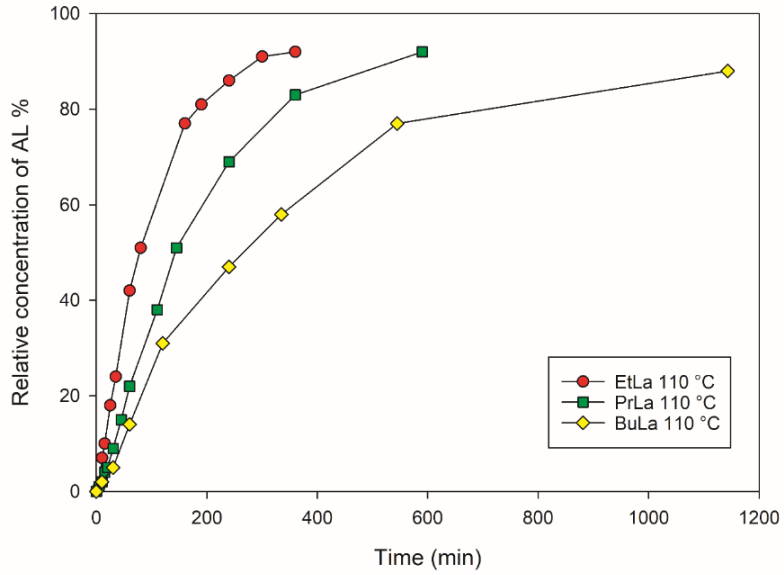

Figure 4.13. Alcoholysis of 12.5 g of PLA at 110 °C, using 50 mL of either EtOH, PrOH, or BuOH, and 1 g Zn(**1**^{Et})$_2$ (300 rpm). Relative concentration of each AL was determined by ^{1}H NMR.

The relative concentration of AL formed during Zn(**2**^{Pr})$_2$ catalysed alcoholysis of PLA is shown in Figure 4.14. Comparing the different alcohol reactions at 110 °C, EtOH displayed the fastest reaction while PrOH and BuOH displayed similar production rate. Comparing the different alcohol reactions at 50 °C, EtOH displayed the faster production rate followed by PrOH and BuOH.

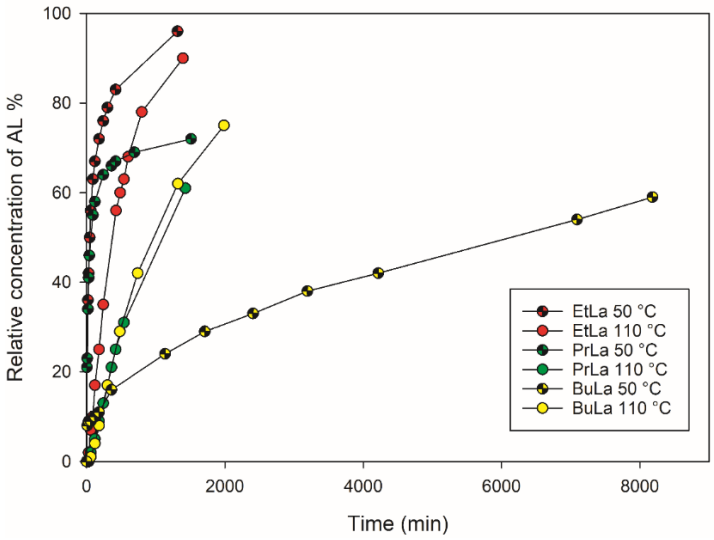

Figure 4.14. Alcoholysis of 12.5 g of PLA at 50 °C and 110 °C, using 50 mL of either EtOH, PrOH, or BuOH, and 1 g Zn(**2**^{Pr})$_2$ (800 rpm). Relative concentration of AL was determined by ^{1}H NMR.

The rates observed with Zn($\mathbf{2}^{Pr}$)$_2$ catalysed alcoholysis support the working hypothesis that longer chain alcohols results in slower alcoholysis. EtOH and PrOH reactions at 50 °C performed better than their counterparts at 110 °C, reaching a higher concentration of AL in a shorter time. BuOH showed the opposite trend: a higher concentration of AL was reached in a shorter time at 110 °C instead of 50 °C. As previously discussed, Zn($\mathbf{2}^{Pr}$)$_2$ exhibits non-Arrhenius behaviour at temperatures ≤ 70 °C. For both EtOH and PrOH reactions at 50 °C, the Zn($\mathbf{2}^{Pr}$)$_2$ non-Arrhenius behaviour causes a significant increase in the reaction rate compared with the higher temperatures studied. Interestingly, EtOH and PrOH at 50 °C have very similar initial rates of AL production. PrLa relative concentration levels off at 70% whereas EtLa relative concentration levels off at around 90%. BuOH at 50 °C had a similar initial rate of AL production but by 30 min the rate had decreased significantly. The relative concentration for BuOH levels off around 60%. To explain why significant non-Arrhenius behaviour is not observed with BuOH at 50 °C, as discussed earlier it could be that its larger molecular size sterically hinders its coordination with the catalyst intermediate.

The activation energies for EtOH, PrOH, and BuOH alcoholysis using Zn($\mathbf{1}^{Et}$)$_2$ are shown in Table 4.9. Comparing E_{a1} for each alcohol, EtOH displayed the greatest value followed by BuOH, and PrOH. This seems counter to the results of Figure 4.13, where ethanolysis generated a greater relative concentration of AL in a shorter time in comparison to propanolysis and butanolysis. This can be explained by the value for E_{a2} and $E_{a\text{-}2}$. For both PrOH and BuOH the value for $E_{a\text{-}2}$ is lower than E_{a2}. A smaller value for $E_{a\text{-}2}$ means the equilibrium lies to the left, favouring the transformation of AL to CE intermediate. While a lower value of E_{a1} means initial cleavage of the PLA chains occurs quicker in PrOH and BuOH, their equilibrium step favours CE formation which explains why a greater AL production rate is seen using EtOH. Alcoholysis using EtOH had an $E_{a\text{-}2}$ greater than E_{a2} favouring AL formation, whereas PrOH and BuOH had

a $E_{a\text{-}2}$ smaller than E_{a2}. This is reflected in their average yields of AL: at 110 °C the Y_{AL} was 37%, 18% and 7% respectively (Table 4.2, Table 4.4, and Table 4.7).

Table 4.9. The activation energies for each step of PLA alcoholysis.

Alcoholysis	E_{a1} (kJ·mol^{-1})	E_{a2} (kJ·mol^{-1})	$E_{a\text{-}2}$ (kJ·mol^{-1})
EtOH	56.33 ± 8.04	53.13 ± 6.43	56.24 ± 18.88
PrOH	27.48 ± 24.66	34.71 ± 25.6	19.54 ± 6.36
BuOH	52.06 ± 15.104	40.87 ± 12.06	19.97 ± 9.68

4.6 Conclusions

In this chapter, a reliable system was designed for the alcoholysis of PLA using two synthesised catalysts Zn(**1**^{Et})$_2$ and Zn(**2**^{Pr})$_2$. EtOH, PrOH, and BuOH, were used as reactants to generate various AL products. The Zn(**1**^{Et})$_2$ reactions followed the trend that a higher temperature resulted in a higher AL production rate. The Zn(**2**^{Pr})$_2$ reactions followed a similar trend at higher temperatures ≥ 90 °C; however, at lower temperatures Zn(**2**^{Pr})$_2$ displayed non-Arrhenius behaviour, where the reaction rate coefficients increase as temperature decreases. This non-Arrhenius phenomenon was observed only in Zn(**2**^{Pr})$_2$ reactions but not Zn(**1**^{Et})$_2$ reactions. McKeown *et al*. reported Zn(**2**^{Pr})$_2$ undergoes ligand dissociation and formation of a new species, this new species facilitates quantum tunnelling effects accelerating the reaction as temperature decreases [188]. According to Table 4.1 and Table 4.6, Zn(**1**^{Et})$_2$ had the greatest initial production of AL at all temperatures ≥ 90 °C. At temperatures ≤ 70 °C, Zn(**2**^{Pr})$_2$ displayed the greatest initial production of AL. For both catalysts, increasing the alcohol chain length decreased the AL production rate. The remarkable non-Arrhenius behaviour of Zn(**2**^{Pr})$_2$ allows for relatively high rates of AL production to be achieved at temperatures as low as 50 °C. However, the catalyst is less stable, and its reactions are less reproducible in comparison to Zn(**1**^{Et})$_2$.

Two kinetic models were successfully applied to fit the relative concentration of the reaction mixtures. A simple first order model was considered as well as a consecutive reaction model

with the second step being in equilibrium. Activation energies were determined using both kinetic models for ethanolysis, propanolysis, and butanolysis using Zn($\mathbf{1}^{Et}$)$_2$. The activation energy for the initial cleavage of PLA during ethanolysis was determined to be E_{a1} = 56.3 ± 8.0 kJ·mol^{-1}, this value is significantly lower than what was found in literature E_a = 112.97 kJ·mol^{-1} [170]. However, the activation energy for butanolysis E_{a1} = 52.0 ± 15.1 kJ·mol^{-1}, is similar to what was reported in literature E_a = 58.88 1 kJ·mol^{-1} [170]. The activation energy for propanolysis was determined to be E_{a1} = 27.5 ± 24.7 kJ·mol^{-1}; the lack of literature means a comparison cannot be made. Zn($\mathbf{1}^{Et}$)$_2$ has potential in industry as a robust and active catalyst for the chemical recycling (alcoholysis) of PLA to generate a range of ALs.

Chapter 5 – Synergistic Dual Catalytic System and Kinetics for the Alcoholysis of Poly(Lactic Acid)

5.1 Chapter Overview

This Chapter describes the investigation of two commercially available catalysts and their synergistic effect on the alcoholysis of PLA. The catalysts $Zn(OAc)_2$ and DMAP were tested both individually and in mixtures. Both MeOH and EtOH were tested but methanolysis was explored further to determine its activation energies. Prof. Andrew Dove (the School of Chemistry at the University of Birmingham) provided help in the original discussion of synergistic dual catalysis. The experimental data were fitted to a simplified kinetic model (equation 7 – 10) detailed in Section §3.6. This chapter is based on the publication, Synergistic Dual Catalytic System and Kinetics for the Alcoholysis of Poly(Lactic Acid) [13].

There are several studies that have investigated the use of dual catalysts, exploiting synergistic effects to obtain enhanced reaction rates [223–225]. Synergistic catalysts can lead to unprecedented reactivities which are not possible using either catalyst alone. This enhanced reactivity has potential to be utilized in chemical recycling, increasing product yield, thus making the overall process more economically viable [223–226]. Typically, dual catalyst systems consist of a transition metal complex coupled with an organocatalyst. A synergistic catalyst complex will only form if there is a great enough difference in pK_a between the two catalysts. Dual catalysis has recently been applied to the chemical recycling of polyesters [231]. Dove *et al.* reported a synergistic effect for $Zn(OAc)_2$ coupled with DMAP resulting in an increased PET depolymerisation rate [232]. There is no prior published literature concerning dual catalysis for the chemical recycling of PLA. The work reported here extends these studies by using mixtures of $Zn(OAc)_2$ and DMAP for PLA alcoholysis. As $Zn(OAc)_2$ and DMAP are commercially available they have the advantage over $Zn(\mathbf{1}^{Et})_2$ and $Zn(\mathbf{2}^{Pr})_2$ as they do not need

to be synthesised, moreover they would be easier to add to a scaled up reaction. The experiments were carried out in the 300 mL Parr autoclave reactor in a semi-batch manner through the addition of alcohol, described in Section §3.4.2. This chapter is structured first by the preliminary methanolysis experiments in Section §5.2 that tested different catalyst mixtures. This is followed by dual catalyst alcoholysis in Section §5.3, which is subdivided into GC results, ^{1}H NMR results, and activation energy (E_a). Finally, Section §5.4 summaries this investigation and establishes a conclusion.

5.2 Preliminary Mixed Catalyst Methanolysis

Preliminary methanolysis experiments were carried out that tested mixtures of $Zn(OAc)_2$ and DMAP in addition to single catalyst reactions. If a synergistic relationship between the catalysts exists, then the dual catalyst experiments would have enhanced reaction rates in comparison to single catalyst experiments. Mixtures of each catalyst (always totalling 0.1 g, 5 wt%) and single catalyst (0.1 g) methanolysis reactions were carried out and analysed by GC, described in Section §3.5.1. Table 5.1 shows the results of each reaction and the initial rate of MeLa production (determined at 60 min). Comparing both single catalyst reactions, methanolysis using 0.1 g $Zn(OAc)_2$ outperformed 0.1 g DMAP by more than double the production rate (5.53×10^{-4} vs 2.45×10^{-4} $g \cdot mL^{-1} \cdot min^{-1}$). $Zn(OAc)_2$ appears to be the superior catalyst in addition to being cheaper than DMAP. Furthermore, $Zn(OAc)_2$ is significantly less toxic than DMAP displaying a much smaller LD_{50} [253,254].

Table 5.1. Methanolysis of PLA at 130 °C and 300 rpm, effect of different amounts of catalyst on; final time (min), final MeLa concentration (%), initial rate of production of MeLa ($g \cdot mL^{-1} \cdot min^{-1}$).

Catalyst (total 0.1 g, 5 wt%)		**Catalyst (mol%)**		**Final time (min)**	**Final MeLa concentration ($g \cdot mL^{-1}$)**	**Initial Rate of Production of MeLa ($g \cdot mL^{-1} \cdot min^{-1}$)**
$Zn(OAc)_2$	**DMAP**	**$Zn(OAc)_2$**	**DMAP**			
0	0.1	0	2.9	300	0.0498	2.45×10^{-4}
0.025	0.075	0.4	2.2	80	0.0543	8.20×10^{-4}
0.05	0.05	0.8	1.5	80	0.0563	8.50×10^{-4}
0.075	0.025	1.2	0.8	120	0.0574	8.38×10^{-4}
0.1	0	1.6	0	180	0.0516	5.53×10^{-4}

Converting each catalyst into mol% (relative to PLA ester groups) 0.1 g of $Zn(OAc)_2$ = 1.6 mol% and 0.1 g of DMAP = 2.9 mol%, detailed in Appendix §8.3.2. This means superior rates were achieved with 0.1 g $Zn(OAc)_2$ despite the PLA ester groups effectively seeing fewer $Zn(OAc)_2$ molecules than in the 0.1 g DMAP experiment. The 0.075 g $Zn(OAc)_2$ / 0.025 g DMAP experiment had a higher initial rate of production of MeLa than the 0.025 g $Zn(OAc)_2$ / 0.075 g DMAP experiment (8.38×10^{-4} and 8.2×10^{-4} $g \cdot mL^{-1} \cdot min^{-1}$ respectively). This result along with the single catalyst reactions further confirms that $Zn(OAc)_2$ is a more active catalyst towards PLA methanolysis than DMAP. The greatest production rate was exhibited by the 0.05g $Zn(OAc)_2$ / 0.05 g DMAP experiment (8.50×10^{-4} $g \cdot mL^{-1} \cdot min^{-1}$). In terms of catalyst mechanisms DMAP coordinates to the nucleophilic alcohol bringing it closer for attack, while its proton in the *ortho*-position activates the ester carbonyl [182]. $Zn(OAc)_2$ initiates transesterification through initial coordination to the alcohol nucleophile followed by a carboxylate shift and coordination to the ester carbonyl [255]. A proposed mechanism for both catalysts is shown in Figure 5.1.

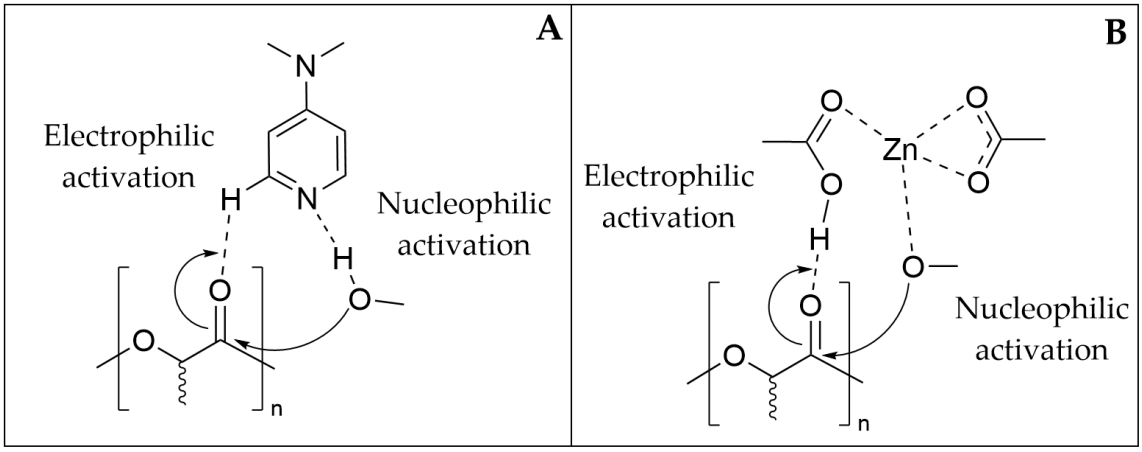

Figure 5.1. Proposed mechanism showing PLA ester electrophilic activation and alcohol nucleophilic activation for **A)** DMAP, and **B)** $Zn(OAc)_2$.

If DMAP is used alongside $Zn(OAc)_2$ the reaction rate increases significantly in comparison to $Zn(OAc)_2$ alone. This implies there is a synergetic effect between the catalysts that enhances the overall reaction rate. This is considered a type II transformation as either of the catalysts alone will lead to the formation of the final product but at a slower rate [225]. Using an equal mass of both catalysts elicited the highest initial rate of production of MeLa, suggesting that a synergetic effect is strongest when there is an equal weight of both catalysts. Both catalysts work by coordinating with the nucleophilic alcohol and PLA ester groups. They are partially cooperative as they both compete to coordinate with the alcohol and ester groups. As there is an excess of alcohol and ester groups in comparison to catalyst molecules their competition to coordinate becomes negligible.

Different stirring speeds were investigated for dual catalysis to see if it influenced their synergistic relationship. Table 5.2 shows the GC results obtained from PLA methanolysis using 0.075 g $Zn(OAc)_2$ / 0.025 g DMAP, at 130°C, and at different stirring speeds. The slowest MeLa production rate was exhibited at stirring speeds 200 and 400 rpm (4.95×10^{-4} and 6.27×10^{-4} $g \cdot mL^{-1} \cdot min^{-1}$ respectively). A stirring speed of 0 rpm generated a greater production rate (7.15×10^{-4} $g \cdot mL^{-1} \cdot min^{-1}$). While increasing the stirring speed to 700 rpm slightly increased the

production rate (7.3 x 10^{-4} g·mL^{-1}·min^{-1}), the greatest production rate was displayed at 300 rpm (8.38 x 10^{-4} g·mL^{-1}·min^{-1}). There was no clear trend with the effect of stirring speed on the reaction. The lack of a clear trend could be explained by one catalyst exhibiting a higher activity at slower stirring speeds, whereas the other catalyst displays a higher activity at faster stirring speeds. (This was explored further in Chapter 6 section §6.3.) Since 300 rpm resulted in the greatest production rate this speed was selected for the proceeding experiments.

Table 5.2. Methanolysis of PLA at 130 °C, 0.075 g $Zn(OAc)_2$ / 0.025 g DMAP, effect of different stirring speeds on; final time (min), final MeLa concentration (%), initial rate of production of MeLa (g·mL^{-1}·min^{-1}) at 60 min.

Stirring speed (rpm)	**Final time (min)**	**Final MeLa concentration (g·mL^{-1})**	**Initial Rate of Production of MeLa (g·mL^{-1}·min^{-1})**
0	120	0.0536	7.15 x 10^{-4}
200	180	0.0502	4.95 x 10^{-4}
300	120	0.0574	8.38 x 10^{-4}
400	120	0.0551	6.27 x 10^{-4}
700	90	0.0536	7.30 x 10^{-4}

5.3 Dual catalyst alcoholysis

The preliminary methanolysis reactions produced the greatest MeLa production rate when an equal weight of $Zn(OAc)_2$ and DMAP was used as well as a stirring speed of 300 rpm. These conditions were selected for dual catalysis alcoholysis using both MeOH and EtOH at a range of temperatures 100 – 130 °C.

5.3.1 GC Results

Samples were taken throughout each methanolysis reaction and analysed by GC. Figure 5.2 shows MeLa concentration (g·mL^{-1}) vs time (min) using an equal mass of $Zn(OAc)_2$ and DMAP at the temperature range 100 – 130 °C. Experiments were repeated (3 – 5 times) at each temperature and results averaged. As expected, a greater temperature resulted in a greater concentration of MeLa in shorter times. The times taken to reach an MeLa concentration of

0.04 g·mL^{-1} were: 50 min (130 °C), 68 min (120 °C), 101 min (110 °C), and 200 min (100 °C). As the temperature decreases the production rate decreases more sharply in magnitude. Furthermore, the lower temperature reactions plateau at a lower final MeLa concentration than the higher temperature reactions.

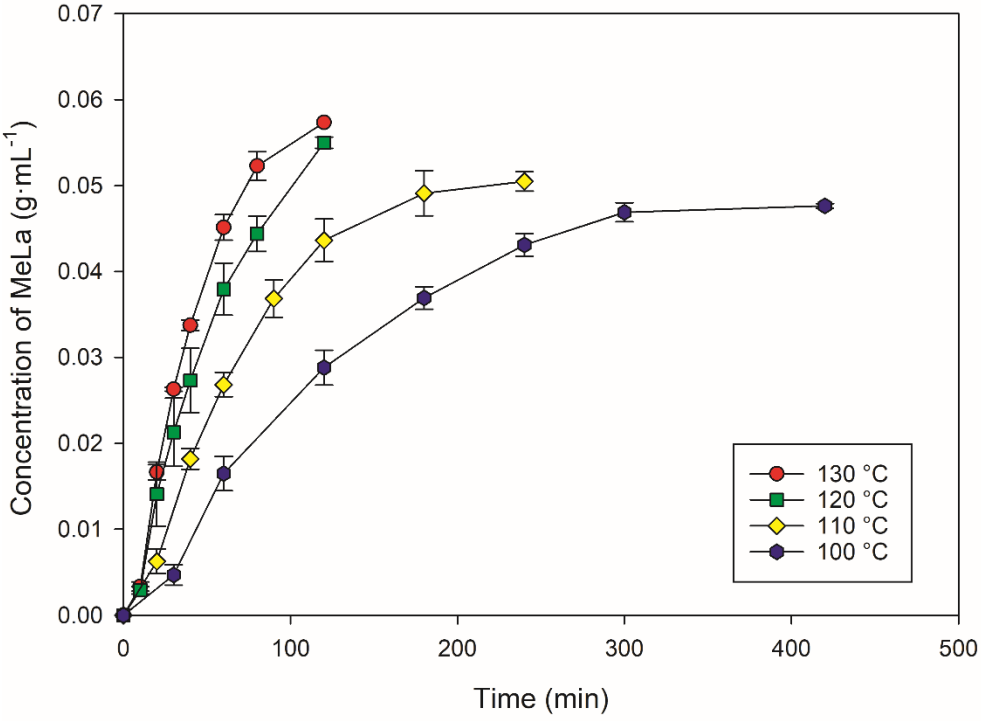

Figure 5.2. Methanolysis of 2 g of PLA at 100 – 130 °C, 300 rpm, using 0.05 g $Zn(OAc)_2$ / 0.05 g DMAP.

Samples were taken throughout each ethanolysis reaction and analysed by GC. Figure 5.3 shows EtLa concentration (g·mL^{-1}) vs time (min) for the ethanolysis of PLA using $Zn(OAc)_2$ and DMAP at the temperature range 110 – 130 °C. Experiments were repeated (2 – 4 times, excluding 110 °C) at each temperature and results averaged. The times taken to reach an EtLa concentration of 0.04 g·mL^{-1} are: 83 min (130 °C), 111 min (120 °C), and 258 min (110 °C). Very similar production rates of EtLa were attained at 120 °C and 130 °C, while decreasing the temperature to 110 °C significantly reduced the production rate.

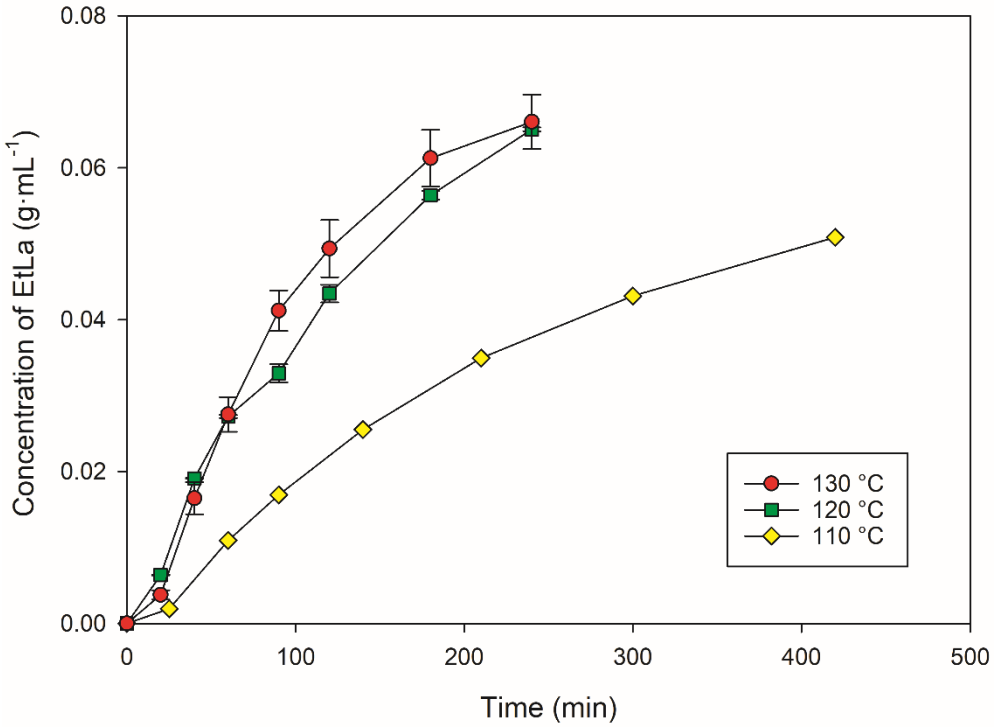

Figure 5.3. Ethanolysis of 2 g of PLA at 100 – 130 °C, 300 rpm, using 0.05 g $Zn(OAc)_2$ / 0.05 g DMAP.

Table 5.3 shows the GC results for the previous two figures to allow for better comparison. The initial rate of production of AL was calculated from the concentration of AL at 60 min. Comparing MeOH and EtOH at 130 °C, methanolysis resulted in a greater initial AL production. The same trend can be seen at 120 °C and 110 °C. The lower reactivity of EtOH can be explained by its increased steric hinderance of its nucleophilic attack in comparison to MeOH [171,177]. There is also a clear relationship in both types of alcoholysis reaction that a higher temperature results in a higher initial rate of AL production. This can simply be explained by the increased kinetic energy of the molecules at a higher temperature, so greater rates of successful collisions between molecules so a faster overall reaction.

A comparison can be made with ethanolysis at 110 °C in Table 4.1 using $Zn(\mathbf{1}^{Et})_2$ and $Zn(\mathbf{2}^{Pr})_2$. $Zn(\mathbf{1}^{Et})_2$ displayed a greater AL production rate in comparison to dual catalysis using $Zn(OAc)_2$ / DMAP (5.18×10^{-4} and 1.82×10^{-4} $g \cdot mL^{-1} \cdot min^{-1}$ respectively). Although $Zn(OAc)_2$ / DMAP

showed a greater AL production rate than Zn(**2**^{Pr})$_2$ at 110 °C (1.82 x 10^{-4} vs 7.46 x 10^{-5} g·mL^{-1}·min^{-1}), the non-Arrhenius behaviour of Zn(**2**^{Pr})$_2$ led to a greater AL production rate at 50 °C (2.51 x 10^{-4} g·mL^{-1}·min^{-1}). Despite Zn(**1**^{Et})$_2$ displaying greater activity at 110 °C and Zn(**2**^{Pr})$_2$ a greater activity at 50 °C, their disadvantage is their required synthesis. It should also be noted that Zn(**1**^{Et})$_2$ and Zn(**2**^{Pr})$_2$ was used at 9 mol% loading whereas Zn(OAc)$_2$ / DMAP was used at 1.6 mol% / 2.9 mol% loading. A greater catalyst loading for the dual experiments would be expected to increase its activity and is investigated further in Chapter 6 Sections §6.2 and §6.3.

Table 5.3. PLA alcoholysis using MeOH and EtOH, 0.05 g of Zn(OAc)$_2$ and 0.05g of DMAP at 300 rpm. The data represents averages of repeat experiments (2 – 5, excluding EtOH 110 °C).

Alcohol	**Temperature (**°C)	**Final time (min)**	**Final AL concentration (g·mL^{-1})**	**Initial rate of AL production (g·mL^{-1}·min^{-1})**
MeOH	130	93	0.0543	7.52 x 10^{-4}
	120	127	0.0564	6.33 x 10^{-4}
	110	188	0.0523	4.47 x 10^{-4}
	100	372	0.0484	2.75 x 10^{-4}
EtOH	130	240	0.0676	4.58 x 10^{-4}
	120	240	0.0651	4.53 x 10^{-4}
	110	420	0.0509	1.82 x 10^{-4}

5.3.2 ^{1}H NMR Results

The GC results for dual catalyst methanolysis showed a greater rate of AL production at any given temperature in comparison to ethanolysis. ^{1}H NMR experiments were only carried out on the methanolysis reactions. Reaction samples were taken periodically throughout each experiment and analysed by ^{1}H NMR, detailed in Section §3.5.2. A simplified kinetic model (equations 3.7 – 3.10) consisting of two consecutive steps was solved by sequential integration and substitution, detailed in Section §3.6. The solution (equation 3.11) was used in SigmaPlot which allowed for the fitting of ^{1}H NMR data (relative concentrations of Int, CE, and AL methine groups) for the determination of k_1 and k_2. It was concluded in Chapter 4 that the

equilibrium step in equation (3.3) only becomes significant at lower temperatures ≤ 70 °C. As this work is in the temperature range 100 – 130 °C it was decided to use a simplified model (equation 3.7) that ignores the equilibrium step. The only literature on PLA alcoholysis kinetics assumes a first order model only considering the initial cleavage of PLA ester groups (Table 2.4). Relative concentrations of methine groups versus time profiles at each temperature are shown in Figure 5.4.

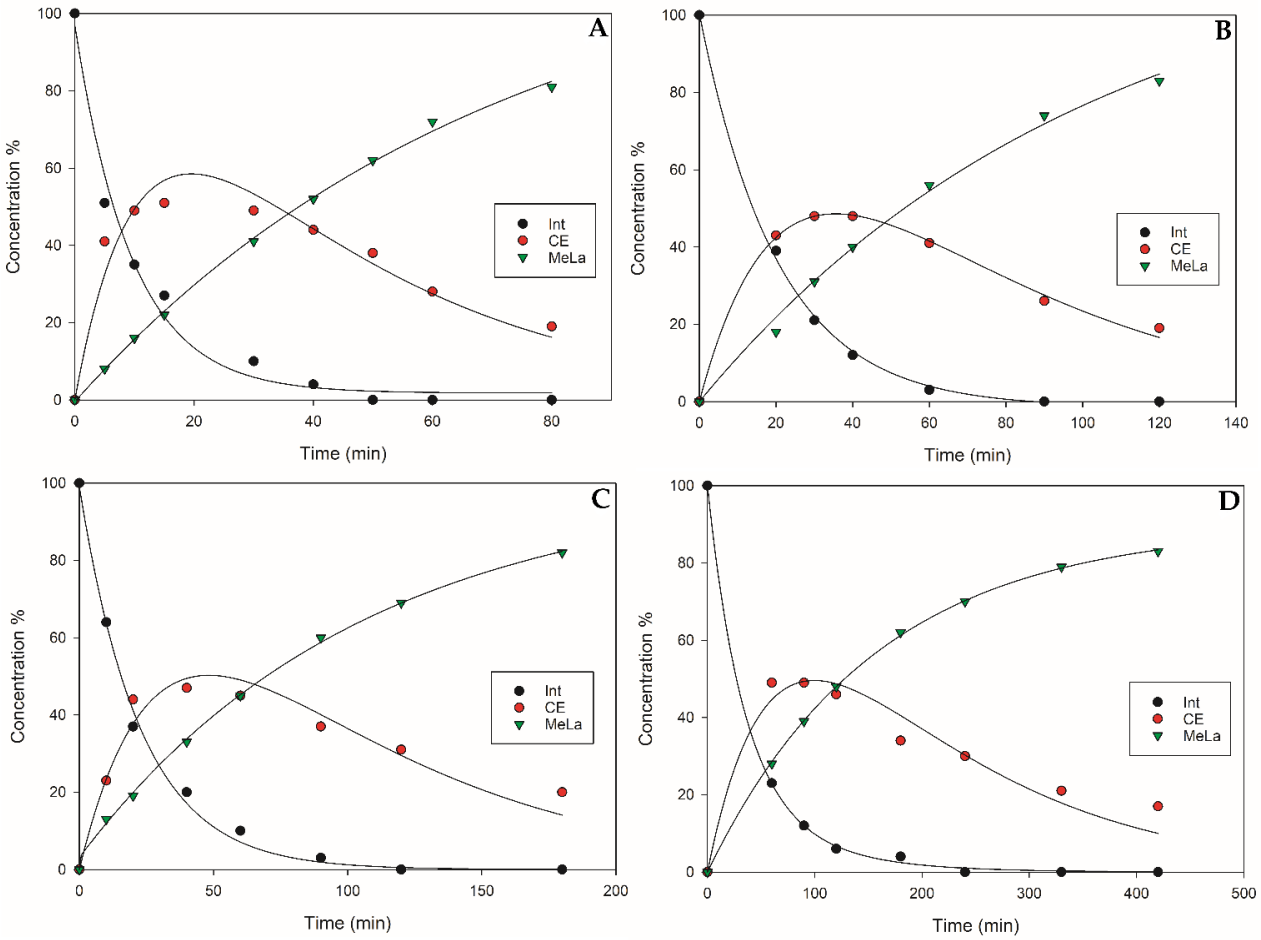

Figure 5.4. $Zn(OAc)_2$ / DMAP **m**ethanolysis reaction profiles obtained from ^1H NMR data fitted in SigmaPlot. (**A**) = 130 °C R^2 = 0.9384, (**B**) = 120 °C R^2 = 0.9954, (**C**) = 110 °C R^2 = 0.9394, (**D**) = 100 °C R^2 = 0.9403.

At 130 °C a maximum concentration of 51% for CE intermediates was reached at 15 min, while 100% conversion of Int groups was reached at 150 min. At 120 °C a maximum concentration

of 48% for CE intermediates was reached at 30 min, while 100% conversion of Int groups was reached at 90 min. At 110 °C a maximum concentration of 47% for CE intermediates occurred at 40 min, while 100% conversion of Int groups was reached at 120 min. At 100 °C a maximum concentration of 49% for CE intermediates was reached at 60 min, 100% conversion of Int groups was only reached at 240 min. The reaction profiles show good fits for the experimental data to the kinetic model.

Conversion of Int groups (X_{Int}), MeLa selectivity (S_{MeLa}), and AL yield (Y_{MeLa}) were calculated according to equations 4.1 – 4.3 (AL was substituted by MeLa). Averages for X_{Int}, S_{MeLa} and Y_{MeLa}, at each temperature were determined to allow for easier comparison, shown in Table 5.4. There is a clear trend that a higher temperature resulted in a higher value for, X_{Int}, S_{MeLa}, and Y_{MeLa}. A higher temperature raises the average kinetic energy of the reactant molecules, thus a greater proportion of molecules will have sufficient energy to overcome the activation energy barrier to form the product AL. By 130 °C conversion of Int methine groups of the PLA chains into oligomers with chain end methines had reached ≈ 100%. The selectivity and yield of MeLa is 70% at 130 °C, meaning the remaining 30% is chain end methine oligomers. The biggest decrease in X_{Int} was seen going from 110 °C to 100 °C; a lower temperature results in a slower reaction so fewer PLA Int groups will be cleaved by 60 min. The biggest decrease in S_{MeLa}, and Y_{MeLa}, was seen going from 130 °C to 120 °C.

Table 5.4. PLA methanolysis at 300 rpm with 0.05 g $Zn(OAc)_2$ and 0.05 g DMAP, conversion of Int groups, MeLa selectivity and MeLa yield at different reaction temperatures.

Temperature (°C)	**Average X_{Int} (%)**	**Average S_{MeLa} (%)**	**Average Y_{MeLa} (%)**
130	100	70	70
120	95	57	54
110	90	47	43
100	79	40	32

X_{Int}, S_{MeLa}, Y_{MeLa}, are determined at 60 min of reaction.

5.3.3 Activation Energy

The ^{1}H NMR relative concentrations of Int, CE, and AL methine groups determined in Section §5.3.2 were fitted to the simplified experimental model, equations (3.7 – 3.11). The solution equation (3.11) was used in SigmaPlot, enabling the determination of the rate coefficients for the fitted experimental data at different temperatures, shown in Table 5.5. The greatest difference between values for k between two repeats was k_1 (4.13×10^{-2} min^{-1}) at 130 °C.

Table 5.5. Estimated rate coefficients for $Zn(OAc)_2$ / DMAP methanolysis experiments at different temperatures.

Temperature (°C)	k_1 **(min^{-1})**	k_2 **(min^{-1})**
130	8.58×10^{-2}	2.74×10^{-2}
130	4.45×10^{-2}	2.75×10^{-2}
120	7.17×10^{-2}	1.75×10^{-2}
120	3.78×10^{-2}	2.03×10^{-2}
110	2.89×10^{-2}	1.43×10^{-2}
110	2.24×10^{-2}	1.11×10^{-2}
110	2.17×10^{-2}	1.22×10^{-2}
100	1.14×10^{-2}	7.90×10^{-3}
100	1.52×10^{-2}	1.03×10^{-2}
100	1.38×10^{-2}	7.01×10^{-3}

The estimated rate coefficients were used to generate Arrhenius plots for PLA methanolysis using $Zn(OAc)_2$ / DMAP, shown in Figure 5.5. According to equation (3.7), alcoholysis of PLA occurs in two consecutive steps. Therefore, there are two rate coefficients (k_1, k_2) corresponding to two activation energies (E_{a1} and E_{a2}). The resulting activation energies are: E_{a1} = 67.99 ± 23.42 kJ·mol^{-1}and E_{a2} = 50.04 ± 10.21 kJ·mol^{-1}. The experimental data show a good fit; each Arrhenius plot has $R^2 \geq 0.85$. The estimated activation energies show that E_{a1} has the greatest range with upper and lower bound values ± 23.42 kJ·mol^{-1}. The activation energy for dual catalysis methanolysis was also determined according to first order kinetics, where only the initial cleavage of PLA Int groups was considered. The integrated rate equation was plotted,

resulting in a linear graph with a negative gradient. The first order E_a was calculated to be 48.32 ± 26.09 kJ·mol^{-1}, which is significantly lower than the value for E_{a1} (67.99 ± 23.42 kJ·mol^{-1}).

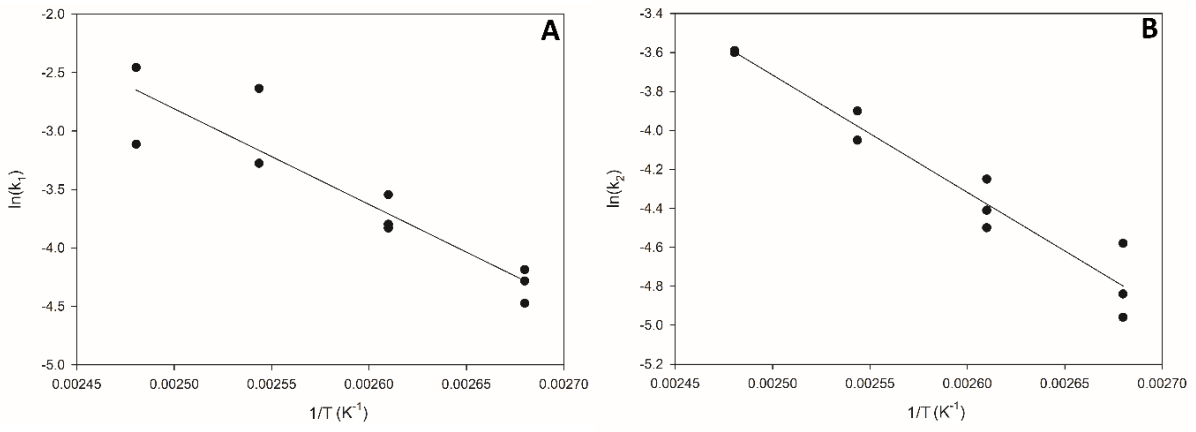

Figure 5.5. Arrhenius plots for methanolysis of 2 g PLA, at 300 rpm, 9 equivalents of MeOH, 0.05 g of $Zn(OAc)_2$ and 0.05g of DMAP. (**A**) k_1 y = -8182.3x + 17.65 R^2 = 0.8486, (**B**) k_2 y = -6021.7x + 11.34 R^2 = 0.941.

A comparison can be made with the activation energies determined in chapter 4. Table 5.6 is a comparison of the activation energies from two different kinetic models and catalysts. Ethanolysis, propanolysis, and butanolysis activation energies were determined according to the kinetic model of two consecutive reaction steps with the second step being in equilibrium (equation 3.4). Methanolysis activation energies were determined according to the kinetic model of two consecutive reaction second step being irreversible (equation 3.7). Methanolysis displayed the greatest E_{a1} = 67.99 kJ·mol^{-1}. Methanolysis showed a large range in the upper and lower bound values for both E_{a1} and E_{a2} (± 23.42 and ± 10.21 kJ·mol^{-1} respectively). While the large range in upper and lower bound values for propanolysis and butanolysis was due to a lack of repeat experiments, methanolysis had enough repeats. The large confidence interval therefore reflects that the kinetic model is less accurate that the one used in chapter 4.

Table 5.6. The activation energies for each step of PLA alcoholysis.

Alcoholysis	E_{a1} (kJ·mol^{-1})	E_{a2} (kJ·mol^{-1})	$E_{a\text{-}2}$ (kJ·mol^{-1})
EtOH[1]	56.33 ± 8.04	53.13 ± 6.43	56.24 ± 18.88
PrOH[1]	27.48 ± 24.66	34.71 ± 25.6	19.54 ± 6.36
BuOH[1]	52.06 ± 15.104	40.87 ± 12.06	19.97 ± 9.68
MeOH[2]	67.99 ± 23.42	50.04 ± 10.21	-

[1] $Zn(1^{Et})_2$ at 9 mol%, [2] $Zn(OAc)_2$ / DMAP at 1.6 mol% / 2.9 mol%

Good results were obtained with the dual catalyst system of $Zn(OAc)_2$ and DMAP. The hypothesis is that a sufficient difference in pK_a is required for enhanced activity. Despite $Zn(OAc)_2$ and DMAP agreeing with the hypothesis, only two catalysts were tested, it is difficult to confirm or disprove this hypothesis. Therefore, further exploration is required to test the effect of pK_a on enhancing catalyst complexes. In Chapter 6 a greater number of catalysts and mixtures are investigated.

5.4 Conclusion

In this chapter a reliable system was designed for the alcoholysis of PLA using an equal mass of $Zn(OAc)_2$ and DMAP. Preliminary methanolysis experiments investigated different mixtures of these catalysts and found dual catalysis experiments resulted in a greater concentration of MeLa in a shorter time in comparison to single catalysis experiments. In addition an equal weight of both $Zn(OAc)_2$ and DMAP resulted in the greatest MeLa production rate in comparison to other mixtures. Dual catalyst alcoholysis was tested in both MeOH and EtOH. Methanolysis resulted in a greater MeLa production rate in comparison to ethanolysis at the same temperature. This result agrees with the conclusion of chapter 4 that a longer carbon chain alcohol leads to a slower alcoholysis reaction by sterically hindering coordination to the catalyst. Both methanolysis and ethanolysis followed the trend that a higher temperature resulted in a greater AL production rate.

A simplified kinetic model consisting of a two-step consecutive reaction was applied to dual catalysis methanolysis. The resulting activation energies were estimated to be: E_{a1} = 67.99 ± 23.42 kJ·mol^{-1} and E_{a2} = 50.04 ± 10.21 kJ·mol^{-1}. Despite a sufficient number of repeats the activation energies have large confidence intervals. Therefore the simplified kinetic model is less accurate than the one used in chapter 4, including an equilibrium step better represents the alcoholysis reaction. A first order model was also established which only considers the initial cleavage of PLA Int groups. According to this kinetic model the activation energy was calculated to be E_a = 48.32 ± 26.09 kJ·mol^{-1}. The use of dual catalysis for the chemical recycling of PLA requires further research. Early results indicate a synergistic effect that enhances the reaction rate. The synergy between cheap readily available catalysts could be utilized in industrial chemical recycling, to attain unprecedented reactivities which are not accessible using either catalyst alone. Increasing PLA depolymerision reaction rates makes the overall process more economically feasible.

Chapter 6 – Methanolysis of Poly(lactic acid) Using Catalyst Mixtures and the Kinetics of Methyl Lactate Production

6.1 Chapter Overview

This Chapter describes the investigation of four commercially available catalysts for the alcoholysis of PLA. The catalysts investigated include: $Zn(OAc)_2$, magnesium acetate tetrahydrate ($Mg(OAc)_2$), DMAP, and triazabicyclodecene (TBD). The catalysts were also tested in mixtures to investigate any synergistic effects. This chapter is based on the publication, Methanolysis of Poly(lactic Acid) Using Catalyst Mixtures and the Kinetics of Methyl Lactate Production [14].

As previously mentioned there are several studies that explore the use of dual catalysis [223–226]. Synergistic dual catalysis can lead to unprecedented reactivities; this enhanced reactivity has potential to be utilized in many industries including the chemical recycling of PLA. A dual catalyst complex will only occur if there is a sufficient difference in pK_a leading to proton transfer and the formation of a stable complex [231]. Since these synergistic complexes function on simple proton transfer, the two catalysts can simply be added to a reaction; if they dissolve homogenously then the complex will form *in situ* [225,226,232]. More recently Dove *et al.* reported dual catalysis for the enhanced depolymerisation of PET [232–234]. The work here builds on our previous publication by testing a larger range of catalysts, and tests the hypothesis that a sufficient difference in pK_a is required for enhanced activity [13]. The experiments were carried out in the 300 mL Parr autoclave reactor in a semi-batch manner through the addition of alcohol, described in Section §3.4.3. This chapter is structured as follows: methanolysis optimisation using $Zn(OAc)_2$ in Section §6.2, single catalyst methanolysis in Section §6.3, mixed catalyst methanolysis in Section §6.4, which is subdivided into GC results, ^{1}H NMR

results, and activation energy. Finally, Section §6.5 summaries this investigation and establishes a conclusion.

6.2 Methanolysis Optimisation using $Zn(OAc)_2$

These experiments were carried out to understand the effect of parameters such as catalyst loading, stirring speed, and MeOH molar equivalents, on the methanolysis of PLA. Developing an understanding of these variables would allow for reaction optimisation in terms of reaction rate and product selectivity. It was decided to use $Zn(OAc)_2$ for these initial optimisation experiments. $Zn(OAc)_2$ is reported to have the best performance among metal acetates, generating the greatest reaction rates [256]. In addition, the results of chapter 5 showed $Zn(OAc)_2$ to have superior activity to DMAP even at a lower mol%. Samples were taken throughout each experiment and analysed by GC to determine the concentration of MeLa (detailed in Section §3.5.1).

Figure 6.1, shows the effect of catalyst loading on MeLa concentration during the methanolysis of PLA at 130 °C. Experiments were repeated (2 – 4 times) at each MeOH equivalent and results averaged. A higher mol% of $Zn(OAc)_2$ resulted in shorter reaction times in order to reach a MeLa concentration of > 0.05 $g \cdot mL^{-1}$. Increasing the catalyst loading from 1 mol% to 2 mol% resulted in the largest increase of MeLa concentration. Increasing the catalyst loading from 2 mol% to 3 mol% also increased the MeLa concentration but less so, while changing the loading from 3 mol% to 4 mol% resulted in only a minor increase in MeLa concentration. A higher mol% of $Zn(OAc)_2$ resulted in a smaller standard error between the repeats for each experiment, likely due to human error associated with weighing out smaller amounts of catalyst. For the mixed catalyst experiments it was therefore decided to use 2 mol% of catalyst; it was assumed the other catalysts would behave similarly in terms of catalyst loading and their effect on

reactivity. 2 mol% loading of $Zn(OAc)_2$ was a balance between using the least amount of catalyst while still obtaining the higher MeLa production rate from higher loadings.

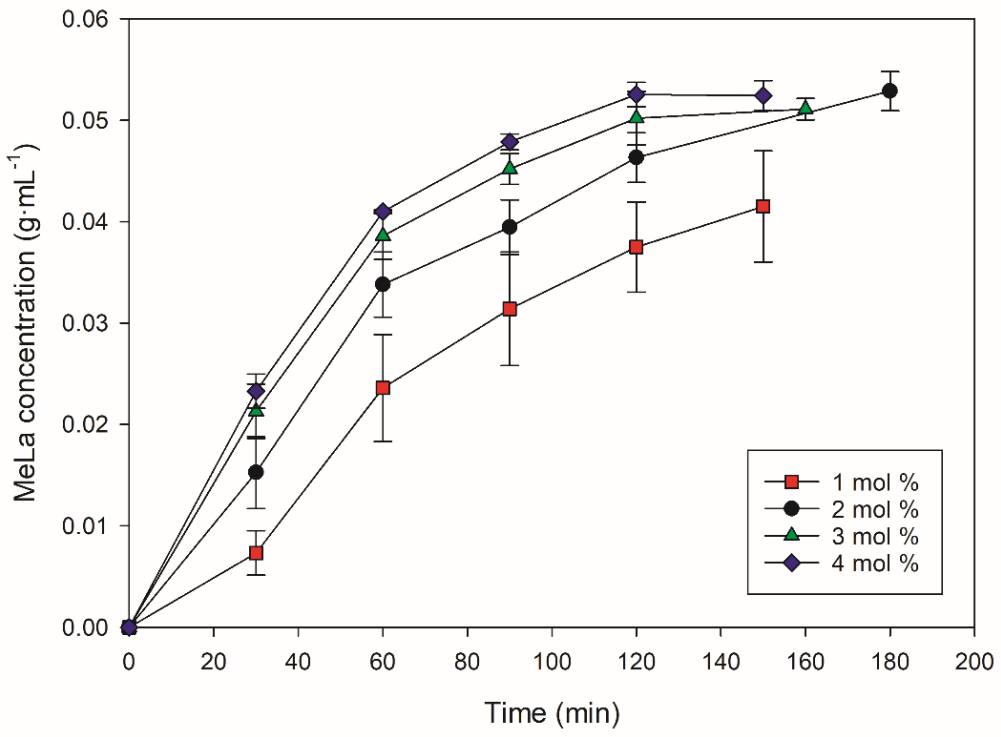

Figure 6.1. Methanolysis of 2 g of PLA at 130 °C, 300 rpm and 9 equivalents of MeOH. Effect of mol% of $Zn(OAc)_2$ (Relative to mol of PLA) on the MeLa concentration ($g \cdot mL^{-1}$) vs. time (min).

Figure 6.2 shows the effect of stirring speed on MeLa concentration during methanolysis at 130 °C. Experiments were repeated (2 – 4 times) at each speed and results averaged. A higher stirring speed of 600 rpm resulted in a MeLa concentration of > 0.05 $g \cdot mL^{-1}$ in shortest times, likely owing to better dispersion of catalyst throughout the vessel, improved rates of mixing, and mass transfer. A higher stirring speed also resulted in a smaller standard error between the repeats for each experiment. Even without stirring (at 0 rpm) the reaction reached completion at 4 h. It was assumed the other catalysts would behave similarly in terms of stirring speed and its effect on activity.

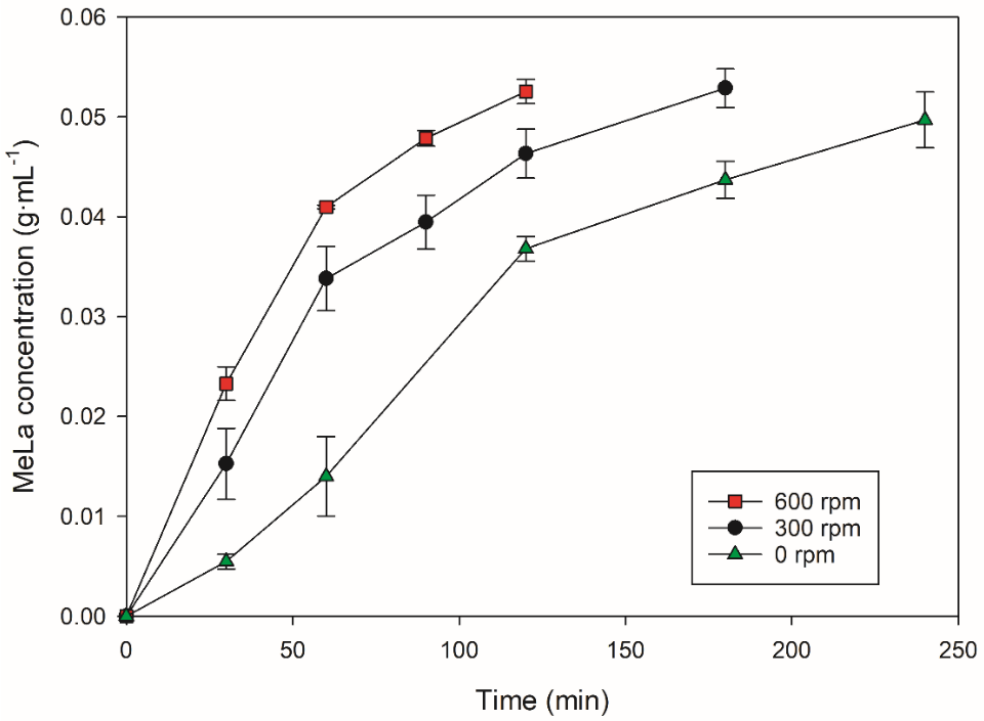

Figure 6.2. Methanolysis of 2 g of PLA at 130 °C, 9 equivalents of MeOH, 2 mol% $Zn(OAc)_2$. Effect of stirring speed (rpm) on the MeLa concentration ($g \cdot mL^{-1}$) vs. Time (min).

The final parameter investigated to optimise the reaction was the molar equivalent of MeOH. Figure 6.3 shows the effect of stirring speed on MeLa concentration during methanolysis using 2 mol% $Zn(OAc)_2$ at 130 °C. A higher equivalent of MeOH resulted in shorter reaction times in order to reach a MeLa concentration of > 0.05 $g \cdot mL^{-1}$. Increasing the molar equivalents of MeOH from 5 to 9 resulted in the largest increase of MeLa production rate. Increasing the equivalents from 9 to 13 also increased the MeLa production rate but by a smaller amount, while increasing the equivalents from 13 to 15 increased the MeLa production rate the least. The classic Lewis acid mechanism for transesterification using $Zn(OAc)_2$ involves the polarization of an ester carbonyl group to the Zn^{2+} centre which helps facilitate nucleophilic attack [257]. Another study reported that $Zn(OAc)_2$ initiates transesterification through a mechanism that involves the initial coordination of the alcohol nucleophile to the metal centre, followed by a carboxylate shift and coordination to the ester group [255].

The latter study could help explain the result that a higher equivalent of MeOH causes greater reaction rates. A higher equivalent of MeOH will result in more MeOH molecules in closer proximity to $Zn(OAc)_2$. Since the catalytic mechanism involves $Zn(OAc)_2$ coordinating to the alcohol nucleophile it could be reasoned that, more MeOH molecules in close proximity to $Zn(OAc)_2$ increases the probability of coordination and thus overall reactivity [197]. This reasoning could also be used to explain why increasing the equivalents of MeOH up to 17 causes the increase in MeLa concentration to plateau. At 17 equivalents, $Zn(OAc)_2$ is becoming fully saturated with MeOH molecules in close proximity; increasing the equivalents of MeOH molecules beyond this limit only marginally increases the probability of coordination.

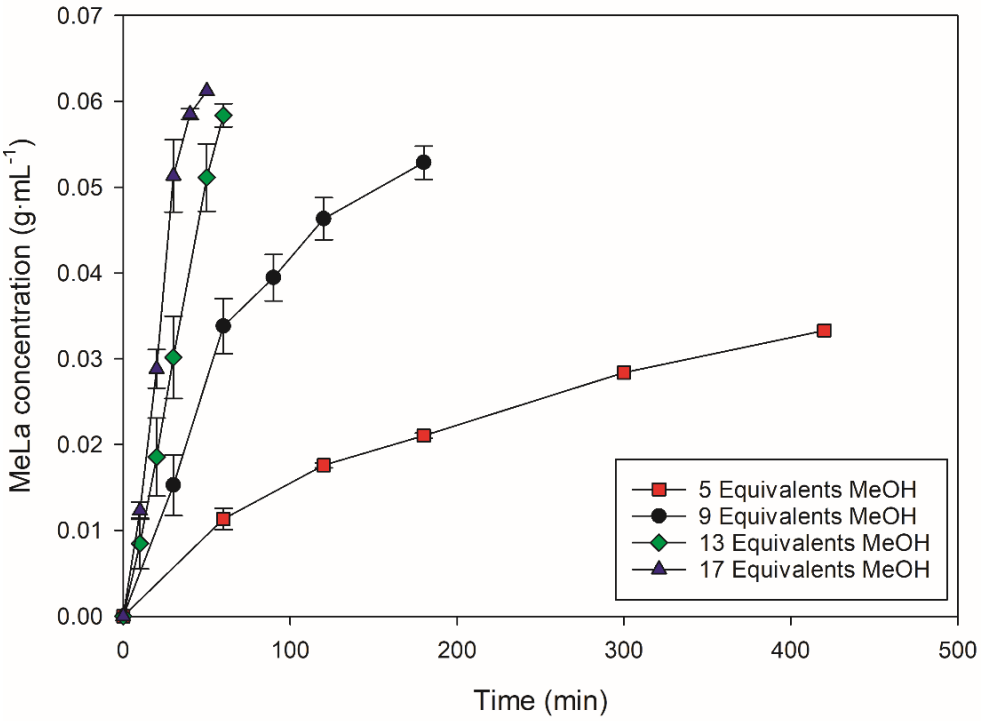

Figure 6.3. Methanolysis of 2 g of PLA at 130 °C, 300 rpm, 2 mol% $Zn(OAc)_2$. Effect of MeOH molar equivalent on the MeLa concentration ($g \cdot mL^{-1}$) vs. time (min).

6.3 Single catalyst methanolysis

It was decided to test the four commercial catalysts for the methanolysis of PLA using the optimised parameters. $Mg(OAc)_2$ was selected as it would allow for a good comparison with

$Zn(OAc)_2$. DMAP and TBD were also chosen as both organocatalysts have been reported to be effective for transesterification. As previously discussed in Section §2.5.5.3.4, both DMAP and TBD are considered bifunctional hydrogen bonding catalysts, and though this mechanism they are effective catalysts for transesterification reactions [179–182]. Table 6.1 shows the results for the methanolysis of PLA using the selected catalysts. Each catalyst was tested at both 9 and 17 equivalents of MeOH and stirring speeds of 300 and 600 rpm.

Table 6.1. Methanolysis of 2 g PLA at 130 °C. The data represents averages of repeat experiments (3-4 repeats).

2 mol% Catalyst	**Speed (rpm)**	**Molar Equivalents of MeOH**	**Final time (min)**	**Final MeLa concentration ($g \cdot mL^{-1}$)**	**Initial rate of MeLa production at 40 min ($g \cdot mL^{-1} \cdot min^{-1}$)**
$Zn(OAc)_2$	300	9	173	0.0538	5.37×10^{-4}
$Zn(OAc)_2$	300	17	48	0.0593	1.42×10^{-3}
$Zn(OAc)_2$	600	17	70	0.0577	1.19×10^{-3}
$Mg(OAc)_2$	300	9	360	0.0449	5.39×10^{-5}
$Mg(OAc)_2$	300	17	107	0.0562	9.09×10^{-5}
$Mg(OAc)_2$	600	17	83	0.0624	1.09×10^{-3}
DMAP	300	9	360	0.0437	3.09×10^{-5}
DMAP	300	17	340	0.0510	4.65×10^{-5}
DMAP	600	17	200	0.0257	2.03×10^{-5}
TBD	300	9	160	0.0501	5.37×10^{-4}
TBD	300	17	140	0.0534	5.27×10^{-4}
TBD	600	17	135	0.0557	6.43×10^{-4}

Comparing the catalysts at 9 equivalents of MeOH: $Zn(OAc)_2$ and TBD displayed the highest initial rate of MeLa production (both 5.37×10^{-4} $g \cdot mL^{-1} \cdot min^{-1}$), followed by $Mg(OAc)_2$ (5.39×10^{-5} $g \cdot mL^{-1} \cdot min^{-1}$), and then DMAP ($3.09 \times 10^{-5}$ $g \cdot mL^{-1} \cdot min^{-1}$). Comparing the catalysts at 17 equivalents of MeOH and 300 rpm: $Zn(OAc)_2$ again displayed the highest average initial rate of MeLa production (1.42×10^{-3} $g \cdot mL^{-1} \cdot min^{-1}$), followed by TBD ($5.27 \times 10^{-4}$ $g \cdot mL^{-1} \cdot min^{-1}$), $Mg(OAc)_2$ (9.09×10^{-5} $g \cdot mL^{-1} \cdot min^{-1}$), and DMAP ($4.65 \times 10^{-5}$ $g \cdot mL^{-1} \cdot min^{-1}$). TBD is the only catalyst that did not display an increase in rate of MeLa production when the equivalent of

MeOH was increased. Of the four catalysts. $Zn(OAc)_2$ exhibited the largest increase in rate of MeLa production when the equivalent of MeOH was increased. At 600 rpm and 17 equivalents of MeOH $Zn(OAc)_2$ again displayed the highest rate of MeLa production (1.19 x 10^{-3} $g \cdot mL^{-1} \cdot min^{-1}$), closely followed by $Mg(OAc)_2$ (1.09 x 10^{-3} $g \cdot mL^{-1} \cdot min^{-1}$), then TBD (6.43 x 10^{-4} $g \cdot mL^{-1} \cdot min^{-1}$), and DMAP significantly slower (2.03 x 10^{-5} $g \cdot mL^{-1} \cdot min^{-1}$).

When increasing the stirring speed from 300 to 600 rpm at 17 equivalents of MeOH $Zn(OAc)_2$ displayed a decrease in rate of MeLa production. However, Figure 6.2 showed $Zn(OAc)_2$ at 9 equivalents of MeOH to increase in MeLa production when stirring was increased from 300 to 600 rpm. A possible explanation is that at a 9 equivalents of MeOH there are fewer MeOH molecules in close proximity to $Zn(OAc)_2$, so mass transfer and stirring speed are more important. At 17 equivalents of MeOH, $Zn(OAc)_2$ becomes surrounded with MeOH molecules, mass transfer and stirring speed become less important. DMAP also displayed a decrease in rate of MeLa production when stirring speed was increased. Similarly, the dual $Zn(OAc)_2$ / DMAP experiment in Table 5.2, exhibited a decrease in MeLa production rate when stirring was increased from 300 to 600 rpm.

On the other hand both $Mg(OAc)_2$ and TBD showed an increase in rate of MeLa production at 600 rpm. As $Mg(OAc)_2$ has a larger size than $Zn(OAc)_2$ it could be argued that it will require a higher equivalent of MeOH to become fully saturated with MeOH in close proximity [197]. Thus, increasing the stirring speed will still increase the mass transfer and reaction rates. As TBD is larger than DMAP the same explanation can be applied. Changing the stirring speed from 300 to 600 rpm caused $Mg(OAc)_2$ to exhibit the most significant difference in production rate (9.99 x 10^{-4} $g \cdot mL^{-1} \cdot min^{-1}$) out of all tested catalyst and conditions. The second most significant difference in production rate (8.83 x 10^{-4} $g \cdot mL^{-1} \cdot min^{-1}$) was displayed by $Zn(OAc)_2$ when MeOH equlivent was increased from 9 to 17.

6.4 Mixed catalyst methanolysis

It was decided to test the four commercial catalysts while using the optimised parameters 600 rpm and 17 equivalents of MeOH, to investigate the effect of catalyst mixtures on the rate of methanolysis. The motivation for this was to find catalyst synergies that have enhanced reactivity in comparison to either catalyst alone. This would unlock the potential for dual catalysis to be used in the chemical recycling of PLA. A faster rate of MeLa production makes industrial PLA alcoholysis more economically feasible.

6.4.1 GC Results

Methanolysis was carried out using the four catalysts in different ratios. If one of these mixtures exhibited a MeLa production rate greater than those in Table 6.1 (at the same conditions), it would imply a synergistic interaction between the catalysts. Samples were taken throughout the reactions and analysed by GC. Experiments were repeated (2 – 4 times) and the results averaged, shown in Table 6.2. In each reaction only 2 mol% total of catalyst was used; all catalysts were dissolved homogenously in the solvent. The greatest initial rate of MeLa production (1.36×10^{-3} g·mL^{-1}·min^{-1}) was displayed by the dual catalyst $Mg(OAc)_2$ / TBD experiment. The rate was greater than the single catalyst $Mg(OAc)_2$ or single catalyst TBD rate (1.09×10^{-3} and 6.43×10^{-4} g·mL^{-1}·min^{-1} respectively) in Table 6.1 at the same conditions. The enhanced reactivity implies a synergistic effect between $Mg(OAc)_2$ and TBD. If the pK_a difference between the two catalysts is great enough then proton transfer occurs, forming a stable acid-base complex capable of enhancing the reaction [231]. $Mg(OAc)_2$ and TBD have a great enough difference in pK_a (8 and 15.2, respectively) to form a stable acid-base complex. The catalysts $Mg(OAc)_2$ / TBD are considered type II partially cooperative; either catalyst alone results in the formation of the product but at a slower rate compared to dual catalysis [225]. As previously discussed in Section §2.5.9: type I are defined as fully cooperative catalysts; type III

are also defined as partially cooperative catalysts (in this case one of the catalysts alone would result in substrate decomposition and formation of side products); and type IV are defined as non-cooperative catalysts [225].

Table 6.2. Methanolysis of 2 g PLA at 130°C, 600 rpm, 17 eq MeOH, and catalyst mixtures 2 mol% total. The data represents averages of repeat experiments (2-4 repeats).

Catalyst (2 mol% total)	**Final time (min)**	**Final MeLa concentration ($g \cdot mL^{-1}$)**	**Initial rate of MeLa production at 40 min ($g \cdot mL^{-1} \cdot min^{-1}$)**
$Zn(OAc)_2$ / TBD (1 : 1)	60	0.0584	1.34×10^{-3}
$Zn(OAc)_2$ / DMAP (1 : 1)	80	0.0608	1.29×10^{-3}
$Mg(OAc)_2$ / TBD (1 : 1)	80	0.0617	1.36×10^{-3}
$Mg(OAc)_2$ / DMAP (1 : 1)	110	0.0602	8.44×10^{-4}
TBD / DMAP (1 : 1)	180	0.0531	2.84×10^{-4}
$Zn(OAc)_2$ / $Mg(OAc)_2$ (1 : 1)	120	0.0561	6.87×10^{-4}
$Zn(OAc)_2$ / TBD / DMAP (1 : 0.5 : 0.5)	90	0.0600	1.27×10^{-3}
$Mg(OAc)_2$ / TBD / DMAP (1 : 0.5 : 0.5)	105	0.0591	8.72×10^{-4}
TBD / $Zn(OAc)_2$ / $Mg(OAc)_2$ (1 : 0.5 : 0.5)	120	0.0529	5.46×10^{-4}
DMAP /$Zn(OAc)_2$ / $Mg(OAc)_2$ (1 : 0.5 : 0.5)	90	0.0581	9.22×10^{-4}
$Zn(OAc)_2$ / $Mg(OAc)_2$ / TBD / DMAP (1 : 1 : 1 : 1)	120	0.0626	7.41×10^{-4}

On the other hand, the $Mg(OAc)_2$ / DMAP experiment resulted in a slower production rate (8.44×10^{-4} $g \cdot mL^{-1} \cdot min^{-1}$) than $Mg(OAc)_2$ alone. $Mg(OAc)_2$ and DMAP have a similar pK_a (8 and 9.6 respectively) so no stable catalyst complex forms. Likewise, a synergistic interaction is not present for the dual $Mg(OAc)_2$ / $Zn(OAc)_2$ experiment, resulting in a slower MeLa production rate (6.87×10^{-4} $g \cdot mL^{-1} \cdot min^{-1}$) than for $Zn(OAc)_2$ alone (1.19×10^{-3} $g \cdot mL^{-1} \cdot min^{-1}$), or $Mg(OAc)_2$

alone (1.09 x 10^{-3} g·mL^{-1}·min^{-1}). As $Zn(OAc)_2$ and $Mg(OAc)_2$ have a similar pK_a (8 and 4.54 respectively) no stable complex forms. The MeLa concentration of $Mg(OAc)_2$ dual catalyst experiments are shown in Figure 6.4. Only $Mg(OAc)_2$ / TBD produced a greater concentration of MeLa in shorter times in comparison to 2 mol% $Mg(OAc)_2$. The experiments showed an initial delay in rate of MeLa production at 15 min with a MeLa significantly lower than the other experiments. The delay was consistent among the 3 repeats but there is no clear explanation. Despite the initial delay, $Mg(OAc)_2$ / TBD exhibited the greatest concentration of MeLa after 40 min.

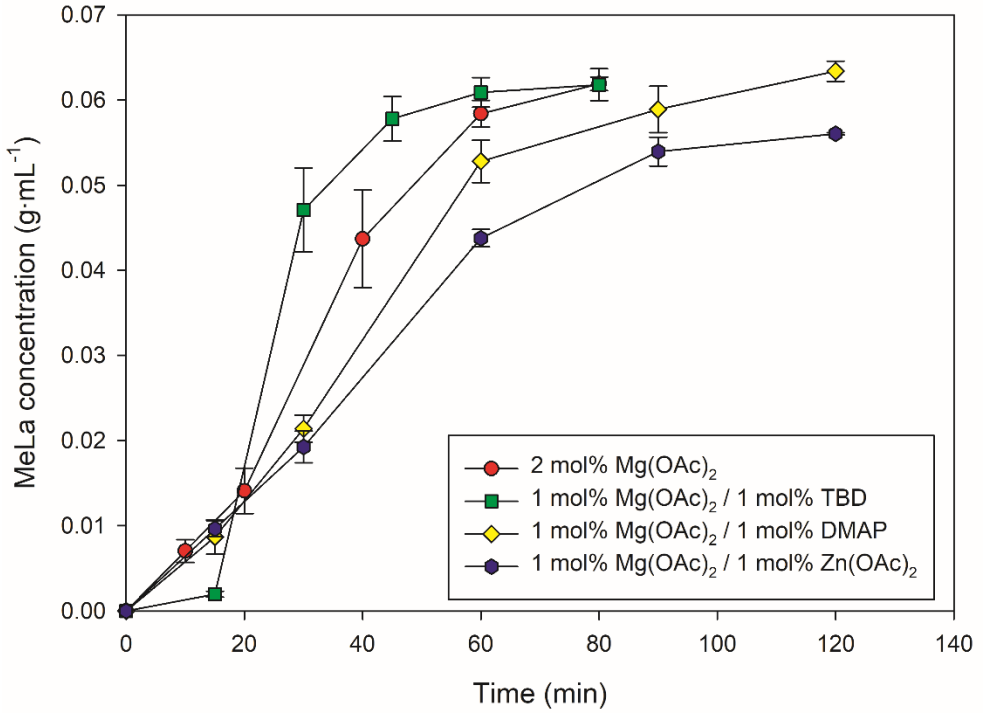

Figure 6.4. Dual catalysts methanolysis of 2 g PLA using $Mg(OAc)_2$ based catalyst mixtures, at 130°C, 600 rpm, and 17 eq MeOH.

$Zn(OAc)_2$ is capable of forming a catalyst complex with both TBD and DMAP due to great enough difference in pK_a (4.54, 15.2, and 9.6 respectively). A sufficient difference in pK_a is necessary for proton transfer to occur forming a stable acid-base complex [231]. If a catalyst pair exhibits a greater activity than either catalyst alone (at the same total mol%) then a catalytic

synergy is present. The $Zn(OAc)_2$ / TBD experiments displayed greater rates of MeLa production (1.34 x 10^{-3} g·mL^{-1}·min^{-1}) than the 2 mol% $Zn(OAc)_2$ experiments (1.19 x 10^{-3} g·mL^{-1}·min^{-1}) in Table 6.1 at the same conditions. Faster rates were also observed for the dual catalyst $Zn(OAc)_2$ / DMAP experiments (1.29 x 10^{-3} g·mL^{-1}·min^{-1}), the faster rate than 2 mol% $Zn(OAc)_2$ again supports the idea of dual catalyst synergy that aids the reaction. The higher rates could be explained by synergistic interactions between the two catalysts, increasing the activation of PLA ester carbonyls facilitating the nucleophilic attack needed for depolymerisation [232]. Synergistic dual catalysis enhances reaction rates by activating both the nucleophile and electrophile. These activated species have a lower HOMO and higher LUMO in comparison to the same species nonactivated [226]. Activation of the nucleophile and electrophile results in a smaller HOMO-LUMO gap and smaller E_a, and this leads to greater reaction rates in comparison to nonactivated species at the same reaction conditions [226].

The MeLa concentration of $Zn(OAc)_2$ dual catalyst experiments are shown in Figure 6.5. Both $Zn(OAc)_2$ / TBD and $Zn(OAc)_2$ / DMAP dual catalyst experiments had faster rates of MeLa production than $Zn(OAc)_2$ alone, while $Zn(OAc)_2$ / $Mg(OAc)_2$ experiments exhibited significantly lower rates. The enhanced rates seen in some dual experiments is not simply the sum of each catalyst's activity but likely a result of a synergistic acid-base complexation. According to Table 6.1 the different rates of MeLa production for 2 mol% of each catalyst are as follows: $Zn(OAc)_2$ (1.19 x 10^{-3} g·mL^{-1}·min^{-1}), $Mg(OAc)_2$ (1.09 x 10^{-3} g·mL^{-1}·min^{-1}), TBD (6.43 x 10^{-4} g·mL^{-1}·min^{-1}) and DMAP (2.03 x 10^{-5} g·mL^{-1}·min^{-1}). Both metal acetates were magnitudes faster than the organocatalysts, yet their combination was the slowest of the dual catalyst experiments.

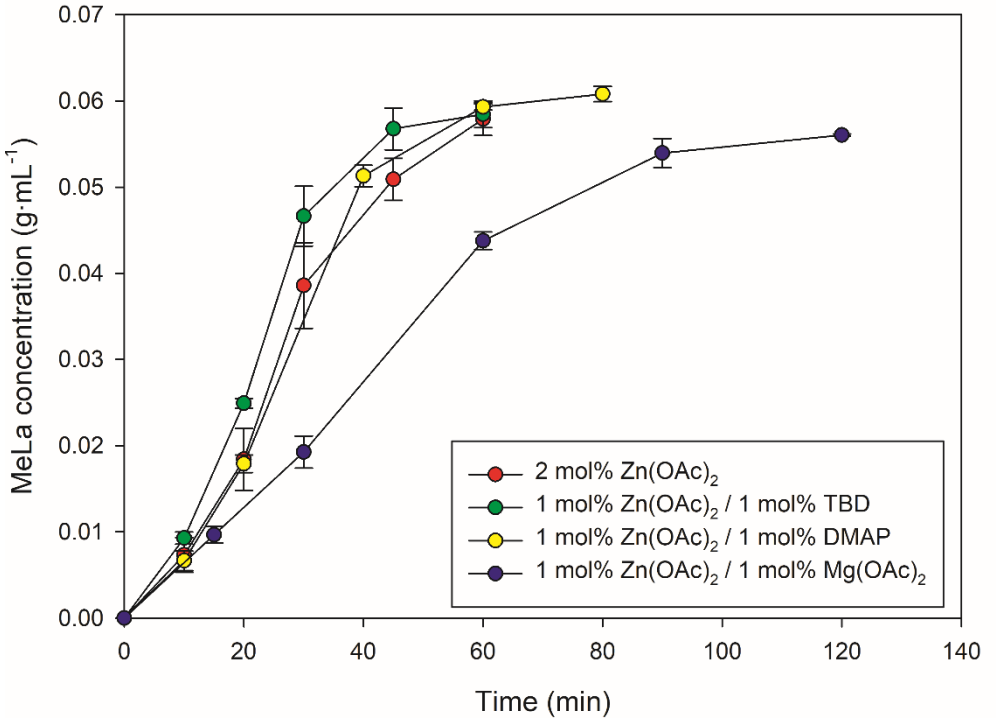

Figure 6.5. Dual catalysts methanolysis of 2 g PLA using $Zn(OAc)_2$ based catalyst mixtures, at 130°C, 600 rpm, and 17 eq MeOH.

Similarly, enhanced reaction rates were not exhibited for the dual TBD / DMAP experiments. These experiments exhibited a MeLa production rate (2.84×10^{-4} g·mL^{-1}·min^{-1}) that was slower than the rate for 2 mol% TBD (6.43×10^{-4} g·mL^{-1}·min^{-1}). Unlike $Zn(OAc)_2$ and $Mg(OAc)_2$, TBD and DMAP have a great enough difference in pK_a (15.2 and 9.6 respectively) yet no enhancing synergy was exhibited. As both TBD and DMAP are bases it can be inferred that catalyst synergy requires both a great enough difference in pK_a and both acid / base components. None of the experiments that use three or four catalysts displayed higher rates when compared to dual catalyst experiments.

6.4.2 ^{1}H NMR Results

According to the GC results, the greatest MeLa production rates were exhibited by the dual catalyst experiments $Mg(OAc)_2$ / TBD (1.36×10^{-3} g·mL^{-1}·min^{-1}) and $Zn(OAc)_2$ / TBD (1.34×10^{-3} g·mL^{-1}·min^{-1}). Both single catalyst $Zn(OAc)_2$ and $Mg(OAc)_2$ experiments demonstrated

relatively fast production rates (1.19×10^{-3} and 1.09×10^{-3} $g \cdot mL^{-1} \cdot min^{-1}$ respectively). Time constraints limited which catalyst/s could be tested further *via* ^1H NMR. The single $Zn(OAc)_2$ and dual $Zn(OAc)_2$ / TBD experiments were selected to determine their activation energies.

Reaction samples were taken periodically throughout each experiment and analysed by ^1H NMR (detailed in Section §3.5.2), to determine the relative concentrations of Int, CE, and AL methine groups. The relative concentrations of the methine groups were fitted to two kinetic models. Both models consist of two consecutive steps only differing in the second step, detailed in §3.6. One model considers the second step to be in **equilibrium** (equations 3.3 – 3.6); the other considers the second step as **irreversible** (equations 3.7 – 3.11). The first step (rate coefficient k_1) relates to the initial cleavage of PLA ester groups *via* a transesterification reaction with an alcohol nucleophile, resulting in two distinct chain end oligomers for each cleavage. The second step (rate coefficient k_2) refers to the nucleophilic attack of a chain end ester group resulting in the formation of MeLa. The reverse step (rate coefficient k_{-2}) represents when the MeLa alcohol group acts as the nucleophile, attacking the ester carbonyl of a chain end to form a larger oligomer.

Equilibrium model - The rate equations (3.4 – 3.6) were solved in MATLAB using a nonlinear square fitting procedure. The relative concentration of methine groups were fitted using this procedure, generating estimates for the rate coefficients (k_1, k_2, k_{-2}). Reaction profiles for the single catalyst $Zn(OAc)_2$ experiments are shown below in Figure 6.6. At 130 °C a maximum concentration of 40% for CE was reached at 15 min, while 100% conversion of Int groups was reached at 60 min. At 120 °C a maximum concentration of 38% for CE intermediates was reached at 15 min, while 100% conversion of Int groups was reached at 90 min. At 110 °C a maximum concentration of 38% for CE intermediates was reached at 15 min, while 100% conversion of Int groups was reached at 90 min. At 100 °C a maximum concentration of 40%

for CE intermediates occurred at 40 min, while 100% conversion of Int groups was reached at 240 min. This procedure was also carried out for the dual $Zn(OAc)_2$ / TBD experiments.

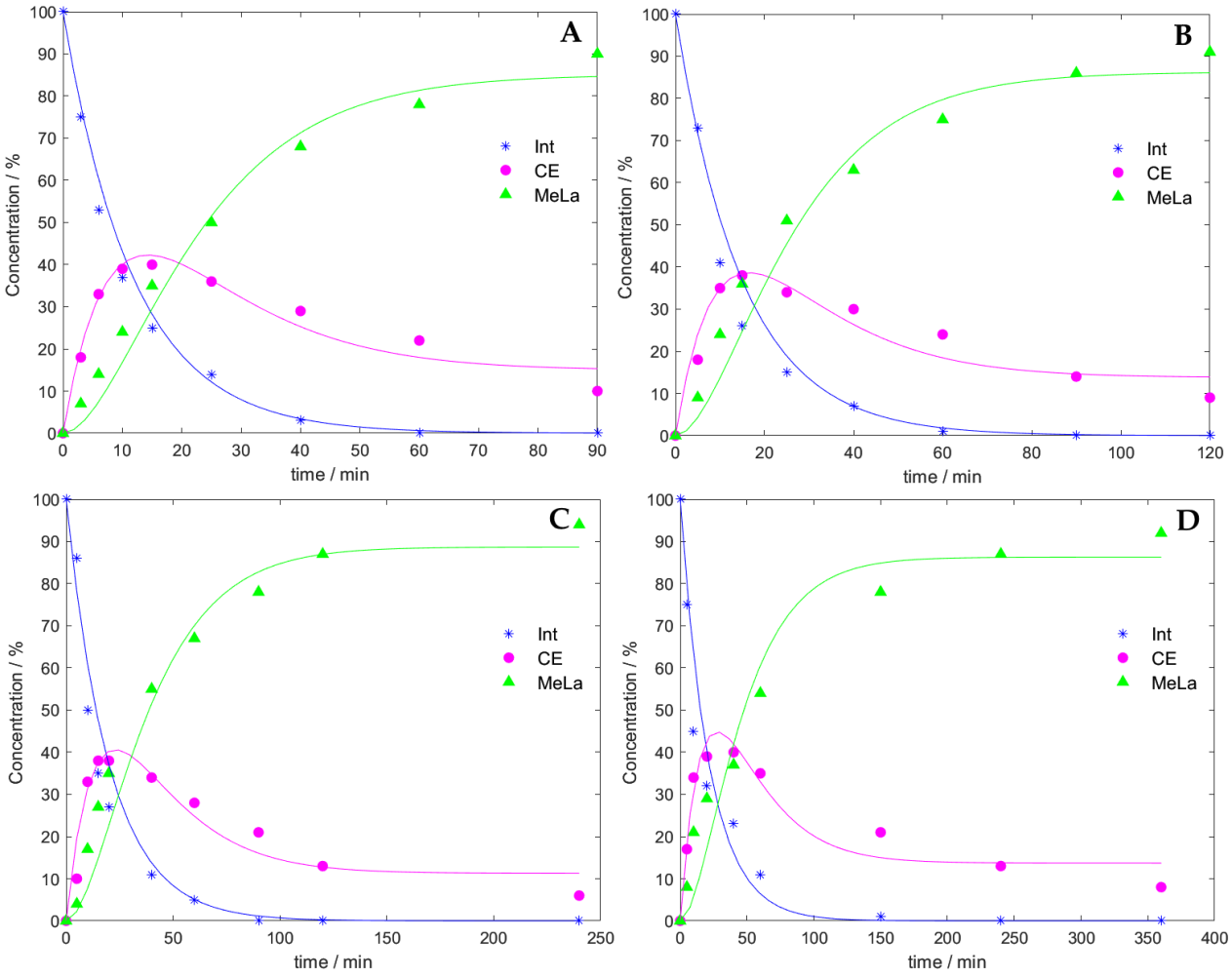

Figure 6.6. $Zn(OAc)_2$ methanolysis reaction profiles obtained from ^1H NMR data fitted in MATLAB. (**A**) = 130 °C, (**B**) = 120 °C, (**C**) = 110 °C, (**D**) = 100 °C.

Irreversible model – the rate equations (3.8 – 3.10) were solved by sequential integration and substitution. The relative concentration of methine groups was fitted to the solution (equation 3.11) using SigmaPlot which enabled for the determination of k_1 and k_2. Reaction profiles for the dual catalyst $Zn(OAc)_2$ / TBD experiments are shown below in Figure 6.7. At 130 °C a maximum concentration of 45% for CE was reached at 15 min, while 100% conversion of Int groups was reached at 25 min. At 120 °C a maximum concentration of 46% for CE

intermediates was reached at 15 min, while 100% conversion of Int groups was reached at 40 min. At 110 °C a maximum concentration of 46% for CE intermediates was reached at 40 min, while 100% conversion of Int groups was reached at 90 min. At 100 °C a maximum concentration of 47% for CE intermediates occurred at 40 min, while 100% conversion of Int groups was reached at 90 min. This procedure was also carried out for the single catalyst $Zn(OAc)_2$ experiments.

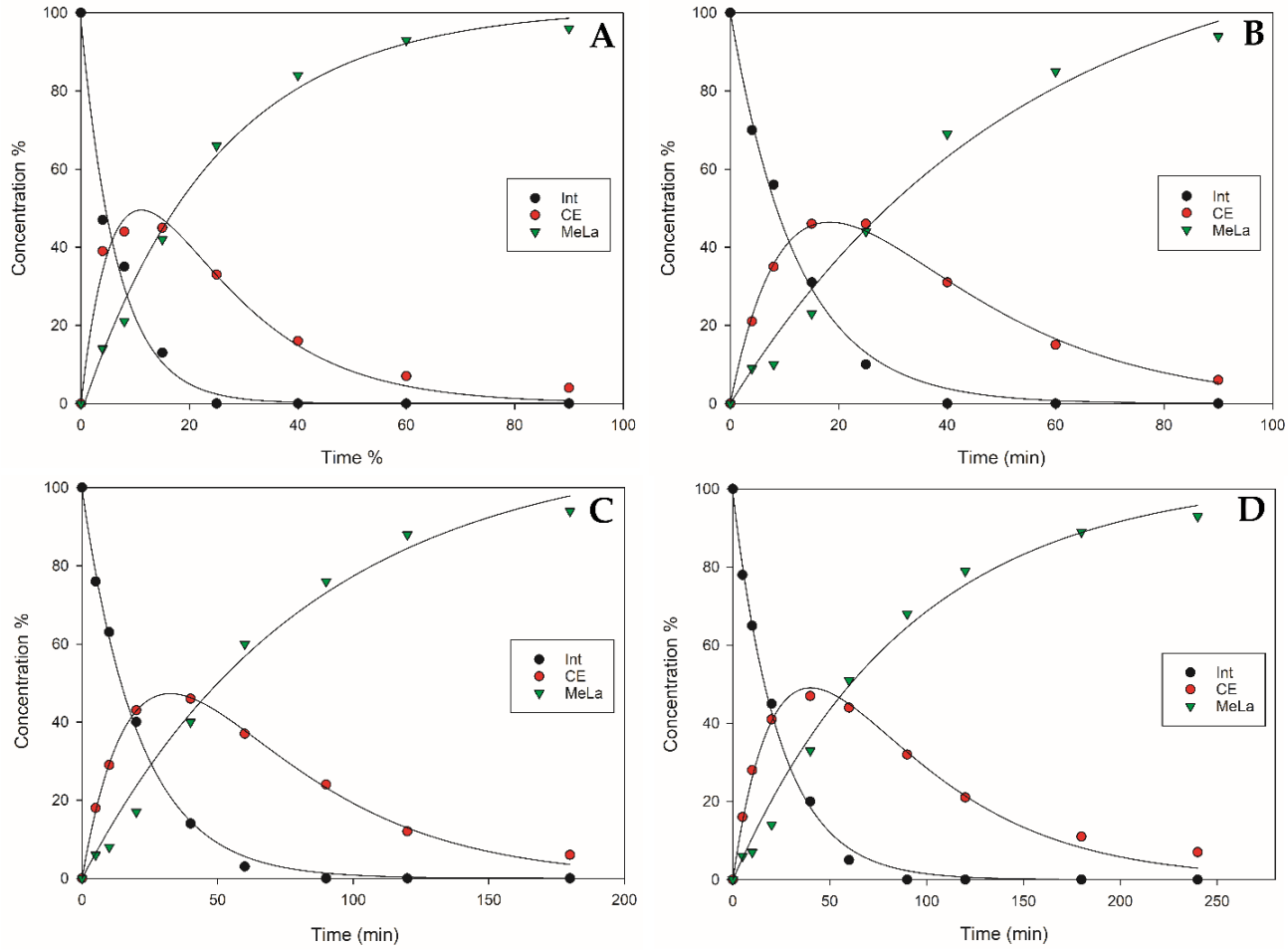

Figure 6.7. $Zn(OAc)_2$ / TBD methanolysis reaction profiles obtained from ^1H NMR data fitted in SigmaPlot. (**A**) = 130 °C R^2 = 0.9764, (**B**) = 120 °C R^2 = 0.9957, (**C**) = 110 °C R^2 = 0.9957, (**D**) = 100 °C R^2 = 0.9853.

Conversion of Int groups (X_{Int}), MeLa selectivity (S_{MeLa}), and MeLa yield (Y_{MeLa}) were calculated according to equations 4.1 – 4.3. Averages for X_{Int}, S_{MeLa} and Y_{MeLa}, at each

temperature were determined to allow for easier comparison, shown in Table 6.3. There is a clear trend that a higher temperature results in a greater X_{Int}, S_{MeLa} and Y_{MeLa}. At 130 °C both catalyst experiments had X_{Int} 100%. However $Zn(OAc)_2$ resulted in a smaller S_{MeLa} and Y_{MeLa} of 81%, while using $Zn(OAc)_2$ / TBD resulted in S_{MeLa} and Y_{MeLa} of 93%. These ^{1}H NMR results add further confirmation to the previous GC results at 130 °C, showing that dual catalyst $Zn(OAc)_2$ / TBD experiments result in a greater production rate of MeLa than either catalyst alone. Interestingly the catalytic performance of $Zn(OAc)_2$ / TBD significantly decreases at lower temperatures. Using $Zn(OAc)_2$ / TBD at 100 °C resulted in an S_{MeLa} and Y_{MeLa} of 53% and 49%. Using $Zn(OAc)_2$ resulted in a greater S_{MeLa} and Y_{MeLa} of 65% and 59%. One explanation is that the enhancing synergistic interaction between $Zn(OAc)_2$ / TBD only comes into effect at temperatures ≥ 120 °C.

Table 6.3. Single catalyst vs. Dual catalyst methanolysis, at 600 rpm, 17 eq MeOH, and a range of temperatures. The data represents averaged repeat experiments (2 repeats).

Catalyst (2 mol% total)	**Temperature (°C)**	**Average X_{Int} (%)**	**Average S_{MeLa} (%)**	**Average Y_{MeLa} (%)**
$Zn(OAc)_2$	130	100	81	81
	120	100	72	72
	110	96	73	70
	100	91	65	59
$Zn(OAc)_2$ / TBD (1 : 1)	130	100	93	93
	120	100	87	87
	110	99	63	62
	100	93	53	49

X_{Int}, S_{MeLa}, Y_{MeLa}, determined at 60 min of reaction.

6.4.3 Activation Energy

The relative concentrations determined in Section §6.4.2 were fitted to both kinetic models, the **equilibrium model** (equations 3.3 – 3.6), and the **irreversible model** (equations 3.7 – 3.11) detailed in Section §3.6. Table 6.4 shows the estimates of rate coefficients for the fitted experimental data using MATLAB and the **equilibrium model**. At 120 and 130 °C the

$Zn(OAc)_2$ experiments displayed a smaller k_1, a larger k_2, and a significantly larger k_{-2}. k_{-2} represents the reverse equilibrium step where the alcohol group of MeLa undergoes transesterification with an CE carbonyl to form a larger oligomer. The significantly larger k_{-2} means MeLa was being converted back to CE oligomers at a much faster rate. As MeLa is being converted back to CE at a higher rate, a lower selectivity and yield for MeLa is observed. The GC results in Table 6.3 confirm this; comparing $Zn(OAc)_2$ and $Zn(OAc)_2$ / TBD at 120 – 130 °C the reactions displayed 100% X_{Int}, but $Zn(OAc)_2$ experiments exhibited a significantly smaller S_{MeLa} and Y_{MeLa}. At 100 and 110 °C both catalyst experiments displayed similar values for k_1, but $Zn(OAc)_2$ had a larger k_2 and k_{-2}. A larger k_2 means there was a greater driving force for MeLa formation, which explains the GC results Table 6.3, as $Zn(OAc)_2$ exhibited larger S_{MeLa} and Y_{MeLa}. At 100 and 110 °C both catalyst experiments exhibited a significantly larger k_2 than k_{-2}. In both cases k_2 was a magnitude greater than k_{-2}, favouring MeLa formation.

Table 6.4. Estimated rate coefficients for each methanolysis experiment, using either $Zn(OAc)_2$ or $Zn(OAc)_2$ / TBD. Rate coefficients were generated using MATLAB and an equilibrium kinetic model.

Catalyst (2 mol% total)	**Temperature (°C)**	k_1 **(min^{-1})**	k_2 **(min^{-1})**	k_{-2} **(min^{-1})**
$Zn(OAc)_2$	130	8.97×10^{-2}	9.14×10^{-2}	1.34×10^{-2}
	130	8.43×10^{-2}	6.75×10^{-2}	1.18×10^{-2}
	120	6.33×10^{-2}	5.37×10^{-2}	1.57×10^{-2}
	120	6.67×10^{-2}	6.49×10^{-2}	1.04×10^{-2}
	110	5.06×10^{-2}	5.19×10^{-2}	5.95×10^{-3}
	110	4.96×10^{-2}	4.27×10^{-2}	5.42×10^{-3}
	100	3.70×10^{-2}	3.66×10^{-2}	4.22×10^{-3}
	100	4.58×10^{-2}	3.18×10^{-2}	5.04×10^{-3}
$Zn(OAc)_2$ / TBD (1 : 1)	130	1.16×10^{-1}	7.20×10^{-2}	2.50×10^{-3}
	130	1.38×10^{-1}	7.04×10^{-2}	3.62×10^{-3}
	120	8.90×10^{-2}	7.71×10^{-2}	6.84×10^{-3}
	120	7.54×10^{-2}	4.46×10^{-2}	9.18×10^{-4}
	110	5.25×10^{-2}	2.83×10^{-2}	2.93×10^{-3}
	110	4.42×10^{-2}	2.54×10^{-2}	1.13×10^{-3}
	100	3.64×10^{-2}	1.98×10^{-2}	2.42×10^{-3}
	100	3.86×10^{-2}	2.06×10^{-2}	1.57×10^{-3}

Table 6.5 shows the estimates of rate coefficients for the fitted experimental data using SigmaPlot and the **irreversible model**. Considering the rate coefficient values at 120 – 130 °C $Zn(OAc)_2$ experiments resulted in a much smaller k_1, and smaller k_2. A smaller k_2 means CE was being converted to MeLa at a slower rate than the $Zn(OAc)_2$ / TBD experiments. Table 6.3 supports this idea as $Zn(OAc)_2$ at 120 – 130 °C exhibited a significantly smaller value for S_{MeLa} and Y_{MeLa}. Considering the rate coefficient values at 100 – 110 °C, $Zn(OAc)_2$ experiments had a smaller k_1 but larger k_2, in comparison to $Zn(OAc)_2$ / TBD experiments. A smaller k_1 means PLA ester groups are cleaved at a slower rate, but the larger k_2 means CE was converted to MeLa at a greater rate. Justifying Table 6.3 $Zn(OAc)_2$ at 100 – 110 °C which resulted in a slightly smaller X_{Int}, but much larger S_{MeLa} and Y_{MeLa}.

Table 6.5. Estimated rate coefficients for each methanolysis experiment, using either $Zn(OAc)_2$ or $Zn(OAc)_2$ / TBD. Rate coefficients were generated using SigmaPlot and a Irreversible kinetic model.

Catalyst (2 mol% total)	**Temperature (°C)**	k_1 **(min^{-1})**	k_2 **(min^{-1})**
$Zn(OAc)_2$	130	5.21×10^{-2}	5.65×10^{-2}
	130	6.29×10^{-2}	4.34×10^{-2}
	120	3.30×10^{-2}	2.62×10^{-2}
	120	4.40×10^{-2}	3.80×10^{-2}
	110	3.37×10^{-2}	3.38×10^{-2}
	110	3.75×10^{-2}	2.91×10^{-2}
	100	2.50×10^{-2}	2.46×10^{-2}
	100	3.04×10^{-2}	1.84×10^{-2}
$Zn(OAc)_2$ / TBD (1 : 1)	130	1.06×10^{-1}	6.59×10^{-2}
	130	1.23×10^{-1}	6.32×10^{-2}
	120	7.30×10^{-2}	6.28×10^{-2}
	120	6.95×10^{-2}	4.18×10^{-2}
	110	4.62×10^{-2}	2.36×10^{-2}
	110	4.01×10^{-2}	2.30×10^{-2}
	100	3.08×10^{-2}	1.61×10^{-2}
	100	3.38×10^{-2}	1.77×10^{-2}

The estimated rate coefficients from both kinetic models were used to generate two types of Arrhenius plots. The **equilibrium model** (equations 3.3 – 3.6), alcoholysis occurs in three steps,

which corresponds to three different Arrhenius plots and activation energies (E_{a1}, E_{a2}, and E_{a-2}). The **equilibrium** Arrhenius plots for 2 mol% $Zn(OAc)_2$ are shown in Figure 6.8. The resulting activation energies are: E_{a1} = 31.20 ± 7.25 kJ·mol^{-1}, E_{a2} = 34.16 ± 12.2 kJ·mol^{-1} and E_{a-2} = 47.93 ± 22.84 kJ·mol^{-1}. The experimental data k_1 and k_2 shows a good fit, with each Arrhenius plot showing an $R^2 \geq 0.089$. On the other hand, k_{-2} show a poorer fit with its R^2 = 0.8147. Its associated activation energy E_{a-2} has the greatest range in upper and lower bound values ± 22.84 kJ·mol^{-1}. This procedure was also carried out for the dual $Zn(OAc)_2$ / TBD experiments; its resulting activation energies are: E_{a1} = 51.12 ± 12.51 kJ·mol^{-1}, E_{a2} = 57.08 ± 20.82 kJ·mol^{-1}and E_{a-2} = 20.06 ± 64.85 kJ·mol^{-1}. The large range in the values for k_{-2} means its associated activation energy E_{a-2} has a large confidence interval.

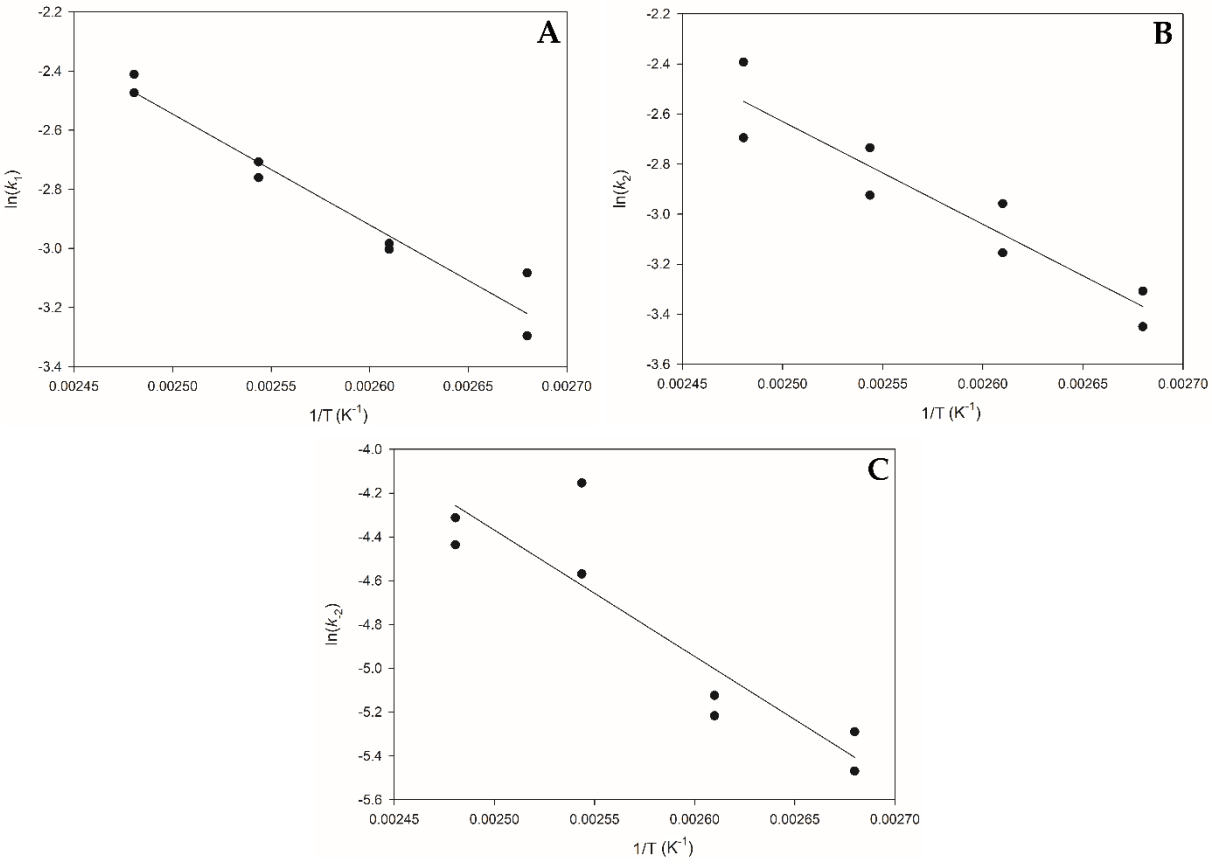

Figure 6.8. Arrhenius plots for methanolysis of 2 g PLA, 2 mol% $Zn(OAc)_2$, 600 rpm, 17 equivalents of MeOH. Values for rate coefficients were obtained from the **equilibrium model**. (**A**) k_1 y = -3754.76x + 6.84 R^2 = 0.9486, (**B**) k_2 y = -4111.22x + 7.65 R^2 = 0.8867, (**C**) k_{-2} y = -5767.58x + 10.05 R^2 = 0.8147.

The **irreversible model** (equations 3.7 – 3.11), alcoholysis occurs in two consecutive steps, which corresponds to two different Arrhenius plots and activation energies (E_{a1} and E_{a2}). The **irreversible** Arrhenius plots for 1 mol% $Zn(OAc)_2$ / 1 mol% TBD are shown in Figure 6.9. The resulting activation energies are: E_{a1} = 53.64 ± 9.65 kJ·mol^{-1} and E_{a2} = 60.18 ± 17.45 kJ·mol^{-1}. The experimental data k_1 and k_2 show a good fit with each Arrhenius plot having an $R^2 \geq 0.92$. In Table 6.5, k_2 had a greater range in values between repeats in comparison k_1, its associated activation energy E_{a2} has the greatest range in upper and lower bound values ± 17.45 kJ·mol^{-1}. This procedure was also carried out for the $Zn(OAc)_2$ experiments; its resulting activation energies are: E_{a1} = 28.17 ± 14.05 kJ·mol^{-1} and E_{a-2} = 31.72 ± 18.91 kJ·mol^{-1}.

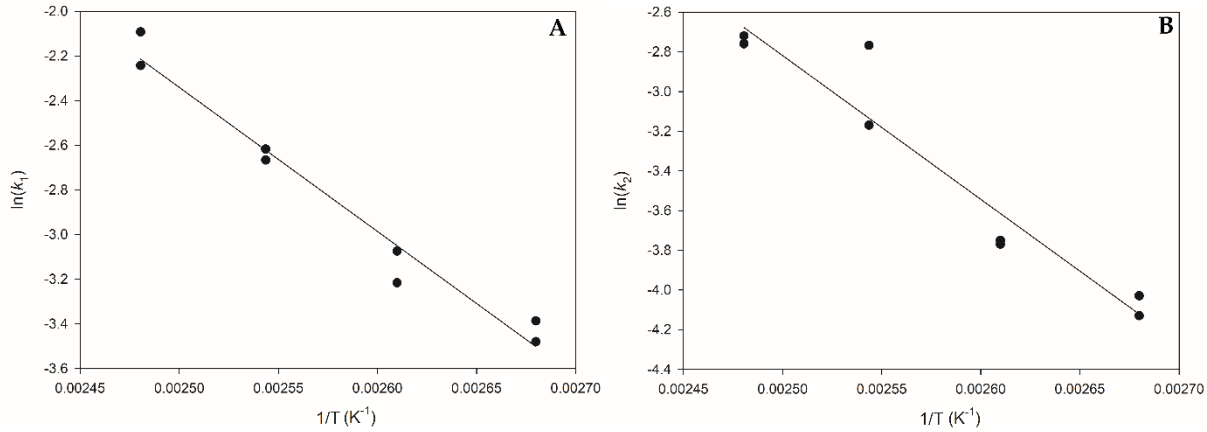

Figure 6.9. Arrhenius plots for methanolysis of 2 g PLA, 1 mol% $Zn(OAc)_2$ / 1 mol% TBD, 600 rpm, 17 equivalents of MeOH. Values for rate coefficients were obtained from the **irreversible model**. (**A**) k_1 y = -6454.97x + 13.80 R^2 = 0.9686, (**B**) k_2 y = -7242.22x + 15.29 R^2 = 0.9223.

The activation energies obtained from the equilibrium model are shown in Table 6.6 (including chapter 4 activation energies). As discussed in Section §4.5, when E_{a-2} is smaller than E_{a2} the equilibrium lies to the left, favouring the transformation of AL to CE oligomer. The opposite is also true: when E_{a-2} is greater than E_{a2}, the equilibrium lies to the right favouring AL formation. Alcoholysis using MeOH[2] had an E_{a-2} greater than E_{a2}. The greater energy barrier for the reverse step means its equilibrium favours the formation of AL. In comparison, alcoholysis using EtOH[1] displayed an E_{a-2} only slighter larger than E_{a2}. This implies AL formation is favoured in

alcoholysis using MeOH[2] instead of EtOH[1]. This can also been seen when comparing their average yield of AL; at 110 °C the Y_{AL} was 70% and 37% respectively (Table 6.3 and Table 4.2). Alcoholysis using MeOH[3] showed the greatest range in the upper and lower bound values for $E_{a\text{-}2}$ (± 64.85). MeOH[3] is omitted from the discussion as its standard error is too large.

Table 6.6. The activation energies for each step of PLA alcoholysis, using an equilibrium kinetic model.

Alcoholysis	E_{a1} (kJ·mol^{-1})	E_{a2} (kJ·mol^{-1})	$E_{a\text{-}2}$ (kJ·mol^{-1})
EtOH[1]	56.33 ± 8.04	53.13 ± 6.43	56.24 ± 18.88
BuOH[1]	52.06 ± 15.104	40.87 ± 12.06	19.97 ± 9.68
MeOH[2]	31.20 ± 7.25	34.16 ± 12.2	47.93 ± 22.84
MeOH[3]	51.12 ± 12.51	57.08 ± 20.82	20.06 ± 64.85

[1] Zn(**1**^{Et})$_2$ at 9 mol%, [2] Zn(OAc)$_2$ at 2 mol% , [3] Zn(OAc)$_2$ / TBD at 1 mol% each.

The activation energies obtained from the irreversible kinetic model are shown in Table 6.7 (Including chapter 5 activation energies). MeOH[3] displayed the smallest activation energy for E_{a1} (28.17 kJ·mol^{-1}), followed by MeOH[2] with a larger E_{a1} (53.69 kJ·mol^{-1}), and MeOH[4] with the largest E_{a1} (67.99 kJ·mol^{-1}). A smaller activation energy for the initial cleavage of PLA ester groups would result in a higher conversion of Int groups. At 110 °C the X_{Int} was 99%, 96%, and 85% for MeOH[3], MeOH[2], and MeOH[4]. (Table 6.3, and Table 5.4). A lower activation energy for the initial step leads to a build-up of CE oligomers during the reaction. Since MeOH[3] had the smaller activation for the E_{a1} there was a greater build-up of CE oligomers, and thus a lower selectivity and yield for AL in comparison to MeOH[2]. At 110 °C the S_{AL} was 63% and 73%, and the Y_{AL} was 62% and 70% respectively (Table 6.3).

Table 6.7. The activation energies for each step of PLA alcoholysis, considering a irreversible kinetic model.

Alcoholysis	E_{a1} (kJ·mol^{-1})	E_{a2} (kJ·mol^{-1})
MeOH[4]	67.99 ± 23.42	50.04 ± 10.21
MeOH[2]	53.64 ± 9.65	60.18 ± 17.45
MeOH[3]	28.17 ± 14.05	31.72 ± 18.91

[4] Zn(OAc)$_2$ / DMAP at 1.6 mol% / 2.9 mol%, [2] Zn(OAc)$_2$ at 2 mol% / , [3] Zn(OAc)$_2$ / TBD at 1 mol% each.

The activation energies were also estimated using a first order kinetic model where only the initial cleavage of PLA was considered, shown in Table 6.8. The first order E_a for MeOH[2] and MeOH[3] was estimated to be 46.57 ± 18.76 kJ·mol^{-1} and 44.12 ± 9.19 kJ·mol^{-1}, shown in Table 6.8 (including chapter 4 / 5 activation energies). MeOH[3] displayed the smallest activation energy E_a (44.12 kJ·mol^{-1}), followed by MeOH[2] with a slightly larger E_a (46.57kJ·mol^{-1}). Both experiments had a lower E_a than the other alcoholysis experiments (MeOH[4], EtOH[1], and BuOH[1]). MeOH[2] and MeOH[3] exhibited a lower E_a despite having lower catalyst loadings than the other alcoholysis experiments.

Table 6.8. The activation energies for each step of PLA alcoholysis, considering a first order kinetic model.

Alcoholysis	**E_a (kJ·mol^{-1})**
EtOH[1]	55.1 ± 10.1
BuOH[1]	52.7 ± 17.7
MeOH[4]	48.32 ± 17.7
MeOH[2]	46.57 ± 18.76
MeOH[3]	44.12 ± 9.19

[1] Zn(**1**^{Et})$_2$ at 9 mol%, [2] Zn(OAc)$_2$ at 2 mol%,[3] Zn(OAc)$_2$ / TBD at 1 mol% each, [4] Zn(OAc)$_2$ / DMAP at 1.6 / 2.9 mol%.

When comparing the activation energies of MeOH[2] and MeOH[3] in Table 6.6, Table 6.7, and Table 6.8, the values are significantly different. For example MeOH[2] displayed the smaller value for E_{a1} and E_{a2} in Table 6.6, whereas, in Table 6.7, MeOH[2] displayed the greater value for E_{a1} and E_{a2}. The choice of kinetic model used has a large effect on the resulting activation energies. Comparisons between activation energies should only be made between values obtained from the same kinetic model. Table 6.8 only considers the initial cleavage of PLA ester groups, assuming first order kinetics. All the literature activation energies for PLA chemical recycling in Table 2.4 also only considered this initial step, which makes the values in Table 6.8 particularly useful. The E_a values in Table 6.8 for MeOH[2], MeOH[3], MeOH[4], are lower than all the literature E_a values for hydrolysis, and pyrolysis. This supports the conclusion

that alcoholysis is the superior chemical recycling method from an environmental perspective, as it requires the mildest operating conditions to achieve complete PLA depolymerisation. The only literature E_a values for alcoholysis that were lower than the E_a values in Table 6.8 were achieved using an IL as the catalyst [174–176]. Out of the reported ILs the lowest activation energies were achieved when the IL was coupled with a metal salt, exploiting a synergic effect between the two catalysts, leading to the small activation energies of E_a = 20.96 kJ·mol^{-1} and 21.28 kJ·mol^{-1} [175,176]. Despite excellent activity and recyclability their industrial use is limited by their high costs and intrinsic viscosity. One other publication reported a smaller E_a values than those in Table 6.8. $FeCl_3$ was used resulting in an E_a of 32.41 kJ·mol^{-1} [173]. However, the paper never disclosed the PLA mass that was depolymerised. It could be possible that this was a small scale experiment ≤ 0.1 g PLA, so the reported E_a might not reflect larger scale experiments.

6.5 Conclusion

In this chapter further studies build upon the previous dual catalyst system by investigating a larger range of commercial catalysts. Four catalysts were tested in different mixtures to explore possible synergistic interactions. Preliminary experiments were carried out using only $Zn(OAc)_2$ in order to optimise other reaction conditions, such as mol%, MeOH equivalents, and stirring speed. A range of mol% were tested, and while 4 mol% exhibited the greatest concentration of MeLa in the shortest time, 2 mol% was selected as a compromise between using the least amount of catalyst possible while still obtaining the enhanced reactivity of a higher mol%. A range of MeOH molar equivalents was tested; increasing the MeOH drastically increased the MeLa production rate. By 17 equivalents the increase in MeLa production rate had plateaued. A range of stirring speeds was tested at 9 equivalents of MeOH and 2 mol% $Zn(OAc)_2$. 600 rpm resulted in the greatest concentration of MeLa in the shortest time. These

optimised parameters were explored for each catalyst $Zn(OAc)_2$, $Mg(OAc)_2$, DMAP, and TBD. TBD was the only catalyst that did not exhibit an increase in MeLa production rate when the molar equivalent of MeOH was increased. Both $Zn(OAc)_2$ and DMAP displayed a slower MeOH production rate when stirring speed was increased from 300 to 600 rpm at 17 equivalents of MeOH. A possible explanation is that at 17 equivalents of MeOH, $Zn(OAc)_2$ or DMAP become saturated with MeOH molecules in close proximity, so mass transfer and stirring speed become less important. On the other hand $Mg(OAc)_2$ is larger than $Zn(OAc)_2$ and TBD is larger than DMAP. The larger sizes mean $Mg(OAc)_2$ and TBD will only become saturated with MeOH molecules in close proximity at a higher equivalents of MeOH, which is why both these catalysts exhibited an increase in MeLa production rate when stirring was increased from 300 to 600 rpm at 17 equivalents of MeOH.

Out of the tested mixed catalyst experiments, a synergistic interaction was present for $Mg(OAc)_2$ / TBD, $Zn(OAc)_2$ / TBD, and $Zn(OAc)_2$ / DMAP. These dual catalyst experiments generated a greater rate of MeLa in comparison to their single catalyst counterparts. For example $Mg(OAc)_2$ / TBD displayed a greater MeLa production rate (1.36×10^{-3} g·mL^{-1}·min^{-1}) then $Mg(OAc)_2$ alone (1.09×10^{-3} g·mL^{-1}·min^{-1}). $Zn(OAc)_2$ / TBD, and $Zn(OAc)_2$ / DMAP exhibited greater MeLa production rates (1.34×10^{-3} and 1.29×10^{-3} g·mL^{-1}·min^{-1} respectively) than $Zn(OAc)_2$ alone (1.19×10^{-3} g·mL^{-1}·min^{-1}). These dual catalysts are considered type II partially cooperative, as either catalyst alone results in the formation of the product but at a slower rate compared to dual catalysis [225]. In order for a synergistic interaction to occur there needs to be great enough difference in pK_a between the two catalysts in addition to having both acid and base character.

The relative concentrations of Int, CE, and MeLa methine groups were calculated for the ^{1}H NMR experiments. The relative concentrations were fitted to three kinetic models: an

equilibrium model consisting of two consecutive steps with the second step being in equilibrium, a non-reversable model consisting of two consecutive steps, and a first order model that only considers the initial cleavage of PLA. For the equilibrium kinetic model $Zn(OAc)_2$ had estimated activation energies of E_{a1} = 31.20 ± 7.25 kJ·mol^{-1}, E_{a2} = 34.16 ± 12.2 kJ·mol^{-1}, and E_{a-2} = 47.93 ± 22.84 kJ·mol^{-1}. $Zn(OAc)_2$ / TBD had estimated activation energies of E_{a1} = 51.12 ± 12.51 kJ·mol^{-1}, E_{a2} = 57.08 ± 20.82 kJ·mol^{-1}, and E_{a-2} = 20.06 ± 64.85 kJ·mol^{-1}. For the non-reversable kinetic model $Zn(OAc)_2$ had estimated activation energies of E_{a1} = 53.64 ± 7.25 kJ·mol^{-1}, and E_{a2} = 60.18 ± 17.45 kJ·mol^{-1}. $Zn(OAc)_2$ / TBD had estimated activation energies of E_{a1} = 28.17 ± 14.05 kJ·mol^{-1}, and E_{a2} = 31.72 ± 18.91 kJ·mol^{-1}. Finally for the first order kinetic model $Zn(OAc)_2$ had estimated activation energies of E_a = 46.57 ± 18.76 kJ·mol^{-1}, and $Zn(OAc)_2$ / TBD had estimated activation energies of E_a = 44.12 ± 9.19 kJ·mol^{-1}.

Chapter 7 – Conclusions and Future Work Recommendations

7.1 Conclusions

The chemical recycling of PLA *via* alcoholysis has successfully been carried out, exploring various alcohols, catalysts, as well as other reaction parameters. Dual catalysis has also been explored, gaining an understanding of synergistic effects that enhance reaction rates. These studies have investigated different kinetic models to best describe PLA alcoholysis. The key strengths and limitations of this project are listed as follows:

Chapter 4 - Kinetics of Alkyl Lactate Formation from the Alcoholysis of Poly(lactic acid)

- Ethanolysis of 12.5 g PLA using 1 g = 9 mol% of Zn(**1**^{Et})$_2$ (50 mL EtOH, 250 mL THF as the solvent) at T = 110 °C, 300 rpm, complete depolymerisation of PLA was observed within 317 min. The calculated yield of EtLa at 60 min was 37%. Ethanolysis of 12.5 g PLA using 1 g = 9 mol% Zn(**2**^{Pr})$_2$ (50 mL EtOH, 250 mL THF as the solvent) at T = 50 °C, 800 rpm, complete depolymerisation of PLA was observed within 1031 min. The calculated yield of EtLa at 60 min was 58%. As Zn(**2**^{Pr})$_2$ exhibited non-Arrhenius behaviour at the tested temperature range it was not possible to obtain reliable fits.
- Propanolysis of 12.5 g PLA using 1 g = 9 mol% Zn(**1**^{Et})$_2$ (50 mL PrOH, 250 mL THF as the solvent) at T = 130 °C, 300 rpm, complete depolymerisation of PLA was observed within 616 min. The calculated yield of PrLa at 60 min was 46%. Propanolysis of 12.5 g PLA using 1 g = 9 mol% Zn(**2**^{Pr})$_2$ (50 mL PrOH, 250 mL THF as the solvent) at T = 50 °C, 800 rpm, complete depolymerisation of PLA was observed within 1509 min. The calculated yield of PrLa at 60 min was 44%.
- Butanolysis of 12.5 g PLA using 1 g = 9 mol% Zn(**1**^{Et})$_2$ (50 mL BuOH, 250 mL THF as the solvent) at T = 130 °C, 300 rpm, complete depolymerisation of PLA was observed within 1062 min. The calculated yield of BuLa at 60 min was 17%. Butanolysis of 12.5 g PLA using

1 g = 9 mol% Zn(**2**^{Pr})$_2$ (50 mL BuOH, 250 mL THF as the solvent) at T = 50 °C, 800 rpm, complete depolymerisation of PLA was observed within 8160 min. The calculated yield of BuLa at 60 min was 9%.

- The working hypothesis was that longer chain alcohols would sterically hinder catalyst coordination, resulting in slower reaction rates. It was observed for both catalysts Zn(**1**^{Et})$_2$ and Zn(**2**^{Pr})$_2$ that increasing the alcohol chain length resulted in a slower reaction. The catalytic performance of Zn(**1**^{Et})$_2$ and Zn(**2**^{Pr})$_2$, at all temperatures ≥ 90 °C Zn(**1**^{Et})$_2$ exhibited the greater initial production of AL, whereas, at temperature ≤ 70 °C Zn(**2**^{Pr})$_2$ the reaction displayed non-Arrhenius behaviour and exhibited the greatest initial production of AL.
- A kinetic model was established and applied to the Zn(**1**^{Et})$_2$ experimental data. The model assumed a two-step consecutive reaction with the second step being in equilibrium. The resulting rate equations were solved in MATLAB, using a minimisation of least squares fitting procedure and estimated rate constants were generated from the experimental ^{1}H NMR data. The rate constants were estimated over a range of temperatures and used to generate Arrhenius plots. A simple first order model only considering the initial cleavage of PLA ester groups was also determined and used to generate an Arrhenius plot.
- The equilibrium model was used to estimate the activation energies for each step of the ethanolysis, propanolysis, and butanolysis reactions. The estimated activation energies for ethanolysis are: E_{a1} = 56.3 ± 8.0 kJ·mol^{-1}, E_{a2} = 53.1 ± 6.4 kJ·mol^{-1}, and E_{a-2} = 56.2 ± 18.9 kJ·mol^{-1}.
- Limitations of these studies: although the non-Arrhenius behaviour of Zn(**2**^{Pr})$_2$ allows for relatively high rates of AL production to be achieved at 50 °C, the catalyst is less stable and its reactions are less reproducible in comparison to Zn(**1**^{Et})$_2$; different alcoholysis reactions used 50 mL of alcohol (either EtOH ≈ 5 molar equivalents relative to ester groups, PrOH ≈ 4

equivalents, or BuOH ≈ 3 equivalents) however, should have used the same molar equivalent of each.

Chapter 5 - Synergistic Dual Catalytic System and Kinetics for the Alcoholysis of Poly(lactic acid)

- Preliminary methanolysis experiments investigated different mixtures of $Zn(OAc)_2$ and DMAP and found that dual catalysis resulted in greater concentrations of MeLa in shorter time in comparison to single catalysis. The working hypothesis was that a sufficient difference in pK_a is required for a synergistic dual catalyst complex to occur and result in enhanced activity.
- Methanolysis of 2 g PLA using 0.5 g = 0.8 mol% of $Zn(OAc)_2$ and 0.5 g = 1.5 mol% of DMAP (10 mL MeOH, 40 mL THF as the solvent) at T = 130 °C, 300 rpm, complete depolymerisation of PLA was observed within 93 min. The calculated yield of MeLa at 60 min was 70%. Ethanolysis of 2 g PLA using 0.5 g = 0.8 mol% of $Zn(OAc)_2$ and 0.5 g = 1.5 mol% of DMAP (14.5 mL EtOH, 35.5 mL THF as the solvent) at T = 130 °C, 300 rpm, complete depolymerisation of PLA was observed within 240 min.
- A simplified kinetic model was established and applied to the dual catalysis experimental data. The model assumed a two-step consecutive reaction with the second step being irreversible. The rate equations were solved by sequential integration and substitution, SigmaPlot was used to fit the ^{1}H NMR data to the resulting solution allowing for the determination of the rate constants. The rate constants were estimated over a range of temperatures and used to generate Arrhenius plots. A simple first order model only considering the initial cleavage of PLA ester groups was also determined and used to generate an Arrhenius plot.
- The irreversible model was used to estimate the activation energies for each step of the methanolysis reaction. The resulting activation energies were estimated to be: E_{a1} = 67.99 ±

23.42 kJ·mol^{-1} and E_{a2} = 50.04 ± 10.21 kJ·mol^{-1}. The first order model estimated the activation energy to be E_a = 48.32 ± 26.09 kJ·mol^{-1}.

- Limitations of these studies: although mixtures of $Zn(OAc)_2$ / DMAP were explored there were used in an equal weight ratio, they should have been tested in an equal molar ratio.

Chapter 6 - Methanolysis of Poly(lactic acid) Using Catalyst Mixtures and the Kinetics of Methyl Lactate Production

- Preliminary methanolysis experiments were carried out using $Zn(OAc)_2$; variables such as catalyst loading, MeOH molar equivalents, and stirring speed were explored. Out of the tested variables, catalyst loading and MeOH equivalents had the most significant effect on the reaction rate. Catalyst loading was tested in the range from 1 mol% to 4 mol%. The 4 mol% experiment showed the greatest reaction rates although 2 mol% was only slightly slower while also saving resources. MeOH equivalents were tested from 5 equivalents to 17 equivalents. Increasing the MeOH equivalent significantly increased the reaction rate; by 17 equivalents the increase in MeLa production rate had plateaued.
- Methanolysis was carried out using a range of catalysts. Methanolysis of 2 g PLA using 2 mol% of either $Zn(OAc)_2$, $Mg(OAc)_2$, DMAP, or TBD (19 mL MeOH, 31 mL THF as the solvent) at T = 130 °C, 600 rpm, complete depolymerisation of PLA was observed at 70, 83, 200, and 135 min respectively.
- Dual catalysis methanolysis was carried out using various mixtures of these catalysts. The dual catalysis experiments using $Mg(OAc)_2$ / TBD, $Zn(OAc)_2$ / DMAP, $Zn(OAc)_2$ / TBD, all exhibited enhanced reaction rates in comparison to either catalyst alone. The enhanced reactivity was due to a synergistic complex between the two catalysts. The working hypothesis was that a dual catalyst complex only occurs if there is a sufficient difference in pK_a between the two catalysts, leading to proton transfer and the formation of a stable complex. However,

the dual catalysis TBD / DMAP experiment did not exhibit enhanced reaction rates despite having a great enough difference in pK_a (15.2 and 9.6 respectively). It was then concluded that synergetic complexes only occur if there is both a sufficient pK_a difference and both acid and base components.

- Methanolysis using $Zn(OAc)_2$ and dual $Zn(OAc)_2$ / TBD was explored further. Methanolysis of 2 g PLA using either 2 mol% $Zn(OAc)_2$ or 1 mol% $Zn(OAc)_2$ / 1 mol% TBD (19 mL MeOH, 31 mL THF as the solvent) at T = 130 °C, 600 rpm, complete depolymerisation of PLA was observed at 70 min and 60 min. The calculated yield of MeLa at 60 min was 81% and 93% respectively.
- The previously established kinetic models were applied to $Zn(OAc)_2$ and dual $Zn(OAc)_2$ / TBD methanolysis to determine Arrhenius plots and activation energies for each reaction step. The equilibrium kinetic model estimated the dual catalysis $Zn(OAc)_2$ / TBD to have activation energies of E_{a1} = 51.12 ± 12.51, E_{a2} = 57.08 ± 20.82, and E_{a-2} = 20.06 ± 64.85.
- Limitations of these studies: although the dual catalysis of $Zn(OAc)_2$ / TBD was explored further by ^1H NMR and activation energy calculated, the other synergistic dual experiments $Zn(OAc)_2$ / DMAP and $Mg(OAc)_2$ / TBD was not tested due to time constraints.

7.2 Future Work Recommendations

This thesis has clearly demonstrated the depolymerision of PLA *via* alcoholysis using a range of catalysts. Due to financial, equipment and time constraint, several experiments/analysis could not be performed in the scope of this work and hence are recommended as future work. They are as follows:

- The economic scaled-up chemical recycling of PLA *via* alcoholysis needs to be addressed. A profitable recycling facility should be able to process at least 5 – 18 kt annually. Several reactor types should be explored, including continuous flow reactors and fixed bed

reactors. Different separation techniques should also be investigated. Overall operating costs as well as environmental impact and profitability should all be considered.

- The catalysts investigated in these alcoholysis studies should be explored for other chemical recycling methods for PLA such as pyrolysis and hydrolysis. Hydrolysis in particular should be explored as its product LA has the largest market share.
- The optimised alcoholysis reactions should also explored for PET. PET has a much larger market share and application than PLA so its chemical recycling is more critical in mitigating plastic pollution. While both PLA and PET are polyesters, PLA has less liable bonds and will require harsher conditions such as a higher working temperature.
- Having established the utility of commercial catalysts for dual catalysis systems with enhanced reactivity, these dual systems should be explored further to gain a deeper understanding of their synergistic mechanisms. Furthermore, if these dual catalysis systems could be immobilized in a fixed bed reactor it would solve several issues with downstream processing and product purification.
- The depolymerision of PLA from mixed plastic sources should be carried out. In particular the mild alcoholysis of PLA from PET sources should be addressed as PLA causes significant issues in PET mechanical recycling facilities.

Reference List

1. Geyer, R.; Jambeck, J.R.; Law, K.L. Production, use, and fate of all plastics ever made. *Sci. Adv.* **2017**, *3*, 1–5, doi:10.1126/sciadv.1700782.
2. World Economic Forum The New Plastics Economy Rethinking the future of plastics. **2016**, 1–36, doi:10.1103/Physrevb.74.035409.
3. Hahladakis, J.N.; Iacovidou, E. Closing the loop on plastic packaging materials: What is quality and how does it affect their circularity? *Sci. Total Environ.* **2018**, *630*, 1394–1400, doi:10.1016/j.scitotenv.2018.02.330.
4. Zalasiewicz, J.; Waters, C.N.; Ivar, J.; Corcoran, P.L.; Barnosky, A.D.; Cearreta, A.; Edgeworth, M.; Jeandel, C.; Leinfelder, R.; Mcneill, J.R.; et al. The geological cycle of plastics and their use as a stratigraphic indicator of the Anthropocene. *Anthropocene* **2016**, *13*, 1–37, doi:10.1016/j.ancene.2016.01.002.
5. Vilaplana, F.; Karlsson, S. Quality concepts for the improved use of recycled polymeric materials: A review. *Macromol. Mater. Eng.* **2008**, *293*, 274–297, doi:10.1002/mame.200700393.
6. Schyns, Z.O.G.; Shaver, M.P. Mechanical Recycling of Packaging Plastics: A Review. *Macromol. Rapid Commun.* **2021**, *42*, 1–27, doi:10.1002/marc.202000415.
7. Ragaert, K.; Delva, L.; Van Geem, K. Mechanical and chemical recycling of solid plastic waste. *Waste Manag.* **2017**, *69*, 24–58, doi:10.1016/j.wasman.2017.07.044.
8. Meys, R.; Frick, F.; Westhues, S.; Sternberg, A.; Klankermayer, J.; Bardow, A. Towards a circular economy for plastic packaging wastes – the environmental potential of chemical recycling. *Resour. Conserv. Recycl.* **2020**, *162*, 105010, doi:10.1016/j.resconrec.2020.105010.
9. European Bioplastics Bioplastics facts and figures Available online: https://docs.european-bioplastics.org/publications/EUBP_Facts_and_figures.pdf (accessed on Jan 10, 2022).
10. Aryan, V.; Maga, D.; Majgaonkar, P.; Hanich, R. Valorisation of polylactic acid (PLA) waste: A comparative life cycle assessment of various solvent-based chemical recycling technologies. *Resour. Conserv. Recycl.* **2021**, *172*, doi:10.1016/j.resconrec.2021.105670.
11. Lamberti, F.M.; Román-Ramírez, L.A.; Wood, J. Recycling of Bioplastics: Routes and Benefits. *J. Polym. Environ.* **2020**, doi:10.1007/s10924-020-01795-8.
12. Lamberti, F.M.; Román-Ramírez, L.A.; Mckeown, P.; Jones, M.D.; Wood, J. Kinetics of alkyl lactate formation from the alcoholysis of poly(lactic acid). *Processes* **2020**, *8*, doi:10.3390/PR8060738.
13. Lamberti, F.M.; Ingram, A.; Wood, J. Synergistic Dual Catalytic System and Kinetics for the Alcoholysis of Poly(Lactic Acid). **2021**, doi:10.3390/pr9060921.

14. Lamberti, F.M.; Rom, L.A.; Dove, A.P.; Wood, J. Methanolysis of Poly(lactic Acid) Using Catalyst Mixtures and the Kinetics of Methyl Lactate Production. **2022**, doi:10.3390/polym14091763.
15. Namazi, H. Polymers in our daily life. *BioImpacts* **2017**, *7*, 73–74, doi:10.15171/bi.2017.09.
16. IUPAC What are polymers? Available online: https://iupac.org/polymer-edu/what-are-polymers/ (accessed on Oct 13, 2021).
17. Seymour, R.B. Polymers are everywhere. *J. Chem. Educ.* **1988**, *65*, 327–334, doi:10.1021/ed065p327.
18. Feldman, D. Polymer history. *Des. Monomers Polym.* **2008**, *11*, 1–15, doi:10.1163/156855508X292383.
19. Percec, V.; Xiao, Q. The Legacy of Hermann Staudinger: Covalently Linked Macromolecules. *Chem* **2020**, *6*, 2855–2861, doi:10.1016/j.chempr.2020.10.007.
20. Tarkanian, M.J.; Hosler, D. America's First Polymer Scientists: Rubber Processing, Use and Transport in Mesoamerica. *Lat. Am. Antiq.* **2011**, *22*, 469–486, doi:10.7183/1045-6635.22.4.469.
21. Hosler, D.; Burkett, S, L.; Tarkanian, M.J. Prehistoric polymers: rubber processing in ancient mesoamerica. *Science*. **1999**, *284*, 1988–1991, doi:10.1126/science.284.5422.1988.
22. Mülhaupt, R. Catalytic polymerization and post polymerization catalysis fifty years after the discovery of Ziegler's catalysts. *Macromol. Chem. Phys.* **2003**, *204*, 289–327, doi:10.1002/macp.200290085.
23. Payne, J.; Jones, M.D. The Chemical Recycling of Polyesters for a Circular Plastics Economy: Challenges and Emerging Opportunities. *ChemSusChem* **2021**, 1–31, doi:10.1002/cssc.202100400.
24. Zheng, Y.; Yanful, E.K.; Bassi, A.S. A review of plastic waste biodegradation. *Crit. Rev. Biotechnol.* **2005**, *25*, 243–250, doi:10.1080/07388550500346359.
25. Grigore, M. Methods of Recycling, Properties and Applications of Recycled Thermoplastic Polymers. *Recycling* **2017**, *2*, 24, doi:10.3390/recycling2040024.
26. Christensen, P.R.; Scheuermann, A.M.; Loeffler, K.E.; Helms, B.A. Closed-loop recycling of plastics enabled by dynamic covalent diketoenamine bonds. *Nat. Chem.* **2019**, *11*, 442–448, doi:10.1038/s41557-019-0249-2.
27. Odian, G. *Principles of polymerization*; Fourth ed.; John Wiley and Sons: New York, 2004; ISBN 0-471-27400-3.
28. Wang, W.; Lu, W.; Goodwin, A.; Wang, H.; Yin, P.; Kang, N.G.; Hong, K.; Mays, J.W. Recent advances in thermoplastic elastomers from living polymerizations: Macromolecular architectures and supramolecular chemistry. *Prog. Polym. Sci.* **2019**, *95*, 1–31, doi:10.1016/j.progpolymsci.2019.04.002.

29. Farah, S.; Anderson, D.G.; Langer, R. Physical and mechanical properties of PLA, and their functions in widespread applications — A comprehensive review. *Adv. Drug Deliv. Rev.* **2016**, *107*, 367–392, doi:10.1016/j.addr.2016.06.012.
30. Cantor, K. *Blown Film Extrusion An Introduction*; Hanser Publishers, 2013; Vol. 53; ISBN 978-1-56990-396-4.
31. Balani, K.; Verma, V.; Agarwal, A.; Narayan, R. Physical, Thermal, and Mechanical Properties of Polymers. In *Biosurfaces: A Materials Science and Engineering Perspective*; 2015; pp. 329–344 ISBN 9781118950623.
32. Grand View Research Plastic Market Size, Share & Trends Analysis Report By Product (PE, PP, PU, PVC, PET, Polystyrene, ABS, PBT, PPO, Epoxy Polymers, LCP, PC, Polyamide), By Application, By End-use, By Region, And Segment Forecasts, 2021 - 2028 Available online: https://www.grandviewresearch.com/industry-analysis/global-plastics-market (accessed on Jan 31, 2022).
33. Geyer, R. Production, use, and fate of synthetic polymers. In *Plastic Waste and Recycling*; Elsevier Inc., 2020; pp. 13–32 ISBN 978-0-12-817880-5.
34. Stephens, R.D.; Williams, R.L.; Keoleian, G.A.; Spatari, S.; Beal, R. Comparative life cycle assessment of plastic and steel vehicle fuel tanks. *SAE Tech. Pap.* **1998**, doi:10.4271/982224.
35. Simon, B.; Amor, M. Ben; Földényi, R. Life cycle impact assessment of beverage packaging systems: Focus on the collection of post-consumer bottles. *J. Clean. Prod.* **2016**, *112*, 238–248, doi:10.1016/j.jclepro.2015.06.008.
36. Stefanini, R.; Borghesi, G.; Ronzano, A.; Vignali, G. Plastic or glass: a new environmental assessment with a marine litter indicator for the comparison of pasteurized milk bottles. *Int. J. Life Cycle Assess.* **2021**, *26*, 767–784, doi:10.1007/s11367-020-01804-x.
37. Sevitz, J.; Brent, A.C.; Fourie, A.B. An Environmental Comparison of Plastic and Paper Consumer Carrier Bags in South Africa: Implications for the Local Manufacturing Industry. *South African J. Ind. Eng.* **2012**, *14*, 67–82, doi:10.7166/14-1-299.
38. Ahamed, A.; Vallam, P.; Iyer, N.S.; Veksha, A.; Bobacka, J.; Lisak, G. Life cycle assessment of plastic grocery bags and their alternatives in cities with confined waste management structure: A Singapore case study. *J. Clean. Prod.* **2021**, *278*, 123956, doi:10.1016/j.jclepro.2020.123956.
39. Worch, J.C.; Dove, A.P. 100th Anniversary of Macromolecular Science Viewpoint: Toward Catalytic Chemical Recycling of Waste (and Future) Plastics. *ACS Macro Lett.* **2020**, 1494–1506, doi:10.1021/acsmacrolett.0c00582.
40. Jambeck, J.; Geyer, R.; Wilcox, C.; Siegler, T.R.; Perryman, M.; Andrady, A.; Narayan, R.; Law, K.L. Plastic waste inputs from land into the ocean. *Publ. Am. Assoc. Adv. Sci.* **2015**, *347*, 768–771, doi:10.1126/science.1260352.

41. Dilkes-Hoffman, L.S.; Pratt, S.; Lant, P.A.; Laycock, B. The Role of Biodegradable Plastic in Solving Plastic Solid Waste Accumulation. In *Plastics to Energy*; Elsevier Inc., 2019; pp. 469–505 ISBN 978-0-12-813140-4.
42. Sudhakar, M.; Trishul, A.; Doble, M.; Suresh Kumar, K.; Syed Jahan, S.; Inbakandan, D.; Viduthalai, R.R.; Umadevi, V.R.; Sriyutha Murthy, P.; Venkatesan, R. Biofouling and biodegradation of polyolefins in ocean waters. *Polym. Degrad. Stab.* **2007**, *92*, 1743–1752, doi:10.1016/j.polymdegradstab.2007.03.029.
43. Zhang, C.; Chen, X.; Wang, J.; Tan, L. Toxic effects of microplastic on marine microalgae Skeletonema costatum: Interactions between microplastic and algae. *Environ. Pollut.* **2017**, *220*, 1282–1288, doi:10.1016/j.envpol.2016.11.005.
44. Bergmann, M.; Gutow, L.; Klages, M. *Marine anthropogenic litter*; Springer Open, 2015; ISBN 978-3-319-16509-7.
45. Cole, M.; Lindeque, P.; Fileman, E.; Halsband, C.; Goodhead, R.; Moger, J.; Galloway, T.S. Microplastic ingestion by zooplankton. *Environ. Sci. Technol.* **2013**, *47*, 6646–6655, doi:10.1021/es400663f.
46. United Nations Enviroment Programme *UNEP Year Book 2014 emerging issues update*; 2014; ISBN 978-92-807-3381-5.
47. Igamberdiev, A.U.; Lea, P.J. Land plants equilibrate O2 and CO2 concentrations in the atmosphere. *Photosynth. Res.* **2006**, *87*, 177–194, doi:10.1007/s11120-005-8388-2.
48. Cox, K.D.; Covernton, G.A.; Davies, H.L.; Dower, J.F.; Juanes, F.; Dudas, S.E. Human Consumption of Microplastics. *Environ. Sci. Technol.* **2019**, *53*, 7068–7074, doi:10.1021/acs.est.9b01517.
49. Wang, F.; Wong, C.S.; Chen, D.; Lu, X.; Wang, F.; Zeng, E.Y. Interaction of toxic chemicals with microplastics: A critical review. *Water Res.* **2018**, *139*, 208–219, doi:10.1016/j.watres.2018.04.003.
50. Sharma, S.; Chatterjee, S. Microplastic pollution, a threat to marine ecosystem and human health: a short review. *Environ. Sci. Pollut. Res.* **2017**, *24*, 21530–21547, doi:10.1007/s11356-017-9910-8.
51. Phillips, K.P.; Tanphaichitr, N. Human exposure to endocrine disrupters and semen quality. *J. Toxicol. Environ. Heal. - Part B Crit. Rev.* **2008**, *11*, 188–220, doi:10.1080/10937400701873472.
52. Hopewell, J.; Dvorak, R.; Kosior, E. Plastics recycling: Challenges and opportunities. *Philos. Trans. R. Soc. B Biol. Sci.* **2009**, *364*, 2115–2126, doi:10.1098/rstb.2008.0311.
53. Cimpan, C.; Maul, A.; Jansen, M.; Pretz, T.; Wenzel, H. Central sorting and recovery of MSW recyclable materials: A review of technological state-of-the-art, cases, practice and implications

for materials recycling. *J. Environ. Manage.* **2015**, *156*, 181–199, doi:10.1016/j.jenvman.2015.03.025.

54. Burat, F.; Güney, A.; Olgaç Kangal, M. Selective separation of virgin and post-consumer polymers (PET and PVC) by flotation method. *Waste Manag.* **2009**, *29*, 1807–1813, doi:10.1016/j.wasman.2008.12.018.
55. Čablík, V.; Topiarzova, R.; Čablíková, L. APPLICATION OF FLOTATION IN SEPARATING PLASTIC MATERIALS. In Proceedings of the International Multidisciplinary Scientific GeoConference; 2014; pp. 811–816.
56. Hearn, G.L.; Ballard, J.R. The use of electrostatic techniques for the identification and sorting of waste packaging materials. *Resour. Conserv. Recycl.* **2005**, *44*, 91–98, doi:10.1016/j.resconrec.2004.08.001.
57. Park, C.H.; Jeon, H.S.; Park, J.K. PVC removal from mixed plastics by triboelectrostatic separation. *J. Hazard. Mater.* **2007**, *144*, 470–476, doi:10.1016/j.jhazmat.2006.10.060.
58. Singh, N.; Hui, D.; Singh, R.; Ahuja, I.P.S.; Feo, L.; Fraternali, F. Recycling of plastic solid waste: A state of art review and future applications. *Compos. Part B Eng.* **2017**, *115*, 409–422, doi:10.1016/j.compositesb.2016.09.013.
59. Al-Salem, S.M.; Lettieri, P.; Baeyens, J. Recycling and recovery routes of plastic solid waste (PSW): A review. *Waste Manag.* **2009**, *29*, 2625–2643, doi:10.1016/j.wasman.2009.06.004.
60. Kumar, S.; Panda, A.K.; Singh, R.K. A review on tertiary recycling of high-density polyethylene to fuel. *Resour. Conserv. Recycl.* **2011**, *55*, 893–910, doi:10.1016/j.resconrec.2011.05.005.
61. Shen, L.; Worrell, E.; Patel, M.K. Open-loop recycling: A LCA case study of PET bottle-to-fibre recycling. *Resour. Conserv. Recycl.* **2010**, *55*, 34–52, doi:10.1016/j.resconrec.2010.06.014.
62. Francis, R. *Recycling of polymers: methods, characterization and applications*; John Wiley and Sons: USA, 2016; ISBN 978-3-527-33848-1.
63. Payne, J.; McKeown, P.; Jones, M.D. A circular economy approach to plastic waste. *Polym. Degrad. Stab.* **2019**, *165*, 170–181, doi:10.1016/j.polymdegradstab.2019.05.014.
64. Nikles, D.E.; Farahat, M.S. New motivation for the depolymerization products derived from poly(ethylene terephthalate) (PET) waste: A review. *Macromol. Mater. Eng.* **2005**, *290*, 13–30, doi:10.1002/mame.200400186.
65. Subramanian, P.. Plastics recycling and waste management in US. *Resour. Conserv. Recycl.* **2000**, *28*, 253–263, doi:10.1016/S0921-3449(99)00049-X.
66. Hites, R.A. Dioxins: An overview and history. *Environ. Sci. Technol.* **2011**, *45*, 16–20, doi:10.1021/es1013664.
67. Niaounakis, M. Introduction to Biopolymers. In *Biopolymers Reuse, Recycling, and Disposal*; 2013; pp. 1–75 ISBN 978-1-4557-3145-9.

68. De Clercq, R.; Dusselier, M.; Sels, B.F. Heterogeneous catalysis for bio-based polyester monomers from cellulosic biomass: Advances, challenges and prospects. *Green Chem.* **2017**, *19*, 5012–5040, doi:10.1039/c7gc02040f.
69. Niaounakis, M. Introduction. In *Biopolymers: Processing and Products*; William Andrew, 2015; pp. 1–77 ISBN 9780323266987.
70. Piemonte, V. Bioplastic Wastes: The Best Final Disposition for Energy Saving. *J. Polym. Environ.* **2011**, *19*, 988–994, doi:10.1007/s10924-011-0343-z.
71. Stephen, J.D.; Mabee, W.E.; Saddler, J.N. Will second-generation ethanol be able to compete with first-generation ethanol? Opportunities for cost reduction. *Biofuels, Bioprod. Biorefining* **2011**, *6*, 159–176, doi:10.1002/bbb.331.
72. Repo, A.; Känkänen, R.; Tuovinen, J.P.; Antikainen, R.; Tuomi, M.; Vanhala, P.; Liski, J. Forest bioenergy climate impact can be improved by allocating forest residue removal. *GCB Bioenergy* **2012**, *4*, 202–212, doi:10.1111/j.1757-1707.2011.01124.x.
73. de Paula, F.C.; de Paula, Carolin. B, C.; Contiero, J. Prospective Biodegradable Plastics from Biomass Conversion Processes. In *Biofuels - State of Development*; IntechOpen: London, 2018; pp. 246–271 ISBN 978-1-78923-346-9.
74. Schmidt, J.; Jia, J. Time and Cost to Commercialize an Oil Shale Surface Retorting Technology. In Proceedings of the Oil Shale Symposium Colorado School of Mines; 2007; pp. 1–9.
75. Shen, L.; Worrell, E.; Patel, M.K. Comparing life cycle energy and GHG emissions of bio- based PET, recycled PET, PLA, and man-made cellulosics. *Biofuels, Bioprod. Biorefining* **2012**, *6*, 625–639, doi:10.1002/bbb.
76. Tabone, M.D.; Cregg, J.J.; Beckman, E.J.; Landis, A.E. Sustainability metrics: Life cycle assessment and green design in polymers. *Environ. Sci. Technol.* **2010**, *44*, 8264–8269, doi:10.1021/es103760e.
77. Chen, L.; Pelton, R.E.O.; Smith, T.M. Comparative life cycle assessment of fossil and bio-based polyethylene terephthalate (PET) bottles. *J. Clean. Prod.* **2016**, *137*, 667–676, doi:10.1016/j.jclepro.2016.07.094.
78. Feldman, R.M.R.; Gunawardena, U.; Urano, J.; Meinhold, P.; Aristidou, A.; Dundon, Catherine, A.; Smith, C. Yeast organism producing isobutanol at a high yield 2011, US 2011/020889 A1.
79. Peters, M.; Taylor, J.D.; Jenni, M.; Manzer, L.E.; Henton, D.E. Integrated process to selectively convert renewable isobutanol to p-xylene 2010, WO 2011/044243 A1.
80. Luo, L.; van der Voet, E.; Huppes, G. An energy analysis of ethanol from cellulosic feedstock-Corn stover. *Renew. Sustain. Energy Rev.* **2009**, *13*, 2003–2011, doi:10.1016/j.rser.2009.01.016.
81. Hendriks, A.T.W.M.; Zeeman, G. Pretreatments to enhance the digestibility of lignocellulosic biomass. *Bioresour. Technol.* **2009**, *100*, 10–18, doi:10.1016/j.biortech.2008.05.027.

82. van Schijndel, J.; Molendijk, D.; van Beurden, K.; Canalle, L.A.; Noël, T.; Meuldijk, J. Preparation of bio-based styrene alternatives and their free radical polymerization. *Eur. Polym. J.* **2020**, *125*, 109534, doi:10.1016/j.eurpolymj.2020.109534.
83. Takeshima, H.; Satoh, K.; Kamigaito, M. Bio-Based Functional Styrene Monomers Derived from Naturally Occurring Ferulic Acid for Poly(vinylcatechol) and Poly(vinylguaiacol) via Controlled Radical Polymerization. *Macromolecules* **2017**, *50*, 4206–4216, doi:10.1021/acs.macromol.7b00970.
84. Mohan, S.K.; Srivastava, T. Microbial deterioration and degradation of Polymeric materials. *J. Biochem. Technol.* **2010**, *2*, 210–215, doi:10.1016/S0964-8305(02)00177-4.
85. Luckachan, G.E.; Pillai, C.K.S. Biodegradable Polymers- A Review on Recent Trends and Emerging Perspectives. *J. Polym. Environ.* **2011**, *19*, 637–676, doi:10.1007/s10924-011-0317-1.
86. Tokiwa, Y.; Calabia, B.P.; Ugwu, C.U.; Aiba, S. Biodegradability of plastics. *Int. J. Mol. Sci.* **2009**, *10*, 3722–3742, doi:10.3390/ijms10093722.
87. Shah, A.A.; Hasan, F.; Hameed, A.; Ahmed, S. Biological degradation of plastics: A comprehensive review. *Biotechnol. Adv.* **2008**, *26*, 246–265, doi:10.1016/j.biotechadv.2007.12.005.
88. Artham, T.; Doble, M. Biodegradation of aliphatic and aromatic polycarbonates. *Macromol. Biosci.* **2008**, *8*, 14–24, doi:10.1002/mabi.200700106.
89. European Bioplastics EN 13432 Certified Bioplastics Performance In Industrial Composting Available online: https://docs.european-bioplastics.org/publications/bp/EUBP_BP_En_13432.pdf (accessed on Jan 10, 2022).
90. Song, J.H.; Murphy, R.J.; Narayan, R.; Davies, G.B.H. Biodegradable and compostable alternatives to conventional plastics. *Philos. Trans. R. Soc. B Biol. Sci.* **2009**, *364*, 2127–2139, doi:10.1098/rstb.2008.0289.
91. Potting, J.; van der Harst, E. Facility arrangements and the environmental performance of disposable and reusable cups. *Int. J. Life Cycle Assess.* **2015**, *20*, 1143–1154, doi:10.1007/s11367-015-0914-7.
92. Niaounakis, M. Recycling of biopolymers – The patent perspective. *Eur. Polym. J.* **2019**, *114*, 464–475, doi:10.1016/j.eurpolymj.2019.02.027.
93. Benn, N.; Zitomer, D. Pretreatment and anaerobic co-digestion of selected PHB and PLA bioplastics. *Front. Environ. Sci.* **2018**, *5*, 1–9, doi:10.3389/fenvs.2017.00093.
94. Madhavan Nampoothiri, K.; Nair, N.R.; John, R.P. An overview of the recent developments in polylactide (PLA) research. *Bioresour. Technol.* **2010**, *101*, 8493–8501, doi:10.1016/j.biortech.2010.05.092.

95. Garlotta, D. A Literature Review of Poly(Lactic Acid). *J. Polym. Environ.* **2001**, *9*, 63–84, doi:https://doi.org/10.1023/A:1020200822435.
96. Henton, D.E..; Gruber, P.; Lunt, J.; Randall, J. Chapter 16. Polylactic Acid Technology. In *Natural Fibers, Biopolymers, and Biocomposites*; 2005; pp. 527–578 ISBN 978-0-8493-1741-5.
97. Rabnawaz, M.; Wyman, I.; Auras, R.; Cheng, S. A roadmap towards green packaging: The current status and future outlook for polyesters in the packaging industry. *Green Chem.* **2017**, *19*, 4737–4753, doi:10.1039/c7gc02521a.
98. Gupta, A.P.; Kumar, V. New emerging trends in synthetic biodegradable polymers - Polylactide: A critique. *Eur. Polym. J.* **2007**, *43*, 4053–4074, doi:10.1016/j.eurpolymj.2007.06.045.
99. Thomas, C.M. Stereocontrolled ring-opening polymerization of cyclic esters: Synthesis of new polyester microstructures. *Chem. Soc. Rev.* **2010**, *39*, 165–173, doi:10.1039/b810065a.
100. Fabra, M.J.; Lopez-Rubio, A.; Lagaron, J.M. Nanostructured interlayers of zein to improve the barrier properties of high barrier polyhydroxyalkanoates and other polyesters. *J. Food Eng.* **2014**, *127*, 1–9, doi:10.1016/j.jfoodeng.2013.11.022.
101. Lu, J.; Tappel, R.C.; Nomura, C.T. Mini-review: Biosynthesis of poly(hydroxyalkanoates). *Polym. Rev.* **2009**, *49*, 226–248, doi:10.1080/15583720903048243.
102. Hamad, K.; Kaseem, M.; Yang, H.W.; Deri, F.; Ko, Y.G. Properties and medical applications of polylactic acid: A review. *Express Polym. Lett.* **2015**, *9*, 435–455, doi:10.3144/expresspolymlett.2015.42.
103. Lemmouchi, Y.; Murariu, M.; Santos, A.M. Dos; Amass, A.J.; Schacht, E.; Dubois, P. Plasticization of poly(lactide) with blends of tributyl citrate and low molecular weight poly(d,l-lactide)-b-poly(ethylene glycol) copolymers. *Eur. Polym. J.* **2009**, *45*, 2839–2848, doi:10.1016/j.eurpolymj.2009.07.006.
104. Parker, K.; Garancher, J.P.; Shah, S.; Fernyhough, A. Expanded polylactic acid - An eco-friendly alternative to polystyrene foam. *J. Cell. Plast.* **2011**, *47*, 233–243, doi:10.1177/0021955X11404833.
105. Niaounakis, M. Foaming and Foamed Products. In *Biopolymers: Processing and Products*; William Andrew, 2015; pp. 327–359 ISBN 9780323266987.
106. Nofar, M.; Park, C.B. Poly (lactic acid) foaming. *Prog. Polym. Sci.* **2014**, *39*, 1721–1741, doi:10.1016/j.progpolymsci.2014.04.001.
107. Abdel-Rahman, M.A.; Tashiro, Y.; Sonomoto, K. Recent advances in lactic acid production by microbial fermentation processes. *Biotechnol. Adv.* **2013**, *31*, 877–902, doi:10.1016/j.biotechadv.2013.04.002.
108. Auras, R.; Harte, B.; Selke, S. An overview of polylactides as packaging materials. *Macromol. Biosci.* **2004**, *4*, 835–864, doi:10.1002/mabi.200400043.

109. Inkinen, S.; Hakkarainen, M.; Albertsson, A.C.; Södergård, A. From lactic acid to poly(lactic acid) (PLA): Characterization and analysis of PLA and Its precursors. *Biomacromolecules* **2011**, *12*, 523–532, doi:10.1021/bm101302t.
110. VanWouwe, P.; Dusselier, M.; Vanleeuw, E.; Sels, B. Lactide Synthesis and Chirality Control for Polylactic acid Production. *ChemSusChem* **2016**, *9*, 907–921, doi:10.1002/cssc.201501695.
111. Lee, H.D.; Lee, M.Y.; Hwang, Y.S.; Cho, Y.H.; Kim, H.W.; Park, H.B. Separation and Purification of Lactic Acid from Fermentation Broth Using Membrane-Integrated Separation Processes. *Ind. Eng. Chem. Res.* **2017**, *56*, 8301–8310, doi:10.1021/acs.iecr.7b02011.
112. Werpy, T.; Petersen, G. Top Value Added Chemicals from Biomass Volume I. *U. S. Dep. Energy* **2004**, doi:10.2172/15008859.
113. Dusselier, M.; Van Wouwe, P.; Dewaele, A.; Makshina, E.; Sels, B.F. Lactic acid as a platform chemical in the biobased economy: The role of chemocatalysis. *Energy Environ. Sci.* **2013**, *6*, 1415–1442, doi:10.1039/c3ee00069a.
114. Singhvi, M.S.; Gokhale, D. V. Lignocellulosic biomass: Hurdles and challenges in its valorization. *Appl. Microbiol. Biotechnol.* **2019**, *103*, 9305–9320, doi:10.1007/s00253-019-10212-7.
115. Shaver, M.P.; Cameron, D.J.A. Tacticity control in the synthesis of poly(lactic acid) polymer stars with dipentaerythritol cores. *Biomacromolecules* **2010**, *11*, 3673–3679, doi:10.1021/bm101140d.
116. Sangeetha, V.H.; Deka, H.; Varghese, T.O.; Nayak, S.K. State of the art and future prospectives of poly(lactic acid) based blends and composites. *Polym. Compos.* **2018**, *39*, 81–101, doi:10.1002/pc.23906.
117. Stanford, M.J.; Dove, A.P. Stereocontrolled ring-opening polymerisation of lactide. *Chem. Soc. Rev.* **2010**, *39*, 486–494, doi:10.1039/b815104k.
118. Ovitt, T.M.; Coates, G.W. Stereoselective Ring-Opening Polymerization of rac-Lactide with a Single-Site, Racemic Aluminum Alkoxide Catalyst: Synthesis of Stereoblock Poly(lactic acid). *J. Polym. Sci. Part A Polym. Chem.* **2000**, *38*, 4686–4692, doi:https://doi.org/10.1002/1099-0518(200012)38:1+<4686::AID-POLA80>3.0.CO;2-0.
119. Qi, X.; Ren, Y.; Wang, X. New advances in the biodegradation of Poly (lactic) acid. *Int. Biodeterior. Biodegradation* **2017**, *117*, 215–223, doi:10.1016/j.ibiod.2017.01.010.
120. Haider, T.P.; Vçlker, C.; Kramm, J.; Landfester, K.; Wurm, F.R. Plastics of the Future? The Impact of Biodegradable Polymers on the Environment and on Society. *Angew. Chemie Int. Ed.* **2019**, *58*, 50–62, doi:10.1002/anie.201805766.
121. Tokiwa, Y.; Calabia, B.P. Biodegradability and Biodegradation of Polyesters. *J. Polym. Environ.* **2007**, *15*, 259–267, doi:10.1007/s10924-007-0066-3.

122. California Department of Resources Recycling and Recovery PLA and PHA Biodegradation in the Marine Environment. (2012).1.
123. Shogren, R.L.; Doane, W.M.; Garlotta, D.; Lawton, J.W.; Willett, J.L. Biodegradation of starch/polylactic acid/poly(hydroxyester-ether) composite bars in soil. *Polym. Degrad. Stab.* **2003**, *79*, 405–411, doi:10.1016/S0141-3910(02)00356-7.
124. Yagi, H.; Ninomiya, F.; Funabashi, M.; Kunioka, M. Mesophilic anaerobic biodegradation test and analysis of eubacteria and archaea involved in anaerobic biodegradation of four specified biodegradable polyesters. *Polym. Degrad. Stab.* **2014**, *110*, 278–283, doi:10.1016/j.polymdegradstab.2014.08.031.
125. Cosate de Andrade, M.F.; Souza, P.M.S.; Cavalett, O.; Morales, A.R. Life Cycle Assessment of Poly(Lactic Acid) (PLA): Comparison Between Chemical Recycling, Mechanical Recycling and Composting. *J. Polym. Environ.* **2016**, *24*, 372–384, doi:10.1007/s10924-016-0787-2.
126. Badia, J.D.; Ribes-Greus, A. Mechanical recycling of polylactide, upgrading trends and combination of valorization techniques. *Eur. Polym. J.* **2016**, *84*, 22–39, doi:10.1016/j.eurpolymj.2016.09.005.
127. Badía, J.D.; Strömberg, E.; Ribes-Greus, A.; Karlsson, S. Assessing the MALDI-TOF MS sample preparation procedure to analyze the influence of thermo-oxidative ageing and thermo-mechanical degradation on poly (Lactide). *Eur. Polym. J.* **2011**, *47*, 1416–1428, doi:10.1016/j.eurpolymj.2011.05.001.
128. Beltrán, F.R.; Lorenzo, V.; Acosta, J.; de la Orden, M.U.; Martínez Urreaga, J. Effect of simulated mechanical recycling processes on the structure and properties of poly(lactic acid). *J. Environ. Manage.* **2018**, *216*, 25–31, doi:10.1016/j.jenvman.2017.05.020.
129. Zenkiewicz, M.; Richert, J.; Rytlewski, P.; Moraczewski, K.; Stepczyńska, M.; Karasiewicz, T. Characterisation of multi-extruded poly(lactic acid). *Polym. Test.* **2009**, *28*, 412–418, doi:10.1016/j.polymertesting.2009.01.012.
130. Cosate de Andrade, M.F.; Fonseca, G.; Morales, A.R.; Mei, L.H.I. Mechanical recycling simulation of polylactide using a chain extender. *Adv. Polym. Technol.* **2018**, *37*, 2053–2060, doi:10.1002/adv.21863.
131. Niaounakis, M. Chapter 16 – Recycling. In *Biopolymers: Processing and Products*; 2015; pp. 481–530 ISBN 9780323266987.
132. Cornell, D.D. Biopolymers in the existing postconsumer plastics recycling stream. *J. Polym. Environ.* **2007**, *15*, 295–299, doi:10.1007/s10924-007-0077-0.
133. Gorrasi, G.; Pantani, R. Hydrolysis and Biodegradation of Poly(lactic acid). *Adv. Polym. Sci.* **2017**, *279*, 119–151, doi:10.1007/12_2016_12.
134. McKeown, P.; Jones, M.D. The Chemical Recycling of PLA: A Review. *Sustain. Chem.* **2020**,

1, 1–22, doi:10.3390/suschem1010001.

135. Rodriguez, E.J.; Marcos, B.; Huneault, M.A. Hydrolysis of polylactide in aqueous media. *J. Appl. Polym. Sci.* **2016**, *133*, 1–11, doi:10.1002/app.44152.
136. Friederike, von B.; Luise, S.; Achim, G. Why degradable polymers undergo surface erosion or bulk erosion. *Biomaterials* **2002**, *23*, 4221–4231, doi:10.1016/s0142-9612(02)00170-9.
137. Piemonte, V.; Sabatini, S.; Gironi, F. Chemical Recycling of PLA: A Great Opportunity Towards the Sustainable Development? *J. Polym. Environ.* **2013**, *21*, 640–647, doi:10.1007/s10924-013-0608-9.
138. De Jong, S.J.; Arias, E.R.; Rijkers, D.T.S.; Van Nostrum, C.F.; Kettenes-Van Den Bosch, J.J.; Hennink, W.E. New insights into the hydrolytic degradation of poly(lactic acid): Participation of the alcohol terminus. *Polymer (Guildf).* **2001**, *42*, 2795–2802, doi:10.1016/S0032-3861(00)00646-7.
139. Tsuji, H.; Ikada, Y. Properties and morphology of poly(L-lactide). II. hydrolysis in alkaline solution. *J. Polym. Sci. Part A Polym. Chem.* **1998**, *36*, 59–66, doi:10.1002/(SICI)1099-0518(19980115)36:1<59::AID-POLA9>3.0.CO;2-X.
140. Tsuji, H.; Daimon, H.; Fujie, K. A new strategy for recycling and preparation of poly(L-lactic acid): Hydrolysis in the melt. *Biomacromolecules* **2003**, *4*, 835–840, doi:10.1021/bm034060j.
141. Tsuji, H.; Saeki, T.; Tsukegi, T.; Daimon, H.; Fujie, K. Comparative study on hydrolytic degradation and monomer recovery of poly(l-lactic acid) in the solid and in the melt. *Polym. Degrad. Stab.* **2008**, *93*, 1956–1963, doi:10.1016/j.polymdegradstab.2008.06.009.
142. Mohd-Adnan, A.F.; Nishida, H.; Shirai, Y. Evaluation of kinetics parameters for poly(l-lactic acid) hydrolysis under high-pressure steam. *Polym. Degrad. Stab.* **2008**, *93*, 1053–1058, doi:10.1016/j.polymdegradstab.2008.03.022.
143. Piemonte, V.; Gironi, F. Kinetics of Hydrolytic Degradation of PLA. *J. Polym. Environ.* **2013**, *21*, 313–318, doi:10.1007/s10924-012-0547-x.
144. Hirao, K.; Shimamoto, Y.; Nakatsuchi, Y.; Ohara, H. Hydrolysis of poly(l-lactic acid) using microwave irradiation. *Polym. Degrad. Stab.* **2010**, *95*, 86–88, doi:10.1016/j.polymdegradstab.2009.10.003.
145. Iñiguez-Franco, F.; Auras, R.; Burgess, G.; Holmes, D.; Fang, X.; Rubino, M.; Soto-Valdez, H. Concurrent solvent induced crystallization and hydrolytic degradation of PLA by water-ethanol solutions. *Polymer (Guildf).* **2016**, *99*, 315–323, doi:10.1016/j.polymer.2016.07.018.
146. Iñiguez-Franco, F.; Auras, R.; Dolan, K.; Selke, S.; Holmes, D.; Rubino, M.; Soto-Valdez, H. Chemical recycling of poly(lactic acid) by water-ethanol solutions. *Polym. Degrad. Stab.* **2018**, *149*, 28–38, doi:10.1016/j.polymdegradstab.2018.01.016.
147. Song, X.; Wang, H.; Yang, X.; Liu, F.; Yu, S.; Liu, S. Hydrolysis of poly(lactic acid) into calcium

lactate using ionic liquid [Bmim][OAc] for chemical recycling. *Polym. Degrad. Stab.* **2014**, *110*, 65–70, doi:10.1016/j.polymdegradstab.2014.08.020.

148. McNeill, I.C.; Leiper, H.A. Degradation studies of some polyesters and polycarbonates-1. Polylactide: General features of the degradation under programmed heating conditions. *Polym. Degrad. Stab.* **1985**, *11*, 267–285, doi:10.1016/0141-3910(85)90050-3.
149. McNeill, I.C.; Leiper, H.A. Degradation studies of some polyesters and polycarbonates-2. Polylactide: Degradation under isothermal conditions, thermal degradation mechanism and photolysis of the polymer. *Polym. Degrad. Stab.* **1985**, *11*, 309–326, doi:10.1016/0141-3910(85)90035-7.
150. Undri, A.; Rosi, L.; Frediani, M.; Frediani, P. Conversion of poly(lactic acid) to lactide via microwave assisted pyrolysis. *J. Anal. Appl. Pyrolysis* **2014**, *110*, 55–65, doi:10.1016/j.jaap.2014.08.003.
151. Feng, L.; Feng, S.; Bian, X.; Li, G.; Chen, X. Pyrolysis mechanism of Poly(lactic acid) for giving lactide under the catalysis of tin. *Polym. Degrad. Stab.* **2018**, *157*, 212–223, doi:10.1016/j.polymdegradstab.2018.10.008.
152. Jamshidi, K.; Hyon, S.H.; Ikada, Y. Thermal characterization of polylactides. *Polymer (Guildf).* **1988**, *29*, 2229–2234, doi:10.1016/0032-3861(88)90116-4.
153. Kaya, H.; Hacaloglu, J. Thermal degradation of polylactide/aluminium diethylphosphinate. *J. Anal. Appl. Pyrolysis* **2014**, *110*, 155–162, doi:10.1016/j.jaap.2014.08.015.
154. Arikado, H. Thermal Catalytic Depolymerization of Poly(L-Lactic acid) Oliomer into LL-Lactide: Effects of Al, Ti, Zn and Zr compounds as catalysts. *Chem. Pharm. Bull.* **1999**, 467–71, doi:10.1248/cpb.47.467.
155. Nishida, H.; Mori, T.; Hoshihara, S.; Fan, Y.; Shirai, Y.; Endo, T. Effect of tin on poly(L-lactic acid) pyrolysis. *Polym. Degrad. Stab.* **2003**, *81*, 515–523, doi:10.1016/S0141-3910(03)00152-6.
156. Mori, T.; Nishida, H.; Shirai, Y.; Endo, T. Effects of chain end structures on pyrolysis of poly(L-lactic acid) containing tin atoms. *Polym. Degrad. Stab.* **2004**, *84*, 243–251, doi:10.1016/j.polymdegradstab.2003.11.008.
157. Fan, Y.; Nishida, H.; Hoshihara, S.; Shirai, Y.; Tokiwa, Y.; Endo, T. Pyrolysis kinetics of poly(L-lactide) with carboxyl and calcium salt end structures. *Polym. Degrad. Stab.* **2003**, *79*, 547–562, doi:10.1016/S0141-3910(02)00374-9.
158. Fan, Y.; Nishida, H.; Mori, T.; Shirai, Y.; Endo, T. Thermal degradation of poly(L-lactide): Effect of alkali earth metal oxides for selective L,L-lactide formation. *Polymer (Guildf).* **2004**, *45*, 1197–1205, doi:10.1016/j.polymer.2003.12.058.
159. De Clercq, R.; Dusselier, M.; Poleunis, C.; Debecker, D.P.; Giebeler, L.; Oswald, S.; Makshina, E.; Sels, B.F. Titania-Silica Catalysts for Lactide Production from Renewable Alkyl Lactates:

Structure-Activity Relations. *ACS Catal.* **2018**, *8*, 8130–8139, doi:10.1021/acscatal.8b02216.

160. Clercq, R. De; Dusselier, M.; Makshina, E.; Sels, B.F. Catalytic Gas-Phase Production of Lactide from Renewable Alkyl Lactates. *Angew. Chemie - Int. Ed.* **2018**, *57*, 3074–3078, doi:10.1002/anie.201711446.
161. Shogren, R.; Wood, D.; Orts, W.; Glenn, G. Plant-based materials and transitioning to a circular economy. *Sustain. Prod. Consum.* **2019**, *19*, 194–215, doi:10.1016/j.spc.2019.04.007.
162. Upare, P.P.; Hwang, Y.K.; Chang, J.S.; Hwang, D.W. Synthesis of lactide from alkyl lactate via a prepolymer route. *Ind. Eng. Chem. Res.* **2012**, *51*, 4837–4842, doi:10.1021/ie202714n.
163. Leibfarth, F.A.; Moreno, N.; Hawker, A.P.; Shand, J.D. Transforming polylactide into value-added materials. *J. Polym. Sci. Part A Polym. Chem.* **2012**, *50*, 4814–4822, doi:10.1002/pola.26303.
164. Pereira, C.S.M.; Silva, V.M.T.M.; Rodrigues, A.E. Ethyl lactate as a solvent: Properties, applications and production processes - A review. *Green Chem.* **2011**, *13*, 2658–2671, doi:10.1039/c1gc15523g.
165. Biddy, M.J.; Scarlata, C.J.; Kinchin, C.M. Chemicals from biomass: A market assessment of bioproducts with near-term potential. *NREL Rep.* **2016**, doi:10.2172/1244312.
166. Leibfarth, F.A.; Moreno, N.; Hawker, A.P.; Shand, J.D. Transforming polylactide into value-added materials. *J. Polym. Sci. Part A Polym. Chem.* **2012**, *50*, 4814–4822, doi:10.1002/pola.26303.
167. Rosales-Calderon, O.; Arantes, V. A review on commercial-scale high-value products that can be produced alongside cellulosic ethanol. *Biotechnol. Biofuels* **2019**, *12*, 1–58, doi:10.1186/s13068-019-1529-1.
168. Filachione, E.M.; Lengel, J.H.; Fisher, C.H. Preparation of Methyl Lactate. *Ind. Eng. Chem.* **1945**, *37*, 388–390, doi:10.1021/ie50424a024.
169. Brake, L.D. Preparation of Alkyl Esters By Depolymerization. **1993**, US Pat. 5264617.
170. Hirao, K.; Nakatsuchi, Y.; Ohara, H. Alcoholysis of Poly(l-lactic acid) under microwave irradiation. *Polym. Degrad. Stab.* **2010**, *95*, 925–928, doi:10.1016/j.polymdegradstab.2010.03.027.
171. Petrus, R.; Bykowski, D.; Sobota, P. Solvothermal Alcoholysis Routes for Recycling Polylactide Waste as Lactic Acid Esters. *ACS Catal.* **2016**, *6*, 5222–5235, doi:10.1021/acscatal.6b01009.
172. Carné Sánchez, A.; Collinson, S.R. The selective recycling of mixed plastic waste of polylactic acid and polyethylene terephthalate by control of process conditions. *Eur. Polym. J.* **2011**, *47*, 1970–1976, doi:10.1016/j.eurpolymj.2011.07.013.
173. Liu, H.; Song, X.; Liu, F.; Liu, S.; Yu, S. Ferric chloride as an efficient and reusable catalyst for methanolysis of poly(lactic acid) waste. *J. Polym. Res.* **2015**, *22*, doi:10.1007/s10965-015-0783-

6.

174. Song, X.; Zhang, X.; Wang, H.; Liu, F.; Yu, S.; Liu, S. Methanolysis of poly(lactic acid) (PLA) catalyzed by ionic liquids. *Polym. Degrad. Stab.* **2013**, *98*, 2760–2764, doi:10.1016/j.polymdegradstab.2013.10.012.
175. Song, X.; Bian, Z.; Hui, Y.; Wang, H.; Liu, F.; Yu, S. Zn-Acetate Containing ionic liquid as highly active catalyst for fast and mild methanolysis of Poly(lactic acid). *Polym. Degrad. Stab.* **2019**, *168*, 108937, doi:10.1016/j.polymdegradstab.2019.108937.
176. Liu, H.; Zhao, R.; Song, X.; Liu, F.; Yu, S.; Liu, S.; Ge, X. Lewis Acidic Ionic Liquid [Bmim]FeCl4 as a High Efficient Catalyst for Methanolysis of Poly (lactic acid). *Catal. Letters* **2017**, *147*, 2298–2305, doi:10.1007/s10562-017-2138-x.
177. Liu, F.; Guo, J.; Zhao, P.; Gu, Y.; Gao, J.; Liu, M. Facile synthesis of DBU-based protic ionic liquid for efficient alcoholysis of waste poly(lactic acid) to lactate esters. *Polym. Degrad. Stab.* **2019**, *167*, 124–129, doi:10.1016/j.polymdegradstab.2019.06.028.
178. Liu, M.; Guo, J.; Gu, Y.; Gao, J.; Liu, F. Versatile Imidazole-Anion-Derived Ionic Liquids with Unparalleled Activity for Alcoholysis of Polyester Wastes under Mild and Green Conditions. *ACS Sustain. Chem. Eng.* **2018**, *6*, 15127–15134, doi:10.1021/acssuschemeng.8b03591.
179. Jehanno, C.; Pérez-Madrigal, M.M.; Demarteau, J.; Sardon, H.; Dove, A.P. Organocatalysis for depolymerisation. *Polym. Chem.* **2019**, *10*, 172–186, doi:10.1039/c8py01284a.
180. Xu, S.; Held, I.; Kempf, B.; Mayr, H.; Steglich, W.; Zipse, H. The DMAP-catalyzed acetylation of alcohols - A mechanistic study (DMAP = 4-(dimethylamino)pyridine). *Chem. - A Eur. J.* **2005**, *11*, 4751–4757, doi:10.1002/chem.200500398.
181. Otera, J. Transesterification. *Chem. Rev.* **1993**, *93*, 1449–1470, doi:10.1021/cr00020a004.
182. Thomas, C.; Bibal, B. Hydrogen-bonding organocatalysts for ring-opening polymerization. *Green Chem.* **2014**, *16*, 1687–1699, doi:10.1039/c3gc41806e.
183. Nederberg, F.; Connor, E.F.; Glausser, T.; Hedrick, J.L. Organocatalytic chain scission of poly(lactides): A general route to controlled molecular weight, functionality and macromolecular architecture. *Chem. Commun.* **2001**, *1*, 2066–2067, doi:10.1039/b106125a.
184. Alberti, C.; Damps, N.; Meißner, R.R.R.; Enthaler, S. Depolymerization of End-of-Life Poly(lactide) via 4-Dimethylaminopyridine-Catalyzed Methanolysis. *ChemistrySelect* **2019**, *4*, 6845–6848, doi:10.1002/slct.201901316.
185. Whitelaw, E.L.; Davidson, M.G.; Jones, M.D. Group 4 salalen complexes for the production and degradation of polylactide. *Chem. Commun.* **2011**, *47*, 10004–10006, doi:10.1039/c1cc13910j.
186. Payne, J.; Mckeown, P.; Mahon, M.F.; Emanuelsson, E.A.C.; Jones, M.D. Mono- and dimeric zinc(II) complexes for PLA production and degradation into methyl lactate – a chemical recycling method. *Polym. Chem.* **2020**, *11*, 2381–2389, doi:10.1039/d0py00192a.

187. Román-Ramírez, Luis, A.; Mckeown, P.; Jones, M.D.; Wood, J. Poly(lactic acid) degradation into methyl lactate catalyzed by a well-defined Zn(II) complex. *ACS Catal.* **2019**, 409–416, doi:10.1021/acscatal.8b04863.
188. Mckeown, P.; Roman-Ramírez, Luis, A.; Bates, S.; Wood, J. Zinc Complexes for PLA Formation and Chemical Recycling : Towards a Circular Economy. *ChemSusChem* **2019**, *12*, 5233–5238, doi:10.1002/cssc.201902755.
189. Román-Ramírez, L.A.; McKeown, P.; Jones, M.D.; Wood, J. Kinetics of Methyl Lactate Formation from the Transesterification of Polylactic Acid Catalyzed by Zn(II) Complexes. *ACS Omega* **2020**, *5*, 5556–5564, doi:10.1021/acsomega.0c00291.
190. Chruszcz, A.; Reeve, S. *Composition of plastic waste collected via kerbside*; 2018;
191. Sherwood, J. Closed-Loop Recycling of Polymers Using Solvents : Remaking plastics for a circular economy. *Johnson Matthey Technol. Rev.* **2019**, *64*, 4–15, doi:10.1595/205651319x15574756736831.
192. Moretti, C.; Hamelin, L.; Jakobsen, L.G.; Junginger, M.H.; Steingrimsdottir, M.M.; Høibye, L.; Shen, L. Cradle-to-grave life cycle assessment of single-use cups made from PLA, PP and PET. *Resour. Conserv. Recycl.* **2021**, *169*, doi:10.1016/j.resconrec.2021.105508.
193. Papong, S.; Malakul, P.; Trungkavashirakun, R.; Wenunun, P.; Chom-In, T.; Nithitanakul, M.; Sarobol, E. Comparative assessment of the environmental profile of PLA and PET drinking water bottles from a life cycle perspective. *J. Clean. Prod.* **2014**, *65*, 539–550, doi:10.1016/j.jclepro.2013.09.030.
194. Maga, D.; Hiebel, M.; Thonemann, N. Life cycle assessment of recycling options for polylactic acid. *Resour. Conserv. Recycl.* **2019**, *149*, 86–96, doi:10.1016/j.resconrec.2019.05.018.
195. Abbasi, S.A. The myth and the reality of energy recovery from municipal solid waste. *Energy. Sustain. Soc.* **2018**, *8*, doi:10.1186/s13705-018-0175-y.
196. E. B. Nauman Chapter 5 Thermal Effects and Energy Balances. In *Chemical Reactor Design, Optimization, and Scaleup*; 2008; pp. 163–197 ISBN 9780470282076.
197. Nauman, E.B. Chapter 1 Elementary Reactions. In *Chemical Reactor Desing, Optimization, and Scaleup*; John Wiley and Sons: Hoboken, New Jersey, 2008; pp. 1–40 ISBN 9780470282076.
198. Nauman, E.B. Chapter 4 Stirred Tanks and Reactor Combinations. In *Chemical Reactor Design, Optimization, and Scaleup*; 2008; pp. 129–161 ISBN 9780470282076.
199. Levenspiel, O. *Chemical reaction engineering*; Wiley-VCH, 1998; Vol. 35; ISBN 978-0-471-25424-9.
200. Zahan, K.A.; Kano, M. Technological progress in biodiesel production: An overview on different types of reactors. *Energy Procedia* **2019**, *156*, 452–457, doi:10.1016/j.egypro.2018.11.086.
201. Eigenberger, G.; Ruppel, W. Catalytic Fixed-Bed Reactors. In *Ullmann's Encyclopedia of*

Industrial Chemistry; Wiley-VCH, 2003; pp. 1–63 ISBN 9783527306732.

202. Andrigo, P.; Bagatin, R.; Pagani, G. Fixed Bed Reactors. *Catal. Today* **1999**, *52*, 197–221, doi:10.1016/S0920-5861(99)00076-0.
203. Stankiewicz, A. Reactive separations for process intensification: An industrial perspective. *Chem. Eng. Process.* **2003**, *42*, 137–144, doi:10.1016/S0255-2701(02)00084-3.
204. Ozdemir, S.S.; Buonomenna, M.G.; Drioli, E. Catalytic polymeric membranes: Preparation and application. *Appl. Catal. A Gen.* **2006**, *307*, 167–183, doi:10.1016/j.apcata.2006.03.058.
205. Dalmon, J, A.; Ertl, G.; Knozinger, H.; Weitkamp, J. *Catalytic Membrance Reactors in Handbook of Heterogeneous Catalysis*; 1997;
206. Vandezande, P.; Gevers, L.E.M.; Vankelecom, I.F.J. Solvent resistant nanofiltration: Separating on a molecular level. *Chem. Soc. Rev.* **2008**, *37*, 365–405, doi:10.1039/b610848m.
207. Abels, C.; Carstensen, F.; Wessling, M. Membrane processes in biorefinery applications. *J. Memb. Sci.* **2013**, *444*, 285–317, doi:10.1016/j.memsci.2013.05.030.
208. Wan, C.F.; Yang, T.; Lipscomb, G.G.; Stookey, D.J.; Chung, T.S. Design and fabrication of hollow fiber membrane modules. *J. Memb. Sci.* **2017**, *538*, 96–107, doi:10.1016/j.memsci.2017.05.047.
209. Beasley, J, K.; Penn, R, E. Hollow fine fiber Vs Flat sheet membranes - A compasion of structures and performane. **1981**, *38*, 361–372.
210. Central, P. Membrane separation processes : Currrent relevance and future opportunities. **2001**, *47*, 1077–1087.
211. Mulder, M, H, V.; Smolders, C, A. Continuous ethanol-production controlled by membrance processes. *Process Biochem* **1986**, *21*, 35–39.
212. Colon, J, C, S, G. On-line removal of volatile fatty acids from CELLS anaerobic bioreactor via nanofiltration. *Life Support Biosph. Sci* **2001**, *7*, 291–299.
213. Timmer, J.M.K.; Kromkamp, J.; Robbertsen, T. Lactic acid separation from fermentation broths by reverse osmosis and nanofiltration. *J. Memb. Sci.* **1994**, *92*, 185–197, doi:10.1016/0376-7388(94)00061-1.
214. Timmer, J.M.K.; van der Horst, H.C.; Robbertsen, T. Transport of lactic acid through reverse osmosis and nanofiltration membranes. *J. Memb. Sci.* **1993**, *85*, 205–216, doi:10.1016/0376-7388(93)85169-W.
215. Hongo, M.; Nomura, Y.; Iwahara, M. Novel method of lactic acid production by electrodialysis fermentation. *Appl. Environ. Microbiol.* **1986**, *52*, 314–319.
216. Wang, Q.; Cheng, G.; Sun, X.; Jin, B. Recovery of lactic acid from kitchen garbage fermentation broth by four-compartment configuration electrodialyzer. *Process Biochem.* **2006**, *41*, 152–158, doi:10.1016/j.procbio.2005.06.015.

217. Nigam, P.S.; Singh, A. Production of liquid biofuels from renewable resources. *Prog. Energy Combust. Sci.* **2011**, *37*, 52–68, doi:10.1016/j.pecs.2010.01.003.

218. Wang, S.; Gu, Y.; Liu, Q.; Yao, Y.; Guo, Z.; Luo, Z.; Cen, K. Separation of bio-oil by molecular distillation. *Fuel Process. Technol.* **2009**, *90*, 738–745, doi:10.1016/j.fuproc.2009.02.005.

219. Keller, T. Reactive Distillation. *Ind. Eng. Chem. Res.* **2000**, *39*, 3953–3957, doi:10.1016/B978-0-12-386878-7.00008-5.

220. Taylor, R.; Krishna, R. Modelling reactive distillation. *Chem. Eng. Sci.* **2000**, *55*, 5183–5229, doi:10.1016/S0009-2509(00)00120-2.

221. Huang, H.J.; Ramaswamy, S.; Tschirner, U.W.; Ramarao, B. V. A review of separation technologies in current and future biorefineries. *Sep. Purif. Technol.* **2008**, *62*, 1–21, doi:10.1016/j.seppur.2007.12.011.

222. Gomis, V.; Font, A.; Pedraza, R.; Saquete, M.D. Isobaric vapor-liquid and vapor-liquid-liquid equilibrium data for the system water + ethanol + cyclohexane. *Fluid Phase Equilib.* **2005**, *235*, 7–10, doi:10.1016/j.fluid.2005.07.015.

223. Zhong, C.; Shi, X. When organocatalysis meets transition-metal catalysis. *European J. Org. Chem.* **2010**, 2999–3025, doi:10.1002/ejoc.201000004.

224. Kim, U. Bin; Jung, D.J.; Jeon, H.J.; Rathwell, K.; Lee, S.G. Synergistic Dual Transition Metal Catalysis. *Chem. Rev.* **2020**, doi:10.1021/acs.chemrev.0c00245.

225. Romiti, F.; Del Pozo, J.; Paioti, P.H.S.; Gonsales, S.A.; Li, X.; Hartrampf, F.W.W.; Hoveyda, A.H. Different Strategies for Designing Dual-Catalytic Enantioselective Processes: From Fully Cooperative to Non-cooperative Systems. *J. Am. Chem. Soc.* **2019**, *141*, 17952–17961, doi:10.1021/jacs.9b05464.

226. Allen, A.E.; MacMillan, D.W.C. Synergistic catalysis: A powerful synthetic strategy for new reaction development. *Chem. Sci.* **2012**, *3*, 633–658, doi:10.1039/c2sc00907b.

227. Muschiol, J.; Peters, C.; Oberleitner, N.; Mihovilovic, M.D.; Bornscheuer, U.T.; Rudroff, F. Cascade catalysis-strategies and challenges en route to preparative synthetic biology. *Chem. Commun.* **2015**, *51*, 5798–5811, doi:10.1039/c4cc08752f.

228. Stephan, D.W.; Erker, G. Frustrated Lewis pair chemistry: Development and perspectives. *Angew. Chemie - Int. Ed.* **2015**, *54*, 6400–6441, doi:10.1002/anie.201409800.

229. Naumann, S.; Scholten, P.B.V.; Wilson, J.A.; Dove, A.P. Dual Catalysis for Selective Ring-Opening Polymerization of Lactones: Evolution toward Simplicity. *J. Am. Chem. Soc.* **2015**, *137*, 14439–14445, doi:10.1021/jacs.5b09502.

230. Del Monte, F.; Carriazo, D.; Serrano, M.C.; Gutiérrez, M.C.; Ferrer, M.L. Deep eutectic solvents in polymerizations: A greener alternative to conventional syntheses. *ChemSusChem* **2014**, *7*, 999–1009, doi:10.1002/cssc.201300864.

231. Basterretxea, A.; Jehanno, C.; Mecerreyes, D.; Sardon, H. Dual Organocatalysts Based on Ionic Mixtures of Acids and Bases: A Step Toward High Temperature Polymerizations. *ACS Macro Lett.* **2019**, *8*, 1055–1062, doi:10.1021/acsmacrolett.9b00481.
232. Delle Chiaie, K.R.; McMahon, F.R.; Williams, E.J.; Price, M.J.; Dove, A.P. Dual-catalytic depolymerization of polyethylene terephthalate (PET). *Polym. Chem.* **2020**, *11*, 1450–1453, doi:10.1039/c9py01920k.
233. Jehanno, C.; Flores, I.; Dove, A.P.; Müller, A.J.; Ruipérez, F.; Sardon, H. Organocatalysed depolymerisation of PET in a fully sustainable cycle using thermally stable protic ionic salt. *Green Chem.* **2018**, *20*, 1205–1212, doi:10.1039/c7gc03396f.
234. Jehanno, C.; Demarteau, J.; Mantione, D.; Arno, M.C.; Ruipérez, F.; Hedrick, J.L.; Dove, A.P.; Sardon, H. Selective Chemical Upcycling of Mixed Plastics Guided by a Thermally Stable Organocatalyst. *Angew. Chemie - Int. Ed.* **2021**, *60*, 6710–6717, doi:10.1002/anie.202014860.
235. Fortune Business Insights Polylactic Acid Market Size, Share and COVID-19 Impact analysis, By Application (Packaging, Textiles, Consumer Goods, Agriculture and Horticulture, and Others), and Regional Forecast, 2021-2028 Available online: https://www.fortunebusinessinsights.com/polylactic-acid-pla-market-103429 (accessed on Apr 21, 2022).
236. Fortune Business Insights Lactic Acid Market Size, Share and COVID-19 Impact Analysis, By Raw Material (Sugarcane, Corn, Yeast Extract, and Others), By Applicaiton (PLA, Food and Beverages, Personal Care, Pharmaceutical, and Others), and Regional Forecast, 2021-2028 Available online: https://www.fortunebusinessinsights.com/lactic-acid-market-102119 (accessed on Jul 21, 2022).
237. Grand View Research Polylactic Acid Market Size, Share & Trends Analysis Report By End-use (Packaging, Textile, Agriculture, Automotive & Transport, Electronics), By Region (North America, APAC, Europe), And Segment Forecasts, 2021 - 2028 Available online: https://www.grandviewresearch.com/industry-analysis/polylactic-acid-pla-market (accessed on Apr 21, 2022).
238. Grand View Research Lactic Acid Market Size, Share & Trends Analysis Report By Raw Material (Sugarcane, Corn, Cassava), By Application (PLA, Food & Beverages), By Region, And Segment Forecasts, 2021 - 2028 Available online: https://www.grandviewresearch.com/industry-analysis/lactic-acid-and-poly-lactic-acid-market (accessed on Apr 21, 2022).
239. Research and Markets Bio-Polylactic Acid Market Research Report by Raw Material (Cassava, Corn, and Sugarcane & Sugar Beet), Form, End User, Region (Americas, Asia-Pacific, and Europe, Middle East & Africa) - Global Forecast to 2027 - Cumulative Impact of COVID-19

Available online: https://www.researchandmarkets.com/reports/4896795/bio-polylactic-acid-market-research-report-by-raw#tag-pos-2 (accessed on Apr 21, 2022).

240. Research and Markets Lactic Acid Market Research Report by Form (Form and Liquid), Application, Region (Americas, Asia-Pacific, and Europe, Middle East & Africa) - Global Forecast to 2027 - Cumulative Impact of COVID-19 Available online: https://www.researchandmarkets.com/reports/5470788/lactic-acid-market-research-report-by-form-form#tag-pos-5 (accessed on Apr 21, 2022).
241. Research and Markets L-lactide - Global Market Trajectory & Analytics Available online: https://www.researchandmarkets.com/reports/5141163/l-lactide-global-market-trajectory-and-analytics#src-pos-1 (accessed on Apr 21, 2022).
242. Research and Markets Global Lactate Esters Market Research Report 2022 (Status and Outlook) Available online: https://www.researchandmarkets.com/reports/5574545/global-lactate-esters-market-research-report-2022#src-pos-1 (accessed on Apr 21, 2022).
243. 360 Market Updates Global ethyl lactate market 2019 by manufacturers, regions, type and application, forecast to 2024 Available online: https://www.360marketupdates.com/global-ethyl-lactate-market-13806819 (accessed on May 21, 2020).
244. Atkins, P.; de Paula, J. *Atkins' Physical chemistry*; 10th ed.; Oxford University Press: Oxford, 2014; ISBN 9780199697403.
245. Giunta, C.J.; Mainz, V. V. Discovery of Nuclear Magnetic Resonance: Rabi, Purcell, and Bloch. In *ACS Symposium Series*; American Chemical Society, 2020; Vol. 1349, pp. 3–20.
246. Vyazovkin, S. On the phenomenon of variable activation energy for condensed phase reactions. *New J. Chem.* **2000**, *24*, 913–917, doi:10.1039/b004279j.
247. Vyazovkin, S. A time to search: Finding the meaning of variable activation energy. *Phys. Chem. Chem. Phys.* **2016**, *18*, 18643–18656, doi:10.1039/c6cp02491b.
248. Silva, V.H.C.; Aquilanti, V.; De Oliveira, H.C.B.; Mundim, K.C. Uniform description of non-Arrhenius temperature dependence of reaction rates, and a heuristic criterion for quantum tunneling vs classical non-extensive distribution. *Chem. Phys. Lett.* **2013**, *590*, 201–207, doi:10.1016/j.cplett.2013.10.051.
249. Aquilanti, V.; Coutinho, N.D.; Carvalho-Silva, V.H. Kinetics of low-temperature transitions and a reaction rate theory from non-equilibrium distributions. *Philos. Trans. R. Soc. A Math. Phys. Eng. Sci.* **2017**, *375*, doi:10.1098/rsta.2016.0201.
250. Sun, J.Y.; Yin, Z.T.; Zhao, D.R.; Sun, B.G.; Zheng, F.P. Qualitative and quantitative research of propyl lactate in brewed alcoholic beverages. *Int. J. Food Prop.* **2018**, *21*, 1351–1361, doi:10.1080/10942912.2018.1466325.
251. Wu, J.; Zheng, Y.; Sun, B.; Sun, X.; Sun, J.; Zheng, F.; Huang, M. The occurrence of propyl

lactate in Chinese Baijius (Chinese liquors) detected by direct injection coupled with gas chromatography-mass spectrometry. *Molecules* **2015**, *20*, 19002–19013, doi:10.3390/molecules201019002.

252. Bajić, D.M.; Živković, E.M.; Šerbanović, S.P.; Kijevčanin, M.L. Experimental measurements and modelling of volumetric properties, refractive index and viscosity of selected binary systems with butyl lactate at 288.15-323.15 K and atmospheric pressure. New UNIFAC-VISCO interaction parameters. *Thermochim. Acta* **2013**, *562*, 42–55, doi:10.1016/j.tca.2013.03.025.
253. ThermoFisher Scientific Safety Data Sheet Zinc acetate Available online: https://www.fishersci.com/store/msds?partNumber=AC370080250&productDescription=ZINC+ACETATE+25GR&vendorId=VN00032119&countryCode=US&language=en (accessed on Dec 3, 2022).
254. ThermoFisher Scientific Safety Data Sheet 4-Dimethylaminopyridine Available online: https://www.fishersci.co.uk/store/msds?partNumber=10504081&productDescription=5GR+4-Dimethylaminopyridine%2C+99%25&countryCode=GB&language=en (accessed on Dec 3, 2022).
255. Reinoso, D.M.; Ferreira, M.L.; Tonetto, G.M. Study of the reaction mechanism of the transesterification of triglycerides catalyzed by zinc carboxylates. *J. Mol. Catal. A Chem.* **2013**, *377*, 29–41, doi:10.1016/j.molcata.2013.04.024.
256. Raheem, A.B.; Noor, Z.Z.; Hassan, A.; Abd Hamid, M.K.; Samsudin, S.A.; Sabeen, A.H. Current developments in chemical recycling of post-consumer polyethylene terephthalate wastes for new materials production: A review. *J. Clean. Prod.* **2019**, *225*, 1052–1064, doi:10.1016/j.jclepro.2019.04.019.
257. Reinoso, D.M.; Damiani, D.E.; Tonetto, G.M. Zinc carboxylic salts used as catalyst in the biodiesel synthesis by esterification and transesterification: Study of the stability in the reaction medium. *Appl. Catal. A Gen.* **2012**, *449*, 88–95, doi:10.1016/j.apcata.2012.09.014.

Chapter 8 – Appendices

Additional information not covered elsewhere in the thesis, and parts of work not ready for publication are presented as a series of Appendices

8.1 Kinetic Models

Throughout this thesis kinetic models have been used to estimate rate constants, Arrhenius plots and activation energies for each reaction step.

8.1.1 First order PLA degradation model

Throughout this thesis a first order kinetic model has been used that only considers the initial cleavage of PLA ester groups. The resulting activation energy E_a is particularly useful as it allows for comparison with the literature values for E_a which also only consider the initial degradation of PLA.

Consider the following elementary reaction

$$Int \overset{k}{\rightarrow} CE$$

The corresponding rate law for this reaction is

$$\frac{d[Int]}{dt} = -k_1[Int]$$

which can be rewritten as

$$\frac{d[Int]}{[Int]} = -kt$$

Integrating this differential equation gives

$$\int \frac{1}{[Int]} d[Int] = -k \int dt \quad \rightarrow \quad \ln[Int] = -kt + C$$

Considering t = 0 and t = *t*

$$\int_0^t \frac{1}{[Int]} d[Int] = -k \int_0^t dt \quad \rightarrow \quad \ln[Int]_t - \ln[Int]_0 = -kt$$

Upon rearranging

$$\ln[Int]_t = \ln[Int]_0 - kt \quad \text{or} \quad [Int]_t = [Int]_0 \exp(-kt)$$

The above equation is in the form of y = c + mx. The concentration of Int gradually falls as the reaction progresses. Plotting ln[*Int*] vs time results in plots of the form shown in Figure 8.1. The gradient of this plot is -*k*. Replotting the data for a range of temperatures enables an Arrhenius plot to be generated, shown in Figure 8.2. The first order E_a was calculated to be 55.1 ± 10.0 kJ·mol^{-1} in this case.

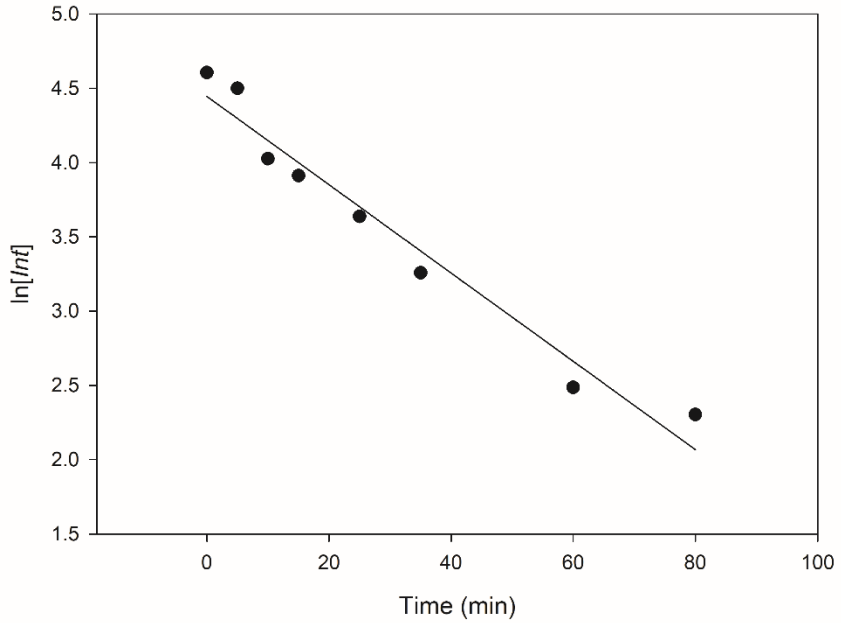

Figure 8.1. ln[*Int*] vs time for ethanolysis of 12.5 g PLA, at 130 °C, 300 rpm, 5 equivalents of EtOH, 9 mol% of Zn(**1**^{Et})$_2$. k_1 y = -0.0297x + 4.45 R^2 = 0.9607.

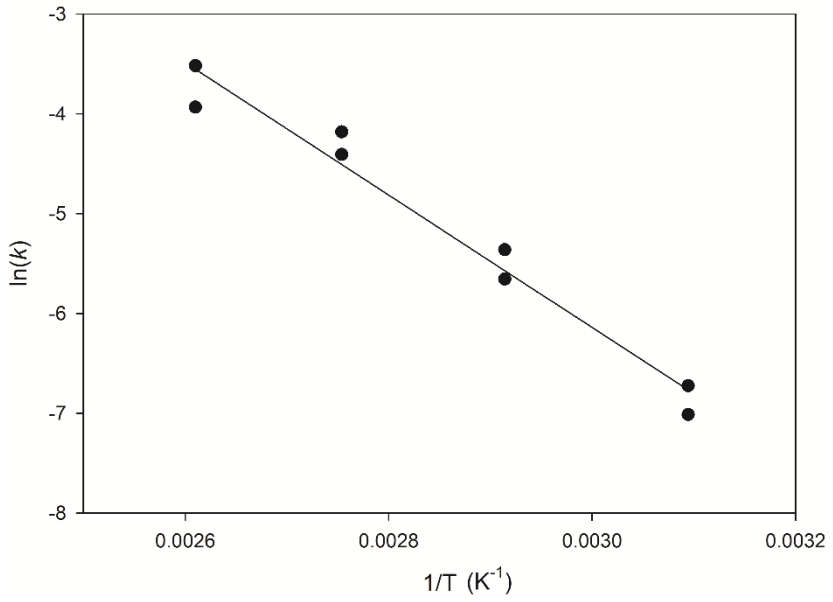

Figure 8.2. Arrhenius plots for ethanolysis of 12.5 g PLA, at 130 °C, 300 rpm, 5 equivalents of EtOH, 9 mol% of Zn(**1**^{Et})$_2$. y = -6634.83x + 13.76 R^2 = 0.9684.

8.1.2 Consecutive second step irreversible model

The equations (3.8 – 3.10) were solved by sequential integration and substitution to produce equation (3.11). The ^{1}H NMR data was then fitted to equation (3.11) using SigmaPlot which enabled for the determination of k_1 and k_2.

$$Int \overset{k_1}{\rightarrow} CE \overset{k_2}{\rightarrow} AL \tag{3.7}$$

$$\frac{d[Int]}{dt} = -k_1[Int] \tag{3.8}$$

$$\frac{d[CE]}{dt} = k_1[Int] - k_2[CE] \tag{3.9}$$

$$\frac{d[AL]}{dt} = k_2[CE] \tag{3.10}$$

$$[CE] = \frac{k_1}{k_2 - k_1}[\exp(-k_1 t) - \exp(-k_2 t)][Int]_0 \tag{3.11}$$

Integrating (3.8) directly gives

$$[Int]_t = [Int]_0 \exp(-kt)$$

Substituting this results into (3.9) gives the differential equation

$$\frac{d[CE]}{dt} + k_2[CE] \;=\; k_1[Int]_0 \exp\,(-k_1 t)$$

This is a first order differential equation of the form

$$\frac{df}{dx} + af = b$$

This has a solution of the form

$$f(x)\exp\left(\int adx\right) = \int exp\left(\int adx\right) bdx + C$$

We need to find f(x), i.e. [CE](t). Substitute kinetic parameters into the above solution

$$[CE](t)\exp\left(\int k_2 dt\right) = \int exp\left(\int k_2 dt\right) k_1[Int]_0 \exp(-k_1 t)\, dt + C$$

Carrying out the integrations gives

$$[CE](t)\exp\left(\int k_2 dt\right) = \int exp\left((k_2 - k_1)t\right) k_1[Int]_0 dt + C$$

$$[CE](t)\exp\left(\int k_2 dt\right) = [Int]_0 \frac{k_1}{k_2 - k_1} exp\left((k_2 - k_1)t\right) + C$$

$$[CE](t) = \exp(-k_2 t)\left[[Int]_0 \frac{k_1}{k_2 - k_1} exp\left((k_2 - k_1)t\right) + C\right]$$

To evaluate the constant C we note that at t=0 [CE] = 0 which gives

$$0 = \left[[Int]_0 \tfrac{k_1}{k_2 - k_1} + C\right] \quad \text{or} \quad C = -\,[Int]_0 (\tfrac{k_1}{k_2 - k_1})$$

Substituting C into the expression for [CE](t) gives

$$[CE](t) = \exp(-k_2 t)\left[[Int]_0 \frac{k_1}{k_2 - k_1} exp\left((k_2 - k_1)t\right) + -\,[Int]_0 (\frac{k_1}{k_2 - k_1})\right]$$

Simplifying this expression give the solution equation

$$[CE] = \tfrac{k_1}{k_2 - k_1}[\exp(-k_1 t) - \exp(-k_2 t)][Int]_0 \qquad (3.11)$$

8.1.3 Consecutive second step in equilibrium model

The experimental data for Chapter 4 and 6 was modelled using the reaction mechanism shown in Equation (3.3 – 3.6), proposed by Román-Ramírez, et al [187]. The differential Equations (3.4 – 3.6) were solved in MATLAB according to the script shown below. The minimisation of least squares fitting procedure in MATLAB estimated the rate constants from the experimental ^{1}H NMR data. The rate constants were estimated for the same reaction over a range of temperatures and used to generate Arrhenius plots to obtain E_a for the reaction.

```
% Script to calculate the rate coefficients
% Prepared by Luis Roman, Sept. 2021.

clear all
clc
format long
global tExp CaExp CbExp CcExp Ca0 Cb0 Cc0
%------------------------------------------------------------------------
%Input
% Use either:
%prompt = 'Input Experimental Data: t, Int, CE, Lact, inside [  ]\n';
%Exp_data = input(prompt)
% or
Exp_data = []
%------------------------------------------------------------------------
%Initial conditions
Ca0 = Exp_data(1,2);
Cb0 = Exp_data(1,3);
Cc0 = Exp_data(1,4);
%------------------------------------------------------------------------
%Vectors of experimental data
tExp = Exp_data(:,1);
CaExp = Exp_data(:,2);
CbExp = Exp_data(:,3);
CcExp = Exp_data(:,4);
%------------------------------------------------------------------------
%Initial estimates
k_ini = [0.05 0.01 0.01];
%------------------------------------------------------------------------
%Minimisation function routine
[k,resnorm,residual,exitflag,output] = lsqnonlin(@fmin_routine,k_ini);
%------------------------------------------------------------------------
%Display results
%------------------------------------------------------------------------
k_ = k'
%------------------------------------------------------------------------
%Computation with fitted values
%final time, min
tf = tExp(length(tExp));
```

```
%time, min
t = linspace(0,tf,50)';
%-------------------------------------------------------------------------
%Concentrations with differential equations solution
Ci0=[Ca0 Cb0 Cc0]; %Initial values
[t Ci]=ode15s(@(t,Ci) diffEqs(t,Ci,k), t,Ci0);
%-------------------------------------------------------------------------
%Conversion, selectivity and yield
Conv=(1-Ci(end,1)/Ca0)*100
Select=Ci(end,3)/Conv*100
Yield= Conv*Select/100
%-------------------------------------------------------------------------
%Graphs
plot(tExp,CaExp,'b*','MarkerFaceColor','b'), hold on
plot(tExp,CbExp,'mo','MarkerFaceColor','m')
plot(tExp,CcExp,'g^','MarkerFaceColor','g')
plot(t,Ci(:,1),'b-',t,Ci(:,2),'m-',t,Ci(:,3),'g-')
xlabel ('time / min'),ylabel ('Concentration / % ')
legend ({'Int','CE','MeLa'},'fontsize',11)
legend boxoff
set(legend,'Location','best');
hold off
%Routine with the function to be minimised
function f = fmin_routine(k)
global tExp CaExp CbExp CcExp Ca0 Cb0 Cc0

% Concentration computation
Ci0=[Ca0 Cb0 Cc0]; %Initial values
[t Ci]=ode15s(@(t,Ci) diffEqs(t,Ci,k), tExp,Ci0);
%function to be minimised
f = [(Ci(:,1)-CaExp)/CaExp (Ci(:,2)-CbExp)/CbExp (Ci(:,3)-CcExp)/CcExp];
end
function dCdt = diffEqs(t,Ci,k)
%-------------------------------------------------------------------------
dCadt = -k(1)*Ci(1);
dCbdt = k(1)*Ci(1) - k(2)*Ci(2) + k(3)*Ci(3);
dCcdt = k(2)*Ci(2) - k(3)*Ci(3);

dCdt = [dCadt dCbdt dCcdt]';
end
```

8.2 Analytical methods

8.2.1 Gas chromatography (GC)

A multiple point external standard calibration curve was prepared using standard solutions covering the range of AL concentrations. A linear response of the detector was determined for MeLa, EtLa, and BuLa (R^2 = 0.9998, 0.9998, and 0.9969 respectively). For PrLa the GC analysis was only qualitative. The calibration curve for EtLa is shown below Figure 8.3.

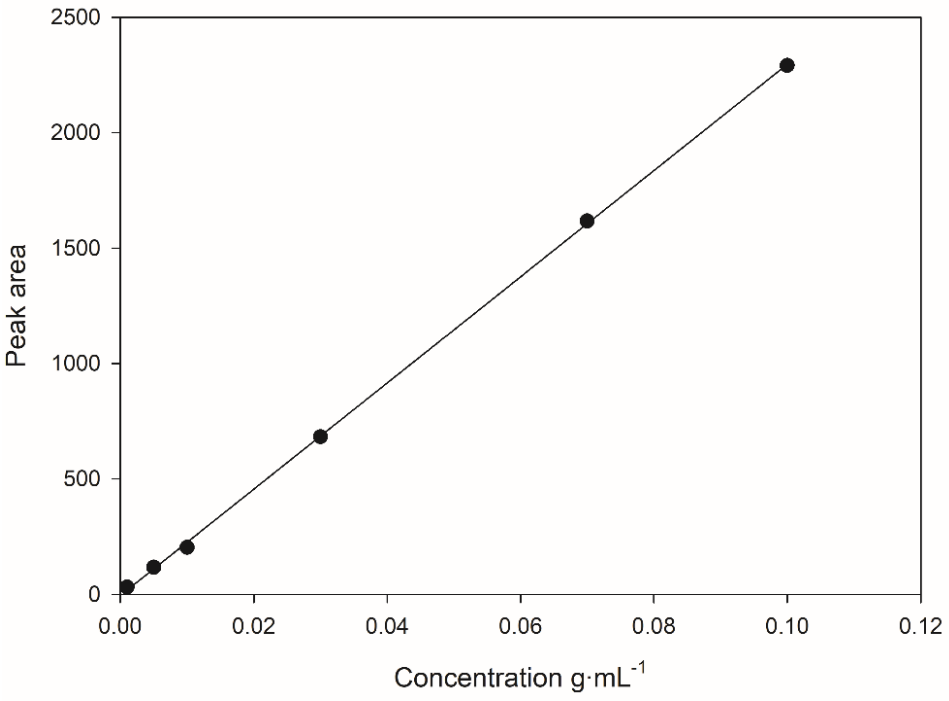

Figure 8.3. GC calibration curve for EtLa. y = 23010.65x -5.056 R^2 = 0.9998.

8.2.2 Proton nuclear magnetic resonance (^{1}H NMR)

According to equation (3.3) there are three possible environments for methine functional groups: internal methine protons along the PLA chains (Int) (δ = 5.09 – 5.21 ppm), two types of chain end methine protons belonging to oligomer fragments (CE) (δ = 4.30 – 4.39 ppm / 5.09 – 5.21 ppm), or methine protons belongs to an alkyl lactate molecule (AL) (δ = 4.23 – 4.29 ppm), shown below in Figure 8.4. By comparing integrals of interest, ^{1}H NMR can be used to determine the ratios of compounds in a reaction mixture. This allows for a relative concentration of each compound to be determined. Reaction samples were dissolved in $CDCl_3$ and chemical shifts were referenced against tetramethylsilane (TMS).

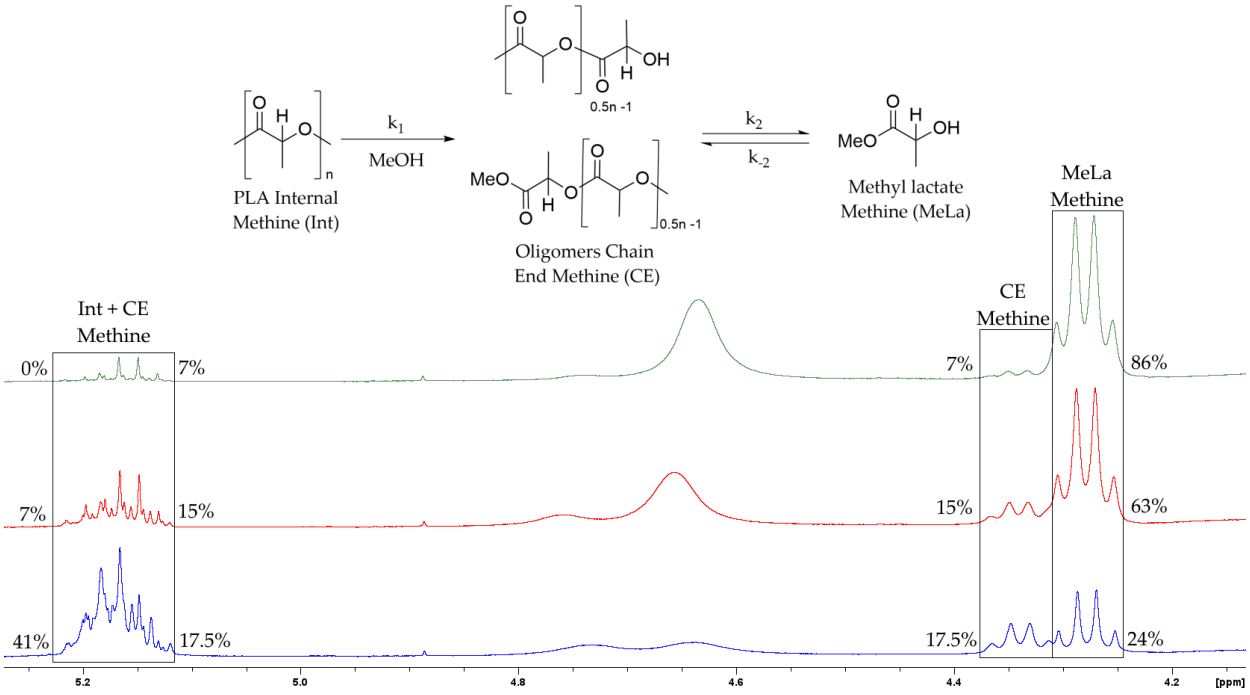

Figure 8.4. ^{1}H NMR (CDCl3, 400 MHz) stacked spectra of a methanolysis reaction at 120 ◦C and the relative percentage of each methine proton Int, CE and MeLa. (Blue spectrum 10 min, Red spectrum 40 min, Green spectrum 90 min).

8.3 Calculations

8.3.1 Calculations in Chapter 4

The mol of ester groups

$$\frac{12.5\ g}{72\ g \cdot mol^{-1}} = 0.1736\ mol$$

The mol of EtOH

$$50\ mL \times 0.789\ g \cdot mL^{-1} = 39.45\ g$$

$$\frac{39.45\ g}{46.07 g \cdot mol^{-1}} = 0.8563\ mol$$

The molar equivalent of EtOH

$$\frac{0.8563\ mol}{0.1736\ mol} = 4.932\ eq$$

The mol of PrOH

$$50\ mL \times 0.803\ g \cdot mL^{-1}\ =\ 40.15\ g$$

$$\frac{40.15\ g}{60.096 g \cdot mol^{-1}} = 0.6681\ mol$$

The molar equivalent of PrOH

$$\frac{0.6681\ mol}{0.1736\ mol} = 3.849\ eq$$

The mol of BuOH

$$50\ mL \times 0.81\ g \cdot mL^{-1}\ =\ 40.5\ g$$

$$\frac{40.5\ g}{74.123\ g \cdot mol^{-1}} = 0.5464\ mol$$

The molar equivalent of BuOH

$$\frac{0.5464\ mol}{0.1736\ mol} = 3.148\ eq$$

The mol of Zn(**1**^{Et})$_2$

$$\frac{1\ g}{644.27\ g \cdot mol^{-1}} = 1.55\ \times 10^{-3}\ mol$$

The mol% of Zn(**1**^{Et})$_2$

$$\frac{1.55\ \times 10^{-3}\ mol}{0.1736\ mol} = (8.93\ \times 10^{-3}\ )\ \times 100 = 8.93\ mol\ \%$$

The mol of Zn(**1**^{Et})$_2$

$$\frac{1\ g}{672.32\ g \cdot mol^{-1}} = 1.487\ \times 10^{-3}\ mol$$

The mol% of Zn(**2**^{Pr})$_2$

$$\frac{1.487\ \times 10^{-3}\ mol}{0.1736\ mol} = (8.57\ \times 10^{-3}\ )\ \times 100 = 8.57\ mol\ \%$$

8.3.2 Calculations in Chapter 5

The mol of ester groups

$$\frac{2\ g}{72\ g \cdot mol^{-1}} = 0.02778\ mol$$

The mol of MeOH

$$10\ mL \times 0.792\ g \cdot mL^{-1} = 7.92\ g$$

$$\frac{7.92\ g}{32.04 g \cdot mol^{-1}} = 0.247\ mol$$

The molar equivalent of MeOH

$$\frac{0.247\ mol}{0.02778\ mol} = 8.89\ eq$$

The mol of EtOH

$$14.5\ mL \times 0.789\ g \cdot mL^{-1} = 11.44\ g$$

$$\frac{11.44\ g}{46.07 g \cdot mol^{-1}} = 0.248\ mol$$

The molar equivalent of EtOH

$$\frac{0.248\ mol}{0.02778\ mol} = 8.93\ eq$$

The mol of $Zn(OAc)_2$

$$\frac{0.5\ g}{219.51\ g \cdot mol^{-1}} = 2.279 \times 10^{-4}\ mol$$

The mol% of $Zn(OAc)_2$

$$\frac{2.279 \times 10^{-4}\ mol}{0.02778\ mol} = (8.204 \times 10^{-4}) \times 100 = 0.8\ mol\ \%$$

The mol of DMAP

$$\frac{0.5\ g}{122.17\ g \cdot mol^{-1}} = 4.0927 \times 10^{-4}\ mol$$

The mol% of DMAP

$$\frac{4.0927\ \times 10^{-4}\ mol}{0.02778\ mol} = (1.4734 \times 10^{-3}\ ) \times 100 = 1.5\ mol\ \%$$

8.3.3 Calculations in Chapter 6

The mol of ester groups

$$\frac{2\ g}{72\ g \cdot mol^{-1}}\ =\ 0.02778\ mol$$

The mol of MeOH

$$19\ mL \times 0.792\ g \cdot mL^{-1}\ =\ 15.048\ g$$

$$\frac{15.048\ g}{32.04 g \cdot mol^{-1}} = 0.4697\ mol$$

The molar equivalent of EtOH

$$\frac{0.4697\ mol}{0.02778\ mol} = 16.91\ eq$$

The mol of $Zn(OAc)_2$

$$\frac{0.122\ g}{219.51\ g \cdot mol^{-1}} = 5.56\ \times 10^{-4}\ mol$$

The mol% of $Zn(OAc)_2$

$$\frac{5.56\ \times 10^{-4}\ mol}{0.02778\ mol} = (2.001\ \times 10^{-2}\ )\ \times 100 = 2\ mol\ \%$$

The mol of $Mg(OAc)_2$

$$\frac{0.119\ g}{214.45\ g \cdot mol^{-1}} = 5.55\ \times 10^{-4}\ mol$$

The mol% of $Mg(OAc)_2$

$$\frac{5.55\ \times 10^{-4}\ mol}{0.02778\ mol} = (1.99\ \times 10^{-2}\ )\ \times 100 = 0.8\ mol\ \%$$

The mol of DMAP

$$\frac{0.0679\ g}{122.17\ g \cdot mol^{-1}} = 5.56\ \times 10^{-4}\ mol$$

The mol% of DMAP

$$\frac{5.56\ \times 10^{-4}\ mol}{0.02778\ mol} = (2.001\ \times 10^{-2}\ )\ \times 100 = 2\ mol\ \%$$

The mol of TBD

$$\frac{0.0774\ g}{139.2\ g \cdot mol^{-1}} = 5.56\ \times 10^{-4}\ mol$$

The mol% of $Zn(OAc)_2$

$$\frac{5.56\ \times 10^{-4}\ mol}{0.02778\ mol} = (2.001\ \times 10^{-2}\ )\ \times 100 = 2\ mol\ \%$$